JOURNAL OF RESEARCH

OF THE U.S. GEOLOGICAL SURVEY

MAY–JUNE 1976
VOLUME 4, NUMBER 3

Scientific notes and summaries of investigations in geology, hydrology, and related fields

U.S. DEPARTMENT OF THE INTERIOR

UNITED STATES DEPARTMENT OF THE INTERIOR
THOMAS S. KLEPPE, Secretary
GEOLOGICAL SURVEY
V. E. McKelvey, Director

For sale by the Superintendent of Documents, U.S. Government Printing Office, Washington, DC 20402. Annual subscription rate $18.90 (plus $4.75 for foreign mailing). Single copy $3.15. Make checks or money orders payable to the Superintendent of Documents.

Send all subscription inquiries and address changes to the Superintendent of Documents at the above address.

Purchase orders should not be sent to the U.S. Geological Survey library.

Library of Congress Catalog-card No. 72-600241.

The Journal of Research is published every 2 months by the U.S. Geological Survey. It contains papers by members of the Geological Survey and their professional colleagues on geologic, hydrologic, topographic, and other scientific and technical subjects.

Correspondence and inquiries concerning the Journal (other than subscription inquiries and address changes) should be directed to Anna M. Orellana, Managing Editor, Journal of Research, Publications Division, U.S. Geological Survey, 321 National Center, Reston, VA 22092.

Papers for the Journal should be submitted through regular Division publication channels.

The Secretary of the Interior has determined that the publication of this periodical is necessary in the transaction of the public business required by law of this Department. Use of funds for printing this periodical has been approved by the Director of the Office of Management and Budget through June 30, 1980.

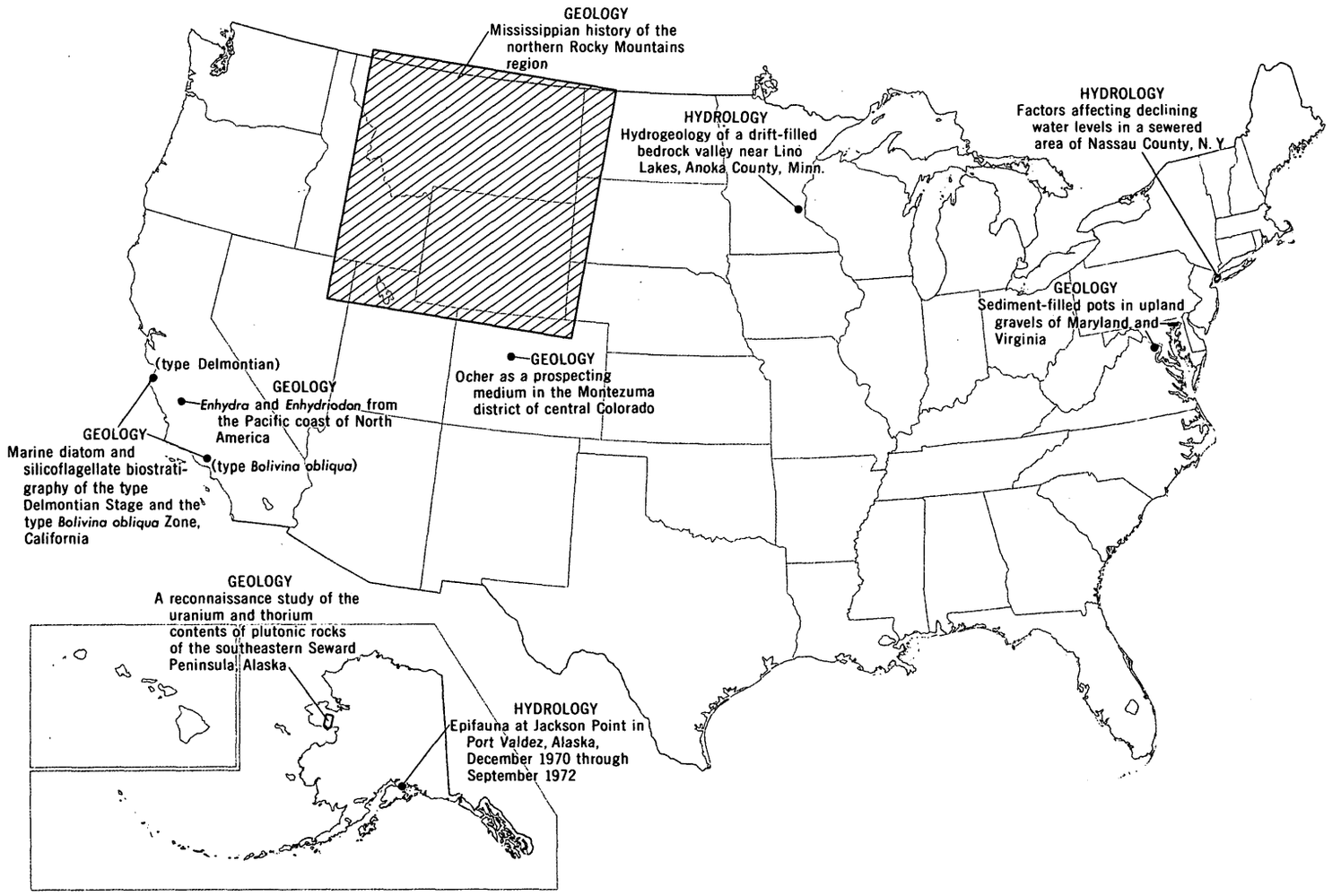

GEOGRAPHIC INDEX TO ARTICLES

See "Contents" for articles concerning areas outside the United States and articles without geographic orientation.

JOURNAL OF RESEARCH

of the

U.S. Geological Survey

Vol. 4 No. 3 May–June 1976

CONTENTS

ABBREVIATIONS

A ---------ampere
Å ---------angstrom
ADP ------ammonium dihydrogen phosphate
atm -------atmosphere
avg -------average
B.P. ------before present
b.y. -------billion years
°C --------degree Celsius
calc -------calculated
c/s -------counts per second
dc --------direct current (d-c as unit modifier)
deg -------degree
diam -----diameter
eq --------equation
EROS ----Earth Resources Observation System
g-mol -----gram-mole
ID --------inside diameter
J ---------joule
Jtu -------Jackson turbidity unit
K ---------kelvin
kPa -------kilopascal
kV --------kilovolt
lm --------lumen
M --------molarity; molar (concentration)
meq -------milliequivalent
MIBK ----methyl isobutyl ketone
min -------minute
ml --------millilitre
mol -------mole
m.y. ------million years
μcal -----microcalorie
μg --------microgram
μl --------microlitre
μm -------micrometre
N --------normality
nm -------nanometre
OD -------outside diameter
ppb -------part per billion
ppm ------part per million
quad. -----quadrangle
RAP ------rubidium acid phthalate
wt --------weight
w/v ------weight per volume
yd --------yard
yr --------year

METRIC-ENGLISH EQUIVALENTS

Metric unit		English equivalent	
Length			
millimetre (mm)	=	0.03937	inch (in)
metre (m)	=	3.28	feet (ft)
kilometre (km)	=	.62	mile (mi)
Area			
square metre (m^2)	=	10.76	square feet (ft^2)
square kilometre (km^2)	=	.386	square mile (mi^2)
hectare (ha)	=	2.47	acres
Volume			
cubic centimetre (cm^3)	=	0.061	cubic inch (in^3)
litre (l)	=	61.03	cubic inches
cubic metre (m^3)	=	35.31	cubic feet (ft^3)
cubic metre	=	.00081	acre-foot (acre-ft)
cubic hectometre (hm^3)	=	810.7	acre-feet
litre	=	2.113	pints (pt)
litre	=	1.06	quarts (qt)
litre	=	.26	gallon (gal)
cubic metre	=	.00026	million gallons (Mgal or 10^6 gal)
cubic metre	=	6.290	barrels (bbl) (1 bbl=42 gal)
Weight			
gram (g)	=	0.035	ounce, avoirdupois (oz avdp)
gram	=	.0022	pound, avoirdupois (lb avdp)
tonne (t)	=	1.1	tons, short (2,000 lb)
tonne	=	.98	ton, long (2,240 lb)
Specific combinations			
kilogram per square centimetre (kg/cm^2)	=	0.96	atmosphere (atm)
kilogram per square centimetre	=	.98	bar (0.9869 atm)
cubic metre per second (m^3/s)	=	35.3	cubic feet per second (ft^3/s)

Metric unit		English equivalent	
Specific combinations—Continued			
litre per second (l/s)	=	.0353	cubic foot per second
cubic metre per second per square kilometre [$(m^3/s)/km^2$]	=	91.47	cubic feet per second per square mile [$(ft^3/s)/mi^2$]
metre per day (m/d)	=	3.28	feet per day (hydraulic conductivity) (ft/d)
metre per kilometre (m/km)	=	5.28	feet per mile (ft/mi)
kilometre per hour (km/h)	=	.9113	foot per second (ft/s)
metre per second (m/s)	=	3.28	feet per second
metre squared per day (m^2/d)	=	10.764	feet squared per day (ft^2/d) (transmissivity)
cubic metre per second (m^3/s)	=	22.826	million gallons per day (Mgal/d)
cubic metre per minute (m^3/min)	=	264.2	gallons per minute (gal/min)
litre per second (l/s)	=	15.85	gallons per minute
litre per second per metre [(l/s)/m]	=	4.83	gallons per minute per foot [(gal/min)/ft]
kilometre per hour (km/h)	=	.62	mile per hour (mi/h)
metre per second (m/s)	=	2.237	miles per hour
gram per cubic centimetre (g/cm^3)	=	62.43	pounds per cubic foot (lb/ft^3)
gram per square centimetre (g/cm^2)	=	2.048	pounds per square foot (lb/ft^2)
gram per square centimetre	=	.0142	pound per square inch (lb/in^2)
Temperature			
degree Celsius (°C)	=	1.8	degrees Fahrenheit (°F)
degrees Celsius (temperature)	=	[(1.8×°C)+32]	degrees Fahrenheit

Jour. Research U.S. Geol. Survey
Vol. 4, No. 3, May–June 1976, p. 253–254

INTERMEDIATE-SCALE MAPPING

By J. LeROY WARD, Reston, Va.

Abstract.—The U.S. Geological Survey has introduced an intermediate-scale map series (1:100,000 and 1:50,000) in response to the demand for maps at scales between the 1:24,000 and 1:250,000 standard series. The goal is to provide basic cartographic data at the level of detail and in the format selected by Federal, State, regional, county, and other users. A major innovation is the preparation of feature-separation drawings which provide great flexibility in constructing maps. The new series is designed with digitization in mind, ultimately to facilitate forming a digital cartographic data base.

In response to the increasing demand for maps at scales that fill the gap between the 1:24,000 and 1:250,000 series, the U.S. Geological Survey has introduced an intermediate-scale (1:100,000 and 1:50,000) map series. These new products reflect the goals of today's National Mapping Program (an expansion of the familiar National Topographic Mapping Program) to make graphic or digital cartographic data and services readily available for a multiplicity of uses. Intermediate-scale maps will provide basic data at the level of detail and in the format selected by Federal, State, regional, county, and other users.

To support U.S. Bureau of Land Management needs, 134 topographic maps at 1:100,000 scale are being prepared initially for critical areas of energy- and mineral-resource development. Similarly, to classify farmlands in 116 counties, the U.S. Soil Conservation Service has requested 1:100,000-scale planimetric bases in county format.

In addition, cooperative projects are underway for 66, 1:50,000-scale maps of counties in Colorado, Pennsylvania, Connecticut, Virginia, and New Mexico, and for 30, 1:100,000-scale maps in Georgia. Other agreements with Federal agencies provide for 30, 1:100,000-scale quadrangles in scattered areas of the Western States. To date, 3, 1:100,000-scale maps have been published—Healdsburg, Calif., Gillette, Wyo., and Reno Junction, Wyo.—and 11, 1:50,000-scale county maps are available, primarily for areas in Colorado and Pennsylvania.

The intermediate-scale base map is a useful tool for Federal agencies that classify and lease public lands and inventory natural resources. At the State and local level, the new series is expected to encourage land-use planning on a larger scale. Because of a number of simplifications in design and construction, either general-purpose or special-purpose base maps can be produced with equal ease, and the data can be stored in digital form.

PRODUCTION

All five mapping centers of the U.S. Geological Survey are producing the new intermediate-scale maps. The maps are derived from available 7.5- and 15-minute topographic maps and (if needed) other sources, such as aerial photographs. A major innovation is the preparation of feature-separation drawings as well as color-separation drawings, which provide great flexibility in constructing maps. For computer compatibility, certain symbols have been modified to forms that lend themselves to trouble-free digitization.

Maps in the 1:100,000-scale series are cast on the Universal Transverse Mercator (UTM) projection with a standard format at 30 minutes north-south and 60 minutes east-west. The component larger scale maps are reduced to 1:100,000, mosaicked on the UTM projection, and updated to some degree (where no large-scale coverage is available, stereocompilation may be required). This base is photographically duplicated to produce numerous guides from which the cartographer selects and separates the map data to be shown.

Much of the 1:24,000-scale map content can be retained; detail such as fence lines, abandoned features, and nonlandmark buildings are excluded. Generally, standard topographic map symbolization is used; however, certain symbols were modified after considerable experimentation with digitization. For example, roads and drainage are symbolized as solid lines, and various line weights indicate classification. Linear features less than 2,000 feet long or areal features less than 1,000 feet in the shortest dimension are not shown.

The number of feature-separation drawings for each map ranges from a minimum of 13 to a maximum of 21. Never before has the user had such an opportunity to obtain at minimal extra cost a map to suit his purpose alone. The selection of map content currently in the program includes:

Feature-separation drawings

Code	*Content*
011	UTM projection and 10-km grid, 7.5-min ticks, State plane-coordinate ticks.
012	Railroads, landmark culture, reservations.
013	Civil boundaries.
014	Most interior and marginal lettering.
015	Public-land survey data, phase 1.
016	Public land survey data, phase 2 (for digitization).
021	Class 1, 2 roads and markers.
022	Class 3–5 roads, State-route markers.
023	Spot elevations (metric), contour conversion table (feet–metres, margin).
031	Contours (continuous lines only, for digitization).
032	Contours (standard treatment).
033	Strip mines and mine dumps, lava, tailings.
034	Sand, gravel, moraine, fill.
041	Perennial and intermittent drainage.
042	Hydrographic lettering.
043	Marsh, swamp.
044	Salt evaporator.
045	Perennial and intermittent open water (fill).
046	Land subject to controlled inundation (fill).
051	National, State, county boundaries (accent tint).
052	Public parks (tint).
053	Forest, game land (tint).
054	Military or Indian reservations, other public areas (tint).

To print any one map, only 5 combined negatives are prepared to produce as many as 11 process colors with mezzotint screens and the 5 standard U.S. Geological Survey press inks: black, magenta, brown, cyan, and yellow. The feature-separation drawings are filed in the Survey's mapping centers, and stable-base film copies may be obtained on request at the cost of reproduction.

FUTURE TRENDS

The new intermediate-scale series embodies several progressive trends in U.S. Geological Survey mapping, namely:

1. Providing cartographic products tailored to both general and special needs.
2. Forming a digital cartographic data base.
3. Developing common mapping methodologies for Federal and State agencies involved in land management.
4. Converting to the SI (Système International) of metric units.

The first fully metric 1:100,000-scale map—Watford City SE, N. Dak. (southeast quarter of the 1:250,000 Watford City)—was recently published. This map was prepared from 32, 7.5-min quadrangles, and the metric contours were interpolated.

Experimentation continues toward promoting simplicity and economy in content, construction, and reproduction for maps of the future. Joint experiments between Federal agencies are resulting in unique map editions, such as topographic–bathymetric maps, image–line maps, and flood-plain maps. Land-use mapping and digitizing are expected to become major operations over the next 5 years; the requirement will likely be intermediate-scale map bases accompanied by at least four overlays. Density-slicing technology is now being explored for semiautomatically extracting map data from imagery.

The ultimate payoff will be the digital cartographic data base. Users will be able to obtain the desired map graphic, whether a television image or hard copy, in the time it takes to make a telephone call. It may not even be necessary to display the map but rather have it serve as a computer model for analyses. The rapid development in the state of the art of automatic data processing puts such capabilities within our grasp in the next decade.

Jour. Research U.S. Geol. Survey
Vol. 4, No. 3, May–June 1976, p. 255–265

FACTORS AFFECTING DECLINING WATER LEVELS IN A SEWERED AREA OF NASSAU COUNTY, NEW YORK

By MURRAY S. GARBER and DENNIS J. SULAM, Mineola, N.Y.

Prepared in cooperation with the Nassau County Department of Public Works

Abstract.—Double-mass-curve analysis of ground-water levels in Nassau County, Long Island, N.Y., shows that the average-weighted ground-water levels in a 32-mi² (83-km²) segment of a sewered area declined 11.8 ft (3.6 m) relative to an adjacent unsewered area to the east during 1953–72. Electric-analog-model analysis indicates that 4.9 ft (1.5 m) of the decline is due to pumping in nearby Queens County, west of the sewered area. Most of the remaining 6.9 ft (2.1 m) of the decline is due to sewering. Streamflow within the sewered area has also declined because of the lowered ground-water levels.

Water levels in western Nassau County, Long Island, N.Y., have declined substantially since 1953. This decline is the result of several factors which include (1) increasing withdrawals of ground water in Queens and Nassau Counties because of increasing population, (2) increasing per capita use of water, (3) decreasing natural recharge related to urban development, (4) decreasing artificial recharge because of gradual changeover from cesspools and septic tanks to sanitary sewers in Nassau County, and (5) the drought on Long Island between 1962 and 1966 (Cohen and others, 1969).

An analysis of the two principal hydrologic factors that have caused the water table to decline in western Nassau County, sewering in Nassau County and pumping of ground water in nearby Queens County, is the subject of this report. The study included a continuation of the graphical-statistical study by Franke (1968) extended to 1972 and the use of an analog model to determine the effect of pumping in nearby Queens County on water levels in the study area.

Acknowledgments.—The authors thank Charles Kirsner, Nassau County Department of Public Works, Division of Sanitation and Water Supply, for providing much of the basic data for this report. The authors also thank R. T. Getzen of the U.S. Geological Survey for his assistance on the analog-model analysis and O. L. Franke, formerly with the Geological Survey, for his valuable advice on the double-mass-curve analysis.

LOCATION AND GENERAL GEOGRAPHIC FEATURES OF STUDY AREA

The study area, known locally as Sewer District 2, is in a highly suburbanized part of western Nassau County entirely south of the major topographic divide. The 70-mi² (180-km²) area includes the west half of the town of Hempstead and the southwest quarter of the town of North Hempstead (fig. 1). The southern three-fourths of the sewer district is a southward-sloping, glacial-outwash plain whose surface lies below an altitude of 100 ft (30 m). The northern one-fourth lies within the Ronkonkoma and the Harbor Hill glacial moraines, areas of rolling topography with altitudes in excess of 100 ft (30 m) and a maximum altitude of about 320 ft (98 m).

The population of Nassau County increased from about 400,000 in 1940 to more than 1,400,000 in 1970 (New York State Division of the Budget, 1973). Rate of growth in population was greatest during the decade 1950–60, when the population of the town of Hempstead alone increased from 448,000 to 767,000 (Long Island Lighting Co., 1971, p. 2). Most of Sewer District 2 lies within the town of Hempstead.

PREVIOUS WORK

The hydrology of Long Island has been described in numerous reports. Most recently, Franke and McClymonds (1972) summarized the hydrologic situation on Long Island. Nitrate concentration of streams and ground water in parts of Nassau County were discussed by Perlmutter and Koch (1972). Kimmel (1971, 1972) prepared maps showing the water table of western long Island in 1969 and 1970, and of all Long Island in March 1970. The effect of urban development

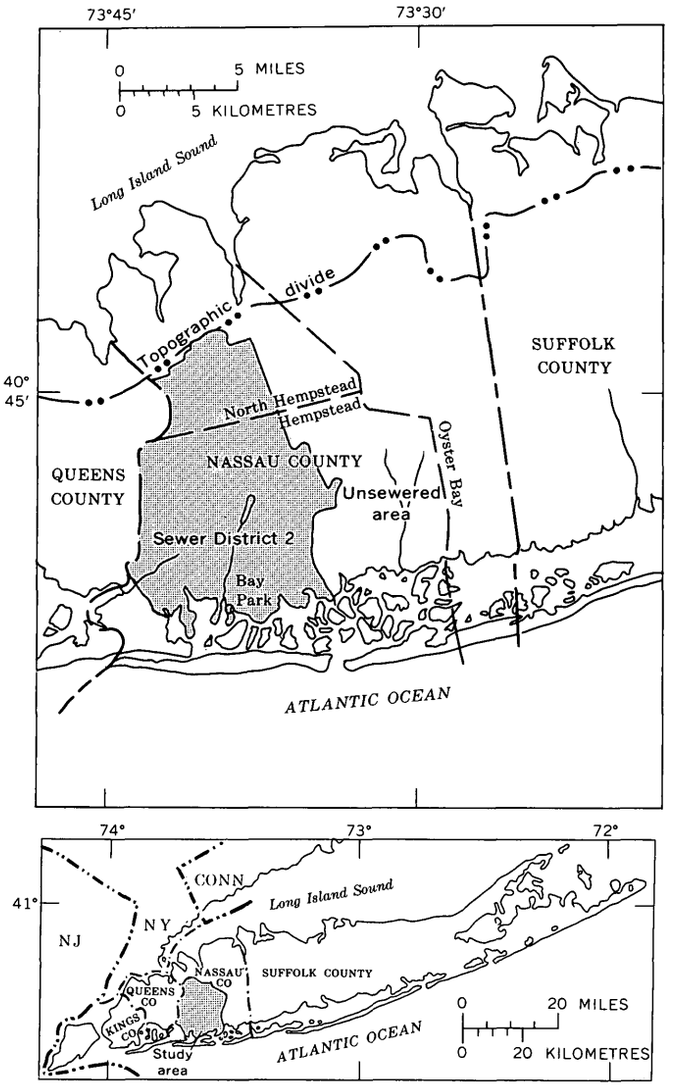

FIGURE 1.—Location of Nassau County, towns, Sewer District 2, and neighboring areas.

on discharge of East Meadow Brook (fig. 3) was examined by Seaburn (1969). The effect of sewering on ground-water levels was analyzed by Franke (1968). Heath, Foxworthy, and Cohen (1966) reported on the changing pattern of ground-water development on Long Island.

HYDROGEOLOGIC BACKGROUND

Long Island is underlain by consolidated bedrock that is overlain by a wedge-shaped mass of unconsolidated sedimentary deposits. The bedrock surface dips southeast from near sea level in northwest Nassau County to 1,600 ft (490 m) below sea level on the south shore at the Suffolk County border. The unconsolidated sedimentary deposits, of Cretaceous age, also dip southeast. Cretaceous beds are mantled nearly everywhere on Long Island by Quaternary glacial deposits. The hydrogeologic units and their water-bearing properties were described in detail by Perlmutter and Geraghty (1963) and are summarized in table 1.

Because Long Island is a true island, recharge to its aquifers is solely from local precipitation, the source of all freshwater to the island. The generally high permeabiity of the surficial glacial deposits allows about half the average annual precipitation of 44 in/yr (1,118 mm) to infiltrate and recharge the water table (Cohen and others, 1968, p. 30 and 44). The ground-water divide lies along the central spine of the island, and recharge to the underlying Magothy and Lloyd aquifers is in the region of this divide as well as in a few other isolated places where heads in the glacial aquifer are higher than those in the underlying aquifers. The Lloyd aquifer is recharged by water moving vertically through confining clay layers that separate the Magothy and Lloyd aquifers.

Water in the aquifers moves laterally away from the ground-water divide, toward either Long Island Sound on the north shore or the bays and the Atlantic Ocean on the south shore, where it contacts saline water in the distal zones of the aquifers. The actual position of the saltwater front varies with aquifer and location and depends on several factors such as head, permeability, and local pumping.

Water that recharges the shallow aquifer but does not percolate downward to recharge deeper aquifers moves laterally from the groundwater divide as underflow and discharges either to the sea or, where valleys intersect the water table, into north- or south-flowing streams. Streams flowing to the ocean represent a major route of freshwater discharge from the hydrologic system.

Reduction of the permeable surface area by extensive construction may lead to a reduction of recharge. However, runoff from precipitation on built-up areas in central Nassau County is received by a network of storm sewers and is commonly routed to recharge basins that are distributed broadly throughout the northern one-fourth of the study area. Because storm water routed to these basins infiltrates the groundwater table, recharge over the area drained is virtually the same as under natural conditions (Seaburn and Aronson, 1974). Storm water is routed to streams in most of the southern three-fourths of the sewered area. Although some of this water returns to the aquifer as stream seepage, recharge in this area is certainly reduced, and streamflow is more variable than under natural conditions.

All public and industrial water supplies for Nassau County are obtained from local aquifers. For the past

TABLE 1.—*Summary of the hydrogeologic properties of strata underlying southern Nassau County*
[Adapted from Perlmutter and Geraghty, 1963, p. 14, 15; hydrologic nomenclature modified from Cohen and others, 1968, p. 18]

Geologic age	Hydrogeologic unit	Approximate range in thickness (feet)	Character	Water-bearing properties
Quaternary:				
Holocene	Artificial fill, salt-marsh deposits, and shore deposits.	0–40	Sand, gravel, clay, silt, organic mud, peat, loam, and shells. Gray and brown.	Sandy beds of moderate to high permeability beneath barrier beaches locally yield fresh or salty water from shallow depths. Clayey and silty beds beneath bays retard saltwater encroachment and confine underlying aquifers.
Pleistocene	Upper glacial aquifer	30–300	Outwash consisting mainly of brown, fine to coarse stratified sand and gravel. Interbedded with a clay layer 0–40 ft thick.	Sand and gravel part of outwash is highly permeable; yields of individual wells are as much as 1,700 gal/min. Specific capacities of wells are as much as 109 (gal/min)/ft of drawdown. Water is fresh except near shorelines. A major aquifer in this area.
	"20-foot" clay	0–40	Clay and silt, gray and grayish-green; some lenses of sand and gravel. Contains shells, Foraminifera, and peat. Altitude of top of unit is about 20 ft below mean sea level. Interbedded with outwash material in southern part of area.	Relatively impermeable confining unit. Retards saltwater encroachment in shallow depths.
	Gardiners Clay	0–40	Clay and silt, grayish-green; some lenses of sand and gravel. Contains lignitic material, shells, glauconite, Foraminifera, and diatoms. Interglacial deposit. Altitude of surface about 50 ft or more below mean sea level.	Relatively impermeable confining layer above Jameco aquifer. Locally contains moderately to highly permeable sand and gravel lenses.
	Jameco aquifer	0–300?	Sand, fine to coarse, dark-gray and brown; gravel. Contains some thin beds of silt and clay. Probably older glacial outwash.	Highly permeable. Yields as much as 1,300 gal/min to individual wells. Specific capacities as high as 135 (gal/min)/ft of drawdown. Contains water under artesian pressure. Water commonly has high iron concentration and is salty near shoreline. A major aquifer in this area.
Upper Cretaceous	Magothy aquifer	200–900	Sand, fine to medium gray; interfingered with lenses of coarse sand, sandy clay, silt, and solid clay. Generally contains gravel in bottom 50–100 ft. Lignite and pyrite are abundant.	Slightly to highly permeable. Principal source of public-supply water in Nassau County. Individual wells yield as much as 2,200 gal/min. Specific capacities as high as 80 (gal/min)/ft of drawdown. Water is mainly under artesian pressure; some wells in southern part of area flow. Water is generally of excellent quality, except where contaminated by salty water in southwestern part of area or by dissolved constituents associated with activities of man. A major aquifer in this area.

TABLE 1.—*Summary of the hydrogeologic properties of strata underlying southern Nassau County*—Continued

Geologic age	Hydrogeologic unit	Approximate range in thickness (feet)	Character	Water-bearing properties
	Raritan clay	100–300	Clay, gray, white, with some red and purple; mainly in solid silty and rarely sandy lenses. Some lenses of sand and gravel. Lignite and pyrite are abundant.	Poorly permeable confining unit. Local lenses and layers of sand and gravel of moderate to high permeability.
	Lloyd aquifer	150–300	Sand, fine to coarse, gray and white, and gravel; some lenses of solid and sandy clay, and clayey sand. Thin beds of lignite locally.	Moderately permeable. Yields as much as 2,000 gal/min to individual wells. Specific capacities as high as 44 (gal/min)/ft of drawdown. Water under artesian pressure; some wells flow. Water of good quality except for high iron concentration. A major aquifer in this area.
Precambrian?	Bedrock		Crystalline, metamorphic, and igneous rocks. Soft, clayey weathered zone at top, as much as 50 ft thick.	Virtually impermeable. Locally contains water along joints and fault zones.

several decades, most of the public-supply water in Nassau County has been pumped from the deep partly confined aquifers (95 percent in 1972); the remainder has been obtained from the shallow unconfined aquifer.

Before sewering, in the early 1950's, large quantities of the water from the deep aquifers were returned to the shallow aquifer through individual cesspools or septic tanks. The net draft on the aquifer system from pumping within Nassau County was therefore close to zero, and the resultant drawdown of water levels was small. However, concentrations of contaminants of the water in the shallow aquifer increased, especially nitrate concentration (Perlmutter and Koch, 1972).

Sewer District 2 was established by Nassau County in the early 1950's to reduce the rate of contamination of the aquifers and to provide an efficient waste-water-disposal system in areas of shallow ground water near the south shore, where cesspools and septic tanks do not work well. The change from disposal of waste water through cesspools and septic tanks to disposal through a communal sewer system has resulted in a significant decrease in the amount of water available for recharge to the upper glacial aquifer. Reduction in waste-water recharge is one of the factors responsible for the lowering of the water table in Sewer District 2. Sewage from the district is routed to a treatment plant at Bay Park near the south shore. Effluent from the plant is discharged to tidewater. Sewage-plant operation was begun in 1953, and sewer hookups to the plant were completed in 1964. Discharge has increased from 5.8 Mgal/d (2.2×10^4 m^3/d) in 1953 to 68 Mgal/d (26×10^4 m^3/d) in 1972 (fig. 2). Mineola and Garden City, having had local sewer systems before the inception of the regional system (Sewer District 2), were the first communities to be connected to the new sewer system in the early 1950's. This resulted in an immediate loss of recharge in the northern part of Sewer District 2.

Pumpage in neighboring Queen County during the study period has not been returned to the aquifer in any significant quantity. Most of this pumpage has been discharged through sewers to the surface-water bodies surrounding the island. As a result, pumpage in Queen County in contrast to that in Nassau County, has constituted a net draft on the aquifer system and has caused water-level drawdowns over wide areas of both counties. In evaluating the cause of any change in water level in Nassau County, pumpage in Queens County is one of the factors that must be considered.

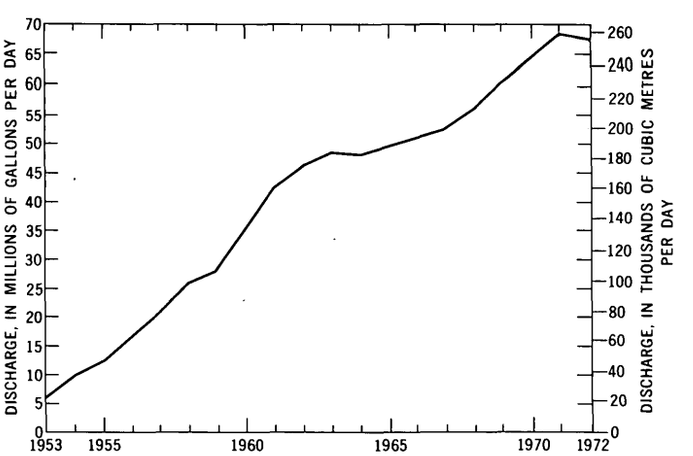

FIGURE 2.—Discharge of Bay Park sewage-treatment plant.

METHOD OF ANALYSIS

The initial step in the analysis was to determine (1) the relationship between ground-water levels in the sewered area and the unsewered area, (2) whether water-level fluctuations in the two areas were proportional to each other before sewering, and (3) whether the proportionality changed with time.

In this study, as in the earlier study by Franke (1968), data were collected in the sewered area and in the unsewered area to the east for comparison. The double-mass-curve analysis, a graphical-statistical method of analysis that can isolate water-level changes due to processes not common to both areas, was applied to the data. The theory of the double-mass curve is based on the fact that a graph of the cumulation of one quantity against the cumulation of another quantity during the same time is a straight line only if the data are proportional. The slope of the line represents the constant of proportionality (Searcy and Hardison, 1960).

A comparison of factors affecting recharge in the sewered and the unsewered areas indicates that the three hydrologic parameters—precipitation, ground-water gradients, and transmissivities—were virtually equivalent in the two areas. The drought in the Northeastern United States during the early 1960's affected the sewered and the unsewered areas almost equally. Thus, in the double-mass-curve technique, the effects of the drought are removed from the results. The analysis therefore isolates the water-level change due to two causes—pumping in Queens County and sewering in Nassau County.

After the double-mass-curve analysis, experiments with an electric analog model were used to estimate the effects of pumpage in Queens County. The experiments permitted isolation of the water-level changes due to sewering alone.

Water-table profiles were developed for sewered and unsewered areas by the method established by Franke (1968). Six lines of wells were selected in Sewer District 2, and six lines of wells were selected in the unsewered areas of Nassau and Suffolk Counties. Well-line numbers preceded by S identify well lines in the sewered area and by U, well lines in the unsewered area. The general location of these well lines is shown in figure 3. Each well line contained four or five wells, extended 3 to 4 mi (5–6 km), and was oriented transverse to the axis of the island. Wells were selected so that the average altitude of the water level in the southernmost well in each line, except line S6, was between 10 and 20 ft (3 and 6 m). Progressively northward, wells were chosen at sites corresponding to roughly a 10–ft (3–m) incremental increase of average water-level altitude. Five of the well lines, S1 through S5 in the sewered area, are near the south shore. Another well line S6, farther inland, near the ground-water divide, exhibits greater water-level fluctuations than well lines S1 through S5. Because of the hydrologic environment of well line S6, data from it cannot be compared directly with the data from well lines S1 through S5; therefore, line S6 is treated separately. Effects of the drought caused greater declines

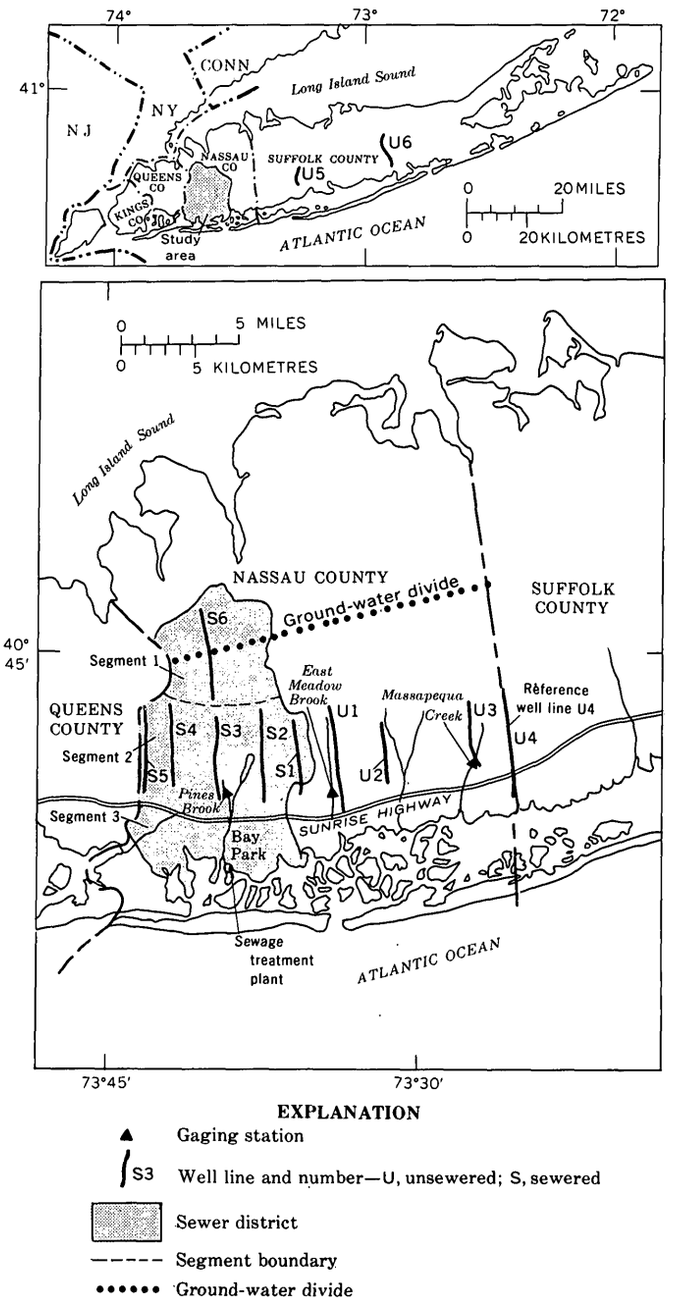

FIGURE 3.—Location of sewage-treatment plant, segments of Sewer District 2, well lines, and streams selected for this study (modified from Franke, 1968, p. B–206).

in water levels in the area of line S6 than in the area of the other S lines.

For this report, Sewer District 2 is divided into three segments (fig. 3). Segment 1, in the northern part of the district, comprises the 17-mi² (44-km²) area surrounding well line S6. Segment 2, in the central part of the district comprises the 32-mi² (83 km²) area surrounding well lines S1 through S5 and is bounded on the south by Sunrise Highway. Segment 3, in the southern part of the district, comprises the 21-mi² (54-km²) subarea of Sewer District 2 south of Sunrise Highway. This segment was excluded from consideration because its proximity to a hydraulic boundary (bays and ocean) makes ground-water levels in the segment less sensitive to changes in the hydrologic regimen.

The annual-average water level from 1938 to 1972 was calculated for each well, and the annual-average water levels for the individual wells in a well line were averaged to determine a composite annual-average water level for each line. Hydrographs (figs. 4 and 5) show the composite annual-average water level for each well line. Also shown in figure 4 is a graph of annual-average precipitation in the study area. The decline in precipitation beginning in 1961 and ending in 1965 indicates the drought on Long Island in the early to middle 1960's.

Water levels at each well line declined in response to the drought but had begun to decline in wells in segments 1 and 2 several years before the start of the drought. Although the hydrographs can be compared directly by observation, such comparison provides

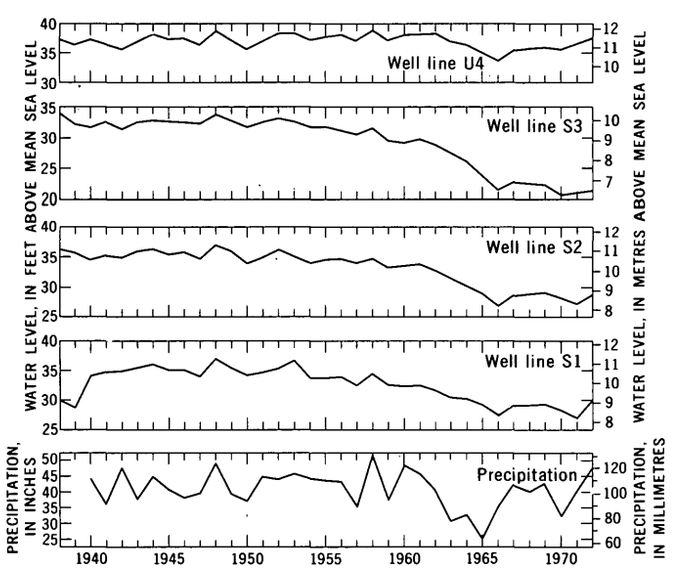

FIGURE 4.—Annual-average water levels at well lines S1, S2, S3, and U4 and annual-average precipitation in the study area.

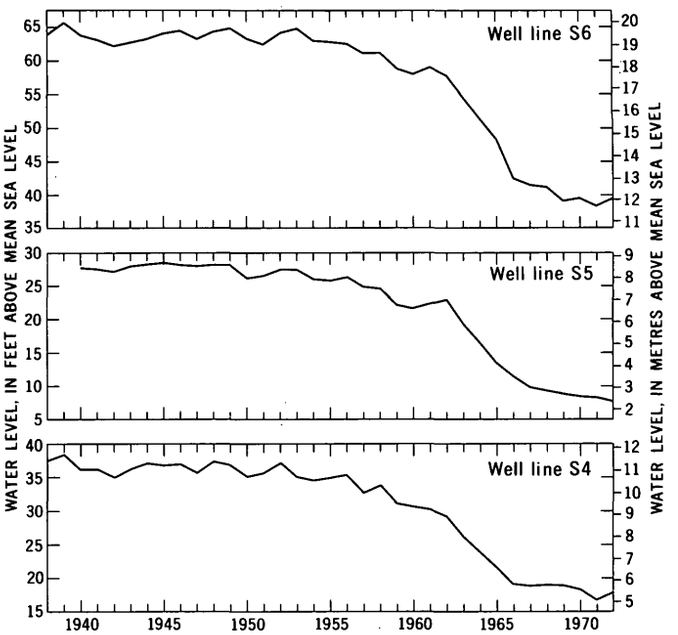

FIGURE 5.—Annual-average water levels at well lines S4, S5, and S6.

little quantitative inference regarding their individual characteristics. Accordingly, the double-mass-curve analysis was used to examine the nature of components in these data. A major inducement in using the double-mass-curve analysis is that it effectively eliminates the effects of the drought. The effect of the drought on the water table in any given part of the island is consistent with the historical relation between precipitation and water level in that part of the island, and does not show up as a deviation in a double-mass-curve analysis.

For this report, cumulative water levels from well lines S1 through S6 and U1 through U6 exclusive of U4 were each plotted against cumulative water levels from well line U4. Well line U4 was used as a reference line because it is sufficiently removed from the sewered area and, hence, is unaffected by sewering; however, it is close enough to the sewered area to share similar areal hydrologic effects.

The relationship between cumulative water levels in reference and individual well lines is described as follows: Let h_r represent water levels for the reference well line and h_l represent water levels for the well line under study. Construct a double-mass curve for each well line by plotting Σh_r on the horizontal axis and Σh_l on the vertical axis. The initial part of the plot, in each graph, is a straight line, which indicates that a simple proportionality of the form

$$\Sigma h_l = k \Sigma h_r \qquad (1)$$

describes the relationship.

This in turn implies that a relationship of the form

$$h_l = kh_r \quad (2)$$

exists between the individual values, h_l and h_r, for the early data.

Beginning in the 1960's, values of Σh_l begin to fall below the straight-line double-mass curves for the sewered area constructed through the earlier data. This is illustrated in figures 6 and 7, which show double-mass curves for well lines S3 and S5 plotted against U4. If Σh_e represents the cumulative water level that would be obtained by extrapolating the straight-line part of the double-mass curve into the 1960's, then for the 1960's part of the graph, in place of equation 1,

$$\Sigma h_e = k\Sigma h_r \quad (3)$$

and, similarly, in place of equation 2,

$$h_e = kh_r, \quad (4)$$

where h_e may be regarded as an extrapolated value giving the water level that would have been observed for the well line if there had been no differences between the hydrologic conditions along the well line and those along the reference line. Furthermore, letting h_l represent the recorded head for the well line, the difference $h_l - h_e$, or $h_l - kh_r$, indicates the change in water level due to processes that affect the well line in question but do not affect the reference well line. This difference is termed "the water-level departure" in this report. Thus, the method of analysis consisted of plotting a double-mass curve to determine k, utilizing equation 4 to determine h_e, and subtracting h_e from the observed water level to determine the departure.

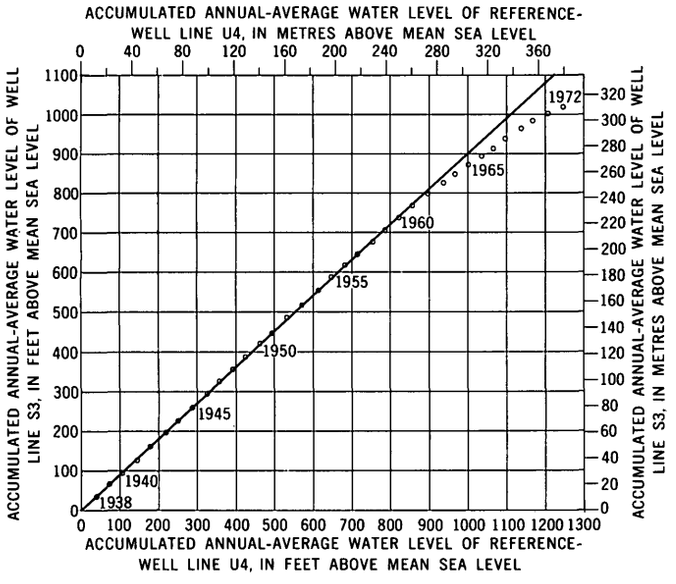

FIGURE 6.—Double-mass curve relating annual-average water levels for reference-well line U4 and annual-average water levels for well line S3.

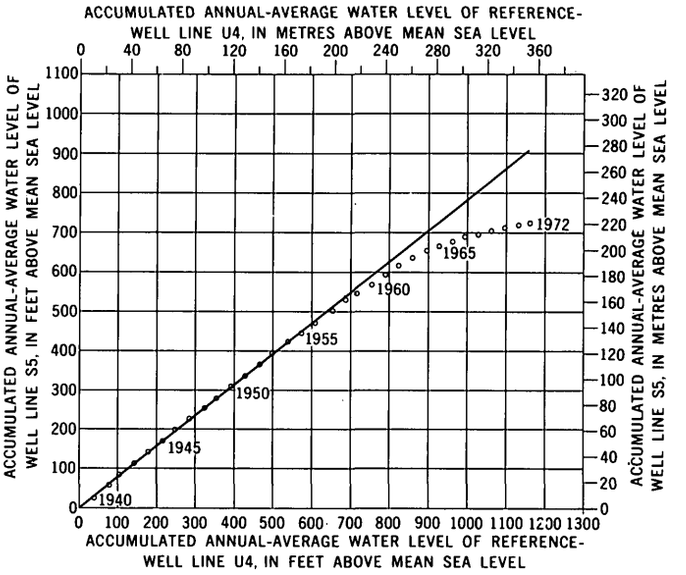

FIGURE 7.—Double-mass curve relating annual-average water levels for reference-well line U4 and annual-average water levels for well line S5.

In an effort to estimate the fraction of water-level departure caused by pumpage in areas of Queens County adjacent to the study area, this pumpage was simulated on a five-layer analog model of the Long Island aquifer system. In the experiment, pumpage in Queens County was the only simulated stress. Drawdowns determined from the analog experiment were subtracted from the water-level departures, utilizing the principle of superposition, to remove the effects of the pumpage in Queens County from the departures. For the analog analysis, pumpage data were collected from several water-supply companies. However, the principal user of ground water in Queens County is the Jamaica Water Supply Co.; a graph showing the magnitude of ground-water withdrawals by this company is shown in figure 8. From 1938 to 1952, pumpage by the company averaged 22 Mgal/d (8.3×10^4 m^3/d) and increased by an average rate of 0.5 Mgal/d (0.18×10^4 m^3/d) each year. Rate of pumpage increased sharply, beginning in 1952, and ultimately reached nearly 54 Mgal/d (20×10^4 m^3/d) in 1972. Pumpage by other suppliers in Queens County was substantially less and was farther removed from the study area than that of the Jamaica Water Supply Co. Accordingly, only the pumpage of this company was used in the analysis.

Pumpage data from the Jamaica Water Supply Co. were categorized into average pumping rates for each aquifer (upper glacial, Jameco, and Magothy), each well field, and each of seven 5-yr periods starting with

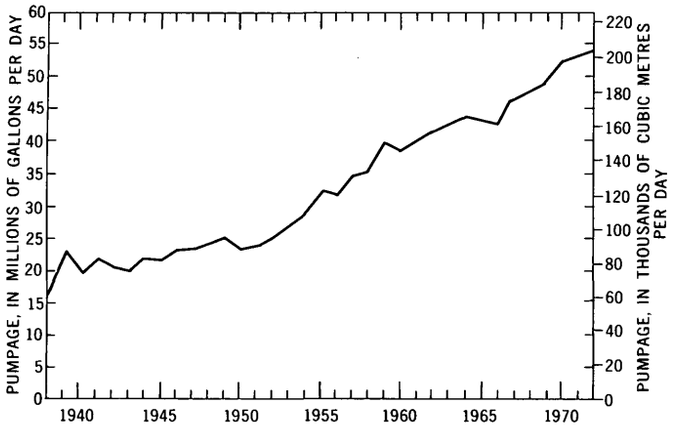

FIGURE 8.—Pumpage from public-supply wells in Queens County, N.Y. (Data from Jamaica Water Supply Co.).

1938. For the analog model experiment, pumpage was assumed to have begun in 1938 even though it had been in progress for many years before that time. Thus categorized, the pumpage data were converted to scaled-model dimensions of electrical current and scaled-time duration for application to the appropriate model nodes. Drawdown as a function of time was read at those model nodes nearest the geographic midpoints of each of the well lines.

In the field, rate of pumpage increased almost uniformly. In the model, increases were programmed as stepwise changes at 5-yr intervals starting in 1938. The increase in rate of pumpage beginning in 1952 (fig. 8) was simulated by stepwise pumpage changes in 1953, 1958, 1963, and 1968 on the model.

Drawdowns determined by the analog model are virtually at equilibrium immediately before the stepwise pumpage change imposed in 1953. The drawdowns are in agreement with the field data of figures 4 and 5, which show little net change in water level before 1953. Accordingly, in correcting water-level departures for the effects of pumpage, the system was assumed to have been near equilibrium before 1953. Drawdowns due to pumping were taken from the analog results as the difference between the water level in 1953 and the water level at the time of measurement. These drawdowns were taken only at the ends of the 5-yr periods of pumping to minimize errors in the results due to use of stepwise changes in withdrawal from the model to simulate continuous increases in actual withdrawal.

The authors recognize that the preceding method of correcting for the effects of pumpage has many shortcomings. Drawdowns as given by the analog model may be in error by as much as 20 percent (R. T. Getzen, oral commun., 1973). However, the technique was considered to be the best available approach and adequate for this report.

RESULTS OF ANALYSIS

Water-level departures for the various well lines in the sewered area are shown in figure 9. Two curves are shown on each graph; one representing the total departure and one representing the departure corrected by the amount attributed to the effects of pumping. Total departures are plotted yearly. The corrected departures are plotted at 5-yr intervals, which correspond to the intervals at which drawdown measurements were taken from the analog analysis.

The corrected departures represent the effects of sewering and possibly of any residual differences between the sewered area and the reference-line area in degree or rate of urbanization. If the reduction in recharge due to urbanization followed the same trend in the reference-line area as in the sewered area, the double-mass curve should be unaffected by this factor, and the calculated departures should reflect only the effects of sewering. Franke (1968) assumes that this condition prevails in the study area.

Water-level declines at individual well lines in the sewered area are shown graphically in figure 10. The water-level decline was largest in segment 1, where it averaged 23.7 ft (7.1 m), of which 4.6 ft (1.4 m) is attributed to pumping in Queens County. Segment 1 is astride the ground-water divide, where water-level changes are generally greatest in the entire sewered area.

Water-level declines at locations in segment 2 ranged from 5.1 ft (1.5 m) in the eastern part of the sewer district to 21 ft (6.3 m) in the westernmost part. Declines attributed to pumping in Queens County ranged from 1.0 ft (0.3 m) in the eastern part to 12.0 ft (3.6 m) in the western part. Magnitude of drawdown is a function of distance from the pumping centers and of pumping duration. Declines attributed to sewering ranged from 3.6 to 12.2 ft (1.1 to 3.7 m). The nonuniform distribution of water-level declines attributed to sewering can be explained, in part, by population-density differences in water use per square mile (Greeley and Hansen, 1971, table V–5). In the area of well lines S4 and S5, where water-level declines were greatest, water use was 2.3 (Mgal/d)/mi^2 or (3,400 m^3/d)/km^2 and 5.50 (Mgal/d)/mi^2 or (8,030 m^3/d)/km^2, respectively. In areas of well lines S1, S2, and S3, water use was less than 1 (Mgal/d)/mi^2 or (1,500 m^3/d)/km^2.

The average water-level departure in segment 2 of the sewered area, relative to water levels in reference-well line U4 in the unsewered area, was evaluated by weighting the departures for each line of wells accord-

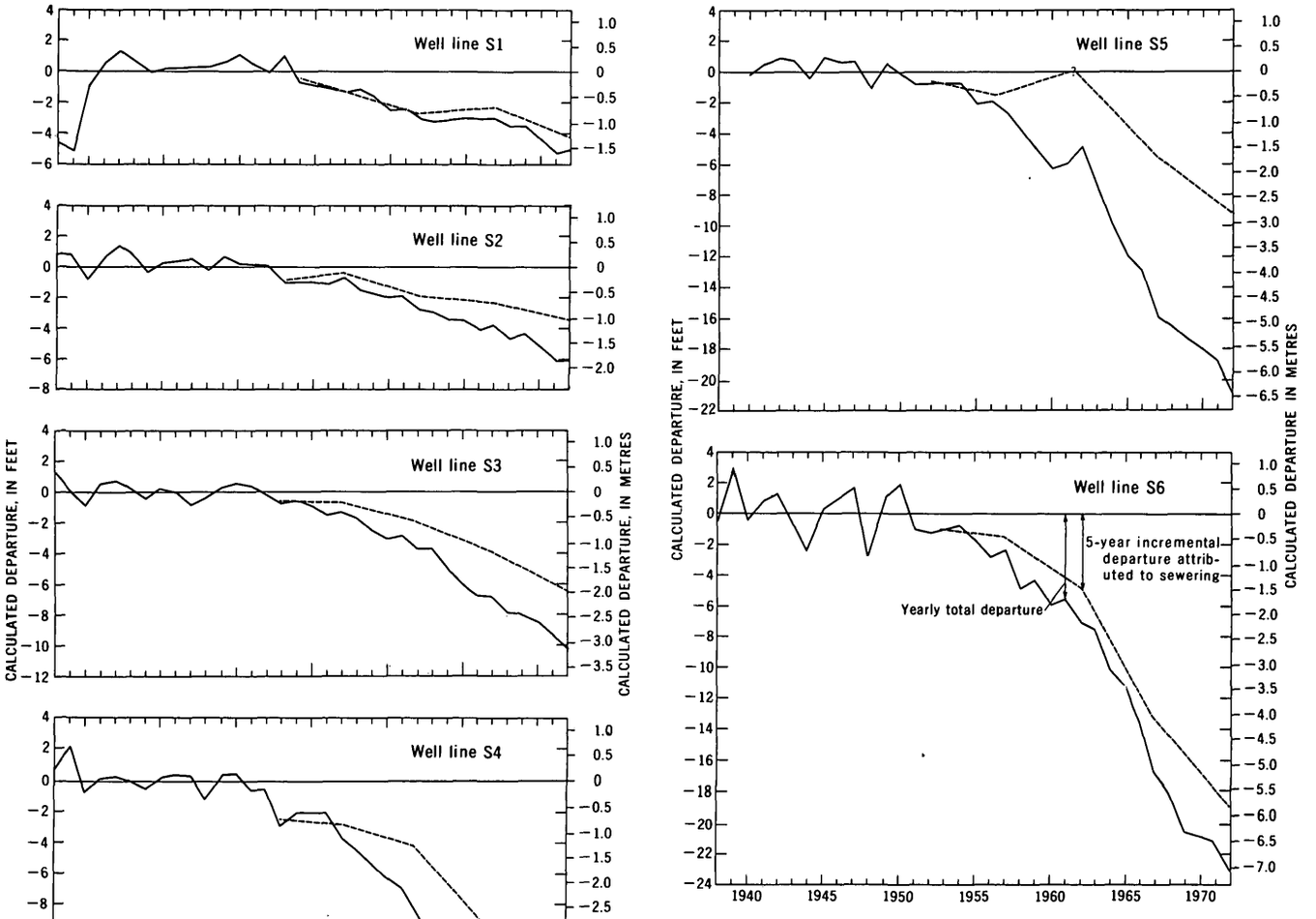

FIGURE 9.—Calculated departures of average water levels and departures attributed to sewering at well lines S1 through S6.

ing to the relative size of the area each line represented (Franke, 1968). Results of this evaluation for one 4-yr period followed by three successive 5-yr periods are shown in figure 11. During this 19-yr period, weighted ground-water levels in segment 2 of the sewered area declined 11.8 ft (3.6 m). Assuming no other factors were involved, decline attributed to sewering accounted for 6.9 ft (2.1 m), and decline attributed to pumping in Queens County accounted for 4.9 ft (1.5 m). As with declines at individual locations, the average weighted decline shows a continued increase with time. Assuming a specific yield of 20 percent for the shallow aquifer, the average loss of ground water from storage in segment 2 of the sewered area was estimated to be 5.0×10^8 gal/mi^2 (7.3×10^5 m^3/km^2) from 1953 to 1972. The average loss of ground water from storage in segment 1 was estimated to be 9.87×10^8 gal/mi^2 (14.4×10^5 m^3/km^2) for the same period. By comparison, the average loss of ground water in segment 3 (area south of Sunrise Highway) was estimated to be 7.8×10^7 gal/mi^2 (1.1×10^5 m^3/km^2).

The streams on Long Island function as local ground-water drains, so large declines of ground-water levels result in corresponding declines in streamflow. To test this hypothesis, the authors plotted a double-mass curve relating annual-average discharge of Massapequa Creek, in the unsewered area, to annual-average discharge at Pines Brook, in the sewered area. Negative deviation of the curve from an initial best-fit, straight-line segment indicated reduction of flow in Pines Brook relative to Massapequa Creek. Calculated departures of annual-average streamflow for Pines Brook are shown in figure 12. The erratic nature of the departure graph can be explained in part by increased annual direct runoff to this stream whose drainage area is serviced by storm sewers. Urban development has

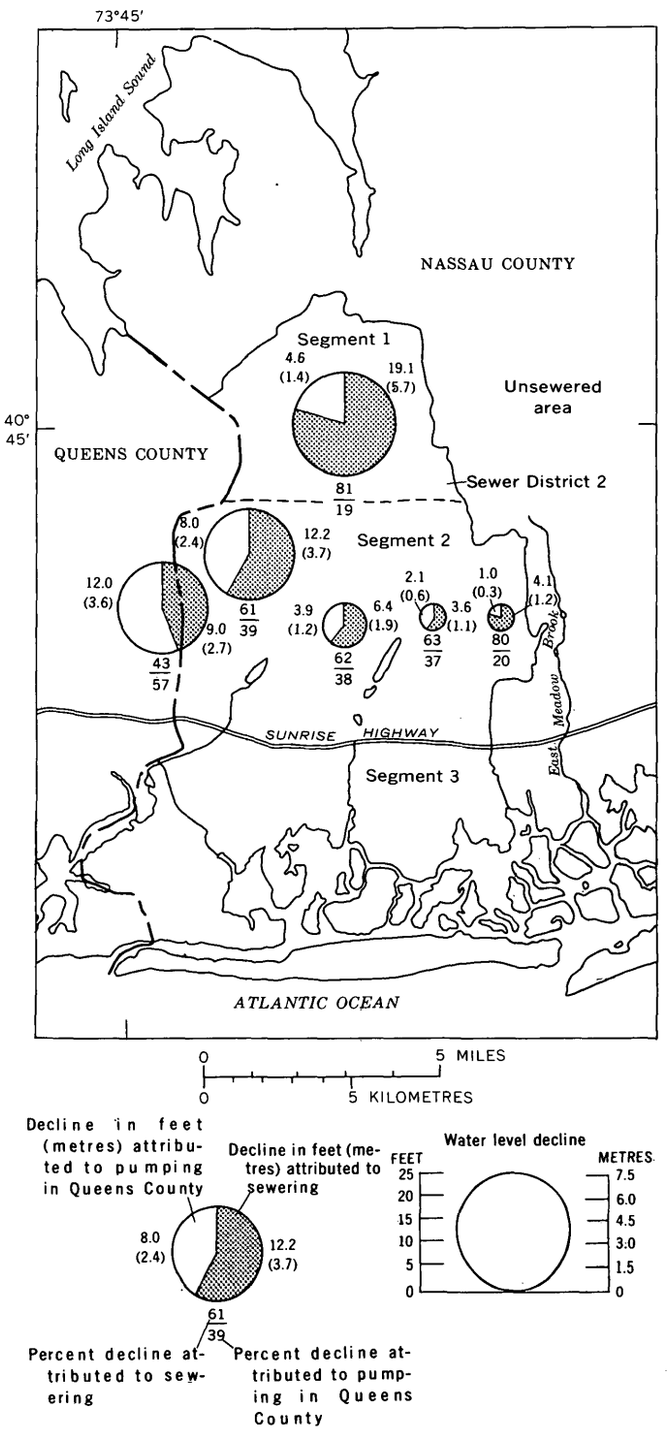

FIGURE 10.—Distribution of water-level declines (1972) at individual well-line locations S1 through S6.

caused a major change in flow characteristics of some streams in urban areas (Seaburn, 1969, p. B7). In Sewer District 2, for instance, direct runoff can account for 50 percent of total streamflow (Greeley and Hansen, 1971, p. 64).

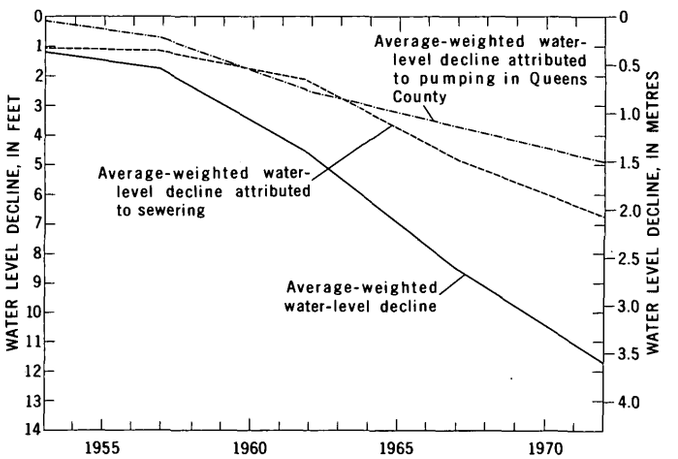

FIGURE 11.—Average-weighted water-level decline, average-weighted decline attributed to sewering, and average-weighted decline attributed to pumping in Queens County in segment 2 of the sewered area.

Decrease in average-annual flow at Pines Brook in the sewered area, relative to Massapequa Creek, was 2.5 ft^3/s (71 l/s) from 1953 to 1972.

A summary of ground-water loss from storage indicates loss from storage for the 20-yr period 1953–1972, inclusive, is 1.7×10^{10} gal (6.4×10^{7} m^3) for segment 1, 1.6×10^{10} gal (6.0×10^{7} m^3) for segment 2, and 0.16×10^{10} gal (0.6×10^{7} m^3) from segment 3, or 3.46×10^{10} gal (1.31×10^{8} m^3) in the three segments. Cumulative loss in the total amount of flow from Pines Brook for this same period amounts to about 1.2×10^{10} gal (4.5×10^{7} m^3). The total loss in ground water storage and in the cumulative amount of streamflow is therefore estimated to be 4.7×10^{10} gal (1.78×10^{8} m^3) for the 20-yr period 1953-1972, or about 16 percent of the total discharge from the Bay Park sewage-treatment plant (3×10^{11} gal or 11.3×10^{8} m^3) for the same period. Thus, the discharge from the Bay Park plant seems to have been roughly six times greater than the apparent losses from the freshwater hydrologic system during 1953 to 1972. This indicates that the reduction in recharge due to the sewering has been balanced, in large part, by

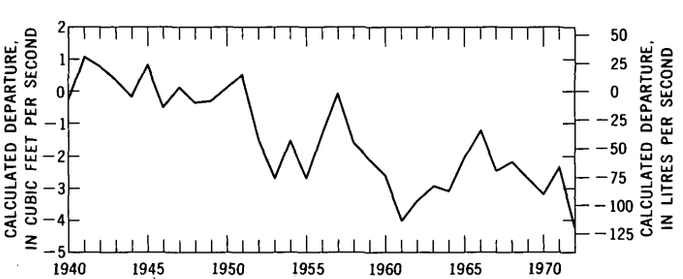

FIGURE 12.—Calculated departures of annual-average discharge of Pines Brook in relation to annual-average discharge of Massapequa Creek.

increased ground-water inflow from adjacent areas and reduced ground-water outflow to the sea. Moreover, one consequence of a reduction in ground-water outflow to the sea would be a landward movement of the salt-water-freshwater interface toward a new equilibrium position. This implies a further loss in freshwater storage in addition to that calculated from declining water levels.

CONCLUSIONS

Results of the double-mass-curve analysis indicate a progressive decline in water levels in the sewered area relative to the unsewered area. The average weighted water-level decline for segment 2 in Sewer District 2 for 1953 to 1972 was 11.8 ft (3.60 m), of which 4.9 ft (1.5 m) can be attributed to pumping in Queens County. At individual well-line locations, water-level declines ranged from 5.1 to 21 ft (1.5 to 6.4 m). Assuming a specific yield of 20 percent for the shallow aquifer in segment 2 of Sewer District 2, the average loss of ground water from storage for this period was estimated to be 5.0×10^8 gal/mi^2 (7.3×10^5 m^3/km^2). Average loss of ground water from storage in segment 1 was 9.87×10^8 gal/mi^2 (14.4×10^5 m^3/km^2). Storage loss in segment 3 was estimated to be 7.8×10^7 gal/mi^2 (1.1×10^5 m^3/km^2). Loss of flow at Pines Brook in the sewered area averaged 2.5 ft^3/s (71 l/s) from 1953 to 1972.

The rate of decline of ground-water levels shows no sign of flattening. Although predictions of future declines are difficult to assess, owing to uncertainties of future magnitude of pumping in Queens County and discharge from the Bay Park sewage-treatment plant, the double-mass-curve analysis of previous and present declines provides a useful means of evaluating the various factors responsible for changes in water levels and aquifer storage. Continuing evaluations of these changes are vital in making well-founded water-management decisions.

REFERENCES CITED

Cohen, Philip, Franke, O. L., and Foxworthy, B. L., 1968, An atlas of Long Island's water resources: New York Water Resources Comm. Bull. 62, 117 p.

Cohen, Philip, Franke, O. L., and McClymonds, N. E., 1969, Hydrologic effects of the 1962–66 drought on Long Island, New York: U.S. Geol. Survey Water-Supply Paper 1879–F, 18 p.

Franke, O. L., 1968, Double-mass-curve analysis of the effects of sewering on ground-water levels on Long Island, New York: U.S. Geol. Survey Prof. Paper 600–B, p. B205–B209.

Franke, O. L., and McClymonds, N. E., 1972, Summary of the hydrologic situation on Long Island, New York, as a guide to water-management alternatives: U.S. Geol. Survey Prof. Paper 627–F, 59 p.

Greeley and Hansen, 1971, Comprehensive public water supply study, CPWS–60: Chicago, Ill., Greeley and Hansen Engineers, 208 p.

Heath, R. C., Foxworthy, B. L., and Cohen, Philip, 1966, The changing pattern of ground-water development on Long Island, New York: U.S. Geol. Survey Circ. 524, 10 p.

Kimmel, G. E., 1971, Water-level surfaces in the aquifers of western Long Island, New York, in 1959 and 1970, *in* Geological Survey research 1971: U.S. Geol. Survey Prof. Paper 750–B, p. B224–B228.

Kimmel, G. E., 1972, The water table on Long Island, New York, in March 1970: Long Island Water Resources Bull. 2, 8 p.

Long Island Lighting Company, 1971, Population survey—Current population estimates for Nassau and Suffolk Counties: Mineola, N.Y., Long Island Lighting Co. 47 p.

New York State Division of the Budget, 1973, New York State statistical yearbook, 1973: New York State Div. Budget, 272 p.

Pearlmutter, N. M., and Geraghty, J. J., 1963, Geology and ground-water conditions in southern Nassau and southeastern Queens Counties, Long Island, New York: U.S. Geol. Survey Water-Supply Paper 1613–A, 205 p.

Perlmutter, N. M., and Koch, Ellis, 1972, Preliminary hydrogeologic appraisal of nitrate in ground water and streams, southern Nassau County, Long Island, New York, *in* Geological Survey research 1972: U.S. Geol. Survey Prof. Paper 800–B, p. B225–B235.

Seaburn, G. E., 1969, Effects of urban development on direct run-off to East Meadow Brook, Nassau County, Long Island, New York: U.S. Geol. Survey Prof. Paper 627–B, 14 p.

Seaburn, G. E., and Aronson, D. A., 1974, Influence of recharge basins on the hydrology of Long Island, New York: U.S. Geol. Survey Water-Supply Paper 2031, 66 p.

Searcy, J. K., and Hardison, C. H., 1960, Double-mass curves; with a section on fitting curves to cyclic data: U.S. Geol. Survey Water-Supply Paper 1541–B, p. 31–66.

Jour. Research U.S. Geol. Survey
Vol. 4, No. 3, May–June 1976, p. 267–276

HYDROGEOLOGY OF A DRIFT-FILLED BEDROCK VALLEY NEAR LINO LAKES, ANOKA COUNTY, MINNESOTA

By T. C. WINTER and H. O. PFANNKUCH,[1]
Denver, Colo., Minneapolis, Minn.

Work done in cooperation with the Minnesota Geological Survey

Abstract.—The bedrock surface of east-central Minnesota is dissected by an intricate network of valleys. These valleys, as much as several hundred feet deep and filled with drift, dissect important sandstone and carbonate-rock aquifers of lower Paleozoic age. A small segment of one of the valleys, in southeastern Anoka County (test site A), is about 335 ft (102 m) deep and 260 ft (79 m) below the bedrock surface. Outside the bedrock valley at site B, 3 mi (4.8 km) from site A, 100 ft (30 m) of drift overlies the bedrock surface. Observation wells were installed at the two sites to determine the vertical ground-water movement between the various aquifer units and the lateral movement between the two sites. An aquifer test of the lowest valley-fill aquifer at site A showed that the observation well completed in the same aquifer as the pumping well responded immediately; whereas a lag of about 100 min occurred between the lower valley fill and uppermost body of sand and gravel. This indicates that the hydraulic connection between these two layers is poor at the immediate site. Test results show that the lower sand-and-gravel aquifer has a transmissivity between 14,000 and 27,000 ft^2/d (1,300 and 2,500 m^2/d). Laboratory analyses of drill cuttings show fair agreement with the hydraulic conductivity derived from aquifer-test analyses. Isopotential and ground-water flow lines for late-winter conditions show downward ground-water movement at each site and some of this water subsequently moves upward to lakes and wetlands. Some water moves from site B through the bedrock aquifers to the valley fill. Although the hydraulic gradient is vertically downward in the valley, much of the drift fill is poorly permeable. This suggests that the quantity of downward-percolating water reaching the lowest valley-fill aquifer is relatively small at the test site. Water-level data for a 2-yr period indicate that there are no reversals in ground-water potential with time. Because valleys cut through a number of bedrock aquifers in the region, they could potentially be an important avenue of contamination from land-surface waste. In addition, the vast network of bedrock valleys in the Twin Cities area might cause contaminants to disseminate rather rapidly throughout a large area.

The bedrock surface of east-central Minnesota is dissected by an intricate network of valleys that incise lower Paleozoic and Precambrian sedimentary rocks. Glacial deposition during the Pleistocene filled the valleys with drift and left the land surface fairly flat. The depths of the buried valleys range from 100 ft to more than 300 ft (30 to 90 m) below land surface. Some of the larger and more extensive valleys were known for some time (Schwartz, 1936; Payne, 1965), but as drilling and subsurface exploration increase in the metropolitan area, more valleys and tributaries to those already known are being discovered.

Hydrologic studies in this area, especially in the Minneapolis–St. Paul metropolitan area (Norvitch and others, 1973), point out the significance of the valleys to understanding the local hydrologic system, but no detailed studies of the valleys have been made. Few available drill logs describe in detail the geology of the valley fill, so the role of the valleys in the hydrologic setting is usually generalized. It is usually assumed the valleys are filled with alluvium with a wide range of grain sizes, but that the alluvium is generally coarse rather than fine and therefore transmits water readily. The valleys, then, are considered favorable avenues for water to recharge readily from the surface and allow water to move between aquifers separated by confining beds.

This study was designed to examine a small segment of a buried valley with emphasis on the hydrologic characteristics of the valley fill and the pattern of ground-water flow between the surface, valley fill, and bedrock aquifers. Studies of this type, at well-chosen locations, should lead to better understanding of the hydrologic system associated with drift-filled bedrock valleys.

The site near Lino Lakes, Anoka County, Minn. (fig. 1), was chosen because it is outside the influence of heavy pumping in the metropolitan area, but is considered a favorable area for future metropolitan development.

[1] Department of Geology and Geophysics, University of Minnesota.

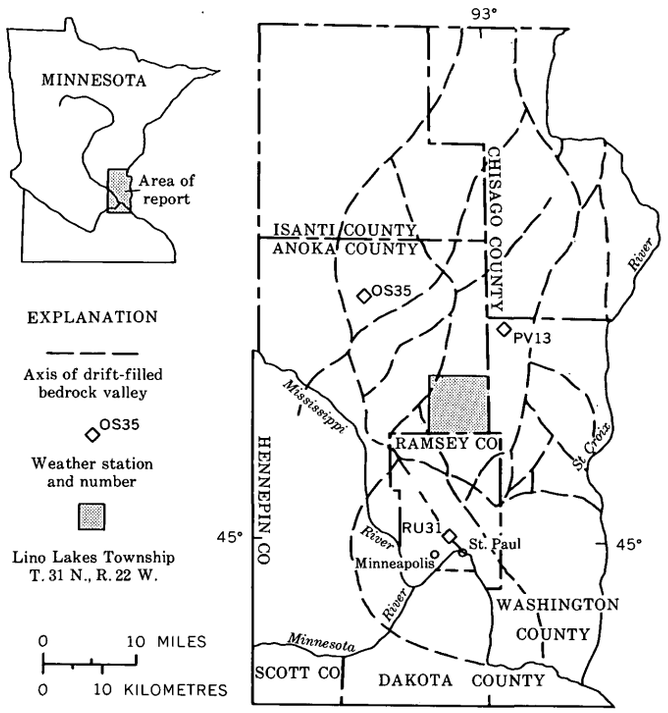

FIGURE 1.—Location of Lino Lakes Township and distribution of buried bedrock valleys in east-central Minnesota.

GEOLOGIC SETTING

Regional geology

Surficial glacial deposits east of the study site consist of reddish-brown sandy till deposited by the Superior lobe. West of the reddish-brown till and partly overlying it is gray clayey till (yellowish brown where oxidized) deposited by the Grantsburg sublobe of the Des Moines lobe. Sand deposits of fluvial and lacustrine origin, part of the Anoka sand plain, overlie the clayey till.

Previous to this study, the type of drift in the valley under study was not known but, at one location, the total thickness is known to be 316 ft (96 m). Outside the valley, the drift is about 75 to 125 ft (23 to 38 m) thick.

Topographic relief in Lino Lakes Township (fig. 2) is slight, typical of the Anoka sand plain. Land surface altitudes generally range from 890 to 910 ft (271 to 278 m) above mean sea level, but rise to more than 950 ft (290 m) in the southeastern part of the township. Wetlands are common along the chain of lakes through which Rice Creek flows.

The bedrock valley, in the northwestern part of Lino Lakes township, dissects the Prairie du Chien Group, Jordan Sandstone, and St. Lawrence Formation, and penetrates the Franconia Formation (fig. 3).

The Franconia Formation, in the study area, is a fine-grained glauconitic sandstone and glauconitic siltstone (Mossler, 1972).

The St. Lawrence Formation in this area is primarily the Lodi Member, a dolomitic siltstone and very fine grained silty, quartz sandstone. The discontinuous lower member, Black Earth Member, herein reinstated, consists of silty dolomite.

The Jordan Sandstone in the study area consists of two members. The basal Norwalk Member is a fine-grained quartz sandstone. The overlying Van Oser Member, herein adopted, is a medium- to coarse-grained quartz sandstone. The Van Oser Member is the most widely distributed member in the Minneapolis–St. Paul area and is commonly the only one present. The Norwalk Member, although discontinuous, is present in the subsurface in southern Anoka County. The Jordan Sandstone generally is between 85 and 100 ft (26 and 30 m) thick. The withdrawal of about 130 Mgal/d (5.7 m^3/s) (1970) makes it the principal source of ground water in the Twin Cities area.

The Prairie du Chien Group, the uppermost bedrock in the study area, consists of two formations—the basal Oneota Dolomite and the overlying Shakopee Formation. The Oneota is a coarsely crystalline dolomite that is locally sandy near the base. The Shakopee Formation consists of two members—the basal New Richmond Sandstone Member and the overlying Willow River Dolomite Member, herein adopted. The New Richmond, discontinuous in the Twin Cities area, is a well-sorted, fine- to medium-grained quartz sandstone. The Willow River Member is finely crystalline dolomite, commonly sandy or oolitic, containing abundant chert in places. The unit is very sandy in the Twin Cities area, especially near the top. The Prairie du Chien Group is generally 125 to 150 ft (38 to 46 m) thick. The general environment of deposition of the bedrock units is discussed by Mossler (1972).

Geology of valley fill at test site

The valley section under investigation is part of a valley underlying a chain of lakes. Because a relationship seems to exist between chains of lakes and buried valleys (Wright, 1973), this feature can be used, with caution, to estimate directional trend and linear extent of buried valleys. On the basis of this assumption, the valley under study is believed by the authors to extend for roughly 20 mi (32 km) (fig. 1). The valley is slightly west of the lake chain and is overlain at the surface by the Anoka sand. The valley trends in a north-northeast direction, and its bottom slopes gently in a south-southwest direction.

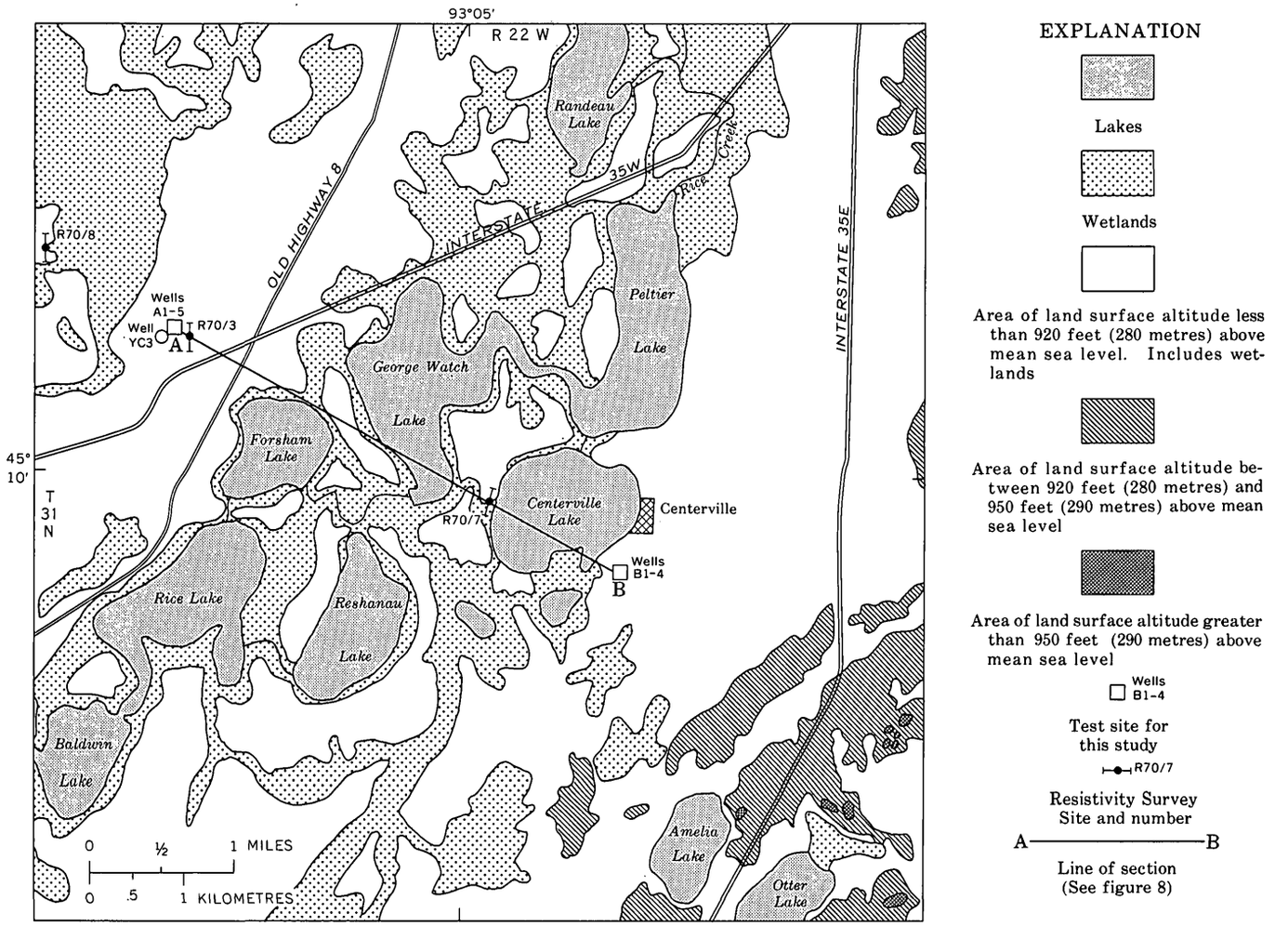

FIGURE 2.—Topography, distribution of lakes and wetlands, and location of data sites in Lino Lakes Township. Wetland boundaries from unpublished map by M. T. Eng, Minnesota Department of Natural Resources.

Because of limitations on drilling and well-construction funds, the study was limited to only one side of the valley. The side toward the Twin Cities was selected because it would be the first to be affected by metropolitan area ground-water pumping.

To define the valley bottom and its east side, electrical resistivity measurements were made to supplement existing drill logs. Because the definition of lithologic boundaries by earth resistivity is accurate to only several tens of feet, especially for greater depths, the main benefit of the survey was in determining the shape and extent of the clay-till layer separating the surface deposits from the lower valley fill.

Two sites were selected for intensive drilling (discussed in detail later); one in the valley and the other on the bedrock upland on the east side. Because interest is chiefly on the valley fill material, a descriptive log of the deepest well at site A is given in table 1.

TABLE 1.—*Lithologic log of well A1 (deepest well at site A)*

Depth		Description
Feet	*Metres*	
0– 45	0 –13.7	Sand, tan, fine; contains a few pebbles of limestone.
45– 50	13.7–15.2	Sand, gray, very fine, uniform.
50– 55	15.2–16.8	Sand, reddish, fine; contains scattered coarse sand.
55– 60	16.8–18.3	Clay, reddish, uniform; contains fine sand and scattered coarse sand.
60– 70	18.3–21.4	Silt, reddish, clayey, uniform.
70– 95	21.4–29.0	Clay, reddish, silty, uniform.
95–100	29.0–30.5	Silt, reddish, uniform.
100–104	30.5–31.7	Silt and very fine sand, brownish.
104–110	31.7–33.6	Sand, brownish, fine, silty.
110–120	33.6–36.6	Sand, brownish, silty; size ranges to medium gravel.
120–124	36.6–37.8	Sand, brownish, fine to medium.
124–155	37.8–47.3	Till, gray, silty; contains limestone pebbles.
155–160	47.3–48.8	Silt, gray, uniform.
160–197	48.8–60.1	Clay, gray, silty, uniform.
197–205	60.1–62.5	Clay and gravel, gray.
205–275	62.5–83.9	Sand and gravel.

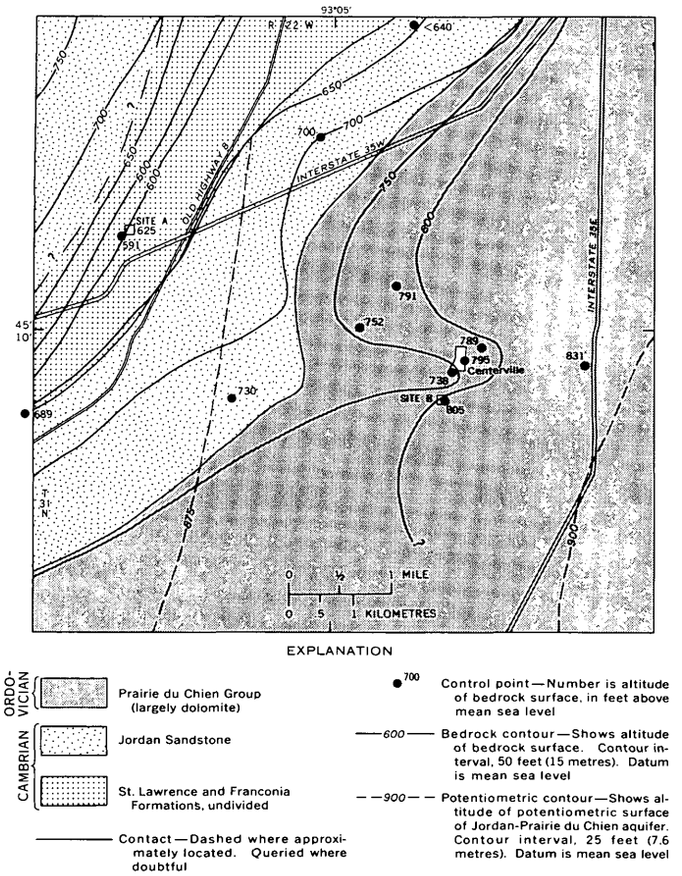

FIGURE 3.—Bedrock geology, bedrock topography, and contours of the potentiometric surface of the Jordan–Prairie du Chien aquifer in Lino Lakes Township. Geology modified from unpublished map by P. K. Sims, Minnesota Geological Survey. Potentiometric surface data from Norvitch and others (1973).

Geophysical (radioactivity) logs were made on the deepest wells at each site to aid in defining lithologic boundaries. The gamma, neutron, and gamma-gamma recordings and their interpretation are given in figures 4 and 5. The logs represent gross results for which corrections for borehole diameter, cement thickness, and borehole fluid, could not be applied because these data were not available.

The geophysical logs for well A1, the deepest at site A, correlate well with the units established by sample cuttings (table 1). The gamma-gamma log especially shows the lower clay layer and indicates that its clay content is higher than that of the upper clay layer. Neutron and gamma-gamma logs corroborate the fact that the top sand is uniform, whereas the bottom sands and gravels are more variable. The amplitude and wave length of the peaks for each unit indicate that a much greater vertical variability in the valley fill exists than

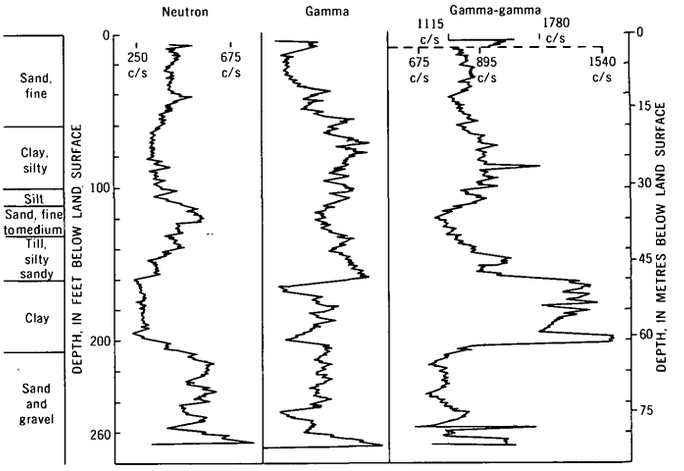

FIGURE 4.—Geophysical logs of well A1.

can be detected from bailer samples taken at 5- to 10-ft (1.5- to 3-m) intervals.

The gamma and gamma-gamma logs of well B1, the deepest well at site B, show the boundary between the drift and bedrock to be at a depth of about 90 ft (27 m). Differentiation between the dolomite and the sandstones is not possible on this log because of the similarity in their natural radiation intensities.

GROUND-WATER HYDROLOGY

A primary goal of this study is to determine the patterns of ground-water flow vertically from the surface and laterally across a valley side. To do this, observation wells were installed in each aquifer unit at two sites in the study area; that is, at Lino Lakes diagnostic center (site A, a group of 5 wells in the valley) and at Centerville (site B, a group of 4 wells outside the valley) (fig. 2). By periodically measuring potentiometric head in each well, vertical movement between the aquifer units and lateral movement between the sites was determined by construction of flow-field diagrams. Sufficient care was taken in the placement of inlets at the bottoms of the wells so that the water-level data truly reflect the head at a given depth. The deep wells were drilled by cable tool and the small-diameter shallow wells were installed by augering. At each location, the wells are about 10 ft (3 m) apart. The Lino Lakes diagnostic center's well (YC3), which is used in the aquifer test analysis, is 1,700 ft (520 m) from site A. Water-level measurements were reduced to a standard datum (mean sea level) and plotted for 1971 and 1972 (fig. 6).

Hydrologic parameters of valley-fill deposits

An aquifer test was run to determine the degree of interconnection between the hydrologic units in the

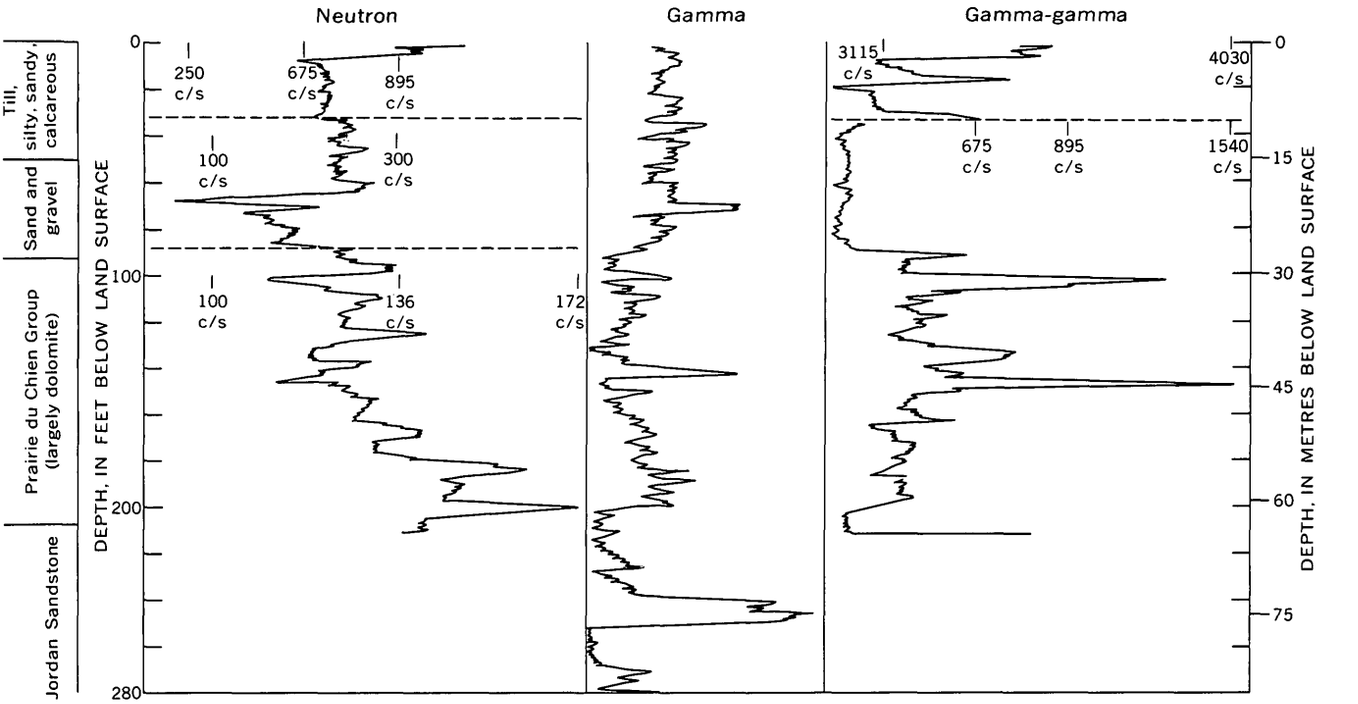

FIGURE 5.—Geophysical logs of well B1.

filled valley. In addition, the aquifer coefficients—hydraulic conductivity (K), transmissivity (T), and storage coefficient (S)—were determined for the lowest sand and gravel aquifer of the valley fill.

Only two sets of drawdown data were used for this evaluation; those for well YC3, with well A1 discharging about 100 gal/min (0.0063 m^3/s), and for well A1 with well YC3 discharging about 440 gal/min (0.028 m^3/s). The Theis method (see Lohman, 1972) of data analysis, used because of the relatively short pumping periods and the large distance between the wells, resulted in the following values for hydrologic parameters for the two tests:

Pumping well		A1	YC3
Drawdown data:			
Transmissivity	ft^2/d	13,835	27,027
	m^2/d	1,280	2,500
Storage coefficient		0.8×10^{-4}	2.5×10^{-4}
Recovery data:			
Transmissivity	ft^2/d	12,904	28,153
	m^2/d	1,194	2,605
Storage coefficient		1.3×10^{-4}	2.7×10^{-4}

The well fields were designed to determine the spatial distribution of head rather than to conduct aquifer tests to obtain a good evaluation of aquifer coefficients. The range of values obtained for hydrologic coefficients, however, lies within the range that can be expected for the type of materials investigated. The lower values for the valley fill agree reasonably well with laboratory measurements and other empirical data (table 2).

TABLE 2.—*Comparison of hydraulic conductivity values, K, in feet per day (metres per day)*

Type of material	Aquifer test	Laboratory measurement	Krumbein and Monk analysis	Empirical data [1]	Literature values
Valley fill (sand and gravel).	198(60)	148(45)	13–2,400 (4.1–738)	127(39)	[2] 160
Bedrock (sandstone and shale).	73(22)	-------	--------	----------	----------
Combined fill and bedrock.	108(33)	-------	--------	----------	----------
Anoka sand.	-------	32(10)	31(9)	40(12)	----------
Clay till units.	-------	0	--------	0.01–0.13 (0.004–0.04)	[3] 0.03–1.3 (0.009–0.4)

[1] Derived by assigning K values to particle-size distribution of samples, as in Winter (1973).
[2] From Lawson (1968) and Lohman (1972).
[3] From Parsons (1970).

Laboratory studies of selected samples of the valley fill were made to assess the intrinsic hydrologic properties of the material. Distinct hydrologic units can be established for the valley-fill material on the basis of particle-size analysis and calculated intrinsic permeability. Values obtained by the field and laboratory pro-

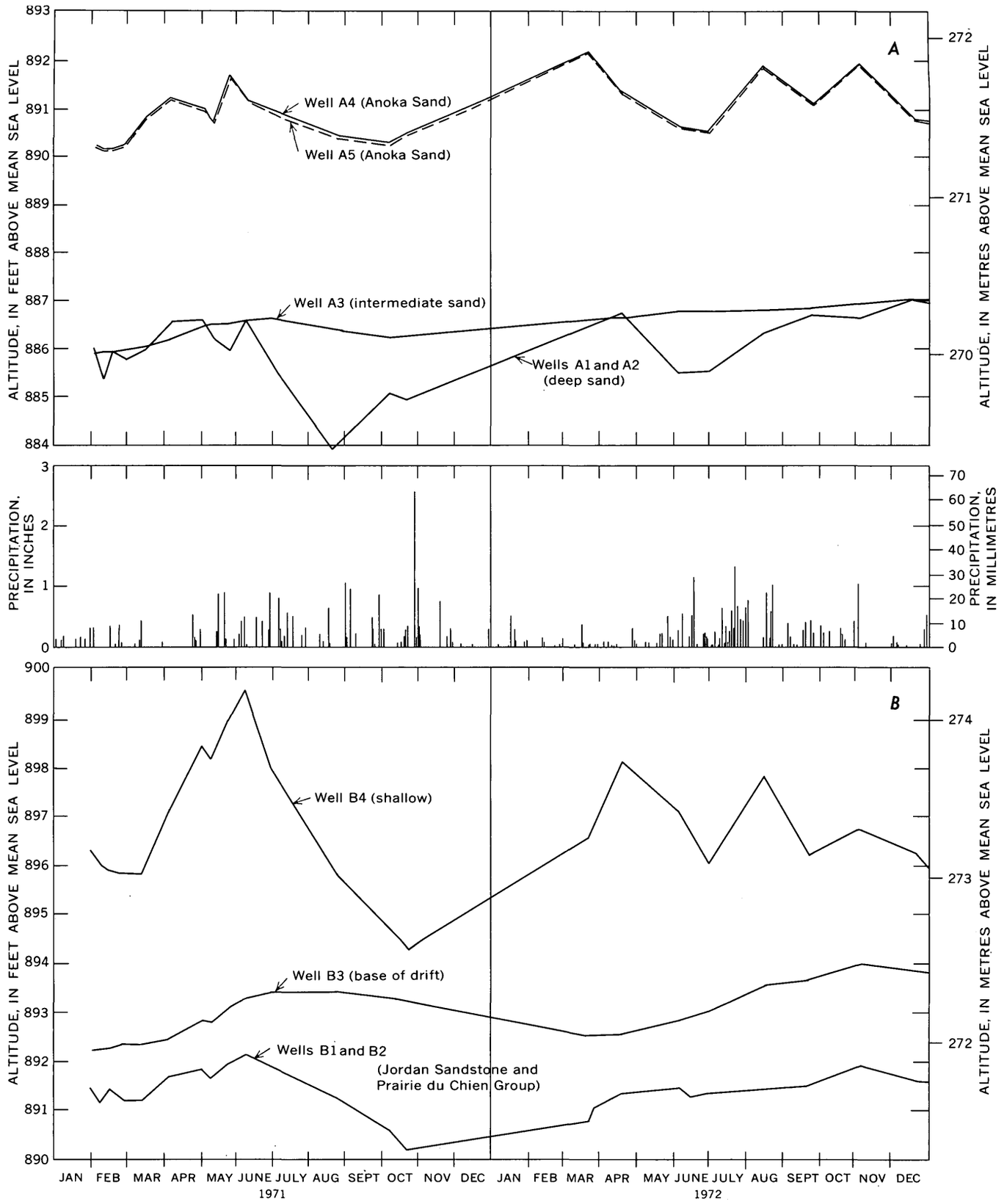

FIGURE 6.—Water-level hydrographs of all observation wells for 1971–72.

cedures (particle-size analyses and constant-head permeameter determinations) are compared with published empirical data and other published values (table 2).

Ground-water movement

The geologic framework described in the previous sections is the framework within which ground water occurs and through which it moves in the study area. Once the water reaches the saturated zone, its movement from recharge to discharge areas is controlled by transmissivity and also by hydraulic potential which is generally depicted in two dimensions by water-table or potentiometric contours.

A contour map of the water table can be used to show the general direction of ground-water movement. In glacial terrain, under natural conditions, the water table usually is a subdued image of the land surface being higher under hills and lower under depressions. Such a configuration indicates that discharge occurs in the lowlands, usually occupied by streams, lakes, or wetlands, adjacent to high areas. Therefore, a generalized topographic map (fig. 2) is used as a basis to show the general direction of ground-water movement. At any place in the study area, the water table is probably not more than 25 ft (7.6 m) below land surface, and in most of the area it is within 10 ft (3 m). In the upper part of the ground-water system in the study area, on a regional scale, water moves from the higher areas along the east side of the area to the wetlands and lakes along Rice Creek (fig. 2).

Much of the ground water in the bedrock and deep-drift units is part of a regional flow system. A map of the potentiometric surface of the Jordan–Prairie du Chien aquifer zone (Norvitch and others, 1973) for the entire Twin Cities area shows potentiometric highs in the aquifer near White Bear Lake, and movement of water to the Mississippi River valley. Lino Lakes Township is in an area of westward movement of water in the Jordan–Prairie du Chien aquifer zone (fig. 3).

To determine the relationship of ground-water flow among the surficial deposits, buried valley deposits, and bedrock, water level observations were used from the five wells at site A and the four wells at site B. At both locations, water levels in the shallower deposits are consistently higher than those in the deeper deposits, indicating downward leakage (fig. 6).

The shallowest well (B4) at Centerville, completed in till, has the highest water level of all the wells. It also shows the largest fluctuations. The water level in this well is generally 3 to 6 ft (0.9 to 1.8 m) higher than in well B3 which is completed at the base of the drift. Water levels in wells B1 and B2, completed in the Jordan Sandstone and Prairie du Chien Group, are identical and are generally about 1 ft (0.3 m) lower than in well B3. The differences in altitude of the water levels indicate that water moves downward through the drift and laterally within the Jordan–Prairie du Chien aquifer zone.

Water levels in shallow wells (A4 and A5) at the diagnostic center are about 4 ft (1.2 m) higher than those in wells completed deeper in the drift. The water levels in wells A1 and A2, completed in the deepest sand and gravel unit, are identical. The water level in well A3, completed in the intermediate sand, is stable, suggesting that the sand may be of limited extent and has poor hydraulic connection with other parts of the ground-water system. As at Centerville, the data at the diagnostic center indicate downward movement of ground water. Within the surficial sand, however, there is a slight upward gradient, the water level in the deeper well being consistently higher than in the shallower well, although the difference is only a few hundredths of a foot.

The response to precipitation and pumping of water levels in wells completed at different depths was also examined in order to evaluate the degree of interconnection of the aquifer zones. A precipitation record for 1971–72 (fig. 6) is compared with the well hydrographs to show infiltration characteristics. A weighted average for the study site was obtained by using precipitation data for three stations, Cedar (OS35), Forest Lake (PV13), and St. Paul (RU31). (See fig. 1.) Seasonal precipitation distribution and the annual precipitation of about 28 in. (71 mm) are typical for this part of Minnesota.

Only intense rainfall in early spring has a marked effect on ground-water levels. This is due to the saturated soil conditions following the spring thaw and a low evapotranspiration rate. Later in the summer, most rainfall is transpired by vegetation. Only very heavy and long rainstorms produce the excess infiltration that actually reaches the water table. For example, the rainy period of May 20–25, 1971, produced the peaks in the hydrographs of wells A4 and A5 on May 28. Water levels in these Anoka sand wells (A4 and A5) peaked almost immediately and those in wells A1, A2, B1, B2, and B4 did not reach a peak until June 11. This suggests a lag of about 2 weeks between the peak rainfall and the peak in ground-water levels resulting from that rainfall in the lower units at both sites as well as to the surficial till at Centerville. These findings indicate only qualitatively the relative response time. Quantitative interpretation might be possible only with continuous records near the well site of both precipitation and ground-water levels.

The composite record of drawdown in all wells during the pumping test indicates the degree of interconnection of the various aquifer zones (fig. 7). Nearly immediate response to pumping was observed in well A2, finished in the same sand as well A1, although at a higher position. The next well that showed the effects of pumping was the diagnostic center's well YC3, about 1,700 ft (518 m) away, where the response came in 19 min. Well A3, completed in a sand of limited extent within till and clay, had the longest delay in response, 200 min. The anomalous drop in drawdown in well A3 at 820 min was probably a consistent measurement error due to a change in observers. The adjusted values show more reasonable readings. Shallow well A5 responded after about 80 min of pumping, but well A4, in the same sand unit, showed an unexplained upward trend. The drawdown of the pumped well fluctuated between 27.3 and 28 ft (8.3 and 8.5 m) and averaged 27.75 ft (8.46 m).

The relative positions of water levels and their response to precipitation and pumping indicate the following hydrologic relationships for the bedrock valley. Infiltration at the land surface is greatly enhanced by the relatively high hydraulic conductivity of the Anoka sand. Movement to deeper aquifers is hindered by the intercalated clay and till layers. It is improbable that large quantities of water pass through this material under the normally occurring head differences at the test site, although some response to large pumping stresses has been shown to exist through those layers. Although the intergranular permeability of tills may be low, flow through fractures and fissures in the till is possible (Williams and Farvolden, 1967). Given the variability in areal extent and the thickness of clay and till units in this area, it is possible that the lower part of this valley has poor hydraulic connection to the surface because of the presence of the clay and till but may be freely connected to the surficial deposits at other locations where the clay and till are thin or nonexistent. There is good hydraulic connection between the lower valley fill and the Franconia Formation.

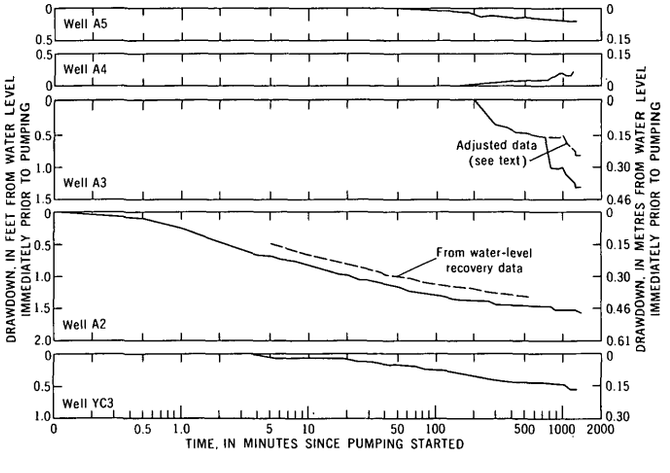

FIGURE 7.—Composite record of drawdown for all wells at site A while well A1 was being pumped.

Lateral movement of water between the valley fill and the incised bedrock units shows water moves into the valley from the bedrock along the east side. Whether this is true for the entire valley is conjectural. Given different cross-sectional geometries and different potentiometric-surface and water-table altitudes, water may move from the valley fill into the bedrock. The well hydrographs indicate that flow directions remain the same throughout the year at this site. In other locations, the inflow-outflow relations may change seasonally. Although not studied specifically here, there are indications (discussed later) that water flows longitudinally down the valley, especially through the coarse bottom material.

To summarize the flow relationships for the study area, a geohydrologic section (fig. 8) was drawn of the area between the diagnostic center (site A) and Centerville (site B). The section was drawn for late-winter hydrologic conditions using data obtained February 19, 1971. This situation represents a fairly stable flow, little affected by sporadic recharge or evapotranspiration. Because of the consistency of relative head differences throughout the year, as determined from well hydrographs, this flow pattern is independent of season. The water table was approximated from the topography and a few measurements in shallow, water-table wells. The altitude of George Watch Lake was estimated from the topographic map (Centerville quadrangle) which shows the lake level to be about 3 ft (1 m) lower than Centerville Lake.

Large quantities of ground water move within the deposits of the Anoka sand plain from the higher topographic areas to George Watch Lake. Smaller quantities of water move downward through the poorly permeable clay and till to the sand and gravel at the base of the drift. In the Centerville area, water moves through the poorly permeable till to Centerville Lake on the east side and downward to the deep sand and gravel and bedrock units. There is also some shallow flow through the Anoka sand to the west side of Centerville Lake.

Relatively large quantities of water move laterally into the area through bedrock and sand and gravel at the base of the drift. A small part of this water moves upward through the till to George Watch Lake, but most of it moves into the drift in the bedrock valley.

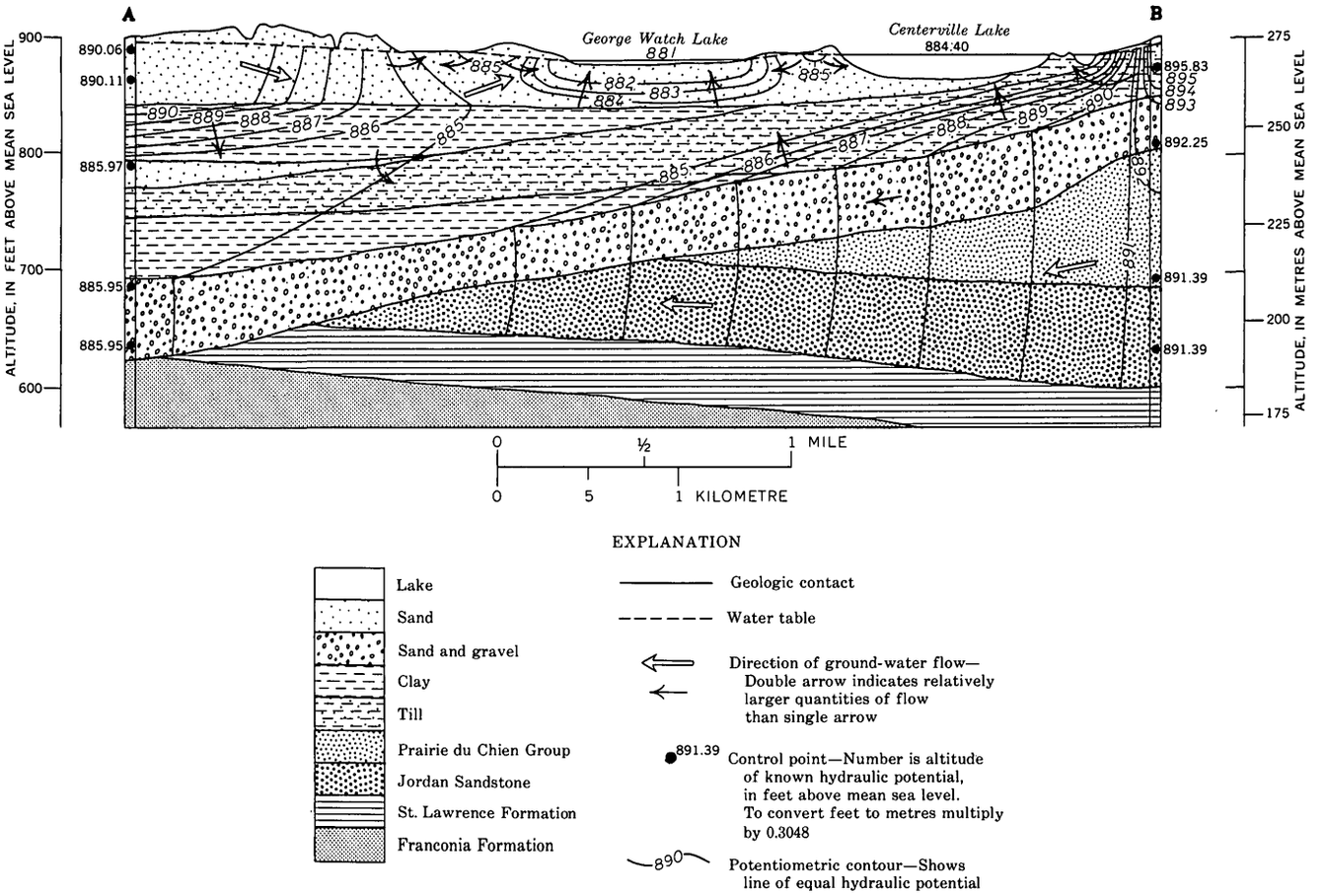

FIGURE 8.—Hydrologic section showing the geology and ground-water movement patterns between sites A and B.

Once the water is in the valley it probably moves perpendicular to the plane of the section, southward down the valley.

ENVIRONMENTAL IMPLICATIONS

From environmental and conservation points of view, the most serious problem associated with drift-filled valleys that incise bedrock in the Minneapolis–St. Paul area are those of water quality.

Several possibilities for water-quality deterioration exist. First, there is the possibility of direct downward percolation of surface water. This in itself is only part of the normal cyclical recharge process, but it may become critical if contaminants are allowed to move downward with the water, thereby creating serious implications about land use above buried bedrock valleys. In each instance, the infiltration and downward transmission capacity of the valley fill are significant factors which should be studied. The existence of poorly permeable till or clay at one site does not preclude substantial downward movement a short distance away. As mentioned earlier, fractures in till may provide important routes for vertical leakage. Also, the extent and geometry of the till bodies should be ascertained because of the great variability in the hydraulic characteristics of these deposits. If the poorly permeable layers are inclined in any direction, percolating water may possibly be diverted downslope to deeper parts of the hydrologic flow system.

Second, confined bottom fill may be more hydraulically conductive than the incised bedrock aquifers and therefore may act as a pipeline to quickly disperse contaminants. Because many of these valleys are interconnected and may form a network of preferred avenues of movement, contaminants may disperse relatively fast throughout the network. For these reasons, it may be necessary to evaluate land-use patterns not only relating to the possibility of vertical movement under the site, but also relating to the possible lateral dispersion pattern, should contaminants enter the channel aquifers.

Third, contaminants carried and dispersed in the valley system could enter the bedrock aquifer where inflow into bedrock occurs. Although at the study site

ground-water flows from the bedrock into the valley, these directions may be reversed elsewhere.

REFERENCES CITED

Lawson, D. W., 1968, Groundwater flow systems in the crystalline rocks of Okanagan Highland, British Columbia: Canadian Jour. Earth Sci., v. 5, p. 813–824.

Lohman, S. W., 1972, Ground-water hydraulics: U.S. Geol. Survey Prof. Paper 708, 70 p.

Mossler, J. H., 1972, Paleozoic structure and stratigraphy of the Twin City region, *in* Sims, P. K., and Morey, G. B., eds., Geology of Minnesota—a centennial volume: St. Paul, Minnesota Geol. Survey, p. 485–497.

Norvitch, R. F., Ross, T. G., and Brietkrietz, Alex, 1973, Water resources outlook for the Minneapolis—St. Paul metropolitan area, Minnesota: St. Paul, Metropolitan Council of the Twin Cities Area, 219 p.

Parsons, M. L., 1970, Groundwater movement in a glacial complex, Cochran District, Ontario: Canadian Jour. Earth Sci., v. 7, p. 869–883.

Payne, C. M., 1965, Bedrock geologic map of Minneapolis, St. Paul, and vicinity: Minnesota Geol. Survey Misc. Map M–1.

Schwartz, G. M., 1936, The geology of the Minneapolis—St. Paul metropolitan area: Minnesota Geol. Survey Bull. 27, 267 p.

Williams, R. E., and Farvolden, R. N., 1967, The influence of joints on the movement of ground water through glacial till: Jour. Hydrology, v. 5, no. 2, p. 163–170.

Winter, T. C., 1973, Hydrogeology of glacial drift, Mesabi Iron Range, northeastern Minnesota: U.S. Geol. Survey Water-Supply Paper 2029–A, 23 p.

Wright, H. E., Jr., 1973, Tunnel valleys, glacial surges, and subglacial hydrology of the Superior Lobe, Minnesota: Geol. Soc. America Mem. 136, p. 251–276.

Jour. Research U.S. Geol. Survey
Vol. 4, No. 3, May–June 1976, p. 277–284

TWO-DIMENSIONAL STEADY-STATE DISPERSION IN A SATURATED POROUS MEDIUM

By AKIO OGATA, Menlo Park, Calif.

Abstract.—A previously developed analytical solution for two-dimensional dispersion is computed for various conditions. These results were then compared with solution of previously developed approximate models of transverse dispersion which were used to analyze experimentally derived concentration distribution. Comparison established that, whenever steady state was reached, the values of dispersion coefficient computed using the approximate expression agreed with values derived from exact expression and in addition allowed a quick computation of the parameter.

Published reports on lateral dispersion in porous medium are still limited in number. Fried and Combarnous (1971) discuss the present-day knowledge of the various aspects of dispersion of fluid in granular medium related to both laboratory and field applications. Although numerical values of lateral dispersion determined from isotropic laboratory models are not abundant, results are consistent. The relative magnitudes of the dispersion coefficients for unidirectional flow in an isotropic medium and the nature of their dependence on the flow rate of the fluid are well documented. These values of the parameter are obtained by utilizing simple laboratory models and solutions of approximate mathematical models. Normally these simplified mathematical models make use of the fact that the longitudinal and transverse dispersion coefficients are independent when certain system of coordinates are used. This fact permits the use of a one-dimensional experimental hydraulic model for verification and the computation of both longitudinal and lateral dispersion coefficients.

With today's capability of digital computers and the advances in numerical techniques, the mathematical simulation of transport phenomenon for any given ground-water flow field is possible provided the parameters are known. The state of the art in numerical computation is such that the differential equation governing dispersion and convection with the superposition of chemical interaction (Rubin and James, 1973) in most instances can be handled with no real difficulty. Also, Smith, Farraday, and O'Connor (1973) discussed recent developments in computing the transport equation by the method of finite elements that circumvents many difficulties posed in finite difference technique. Pinder (1973) used this computational method to develop a predictive model for ground-water contamination in Long Island, N.Y. The limitations of these numerical models stem from the inability to directly apply parameters derived from simplified laboratory models to describe the process in a field situation, thus necessitating a program of curve fitting in the developmental phase of the numerical model.

The difficulties encountered in analysis of transport processes in the real ground-water environment are manifold and stem primarily from the inability to obtain synoptic field data. Although time rate of change of the flow pattern in a ground-water body is small, the diffused point samples available in the study region make it difficult to interpret the data without the basic understanding of the mechanics governing a given process. In all investigations based on a mathematical model, it is assumed that the flow system and all physicochemical processes that occur in the system are known. For example, to describe the simplest process, the physical transport of a substance by fluid flowing through porous materials, it is assumed that the flow vector and the dispersion tensor are completely defined. However, controls in the natural system, such as inhomogeneity of the porous medium which determines path of the fluid flow and hence the coefficient of dispersion, cannot be described mathematically nor simulated in the laboratory. This inability to describe the real system may be reflected in the difference in the magnitude of the dispersion coefficient derived from field and laboratory studies. For example, Pinder (1973) reported values of the dispersion coefficient that are orders of magnitude larger than values obtained for flow in isotropic porous-medium models in the laboratory.

In addition to medium nonhomogeneity, the value of the computed dispersion coefficient depends on the source of contaminant, since the manner in which the tracer or contaminant is introduced into the flow field changes the flow pattern of the host fluid and hence a corresponding change in the pattern of spreading occurs. A limited discussion of this effect is given in Ogata (1963). However, no followup in laboratory or theoretical studies has been initiated. Clearly the injection rate of the source does effect the initial spreading of the tracer and will effect the magnitude of the computed dispersion coefficient when a single parameter or unidirectional velocity is used to describe the flow field. The need to systematically evaluate the effect of the injection rate and geometry of the source on the magnitude of the parameters is apparent. Study of tracer sources located in the porous medium in contrast to medium heterogeneity can be investigated in the laboratory and may be useful in evaluating the use of a mass average velocity to describe the ground-water flow.

Because of mathematical difficulties, initial studies of the transverse dispersion process were based on a model that assumed dispersion parallel to the direction of flow is negligible, for example, Harleman and Rumer (1962) and Ogata (1961). This type of analytical solution coupled with an appropriate laboratory test facilitated determination of parameters because of the simplicity of the resulting expression. A treatment of the two-dimensional dispersion from surface source (Ogata, 1969) is available; however, evaluation requires the numerical integration of the products of the Bessel function. Because of the properties of the Bessel function, numerical evaluation of the solution is time consuming, unless special conditions are considered. For example, along a certain geometric axis, expression reduces sufficiently so that the concentration distribution can be computed with available desk calculators. These expressions, applicable along a fixed axis, were derived and compared with a formula obtained for the simplified one-dimensional dispersion models.

The physical model (fig. 1) considered is the dispersion of a tracer fluid emitted from a circular source of tracer of radius a located at $z=0$. A fluid containing tracer of concentration of C_o is introduced into the semi-infinite medium in region $r<a$ while fluid flowing into the medium from region $r>a$ contains a zero amount of tracer. The flow rate of both fluids into the porous medium at $z=0$ is maintained at an equal and constant rate. Because of symmetry about the z axis, the governing differential equation of the physical transport process for a unidirectional flow field as expressed in cylindrical coordinate is

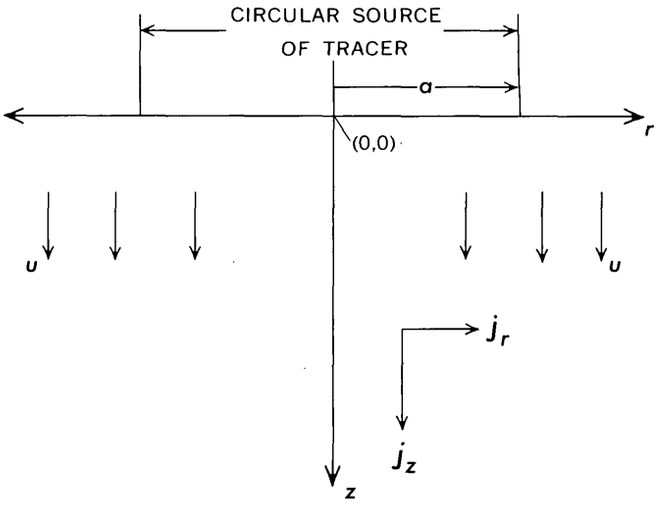

FIGURE 1.—Definition sketch of mathematical model. Symbols defined in text.

$$D_z\frac{\partial^2 C}{\partial z^2}-u\frac{\partial C}{\partial z}+\frac{D_r}{r}\frac{\partial}{\partial r}\left(r\frac{\partial C}{\partial r}\right)=\frac{\partial C}{\partial t}, \tag{1}$$

where u = flow rate in z-direction,
D_z, D_r = dispersion coefficients in z and r directions,
C = concentration,
t = time, and
z, r = space coordinate.

Since solution is obtained by use of the instantaneous point source, the boundary conditions needed for the source of radius a located at surface $z=0$ are

$$\begin{aligned} j&=uC_o, \text{ for } r\leqq a,\\ j&=0, \text{ for } r>a,\\ C(z,r,o)&=0, \end{aligned} \tag{2}$$

where j is the flux of mass.

Consider first the approximate model of transverse dispersion. Since the frontal diffused zone due to the longitudinal dispersion is assumed to develop at a rapid rate, it is assumed that, for the region upstream of this zone, equation 1 is reduced to

$$\frac{D_r}{r}\frac{\partial}{\partial r}\left(r\frac{\partial C}{\partial r}\right)=\frac{\partial C}{\partial t}+u\frac{\partial C}{\partial z}. \tag{3}$$

Only the solution is given here since the details appear in Ogata (1964). Letting $D=D_r$, the solution obtained was

$$\frac{C}{C_0}=\exp\left(-\frac{r^2+a^2}{4Dt}\right)\sum_{m=1}^{\infty}\eta^m I_m(\xi), \tag{4}$$

where $\xi=\dfrac{ra}{2Dt}$, $\eta=\dfrac{a}{r}$, and $I_m(\xi)$ is the modified Bessel function of the first kind of order m. The expression for steady-state dispersion can be obtained by making the substitution $t=z/u$ in equation 4.

For steady-state condition, the concentration distribution along axis $r=0$ is reduced to

$$\left.\frac{C}{C_o}\right|_{r=0} = 1-\exp(-a^2u/4Dz). \quad (5)$$

Also along axis $r=a$, significant reduction of the solution (eq 4) can be obtained; that is

$$\left.\frac{C}{C_o}\right|_{r=a} = \frac{1}{2}\left[1-\exp(-a^2u/2Dz)I_o(a^2u/2Dz)\right]. \quad (6)$$

The above two expressions can be readily computed since functions are tabulated in easily available forms.

Consider now the solution of the differential equation 1 for the boundary conditions prescribed. The development of the solution is described in Ogata (1969) and the result is written

$$\frac{C}{C_0} = \frac{2e^{2\alpha}}{\sqrt{\pi}}\int_0^\beta \exp(-\xi^2-\alpha^2/\xi^2)\left[1-J\left(\frac{a^2}{4\gamma^2\xi^2}, \frac{r^2}{4\gamma^2\xi^2}\right)\right]d\xi \quad (7)$$

where $\alpha = uz/4D_z$,
$\gamma^2 = 4D_zD_r/u^2$,
$\beta^2 = u^2t/4D_z$, and

$$1-J(x,y) = x^{1/2}\int_0^\infty e^{-t}J_0(2t^{1/2}y^{1/2})J_1(2t^{1/2}x^{1/2})\frac{dt}{t^{1/2}},$$

and J_0 and J_1 are Bessel functions of the first kind at orders 0 and 1, and $J(x,y)$ is the Goldstein J-function which appears frequently in heat-flow literature. This function has been computed to a limited extent and its integral cannot be evaluated by classical methods.

The numerical evaluation is time consuming although a subroutine of the product Bessel function is available. Thus, for computation of the value of the lateral dispersion coefficient from experimentally derived concentration distribution, any simplification of the general solution would facilitate analysis. The evaluation of concentration distribution along the centerline of the tracer path $r=0$ and along $r=a$ is considered. For the particle pathline $r=0$, the non-steady-state solution may be written in terms of the tabulated complement of the error function,

$$2\left.\frac{C}{C_o}\right|_{r=0} = \operatorname{erfc}\left(\frac{\alpha}{\beta}-\beta\right) + e^{4\alpha}\operatorname{erfc}\left(\frac{\alpha}{\beta}+\beta\right) - \exp\left[2\alpha-2\sqrt{\alpha^2+\theta^2}\right]\operatorname{erfc}\left[\frac{\sqrt{\alpha^2+\theta^2}}{\beta}-\beta\right] - \exp\left[2\alpha+2\sqrt{\alpha^2+\theta^2}\right]\operatorname{erfc}\left[\frac{\sqrt{\alpha^2+\theta^2}}{\beta}+\beta\right], \quad (8)$$

where $\theta^2 = a^2u^2/4D_zD_r$.

For steady-state dispersion or as $t\to\infty$, equation 8 further reduces to

$$\left.\frac{C}{C_0}\right|_{r=0} = 1-\exp(2\alpha-2\sqrt{\alpha^2+\theta^2}). \quad (9)$$

Plots of equations 8 and 9 for values of $\theta^2=2.75$ and 5.5 are shown in figure 2. The centerline concentration variation with time is shown in these graphs; thus in any given test run the assumption of steady-state dispersion can be tested provided estimates of D_z and D_r are available. The value $\theta^2=2.75$ was chosen since it seemed to fit data obtained in test runs reported previously.

To determine the expression applicable for steady state, consider equation 7 for large times. When $t\to\infty$, or $\beta\to\infty$, the resulting expression which is applicable for the steady-state system may be written,

$$\frac{C}{C_o} = \frac{2e^{2\alpha}}{\sqrt{\pi}}\int_0^\infty \exp(-\xi^2-\alpha^2/\xi^2)\left[1-J\left(\frac{\theta^2}{4\xi^2}, \frac{\rho^2\theta^2}{4\xi^2}\right)\right]d\xi, \quad (10)$$

where $\rho = r/a$, and
$\theta^2 = a^2/\gamma^2$.

The evaluation of the integral involves the expansion

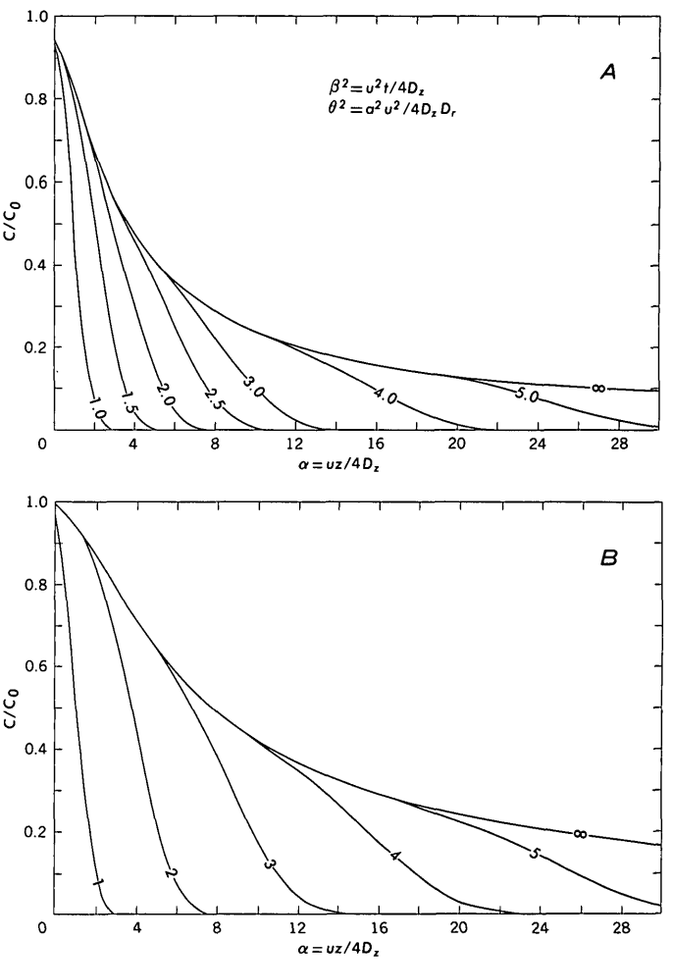

FIGURE 2.—Concentration distribution along centerline. Values of β indicated on curves. *A*, For $\rho=0$ and $\theta^2=2.75$. *B*, For $\rho=0$ and $\theta^2=5.5$.

of the J-function into an infinite series of Bessel function (Luke, 1962), or

$$J(x,y) = e^{-(x+y)} \sum_{k=0}^{\infty} \eta^k I_k(\xi), \eta<1$$

$$= 1 - e^{-(x+y)} \sum_{k=1}^{\infty} \eta^{-k} I_k(\xi), \eta>1$$

where $\eta = y/x$ and $\xi = 2\sqrt{xy}$, and $I_k(\xi)$ is the modified Bessel function of the first kind of order k.

Substituting the first series for $J(x,y)$ in equation 10, the expression applicable for region $\eta<1$ is

$$\frac{C}{C_o} = \frac{2e^{2\alpha}}{\sqrt{\pi}} \int_0^{\infty} e^{-\xi^2 - \alpha^2/\xi^2} \left\{ 1 - \exp\left[-(1+\rho^2)\right] \frac{\theta^2}{4\xi^2} \sum_{n=0}^{\infty} \rho^n I_n \left(\frac{\rho\theta^2}{2\xi^2} \right) \right\} d\xi = \frac{2e^{2\alpha}}{\sqrt{\pi}} \int_0^{\infty} \exp\left(-\xi^2 - \alpha^2/\xi^2\right) d\xi - \frac{2e^{2\alpha}}{\sqrt{\pi}} \int_0^{\infty} \exp\left\{-\xi^2 - \left[4\alpha^2 + (1+\rho^2)\theta^2\right]/4\xi^2\right\} \sum_{n=0}^{\infty} \rho^n I_n \left(\frac{\rho\theta^2}{2\xi^2} \right) d\xi. \tag{11}$$

The value of the first integral in equation 11 is one; hence, changing the order of integration and summation in the second term, equation 11 may be expressed as

$$\frac{C}{C_o} = 1 - \frac{2e^{2\alpha}}{\sqrt{\pi}} \sum_{n=0}^{\infty} \rho^n \int_0^{\infty} \exp\left\{-\xi^2 - \left[4\alpha^2 + (1+\rho^2)\theta^2\right]/4\xi^2\right\} I_n \left(\frac{\rho\theta^2}{2\xi^2} \right) d\xi. \tag{12}$$

Equation 12 may be integrated by expanding I_n into an infinite series and integrating term by term. However, the procedure may be simplified by first writing I_n in terms of the confluent hypergeometric function $\phi(a,c;x)$; that is (Erdelyi and others, 1953, p. 265)

$$I_\nu(x) = \frac{1}{\Gamma(\nu+1)} \left(\frac{x}{2} \right)^{\nu} e^{-x} \phi\left(\tfrac{1}{2}+\nu, 1+2\nu, 2x\right)$$

or $$\frac{C}{C_o} = 1 - \frac{2e^{2\alpha}}{\sqrt{\pi}} \sum_{n=0}^{\infty} \rho^n \int_0^{\infty} \exp\left\{-\xi^2 - \left[4\alpha^2 + (1+\rho^2)\theta^2\right]/4\xi^2\right\} \frac{\exp\left(-\rho\theta^2/2\xi^2\right)}{\Gamma(n+1)} \left(\frac{\rho\theta^2}{4\xi^2} \right)^n \phi\left(\tfrac{1}{2}+n, 1+2n; \frac{\rho\theta^2}{\xi^2} \right) d\xi. \tag{13}$$

The equation 12 is rewritten,

$$\frac{C}{C_o} = 1 - \frac{2e^{2\alpha}}{\sqrt{\pi}} \sum_{n=0}^{\infty} \frac{(\rho\theta/2)^{2n}}{\Gamma(n+1)} \int_0^{\infty} \exp\left(-\xi^2 - \frac{4\alpha^2 + (1+\rho)^2\theta^2}{4\xi^2} \right) \phi\left(\tfrac{1}{2}+n, 1+2n; \frac{\rho\theta^2}{\xi^2} \right) \frac{d\xi}{\xi^{2n}}. \tag{14}$$

By definition $\phi(a,c;x)$, confluent hypergeometric series, is a geometric series of the form

$$\phi\left(\tfrac{1}{2}+n, 1+2n; \frac{\rho\theta^2}{\xi^2} \right) = \sum_{m=0}^{\infty} \frac{(\frac{1}{2}+n)_m}{(1+2n)_m} \left(\frac{\rho\theta^2}{\xi^2} \right)^m \frac{1}{m!}$$

where $(a)_0 = 1$, $(a)_m = (1)(2)(3) \ldots (a+m-1)$. Thus expanding the hypergeometric function and substituting the result in equation 14 gives

$$\frac{C}{C_o} = 1 - \frac{2e^{2\alpha}}{\sqrt{\pi}} \sum_{n=0}^{\infty} \frac{(\rho\theta/2)^{2n}}{\Gamma(n+1)} \int_0^{\infty} \exp\left[-\xi^2 - \frac{4\alpha^2 + (1+\rho)^2\theta^2}{4\xi^2} \right] \sum_{m=0}^{\infty} \frac{(\frac{1}{2}+n)_m}{(1+2n)_m} \left(\frac{\rho\theta^2}{\xi^2} \right)^m \frac{1}{m!} \frac{d\xi}{\xi^{2n}}. \tag{15}$$

Changing order of integration and summation

$$\frac{C}{C_o} = 1 - \frac{2e^{2\alpha}}{\sqrt{\pi}} \sum_{n=0}^{\infty} \frac{(\rho\theta/2)^{2n}}{n!} \sum_{m=0}^{\infty} \frac{(\rho\theta^2)^m}{m!} \frac{(\frac{1}{2}+n)_m}{(1+2n)_m} \int_0^{\infty} \exp\left[\xi^2 - \frac{4\alpha^2 + (1+\rho)^2\theta^2}{4\xi^2} \right] \frac{d\xi}{\xi^{2m+2n}}. \tag{16}$$

Note that the integral in equation 16 is the integral form of the modified Bessel function. This can be seen clearly by first letting

$$\xi^2 = \left[4\alpha^2 + (1+\rho)^2\theta^2\right]\lambda^2 = \chi^2\lambda^2.$$

Substituting the above expression into the integral in equation 16 results in

$$I = \int_0^{\infty} \exp\left(-\chi^2\lambda^2 - \frac{1}{4\lambda^2} \right) \frac{\chi\, d\lambda}{(\chi^2\lambda^2)^{m+n}} = \int_0^{\infty} \exp\left(-\chi^2\lambda^2 - \frac{1}{4\lambda^2} \right) \chi^{-2(m+n)+1} \frac{d\lambda}{\lambda^{2(m+n)}}.$$

Gray, Mathews, and MacRobert (1952, p. 51), give the identity

$$K_n(z) = \frac{1}{(2z)^n} \int_0^{\infty} e^{\left(-z^2\xi^2 - \frac{1}{4\xi^2}\right)} \xi^{-2n-1}\, d\xi$$

where $K_n(z)$ is the modified Bessel function of the second kind of order n.

To conform with the above identity, write integral I as

$$I = \frac{2^{k-\frac{1}{2}} \chi^{\frac{1}{2}}}{(\chi)^k} \frac{1}{(2\chi)^{k-\frac{1}{2}}} \int_0^{\infty} e^{-\chi^2\lambda^2 - \frac{1}{4\lambda^2}} \frac{d\lambda}{\lambda^{2(k-\frac{1}{2}+1)}}$$

where $k = m+n$.

Thus $$I = \left(\frac{2}{\chi} \right) \frac{(2\chi)^{\frac{1}{2}}}{2} K_{k-\frac{1}{2}}(\chi).$$

Resubstituting into equation 6,

$$\frac{C}{C_o} = 1 - \frac{e^{2\alpha}}{\sqrt{\pi}} \sum_{n=0}^{\infty} \frac{\left(\frac{\rho\theta}{2} \right)^{2n}}{n!} \sum_{m=0}^{\infty} \frac{(\rho\theta^2)^m}{m!} \frac{(\frac{1}{2}+n)_m}{(1+2n)_m} \left(\frac{2}{\chi} \right)^{m+n}$$

$$(2\chi)^{\frac{1}{2}} K_{m+n-\frac{1}{2}}(\chi) = 1 - \frac{e^{2\alpha}}{\sqrt{\pi}} (2\chi)^{\frac{1}{2}} \sum_{n=0}^{\infty} \frac{\left(\frac{\rho^2\theta^2}{\chi} \right)^n}{n!} \sum_{m=0}^{\infty} \frac{\left(\frac{2\rho\theta^2}{\chi} \right)^m}{m!} \frac{(\frac{1}{2}+n)_m}{(1+2n)_m} K_{m+n-\frac{1}{2}}(\chi). \tag{17}$$

The first two values of half-order modified Bessel function are obtained from the formulas

$$K_{1/2}(z)=\sqrt{\frac{\pi}{2z}}e^{-z}=\sqrt{\frac{\pi}{2z}}e^{-z}k_0 \text{ and}$$

$$K_{3/2}(z)=\sqrt{\frac{\pi}{2z}}e^{-z}(1+z^{-1})=\sqrt{\frac{\pi}{2z}}e^{-z}k_1.$$

All other values of the function can be obtained by using the recurrence relationship of the Bessel function which is given as

$$k_{n+1}(z)=k_{n-1}(z)+\frac{2n+1}{z}k_n(z).$$

Thus equation 16 expressed in the exponential form of the half-order modified Bessel function equation may be rewritten

$$1-(C/C_o)\,e^{-2\alpha+\chi}=\sum_{n=0}^{\infty}\frac{\left(\frac{\rho A}{4}\right)^n}{n!}\sum_{m=0}^{\infty}\frac{A^m}{m!}\frac{(1/2+n)_m}{(1+2n)_m}$$
$$k_{m+n-1}(\chi);\rho<1 \qquad (18)$$

where $A=2\rho\theta^2/\chi$. Note that because the modified Bessel function is an even function $k_{-1}=K_{-1/2}=K_{1/2}=k_0$.

In a similar way, an expression applicable for the region $\rho>1$ was obtained. The J-function for $\rho>1$ is

$$J\left(\frac{\theta^2}{4\xi^2},\frac{\rho^2\theta^2}{4\xi^2}\right)=1-\exp[-(1+\rho^2)\theta^2/4\xi^2]\sum_{k=1}^{\infty}\left(\frac{1}{\rho}\right)^k I_k\left(\frac{\rho\theta^2}{2\xi^2}\right).$$

Substituting the above expression into the integral equation 15 gives

$$\frac{C}{C_o}=\frac{2e^{2\alpha}}{\sqrt{\pi}}\int_0^{\infty}\exp(-\xi^2-\alpha^2/\xi^2)\exp[-(1+\rho^2)\theta^2/4\xi^2]\sum_{n=1}^{\infty}\left(\frac{1}{\rho}\right)^n I_n\left(\frac{\rho\theta^2}{2\xi^2}\right)d\xi.$$

This expression is the same as the second term in equation 16 where ρ is replaced by $1/\rho$; hence, the expression for steady-state concentration distribution in region $\rho>1$ can be written immediately by replacing the ρ^n by $\left(\frac{1}{\rho}\right)^n$ in equation 18 or

$$\frac{C}{C_o}=e^{2\alpha-\chi}\sum_{n=1}^{\infty}\frac{\left(\frac{A}{4\rho}\right)^n}{n!}\sum_{m=0}^{\infty}\frac{A^m(1/2+n)_m}{m!(1+2n)_m}k_{m+n-1}(\chi);\rho>1.$$

For $\rho=1$, the resulting solution is simplified and may be written

$$\left.\frac{C}{C_o}\right|_{r=a}=\tfrac{1}{2}[1-\exp(2\alpha-2\sqrt{\alpha^2+\theta^2})]-\frac{2e^{2\alpha}}{\sqrt{\pi}}\sum_{m=1}^{\infty}\frac{(1/2)_m}{(n!)^2}\frac{\theta^{2m}}{(\sqrt{\alpha^2+\theta^2})^{m-1/2}}K_{m-1/2}(2\sqrt{\alpha^2+\theta^2}). \qquad (20)$$

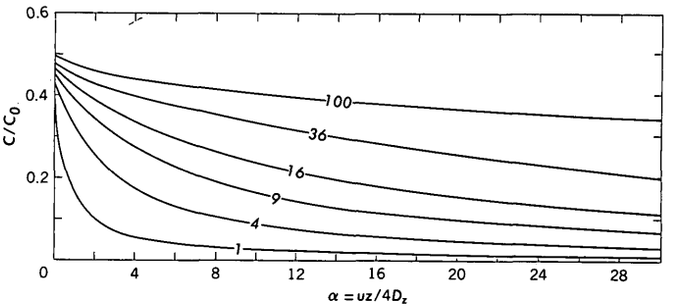

FIGURE 3.—Concentration distribution along $\rho=1$. Values of θ^2 indicated on curves.

Plot of the above equation for various values of θ^2 is shown in figure 3.

Equations 18, 19, and 20 are the complete series representation of the discontinuous integral, equation 10. The series as represented converged rapidly so that a desk-top programable calculator was used to compute the series. Typical curves of concentration distribution for various values of θ^2 are shown in figure 4. These plots represent the distribution in a given cross section of the porous material.

When steady-state experimental data are available at various cross sections of the porous medium, a series of computed curves such as those shown in figure 4 may be used as a type curve and dispersion coefficient determined by the process of curve fitting. However, since the solution is simpler when axis $r=0$ or $r=a$ is considered, it would be advantageous to use these formulas to compute the magnitude of the dispersion coefficient. In some experiments, the variation of concentration along these two axes may not be large enough to be useful; hence, the ratio of the concentrations along $r=a$ and $r=0$ may be used to correlate theoretical and experimental values. A plot of these ratios for various θ is shown in figure 5. This ratio is also useful when the value of C_o is suspect such as in the experiment reported previously where the amount adsorbed by the porous medium was used to determine liquid concentration.

The two-dimensional model was developed in order to evaluate the validity of the approximate transverse dispersion models shown as equations 4, 5, and 6. The approximate model was used to assimilate data of the experimental model described by Skibitzke, Chapman, Robinson, and McCullough (1961). Because of the complexity of the solution of the exact model, complete numerical evaluation of the nonsteady-state dispersion process was not attempted. To determine the range of validity of the approximate model, computation of the steady-state dispersion for the special case of $r=0$ was

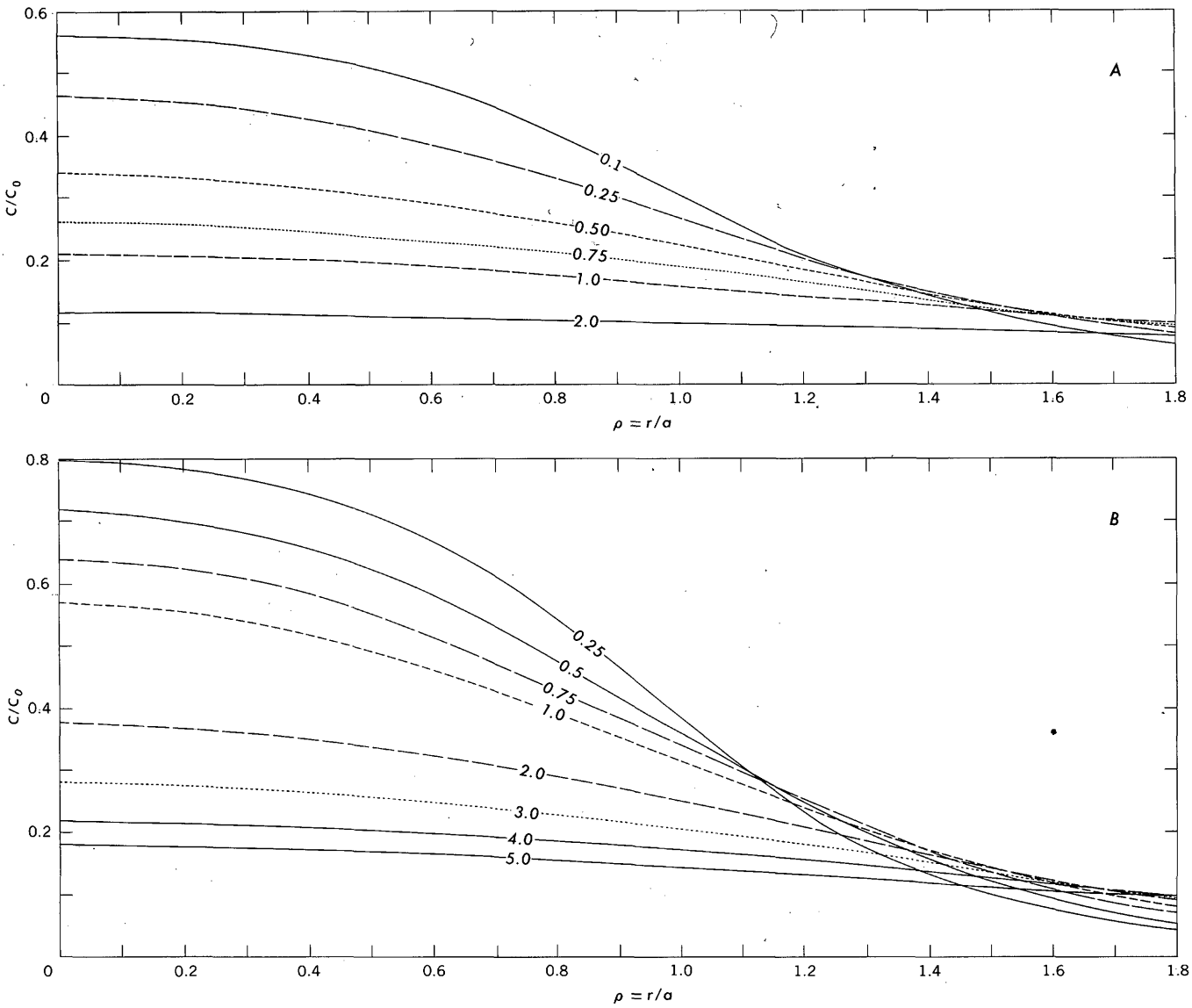

FIGURE 4.—Radial concentration distribution. Values of α indicated on curves. *A*, For $\theta^2=1$. *B*, For $\theta^2=4$. *C*, For $\theta^2=9$.

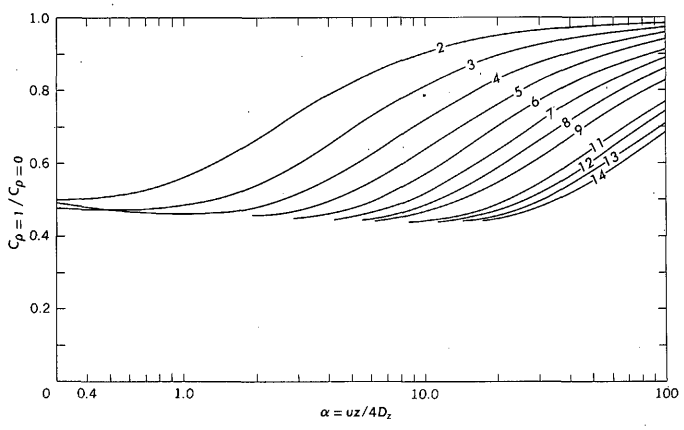

FIGURE 5.—Ratios of concentration for $\rho=0$ and $\rho=1$. Values of θ indicated on curves.

carried out. The comparison of these two solutions is shown in figure 6. For most values of θ observed in the laboratory, the approximate expression, which contains the single dispersion coefficient D_r, approaches the exact solution rapidly. Thus, whenever the test is continued for some time, the approximate solution can be used to obtain a quick estimate of the transverse dispersion coefficient.

This surface source model two-dimensional dispersion study was chosen since this mathematical model can be readily simulated in the laboratory. Also the spreading of the tracer in a homogeneous porous material may be controlled by the rate of injection of the tracer fluid relative to the surrounding fluid flow. Laboratory studies of other injection sources of vari-

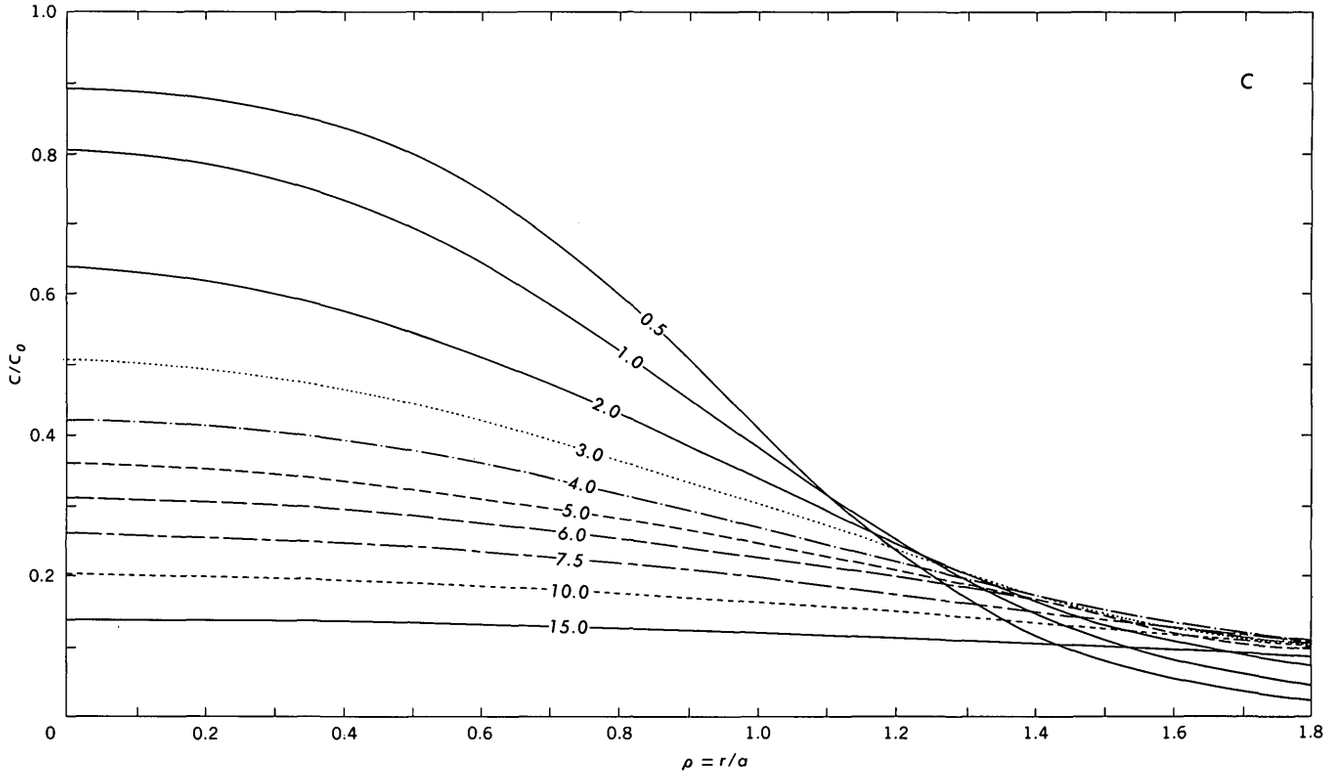

FIGURE 4.—Continued.

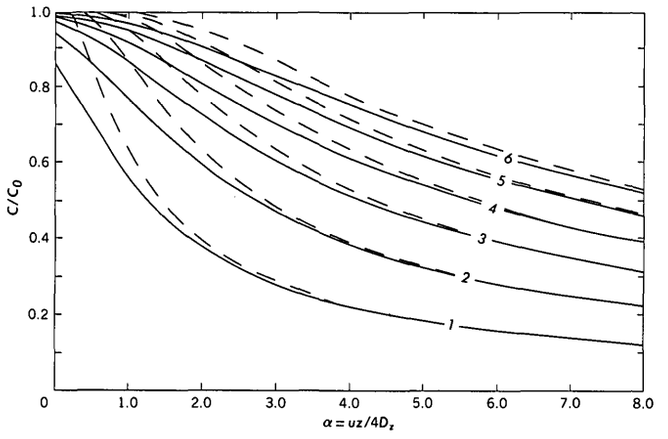

FIGURE 6.—Comparison of centerline concentration. Solid line, exact model; dashed line, approximate model.

ous strengths need to be carried out in order to evaluate the effect of the source on the lateral dispersion. Additional laboratory studies and the correlation with mathematical models would further delineate the effect of nonhomogeneity encountered in the actual system. Studies along this line would aid in the correlation of field- and laboratory-derived magnitudes of the dispersion coefficient especially when the convective transport is based on the mass average velocity.

REFERENCES CITED

Erdelyi, Arthur, Magnus, Wilhelm, Oberhettinger, Fritz, and Tricomi, F. G., 1953, Higher transcendental function, v. II: New York, McGraw-Hill, 396 p.

Fried, J. J., and Combarnous, M. A., 1971, Dispersion in porous media, *in* Ven Te Chow, ed., Advances in hydroscience: New York, Academic Press, v. 7, p. 170–282.

Gray, Andrew, Mathews, G. B., and MacRobert, T. M., 1952, A treatise on Bessel functions: London, MacMillan and Co., Ltd., 327 p.

Harleman, D. R. F., and Rumer, R. R., Jr., 1962, The dynamics of salt-water intrusion in porous media: Massachusetts Institute of Technology Hydrodynamics Lab. Rept. 55, 125 p.

Luke, Y. L., 1962, Integrals of Bessel functions: New York, McGraw-Hill, 419 p.

Ogata, Akio, 1961, Transverse diffusion in saturated isotropic granular media: U.S. Geol. Survey Prof. Paper 411–B, 8 p.

———1963, Effect of the injection scheme on the spread of tracers in ground water reservoirs: U.S. Geol. Survey Prof. Paper 475–B, p. B199–B202.

———1964, The spread of dye stream in an isotropic granular medium: U.S. Geol. Survey Prof. Paper 411–G, 11 p.

———1969, Two-dimensional dispersion in a granular medium-disk source emitting at constant rate: U.S. Geol. Survey Prof. Paper 650–D, p. 260–264.

Pinder, George F., 1973, A Galerkin-finite element simulation of groundwater contamination on Long Island, New York: Water Resources Research, v. 9, no. 6, p. 1657–1670.

Rubin, Jacob, and James, R. V., 1973, Dispersion-affected transport of reacting solutes in saturated porous media: Galerkin method applied to equilibrium-controlled exchange in unidirectional steady water flow: Water Resources Research, v. 9, no. 5, p. 1332–1356.

Skibitzke, H. E., Chapman, H. T., Robinson, G. M., and McCullough, R. A., 1961, Radio tracer techniques for the study of flow in saturated porous material: Internat. Jour. Appl. Radiation and Isotopes, v. 10, no. 1, p. 38–46.

Smith, I. M., Farraday, R. V., and O'Connor, B. A, 1973, Rayleigh-Ritz and Galerkin-finite elements for diffusion-convection problems: Water Resources Research, v. 9, no. 3, p. 593–606.

Jour. Research U.S. Geol. Survey
Vol. 4, No. 3, May–June 1976, p. 285–291

A SIMPLIFIED SLOPE-AREA METHOD FOR ESTIMATING FLOOD DISCHARGES IN NATURAL CHANNELS

By H. C. RIGGS, Reston, Va.

Abstract.—Discharge of a stream may be computed from the slope of the water surface, the cross-sectional area, and an estimate of channel roughness. This, the slope-area method, is widely used to compute flood peak discharges from high-water marks. Reliability of a computed discharge depends largely on the roughness coefficient, which must be estimated. This paper shows that results of comparable accuracy can be obtained from area and slope alone in natural channels; a roughness coefficient is not needed because roughness and slope are related. The estimating equation and suggestions for application of the simplified method are included.

The slope-area method is widely used to compute peak discharge after the passage of a flood. A reach of uniform channel is selected on which the flood profile on both banks can be defined from high-water marks. Surveys of these high-water marks and of channel cross sections and estimates of the roughness coefficient in the Manning equation are required. The method is described by Benson and Dalrymple (1968) and by Dalrymple and Benson (1967).

Although judgment is required in selecting the stream reach and in interpreting the profiles from high-water marks, the major subjectivity is in selection of the roughness coefficient n in the Manning equation

$$Q = \frac{1.49}{n} A R^{2/3} S^{1/2}$$

where Q is discharge in cubic feet per second, A is cross-sectional area in square feet, R is the hydraulic radius in feet (cross-sectional area divided by the wetted perimeter), and S is the slope of the energy gradient. Guides to selection of n are given in many texts. The guide by Barnes (1967) for estimating the roughness coefficient in natural channels includes color photographs of stream reaches for which the coefficients have been computed from channel surveys and known peak discharges.

Study of the photographs and the computed (verified) values of n in Barnes' (1967) report will show some apparent inconsistencies; for example, between Cache Creek and Boundary Creek. These inconsistencies are thought to arise from two sources. First, the roughness coefficient of a natural channel is due to bed roughness, bank irregularity, effect of vegetation(if any), depth of water, channel slope, and perhaps other factors. No objective way of evaluating and combining these factors into one coefficient is available. Second, a verified value of a roughness coefficient is affected by the inaccuracies in each of the other variables in the Manning equation. Inaccuracies may arise because of a poorly defined water-surface profile or nonrepresentative cross sections. A poorly defined profile may be caused by poor high-water marks, bank irregularity at the high-water line, or a changing cross-sectional area and shape throughout the reach. In rough cross sections the detail to which the cross section is surveyed will affect the computed area and thus the computed roughness coefficient.

Several investigators have related the verified roughness coefficients to channel bed roughness and to the vertical velocity distribution. See Boyer (1954), Graf (1966), and Limerinos (1970). However, such relations have limited use because bed roughness is only part of the total roughness in most channels, and the vertical velocity distribution generally is not known at sites where a slope-area measurement is made.

Thus the roughness coefficient still must be selected by judgment based on guidelines and experience. Whether this is a disadvantage or not depends on the accuracy of results. How accurate are slope-area measurements? This has been a subject of discussion for many years. Opinions range from claims of high accuracy to the comment of a prominent (unnamed) hydraulic engineer who was quoted by Henry Beckman (written commun., 1925) as saying that, whenever results obtained by the slope-area method came nearer than 25 percent to the correct result, it was due either to accident or to a second choice of factors to use in the formula after the first choice had gone amiss. Fifty years later, wide differences of opinion as to the accuracy of the method still exist.

Those with experience in slope-area measurements can recognize reaches where good results can be ex-

pected. But how good is good? An answer to this is now possible. Estimates of the roughness coefficient were recorded on field notes of some surveys of channel reaches for which the coefficient was computed from known peak discharge. Estimated roughness coefficients by each individual and the computed (verified) coefficients are shown in table 1. All reaches listed in table 1 are ones in which the flow was contained in a single channel.

Table 1 shows a surprisingly small difference among estimates by individual observers for most of the streams. That table also indicates that estimates of roughness coefficient tend to be better on some types of reaches than on others. Estimates were poor on Salt-Roca, Cache–Lower Lake, Cachuma–Santa Ynez, Sycamore–McDowell, and Hominy–Candler. One might conclude from this table that experienced observers can make acceptable subjective estimates of the roughness coefficients in channels typified by that of W. Fk. Bitterroot–Conner but that better guidelines are needed for unusual channels. Nearly all the estimates in table 1 were made by observers with extensive experience in this type of work. Less experienced observers would do less well on the average. Thus, a less subjective method is needed.

Some measurable channel characteristic related to the roughness coefficient might permit an objective selection of the latter. Channel (or water-surface) slope is one such characteristic. It has been known for years

TABLE 1.—*Estimated and verified values of the channel roughness coefficient* n

[The first 20 streams are included in Barnes' (1967) report; the rest are from unpublished verifications]

Stream reach	Estimated n				Verified n
Clark Fork–St. Regis, Mont	0.035	0.030	0.035	0.035	0.028
Clark Fork above Missoula, Mont.	.035	.035	.035	----	.030
Salt–Roca, Nebr	.045	.045	----	----	.030
Blackfoot—Ovando, Mont	.035	----	----	----	.031
Coeur d'Alene–Prichard, Idaho	.035	.038	.040	.030	.032
Rio Chama–Chamita, N. Mex	.035	.025	----	----	.032
Clearwater–Kamiah, Idaho	.035	.035	.035	----	.033
W. Fk. Bitterroot–Conner, Mont.	.040	.035	.035	----	.036
Yakima–Umtanum, Wash	.032	----	----	----	.036
Wenatchee–Plain, Wash	.037	.035	.030	.035	.037
Moyie–Eastport, Idaho	.030	.035	.035	.030	.038
Spokane–Spokane, Wash	.038	.035	.035	----	.038
M. Fk. Flathead–Essex, Mont	.038	.040	.038	----	.041
Catherine—Union, Oreg	.042	.045	.040	.040	.043
Chiwawa–Plain, Wash	.038	----	----	----	.043
Grande Ronde–LaGrande, Oreg	.038	.040	.040	.038	.043
S. Fk. Clearwater–Grangeville, Idaho.	.050	.045	.048	----	.051
Cache–Lower Lake, Calif	.082	.074	----	----	.053
Boundary–Porthill, Idaho	.065	.075	----	----	.073
Rock–Darby, Mont	.070	.065	.075	----	.075
Salmon–Whitebird, Idaho	.04	.04	.04	----	.040
Sulfur Fork Red–Adams, Tenn	.05	.09	----	----	.050
Cachuma–Santa Ynez, Calif	.045	.055	----	----	*.07
Sycamore–McDowell, Ariz	.032	----	----	----	.020
Salt–Lincoln, Nebr	.035	.042	----	----	*.03
Bijou–Wiggins, Colo	.025	----	----	----	*.025
Deckers–Morgantown, W. Va	.035	----	----	----	.035
Millers–Erving, Mass	.037	.042	----	----	.037
Neversink–Godeffroy, N. Y	.035	----	----	----	.035
Hominy–Candler, N. C	.045	----	----	----	.060

* Varies depending on interpretation of data.

that the roughness coefficient is related to slope in natural channels but, in practice, the two have been considered independent. The degree of relation between roughness coefficient, n, and the square root of the water-surface slope is shown in figure 1 using data from Barnes' (1967) report. A relation of this type might be used to modify an estimated n according to slope; or one might conclude that the two variables are so highly related that only one of the two is needed in computing discharge. The latter is the basis for the simplified method described in the next section.

THE SIMPLIFIED METHOD

The existence of a relation between channel roughness and water-surface slope in natural channels suggests that discharge might be computed without using a roughness coefficient and without defining the relation of roughness coefficient to slope. Assuming that

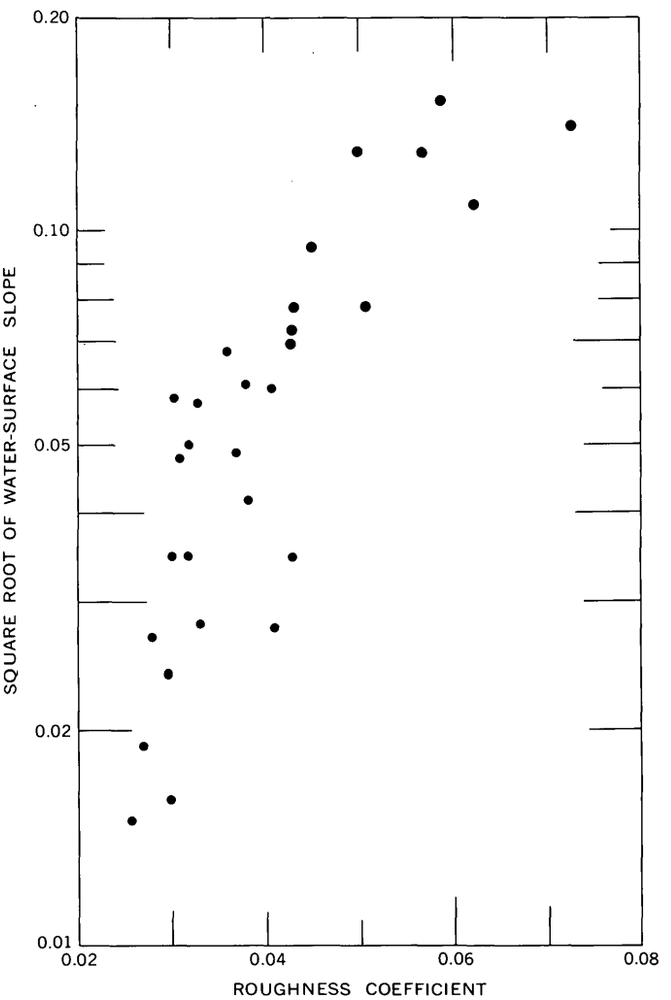

FIGURE 1.—Relation of roughness coefficient to square root of water-surface slope.

the slope will replace n and that the hydraulic radius, R, is closely related to cross-sectional area, A, the Manning equation is reduced to the model

$$Q = aA^bS^c$$

if S is redefined as water-surface slope.

Using areas and slopes from Barnes' (1967) report, the following equation was derived (Riggs, 1974):

$$\log Q = 0.53 + 1.295 \log A + 0.316 \log S \quad (1)$$

where Q is in cubic metres per second. A is in square metres, and S is dimensionless. The standard error is about 20 percent.

Subsequent study of the data indicated that the relation with slope is not log linear. Accordingly the data were reanalyzed in English units with the following result which is the basis for the simplified method:

$$\log Q = 0.366 + 1.33 \log A + 0.05 \log S - 0.056 (\log S)^2 \quad (2)$$

where Q is in cubic feet per second, A is in square feet, and S is dimensionless. The standard error is about the same as before but this latter equation fits the data better throughout the range. Comparison of results from equation 2 with those that would have been obtained by the conventional slope-area method is possible for stream reaches (table 1) for which the survey-party members selected n values prior to verification. These reaches are listed in table 2 along with the mean of the estimates of n for each reach, the known discharge, the discharge computed by the conventional slope-area method using the mean n, and the discharge computed by the simplified method (eq 2). Results are plotted in figure 2. These plots indicate little difference in relia-

TABLE 2.—*Evaluation of slope-area method and simplified method*

[See table 1 for reach locations and estimated n values]

Stream reach	Mean, $\bar{n}$, of estimated n values	Discharge		
		Known	Using $\bar{n}$	By eq 2
Clark Fork	0.034	68,900	56,700	59,300
Clark Fork	.035	31,500	27,000	31,100
Salt	.045	1,860	1,240	1,620
Blackfoot	.035	8,200	7,300	8,510
Coeur d'Alene	.036	11,300	9,400	9,660
Rio Chama	.030	1,060	1,130	1,110
Clearwater	.035	99,000	93,400	114,000
W. Fk. Bitterroot	.037	3,880	3,780	3,460
Yakima	.032	27,700	31,200	26,200
Wenatchee	.034	22,700	24,700	22,900
Moyie	.032	8,030	9,400	8,360
Spokane	.036	39,600	42,200	43,300
M. Fk. Flathead	.039	14,500	15,400	14,800
Catherine	.042	1,740	1,790	1,410
Chiwawa	.038	5,880	6,650	6,170
Grande Ronde	.039	4,620	5,100	4,720
S. Fk. Clearwater	.048	12,600	13,400	13,800
Cache	.078	3,840	2,610	3,630
Boundary	.07	2,530	2,640	3,180
Rock	.07	1,500	1,600	1,580
Salmon	.04	101,000	101,000	114,000
Sulfur Fork Red	.07	10,100	7,220	10,100
Cachuma	.05	776	------	1,120
Sycamore	.032	2,300	1,440	1,420
Salt	.038	29,200	------	21,700
Bijou	.025	7,900	------	8,830
Deckers	.035	3,100	3,100	2,630
Millers	.040	5,700	5,350	7,470
Neversink	.035	10,100	10,100	11,000
Hominy	.045	6,800	5,100	8,140

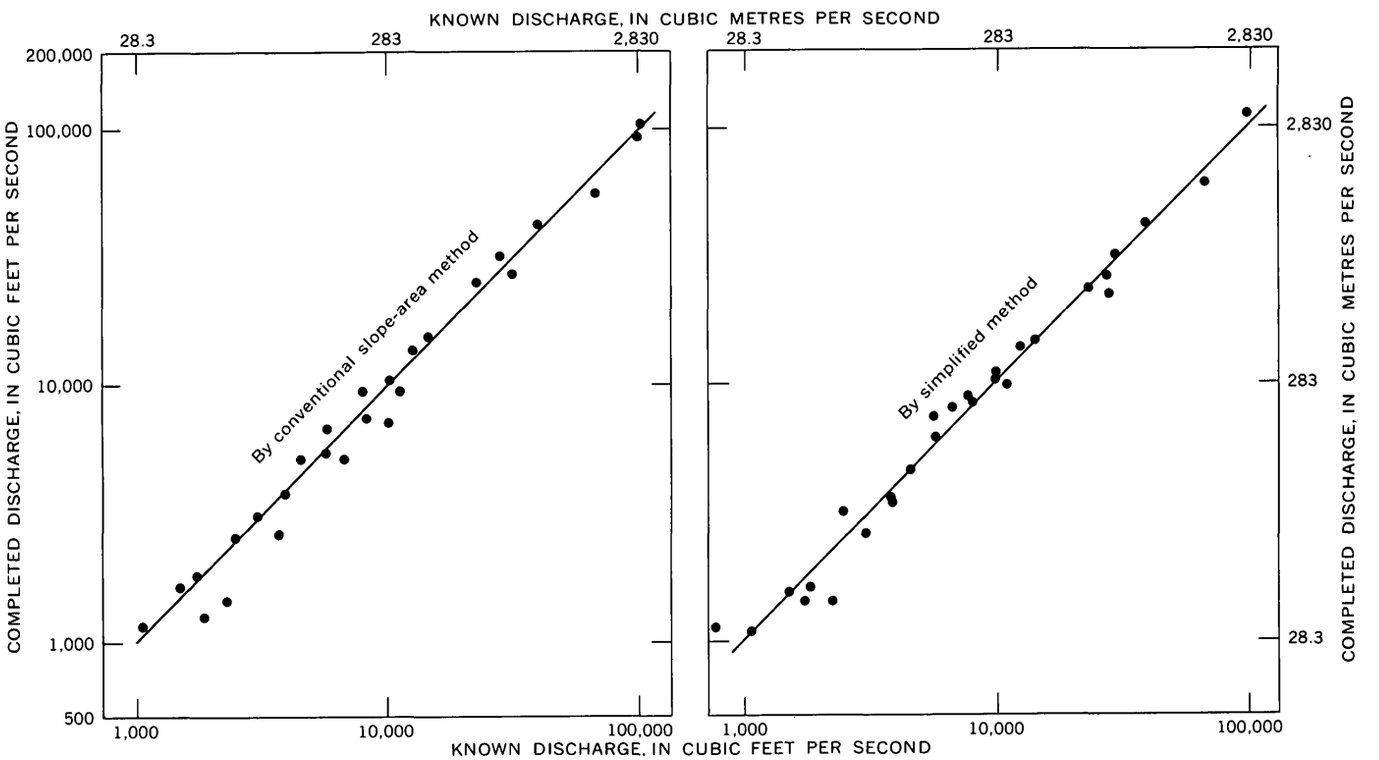

FIGURE 2.—Comparison of known peak discharges with those computed by two methods (data from table 2).

bility of the two methods. Most of the channel reaches used in this test were favorable for use of the slope-area method, and the hydrologists who made most of the surveys had broad experience in selecting n.

The applicability of the simplified method was further tested on 44 slope-area verifications not used in its derivation. Data from these verifications and the discharge computed by the simplified method are shown in table 3. Some of these verifications are of poor quality because of unfavorable channel characteristics, poor high-water marks, channel modification by man, or backwater. However, the peak discharges should be reliable because they are based on discharge measurements or short rating extensions. Comparisons of known discharge with discharge computed by equation 2 are shown in figure 3. These computed discharges are less reliable than those in figure 2 because the reaches used were not as good. However, no bias is indicated. The data on which table 3 and figure 3 are based did not include estimated values of n; thus the discharges cannot be computed by the conventional slope-area method for comparison with those by the simplified method. However, the verified n is indefinite for some stream reaches in table 3, and it could not be computed at all for others. This indicates that, had n been estimated at each of these streams, the discharge computed by the slope-area method also would have been considerably in error.

A FURTHER SIMPLIFICATION

In developing the simplified method it was found that, for nearly full channels of a certain type, discharge may be computed reliably from mean cross-sectional area alone. The relation, shown in figure 4, is

TABLE 3.—*Application of the simplified method to data not used in its derivation*

Stream	Date	Area	Slope	Verified n	Discharge	
					Known	By eq 2
Red Willow, Nebr	8–25–50	297	0.00067	0.015	1,790	855
Rio Grande, N. Mex	5–12–52	1,057	.00091	.015	6,380	5,230
Rio Grande, N. Mex	6–17–52	1,036	.00113	--------	6,100	5,530
Bijou, Colo	8–22–52	1,097	.00343	.02–0.03	7,900	8,830
Pecos, N. Mex	6–24–51	258	.00032	0.25	457	518
S. Fk. Cheyenne, Wyo	5–23–52	1,279	.00185	.026	7,900	8,780
Elkhorn, Nebr	6–26–56	1,240	.00043	.016	6,960	4,760
Lance, Wyo	6–27–52	1,010	.002	.027	5,400	6,590
Little Colorado, Ariz	7–27–40	2,681	.0028	.015	20,100	27,100
Little Colorado, Ariz	7–27–40	2,037	.00725	.05–0.055	20,100	25,300
Trinity, Tex	5–06–50	[1] 5,547	.00055	.065–0.07	25,000±	38,700
Wissahickon, Pa	2–26–62	577	.00158	(?)	2,460	2,880
Cullasaja, N.C	6–16–49	1,702	.00133	.07	8,450	11,400
Deckers, W. Va	4–13–48	391	.00573	.035	3,100	2,630
French Broad, N.C	8–28–49	2,312	.00079	.047	10,100	14,000
Croton, N.Y	3–31–51	726	.0103	.063	4,670	7,090
Cane, N.C	3–28–48	339	.0010	(?)	1,360	1,190
Hominy, N.C	6–16–49	1,219	.00179	.060	6,800	8,140
John Day, Oreg	5–23–48	2,896	.00188	.032	23,000	26,200
Millers, N.Y	3–22–48	912	.00438	.037	5,700	7,470
Mills, N.C	6–16–49	954	.00145	(?)	5,300	5,440
Neversink, N.Y	3–22–48	1,366	.00279	.035	10,100	11,000
Antelope, Nebr	6–17–54	85.4	.00278	(?)	445	277
Captina, Ohio	2–27–62	796	.00047	(?)	3,630	2,740
Antelope, Nebr	5–23–54	18.4	.0021	.029	45	33
Antelope tributary, Nebr	5–01–54	6.3	.0072	.063	10.8	12
Tenaya, Calif	5–17–50	170	.005	.034	886	833
Tenaya, Calif	5–16–50	184	.00202	.033	920	687
Merced, Calif	5–17–50	380	.0097	.067	1,990	2,950
Merced, Calif	5–17–50	464	.00453	.060	1,990	3,070
Merced, Calif	5–20–50	694	.0104	.088	3,950	6,690
Sulfur, Tenn	5–12–49	1,900	.00067	.050	10,100	[2] 10,100
Twelvepole, W. Va	2–14–48	2,496	.00045	.05+	9,350	12,300
San Gabriel, Calif	1–04–64	112	.00109	.032	211	283
Alder, Ariz	2–11–63	36.2	.0181	.067	117	152
Piru, Calif	7–24–62	66.6	.0042	.031	281	227
Cachuma, Calif	2–11–62	171	.0136	(?)	776	1,120
Sycamore, Ariz	2–11–63	240	.0064	.020	2,300	1,420
Salmon, N.Y	4–02–52	141	.0109	.05–0.066	676	814
Salmon, N.Y	4–08–52	136	.0109	.05–0.066	623	776
Salmon, Idaho	6–03–48	9,371	.00148	.040	101,000	114,000
Powder, Wyo	5–24–52	2,110	.00107	--------	22,000	13,900
Salt, Nebr	5–09–50	3,704	.0005	(?)	29,200	21,700
Paradise, Wash	2–28–48	41.8	.0009	.030	90.4	66

[1] Main channel.
[2] Overflow (10 percent) not included.

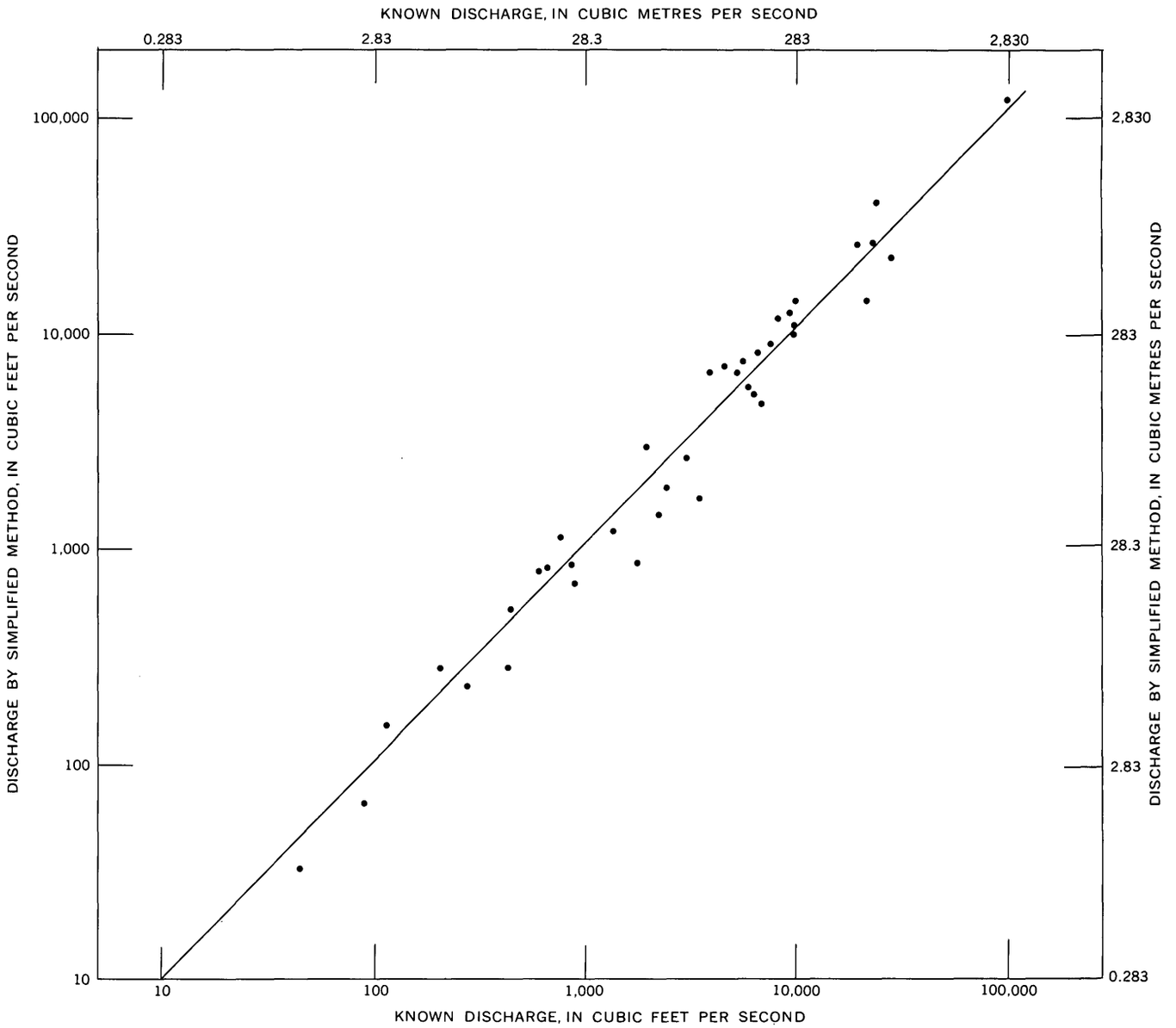

FIGURE 3.—Further evaluation of the simplified method (data from table 3).

based largely on channels in the Pacific Northwest and applies to full channels. Part-full discharges in these channels will be less than the discharges shown by the relation.

Study of the photographs of streams in Barnes' (1967) report should lead to the ability to recognize such stream channels. Figure 4 provides a reconnaissance tool for estimating discharge of near bankfull channels of this type; it is not the simplified method.

APPLICATION OF THE SIMPLIFIED METHOD

Criteria

The reach should be selected according to the same criteria used for a conventional slope-area measurement except that a uniform cross-sectional area throughout is preferable to a contracting reach. Ideally, the reach should be 4 or 5 channel widths long in order that the water-surface slope can be measured accurately. The method has been verified only for nearly full natural channels without substantial overbank flow and without backwater from constrictions or a flooding tributary. Thus it is recommended only for such channels at this time.

These criteria are not as restrictive as they may seem. Necessity often forces the use of the best available reach, which may have undesirable characteristics both for the simplified method and for the conventional slope-area method. Thus a reach which does not meet

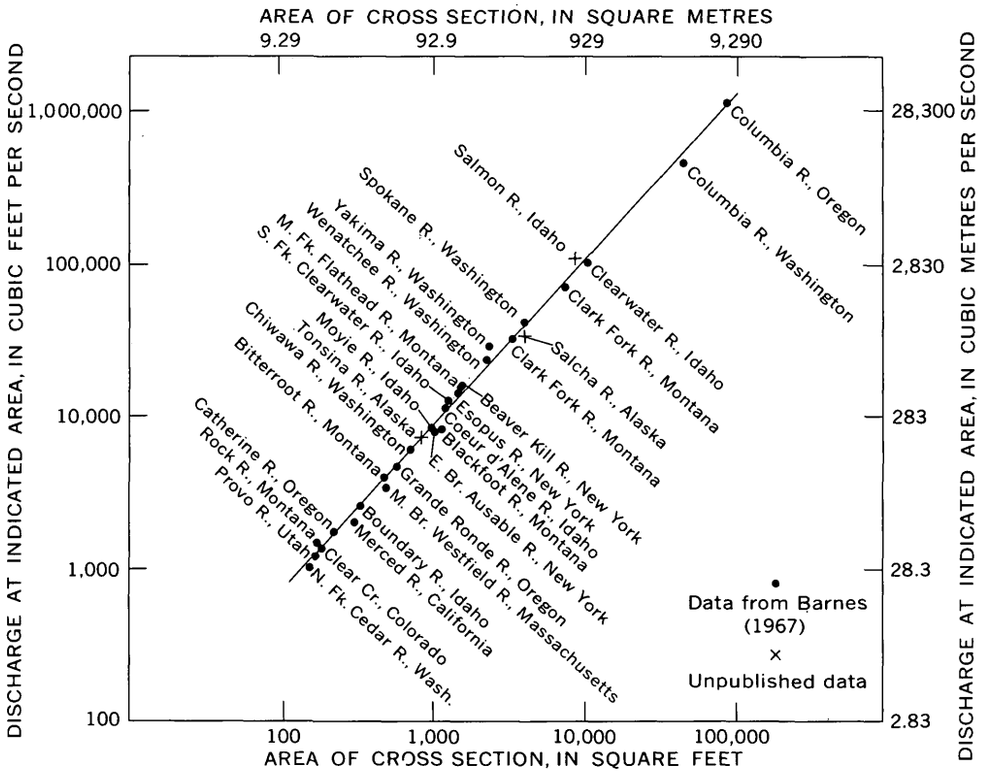

FIGURE 4.—Relation of discharge to channel cross-sectional area for full channels typified by those in Pacific Northwest.

the criteria is used when there is no better way to estimate the flood peak. Table 3 and figure 3 indicate the accuracy attainable by the simplified method from poor or unusual channel reaches.

Procedure

1. To determine peak discharge of a flood from high-water marks:
   (a) Define slope of water surface from high-water marks as a straight line throughout the reach.
   (b) Measure three cross sections so located that their average defines the average cross-sectional area in the reach.
   (c) Apply equation.
2. To determine discharge corresponding to a specific stage, either arbitrarily selected or from a few high-water marks:
   (a) Define water-surface slope as bed slope or slope of water surface at existing stream stage.
   (b) Project defined water-surface slope through specified stage.
   (c) Survey three cross sections and average the areas.
   (d) Apply equation.

Advantages

1. No subjective estimate of a roughness coefficient is required; both cross-sectional area and slope can be measured.
2. A water-surface profile based on high-water marks throughout the reach is desirable, but well-defined water-surface elevations at the ends of the reach may be adequate.
3. Computation of discharge is simple; and one answer is obtained. There is little room for subjective judgments either by the originator or by the reviewer.
4. Two or more measurements at different stages in the same reach will give consistent answers.
5. The method can be applied where only one high-water mark is found.
6. The method appears to give results comparable in accuracy to those from the slope-area method for natural streams.

REFERENCES CITED

Barnes, H. H., Jr., 1967, Roughness characteristics of natural channels: U.S. Geol. Survey Water-Supply Paper 1849, 213 p.

Benson, M. A., and Dalrymple, Tate, 1968, General field and and office procedures for indirect discharge measurements: U.S. Geol. Survey Techniques Water-Resources Inv., book 3, chap. A1, 30 p.

Boyer, M. C., 1954, Estimating the Manning coefficient from an average bed roughness in open channels: Am. Geophys. Union Trans., v. 35, no. 6, pt. 1, p. 957–961.

Dalrymple, Tate, and Benson, M. A., 1967, Measurement of peak discharge by the slope-area method: U.S. Geol. Survey Techniques Water-Resources Inv., book 3, chap. A2, 12 p.

Graf, W. H., 1966, On the determination of the roughness coefficient in natural and artificial waterway: Internat. Assoc. Sci. Hydrology Bull., 11th year, no. 1, p. 59–68.

Limerinos, J. T., 1970, Determination of the Manning coefficient from measured bed roughness in natural channels: U.S. Geol. Survey Water-Supply Paper 1898–B, 47 p.

Riggs, H. C., 1974, Proposed hydrologic analyses of streamflow for Brazil: U.S. Geol. Survey open-file rept., 18 p.

Jour. Research U.S. Geol. Survey
Vol. 4, No. 3, May–June 1976, p. 293–297

DEVELOPMENT OF A STANDARD RATING FOR THE PRICE PYGMY CURRENT METER

By VERNE R. SCHNEIDER and GEORGE F. SMOOT,
Bay Saint Louis, Miss., Reston, Va.

Abstract.—Fifty new Price pygmy current meters, 50 used Price pygmy meters with used rotors, 50 used Price pygmy meters with new rotors, and 26 used Price pygmy meters with straight uniform (nonbeaded) contact wires were rated individually in a towing tank. A standard rating of $V=0.961N+0.039$ ($V=0.293N+0.012$), where V is the velocity in feet per second (metres per second) and N is the meter rotation in revolutions per second, was established for the group of new meters. Repeated ratings of two new meters showed that under the best rating conditions, the individual Price pygmy rating is repeatable to within 1 percent.

The standard errors of velocities predicted using the individual ratings and the standard ratings were compared. The use of the standard rating resulted in statistically higher standard errors than the individual ratings for all groups of meters. However, the differences are a fraction of 1 percent higher and are not of concern for practical purposes. The individual ratings and standard rating for the used meters with new straight contact wires were found to be statistically similar to the ratings for the new meters. Continuation of the use of individual ratings of Price pygmy current meters is probably unnecessary with the implementation of precise standards in their manufacture, rating of a random sample, and use.

The practice of rating each individual Price pygmy current meter (fig. 1) was adopted in the early days of stream gaging when the tolerance allowed in the manufacture of meters was much greater than it is today. If identical meters could be produced by rigid control in manufacturing, a standard rating could be used. A random sample of meters from each production run would be selected for rating to continuously verify the standard rating. In addition, measurements to maintain quality control of the manufacturing process would be required.

Smoot and Carter (1968) reported the results of tests leading to the standard rating of the Price AA meter. They conducted tests to determine the repeatability of rating data, to compare velocities predicted with individually rated meters and standard ratings, and to study effects of wearing parts on meter ratings. A study was also made of the change in rating after field use of meters. These tests concluded that (1) a single rating for a group of current meters of one manufacturer fits all observations as well as individual ratings fit the observations for the individual meter; (2) the standard error of the single rating for a group of meters is due to random errors in the observations rather than differences in meters; and (3) physical changes in the pivot and upper bearing have little influence on the rating, but damage to the bucket wheel can cause appreciable change in the rating. The results of the study by Smoot and Carter (1968) were used to design this study.

PROCEDURE

Pygmy current meters used by the U.S. Geological Survey for streamflow measurements are rated individually by towing the meters in a tank of still water at six different speeds, 0.25, 0.50, 0.75, 1.50, 2.20, and 3.00 feet per second (0.076, 0.152, 0.229, 0.457, 0.671, and 0.915 metre per second). Two runs are made at each speeed, one in each direction in the tank, to average out any minor directional differences. The distance traveled, time of travel, and the number of revolutions of the bucket wheel (rotor speed) are recorded as basic data. The velocity, V, is the ratio of distance to time; the rotor speed, N, is the ratio of the number of revolutions of the bucket wheel to the time; and the meter efficiency is the ratio of the number of revolutions of the bucket wheel to the distance traveled. The meter efficiency, ranging from about 0.90 to 1.05 revolutions per foot (2.95 to 3.44 revolutions per metre) for the pygmy meter, is a useful variable for detecting errors in the rating procedure and malfunctions of the meter. The meter rating is determined from these data by a least-squares fit and is expressed as a linear equation

$$V=KN+C, \qquad (1)$$

where K and C are the rating constants. Equation 1 is used to generate a rating table for field use.

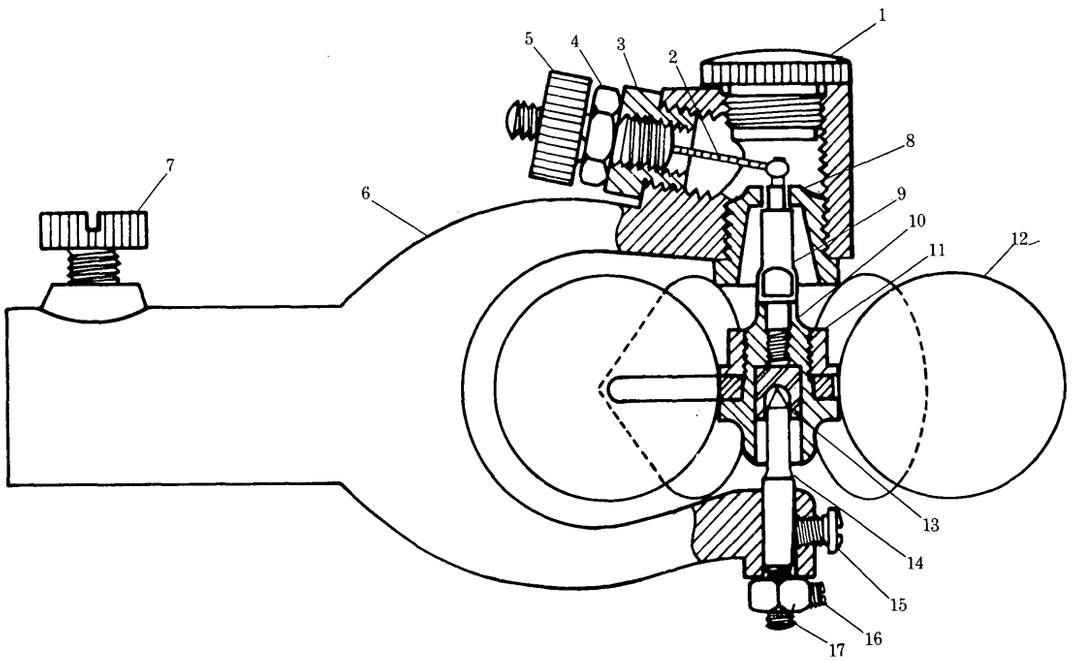

FIGURE 1.—Assembly diagram of pygmy current meter.

To determine the feasibility of a standard rating for the pygmy current meter, a group of 50 new meters manufactured to the same specifications was studied. Two of the new meters were selected at random for a study of the repeatability of rating data. The 50 meters were each calibrated, and the data were used to obtain an average rating for the group.

The bucket wheels of 50 used meters were replaced with new bucket wheels to determine the effects of using new bucket wheels. These meters, some of which were quite old, came from a variety of manufacturers. Another group of 50 used meters whose bucket wheels were found to be in good condition was selected. In addition, a group of the meters whose beaded contact wires were replaced with a straight alloy wire was studied. These tests were run to determine the factors affecting the use of the standard rating for old meters.

All meters tested were purchased by the Survey and conform to the same design specifications, which have not changed since at least 1946. Although different manufacturers and manufacturing techniques have been used, the rating facilities are now more accurate.

REPEATABILITY OF RATING DATA

A large number of runs were made with two new meters at each velocity to establish the repeatability of the data obtained in the tow tank. Care was taken to select days when the the temperature-driven velocity currents in the tank were small. A rating in the form of equation 1 was established by least squares using all the data for each meter. These ratings, $V=0.987N+0.029$ and $0.945N+0.030$ ($V=0.301N+0.007$ and $0.288N+0.009$) were used to adjust all of the data so that each velocity was obtained with a constant rotor speed. The constant rotor speed used was computed from the ratings for each tow vehicle speed. Then each sample velocity was adjusted to the constant rotor speed by sliding it parallel to the rating for each meter. The standard deviation of the velocity expressed as a percentage of the mean velocity is shown in table 1. The maximum error inherent in measuring distance and time in the tank is approximately 0.1 percent. The balance of the error is explained by physical differences in the construction of the meter, residual velocity currents in the tow tank, and other small random errors inherent in the rating procedure. The errors are virtually inseparable.

TABLE 1.—*Repeatability of rating data*

Mean velocity (feet per second)[1]	Number of runs	Standard deviation of velocity indicated by meter as percent of mean velocity	
		Meter Y–0033	Meter Y–0044
0.25	85	1.29	0.98
.50	40	.65	.61
.75	40	.94	1.27
1.52	30	.54	.43
2.24	20	.38	.33
3.03	20	1.14	.33

[1] To change feet per second to metres per second, multiply by 0.3048.

In general the pygmy meter data are more repeatable than those of the Price AA meter as reported by Smoot and Carter (1968). This does not imply that the Price pygmy meter is a more stable meter than the Price AA. The tests reported by Smoot and Carter (1968) were conducted in an older tow tank. The methods of measuring distance and time were different and probably less accurate than the methods presently used. The same factors causing error existed in both situations, but the improvement in the tow vehicle has resulted in improved accuracy and precision.

COMPARISON OF INDIVIDUAL AND AVERAGE RATINGS

The rating data and equations were available for four groups of meters:

Group 1—Fifty new Price pygmy meters.

Group 2—Fifty used Price pygmy meters whose bucket wheels were found to be in good condition and were not replaced.

Group 3—Fifty used Price pygmy meters whose bucket wheels were replaced during the repair process with new bucket wheels.

Group 4—Twenty-six used meters with used bucket wheels whose beaded contact wires were replaced with straight (nonbeaded) alloy wire.

The following information was used: (1) 12 observations of car velocity V and the corresponding rotor speed N for each meter; (2) a rating equation for each individual meter; and (3) an average rating computed for the group of new meters. The average rating equation for the new meters is

$$V=0.961N+0.039. \qquad (2)$$

Equation 2 is used as the standard rating for purposes of comparison in this paper.

Standard errors were computed at each two-vehicle speed for each group of meters. The measured rotor speed was used to compute velocity from the individual ratings and from the standard rating (eq 2) for each rating point. The standard error of the velocity using the individual rating was computed from the deviation of the measured velocity from the individual rating for each meter and summed over all meters for the group. The standard error of the velocity using the standard rating (eq 2) was computed from the deviation of the measured velocity for each meter from the standard rating (eq 2). The square of the standard error is approximately equal to the variance of the rating data at each two vehicle speed. The F-distribution was used to test the hypothesis that the variances of the rating data at each tow vehicle speed of two groups of meters are equal.

Group 1

The 50 new pygmy meters were used to study the comparability of using individual and standard ratings. The results, standard error as a percentage of the mean, are summarized in table 2.

TABLE 2.—*Comparison of standard errors computed using individual and standard rating equations for the group of 50 new meters*

Velocity (feet per second)[1]	Standard error as percent of mean velocty		Statistical comparison of individual and standard ratings[2]
	Individual rating	Standard rating	
0.25	4.18	4.45	a
.50	1.36	1.76	a
.75	1.04	1.60	b
1.50	.95	1.39	b
2.20	.61	1.12	b
3.00	.46	1.04	b

[1] To change feet per second to metres per second, multiply by 0.3048.
[2] a, not significantly different at the 5-percent level of significance; b, significantly different at the 5-percent level of significance.

A standard rating fits the observed data for a group of meters with almost the same accuracy as the individual equations fit the corresponding data for the individual meter. However, the differences are statistically significant at the 5-percent level for the sample velocities, 0.75, 1.50, 2.20, and 3.00 ft/s (0.229, 0.457, 0.671, and 0.915 m/s).

The standard errors in table 2 are larger than those reported for a single meter in table 1. The difference is probably explained by the fact that the individual ratings were obtained over a wider range of tow-tank conditions (primarily small temperature-driven velocity currents). Even though the meters are manufactured to close tolerances, small physical differences probably contribute to the observed errors.

Examination of the data in table 2 indicates that the standard error for the standard rating is only a fraction of 1 percent larger than that for the individual rating for each sample velocity. Therefore, for all practical purposes, the individual rating and standard rating yield identical results for the new meters.

Because of its size, the pygmy meter is often used as a low-velocity meter in shallow flows. The data indicate that the errors increase significantly for low velocities.

Group 2

Fifty used meters whose bucket wheels were found to be in good condition, and, therefore, not replaced, were used to study the effects of used bucket wheels. The individual and standard rating results are shown in table 3. Comparison of the results show that the standard error due to the use of the standard rating

TABLE 3.—*Comparison of standard errors computed using individual and standard rating equations for the group of 50 used meters with used bucket wheels*

Velocity (feet per second)[1]	Standard error as percent of mean velocity		Statistical comparison of individual and standard ratings[2]
	Individual rating	Standard rating	
0.25	4.26	5.12	a
.50	1.68	2.22	b
.75	1.19	1.88	b
1.50	.95	1.92	b
2.20	.61	1.76	b
3.00	.50	1.74	b

[1] To change feet per second to metres per second, multiply by 0.3048.
[2] a, not significantly different at the 5-percent level of significance; b, significantly different at the 5-percent level of significance.

is consistently higher than the individual rating. These results are significantly different at the 5-percent level for the sample velocities 0.50, 0.75, 1.50, 2.20, and 3.00 ft/s (0.152, 0.229, 0.457, 0.671, and 0.915 m/s).

Group 3

The ratings of 50 used meters whose bucket wheels were replaced during the repair process were studied to determine the effect of using new bucket wheels. Comparison of the standard errors computed using the individual and standard ratings (eq 2) is made in table 4. The standard error due to the use of the standard rating is consistently higher than that due to the individual rating. The differences are not statistically different at the 5-percent level for the sample velocity 0.75 (0.229).

TABLE 4.—*Comparison of standard errors computed using individual and standard rating equations for the group of 50 used meters with used bucket wheels*

Velocity (feet per second)[1]	Standard error as percent of mean velocity		Statistical comparison of individual and standard ratings[2]
	Individual rating	Standard rating	
0.25	4.55	6.01	b
.50	1.86	2.45	b
.75	1.29	1.57	a
1.50	.94	1.25	b
2.20	.69	.85	b
3.00	.64	1.38	b

[1] To change feet per second to metres per second, multiply by 0.3048.
[2] a, not significantly different at the 5-percent level of significance; b, significantly different at the 5-percent level of significance.

Group 4

The effect of the contact wire was studied using a group of 26 used meters whose beaded contact wires were replaced with a 0.25-millimetre diameter straight wire. The composition of the wire was 35 percent palladium, 30 percent silver, 15 percent copper, 10 percent platinum, and 10 percent gold. The results are compared in table 5.

The standard error due to the use of the standard rating again is consistently higher than the individual rating. The differences are statistically significant at the 5-percent level for sample velocities 0.50, 0.75, 1.50, 2.20, and 3.00 ft/s (0.152, 0.229, 0.457, 0.671, and 0.915 m/s).

TABLE 5.—*Comparison of standard errors computed using individual and standard rating equations for the group of 26 used meters with straight contact wires*

Velocity (feet per second)[1]	Standard error as percent of mean velocity		Statistical comparison of individual and standard ratings[2]
	Individual rating	Standard rating	
0.25	3.81	4.98	a
.50	1.56	2.43	b
.75	1.02	1.87	b
1.50	0.84	1.48	b
2.20	0.48	1.42	b
3.00	0.47	1.52	b

[1] To change feet per second to metres per second, multiply by 0.3048.
[2] a, not significantly different at the 5-percent level of significance; b, significantly different at the 5-percent level of significance.

COMPARISONS OF GROUPS OF METERS

Using the four groups of meters in various combinations, the following three factors affecting meter performance were tested: (1) The effect of using used bucket wheels on used meters was studied by comparing group 2 to group 1; (2) the effect of new bucket wheels on used meters was studied by comparing group 3 to group 1; and (3) the effect of the contact wire was studied by comparing group 4 to group 1.

The individual and standard ratings of all groups of meters were compared to the individual and standard ratings for group 1 to determine if the physical properties of the meters would affect their rating.

The results of the statistical analysis are summarized in tables 6 and 7. The comparison of the individual ratings is summarized in table 6 and the standard ratings in table 7.

TABLE 6.—*Statistical comparison of the variances of the individual rating equations for the groups of meters*
[a, not significantly different at the 5-percent level of significance]

Velocity (feet per second)[1]	Group 2 versus group 1	Group 3 versus group 1	Group 4 versus group 1
0.25	a	a	a
.50	a	a	a
.75	a	a	a
1.50	a	a	a
2.20	a	a	a
3.00	a	a	a

[1] To change feet per second to metres per second, multiply by 0.3048.

TABLE 7.—*Statistical comparison of the variance of the standard rating equations for the groups of meters*
[a, not signficantly different at the 5-percent level of significance; b, significantly different at the 5-percent level of significance]

Velocity (feet per second)[1]	Group 2 versus group 1	Group 3 versus group 1	Group 4 versus group 1
0.75	a	b	a
.50	a	b	a
.75	a	a	a
1.50	b	a	a
2.20	b	a	a
3.00	b	b	b

[1] To change feet per second to metres per second, multiply by 0.3048.

The individual ratings of group 2 (table 6) results are not significantly different at the 5-percent level from the group 1 meters. The standard rating results (table 7) were found to be significantly different at the 5-percent level for the sample velocities 1.50, 2.20, and 3.00 ft/s (0.457, 0.671, and 0.915 m/s).

The individual and standard rating results of group 3 were compared to the group 1 meters. The individual rating results (table 6) are not significantly different from the group 1 meters at the 5-percent level. The standard rating results (table 7) are significantly different at the 5-percent level for sample velocities 0.25, 0.50, and 3.00 ft/s (0.076, 0.152, and 0.915 m/s).

The individual rating results of group 4 (table 6) are not significantly different at the 5-percent level from the group 1 meters. The standard rating results (table 7) are not significantly different at the 5-percent level from the group 1 meters for all sample velocities except 3.00 ft/s (0.915 m/s).

RESULTS

In all cases the use of individual ratings were found to give results which were not statistically different from the group 1 meters (table 2). This result implies that the physical differences in the meters and other random errors can, in effect, be accounted for in the rating process. The errors in the individual ratings are an indication of the expected error due to the meter for velocity measurements made with individually rated pygmy meters.

The results (table 7) obtained in using the standard rating (eq 2) are statistically different from the group 1 meters at several specific velocities. When a new beaded wire contact was used in the case of the group 1 meters and the uniform straight contact wire was used in the case of the group 4 meters, statistically similar results were obtained. The favorable comparison of the standard rating results to the group 1 meters indicates that the use of the straight uniform contact wire affects the rating results beneficially. If the rating results were the only consideration, it would be beneficial to replace all contact wires with the straight alloy wire. The difference observed for the other two groups of meters may be related to the fact that many used contact wires were left on the used meters when repaired. The repair records do not indicate what action was taken. Meters to be repaired have had a variety of nonstandard (penta counter contact, five-strand wire, no bead, and so forth) contact wires as replacements, wires of varying stiffness, and solder in the wire braid. In the repair process, wires are replaced when they are obviously faulty or nonstandard. However, there is considerable variability in stiffness among contact wires on the old meters as rated. For any individual meter, the contact wire stiffness would be accounted for in the rating; thus, it would not increase the standard error of the individual ratings. When compared to the standard rating, the variability could cause a wider scatter in the ratings, especially at low velocities, and a higher standard error.

SUMMARY AND CONCLUSIONS

Individual ratings of Price pygmy meters are probably unnecessary for practical purposes even though the differences between the individual and standard ratings are statistically significant. The actual standard error of the standard rating is a fraction of 1 percent larger than the individual rating for new meters. There is no statistical difference between individual ratings of new meters, used meters with new bucket wheels, used meters with used bucket wheels, or used meters with used bucket wheels and new contact wires. This suggests that physical differences in the meter and other random errors are accounted for in the rating process. An analysis of the results using the standard rating indicates that the contact wire has a small but statistically significant effect on the rating. The contact wire should be standardized and replaced whenever necessary.

On the basis of these results, by setting rigid standards during the manufacturing process and establishing a quality control procedure, a standard rating could be implemented for the pygmy current meter. Appreciable money could be saved in eliminating the need for individual ratings without sacrificing accuracy of current-meter measurements; and, in addition, the need for a central repair facility could be eliminated.

REFERENCE CITED

Smoot, G. F., and Carter, R. W., 1968, Are individual current meter ratings really necessary? Am. Soc. Civil Engineers, Jour. Hydraulics Div., v. 94, no. HY2, p. 391–397.

Jour. Research U.S. Geol. Survey
Vol. 4, No. 3, May–June 1976, p. 299–304

EPIFAUNA AT JACKSON POINT IN PORT VALDEZ, ALASKA, DECEMBER 1970 THROUGH SEPTEMBER 1972

By JON W. NAUMAN and DONALD R. KERNODLE, Anchorage, Alaska

Abstract.—A biological sampling program at Jackson Point in Port Valdez, Alaska, was begun in December 1970. Sixteen artificial substrate samplers (8 multiplate and 8 rock-filled baskets with net liners) were retrieved after 2 to 4 months' exposure. The most common groups in order of their abundance were Copepoda, Foraminifera, Nematoda, and Ostracoda during winter; Copepoda, Nematoda, Cirripedia, and Foraminifera, during spring; Pelecypoda, Amphipoda, Insecta, and Cirripedia during summer; and Pelecypoda, Copepoda, Insecta, and Nematoda during fall. The most abundant species collected during the study were the blue mussels (*Mytilus edulis*), copepods (*Harpacticus* sp.), midges (*Clunio* sp., Chironomidae), and fairy shrimp (unidentified amphipods). During the summer and fall of 1972 the total number of epifaunal organisms was 22 times greater than during the same period in 1971, with *Mytilus edulis* comprising 88 percent of the community in 1972 (more than triple the percentage for 1971). The two sampler types collected approximately the same major groups of organisms; however, the multiplate samplers collected an average of 1.6 times more organisms than the basket samplers. The basket sampler, on the other hand, collected three more species per sample than did the multiplate samplers, resulting in species diversities 0.3 to 0.6 greater than those of the multiplate samplers. Diversity values were lower during 1972, except for the spring sample. Seasonal diversity varied from a low of 0.36 in the summer of 1972 to a high of 3.99 in the fall of 1971.

After the discovery of the Prudhoe Bay oil field on the Alaskan North Slope, the U.S. Geological Survey undertook a preconstruction biological sampling program along the trans-Alaska pipeline corridor (Nauman and Kernodle, 1974). This study included a preliminary qualitative epifaunal sampling program at the proposed terminal site, Jackson Point in Port Valdez.

Studies at Jackson Point were initiated to (1) test the feasibility of using artificial substrate samplers in a subarctic marine fiord estuary, (2) expand knowledge of the structure of the biotic community near the terminal site, (3) supplement studies of benthic and littoral biotic communities conducted by other agencies, and (4) set up a preconstruction baseline biological sampling program at the terminal site.

Epifaunal organisms are abundant in estuaries and coastal waters. These organisms comprise that part of the aquatic community which lives attached to or crawls on the bottom, particularly on such substrates as rocks, pilings, and buoys. These substrates are easy to simulate and therefore this group of organisms is easily collected on artificial substrates.

Because most epifaunal organisms are immobile and adapted to specific conditions, but restricted in their distribution by physical environmental conditions, they can be used to detect changes in water quality. Increased suspended sediment from construction activities or pollution resulting from oil spills or pipeline leaks can have deleterious effects on many epifaunal species (Pearce, 1972). Monitoring the epifaunal community may permit detection of pollution.

Cory (1967) summarized the history and use of artificial substrates in marine studies and demonstrated that both quantitative and qualitative biological data could be obtained from test panels. The use of artificial substrates for freshwater benthic invertebrate studies is well documented (Slack and others, 1973) and has been the major biological sampling technique of the Geological Survey, particularly in its national stream-quality accounting network.

To our knowledge, except for the intertidal surveys conducted in Prince William Sound by Haven (1971), Mueller (1973), Nybakken (1971), Natasha Smith (written commun., 1972), and the environmental studies of Port Valdez by Feder, Mueller, Dick, and Hawkins (1973), no studies of marine epifaunal organisms collected on artificial substrates have been reported in Alaska.

Port Valdez is a subarctic marine fiord and an embayment of Prince William Sound (fig. 1). It is 21 km (13 mi) long and 4.5 km (2.8 mi) wide with a maximum depth of 240 m (787 ft). The weather at Port Valdez is influenced by subarctic winds off the Chugach Mountains and off the Valdez Glacier. The effects of these winds are moderated by ocean currents coming

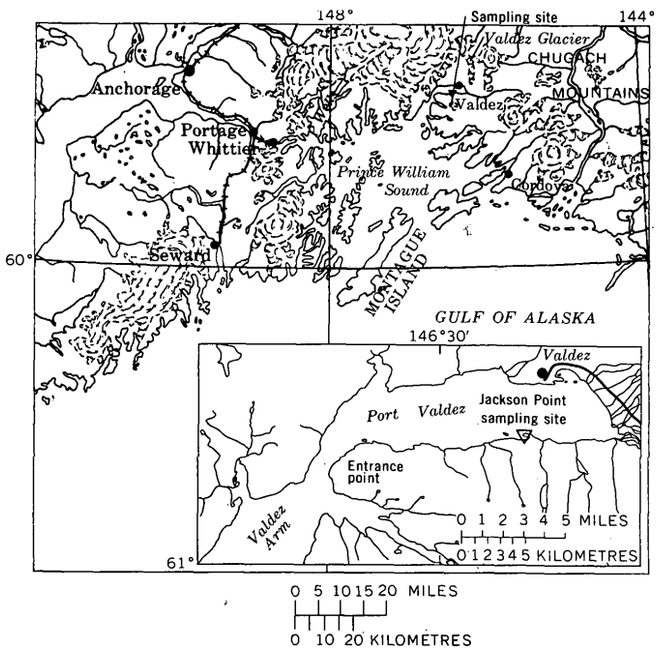

FIGURE 1.—Location of sampling site in Port Valdez.

through Prince William Sound (Searby, 1968). The hydrography and circulation in Port Valdez are controlled by tides, precipitation, freshwater runoff, winds, and surface air temperatures (Muench and Nebert, 1973).

Jackson Point, the study site, is the outermost westerly tip of a small peninsula paralleling the southern shoreline of Port Valdez (fig. 1) and was the site of the Jackson Point Cannery prior to the 1964 earthquake (Coulter and Migliaccio, 1966).

SAMPLING METHODS

This study was conducted from September 25, 1970, to September 22, 1972. Two types of samplers were used: A multiplate sampler (Fullner, 1971) (fig. 2) and a collapsible vegetable washbasket lined with nylon-screen cloth having a mesh opening of 216 μm and filled with 40 rocks ranging from 25 to 50 mm (1 to 2 in) in diameter (fig. 3). The samplers were retrieved after 2 to 4 months' exposure, the longer exposures occurring during the winter.

One basket sampler was installed in September 1970 and retrieved in December 1970; however, this sample had been exposed repeatedly to air during low tides and therefore it was discarded. At this time the decision was made to use one multiplate and one basket sampler per season. In December 1970, one multiplate and one basket sampler were attached to a mooring line on shore and placed on the bottom about 6 m (20 ft) offshore from the high-tide line. This first set of samples was retrieved in April 1971 and, for convenience of discussion, is designated the spring 1971 sample and marks the beginning of the study for this report.

Samples installed in April or May and retrieved in July are designated summer samples. Fall samples are those installed in July and retrieved in September. The same schedule was followed during 1971 and 1972. Only one set of samples was designated as winter; this set was installed in September 1971 and retrieved in February 1972.

The spring 1971 multiplate sampler was discarded after it was determined that it had been repeatedly

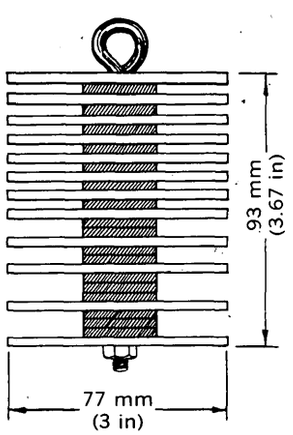

FIGURE 2.—Multiplate sampler.

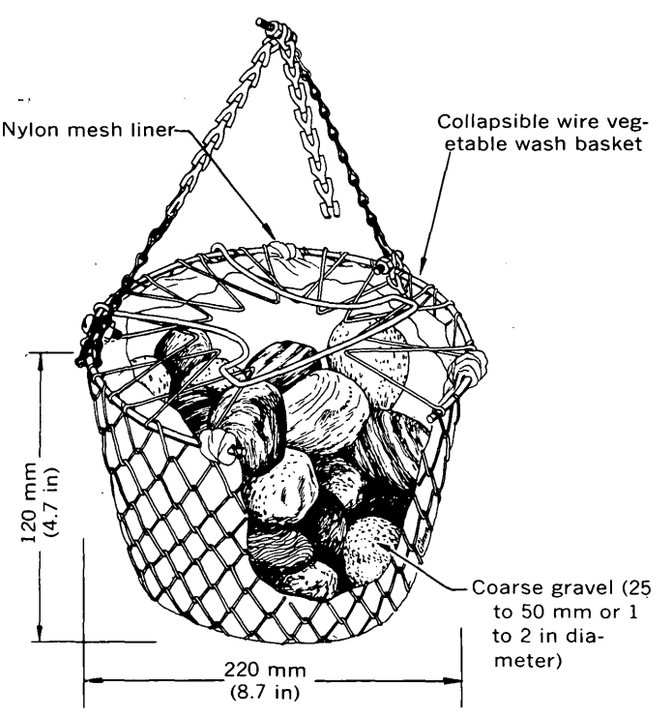

FIGURE 3.—Basket sampler.

exposed to air. In May 1971, an attempt was made to suspend a multiplate sampler from a surface float at a predetermined depth beneath the water surface. This method failed because of improper mooring and the multiplate sank to the bottom near the other samplers. This multiplate sampler was later recovered, after 4 months' exposure, and its specimens have been included in the analysis as part of the fall 1971 sample. In July 1971 an offshore platform was constructed, making it possible to place samplers 0.9 m (3 ft) below mean tide level of 1.9 m (6.3 ft) (U.S. Dept. of Commerce, 1951).

Epifaunal organisms were preserved in 40 percent isopropyl alcohol at the time of collection. In the laboratory, major taxonomic groups were separated and identified. Separated samples were then sent to Dr. G. J. Mueller, curator of the Marine Sorting Center of the University of Alaska, for species identification. We are most grateful to Dr. Mueller for this service.

Water-quality data were collected at the site at the time of retrieval of the samplers. These data as well as summary of data collected near Jackson Point by Hood, Shiels, and Kelley (1973) are presented in table 1.

TABLE 1.—*Physical and water-quality parameters from data collected near Jackson Point, Alaska, from fall 1970 to fall 1972*

[Precipitation average was 152 cm/yr and tide range was 3.7 m (12 ft)]

Parameter	Range
Air temperature	−6° - 21°C
Water temperature	−2.5°- 11.0°C
Salinity	24 - 32.5 mg/l
Dissolved oxygen	6.3 - 8.2 mg/l
pH	7.2 - 8.9
Alkalinity HCO_3	42 -144 mg/l
Turbidity	1 - 8 Jtu
Chlorophyll *a*	0.1 - 11.0 mg/l
Current velocity	2 - 3 cm/s

RESULTS AND DISCUSSION

The average seasonal epifaunal community composition and species abundance based on collections from multiplate and basket samplers from December 1, 1970, through September 22, 1972, are shown in table 2. (A basket sampler installed in September 1970 and a multiplate sampler installed in December 1970 have been excluded from this table for reasons stated previously.) Data in this table are given as averages for two sampler types in order to simplify description of seasonal species abundance and community composition. Although the taxa varied seasonally, a composite of all samples indicate that the dominant groups, in order of abundance, were Pelecypoda, Copepoda, and immature Insecta (table 3). Individuals of the pelecypod *Mytilus*

TABLE 2.—*Epifauna seasonal abundance averaged from multiplate and basket samplers collected December 1970 to September 1972*

TAXA		Summer[1]		Fall[1]		Winter	Spring		Total collection
		1971	1972	1971[3]	1972	1971–72	1971[2]	1972	
Foraminifera (forams)	*Elphidium frigidum*	----	----	----	----	346	350	61	757
	Unidentified Foraminifera	----	----	1	----	----	7	----	8
Turbellaria (flat worms)	Unidentified Turbellaria	----	----	1	----	----	----	----	1
Nematoda (nematodes)	Unidentified Nematoda	4	49	17	76	152	650	32	980
Polychaeta (marine worms)	*Capitella capitata*	----	----	----	16	----	----	----	16
	Eteone longa	----	----	----	----	----	----	10	10
	Harmothoe imbricata	----	2	----	----	2	----	----	4
	Heteromastus filigormis	20	4	----	2	----	----	----	26
	Nereis sp.	----	----	----	----	----	----	1	1
	Pectinaria sp.	----	----	----	----	3	----	----	3
	Polydora quadrilobata	----	----	----	14	----	----	----	14
	Polydora sp.	----	3	----	----	----	----	----	3
	Sphaerosyllis erinaceus	----	----	----	24	----	----	----	24
	Syllidae	----	----	4	----	----	----	----	4
Ostracoda (seed shrimp)	*Leptocythere* sp.	68	26	35	52	88	70	21	360
Copepoda (copepods)	Unidentified nauplii	----	----	11	----	----	----	----	11
	Halectinosoma finmarchicum	6	1	9	15	66	----	53	150
	Halectinosoma sp. A	22	18	57	314	264	115	29	819
	Harpacticus sp.	27	19	17	291	454	371	314	1,493
	Harpacticus sp. (nauplii)	----	----	28	----	----	----	----	28
	Heterolaophonte cf. *H. mendax*	9	18	6	134	54	90	190	501
	Mesocha pygmea	4	----	4	64	15	13	4	104
	Unknown sp. A	9	9	6	----	149	51	50	274
	Unknown sp. B	22	30	12	----	601	50	560	1,275
	Unknown sp. C	1	----	----	----	22	----	19	42
Cumacea (shrimplike crustaceans)	*Leucon nasica*	----	----	----	2	----	----	----	2
Cirripedia (barnacles)	*Balanus balanoides*	316	112	33	----	----	150	75	686
	Balanus balanoides cyprid	----	----	----	----	----	100	177	277

See footnotes at end of table.

TABLE 2.—*Epifauna seasonal abundance averaged from multiplate and basket samplers collected December 1970 to September 1972*—Continued

TAXA		Summer[1]		Fall[1]		Winter	Spring		Total collection
		1971	1972	1971[3]	1972	1971–72	1971[2]	1972	
Isopoda (isopods)	*Gnorimosphaeroma oregonensis*	----	4	----	4	----	----	----	8
	Limnoria (phycolimnoria) algarum	----	----	3	12	1	----	1	17
	Pentidotea wosensenskii	----	----	----	4	----	----	----	4
	Unidentified Isopoda	----	----	----	----	4	----	----	4
Amphipoda (fairy shrimp)	Unidentified amphipods	3	1,293	2	70	46	----	9	1,423
	Unidentified amphipods tube	----	----	1	----	----	----	----	1
Natantia (shrimp)	*Heptacarpus brevirostris*	----	----	----	----	1	----	----	1
	Pandalus hypsinotus	----	----	----	----	1	----	----	1
Brachyura (crabs)	*Hemigrapsus oregonensis*	----	----	1	----	----	1	----	2
Anomura (hermit crabs)	*Pagurus hirsutiusculus*	----	8	3	8	1	----	----	20
Pelecypoda (clams)	*Crenella* cf. *C. grisea*	----	----	59	----	----	----	----	59
	Hiataella arctica	----	24	13	----	----	----	----	37
	Macoma inconspicua	----	----	----	----	16	----	----	16
	Modiolus modiolus	----	----	21	----	----	----	----	21
	Mytilus edulis	1,084	51,510	13	6,158	37	10	77	58,889
Gastropoda (snails)	*Alvania compacta*	----	29	----	----	----	----	1	30
	Collisella persona	24	----	4	----	1	2	2	33
	Lacuna marmorata	24	----	4	70	43	1	5	147
	Littorinia sitkana	4	----	1	----	----	----	----	5
	Rissoella translucens	----	44	1	----	----	----	----	45
	Unidentified veliger	12	----	----	----	----	----	----	12
Insecta (midges)	*Clunio* sp. (larvae)	252	820	55	290	7	40	25	1,489
	Clunio sp. (pupa)	----	6	----	----	----	----	----	6
(beetles)	*Diaulota* sp. (larvae)	----	----	----	----	----	10	----	10
Echinodermata (sea stars)	*Evastarius trocheli*	----	----	----	----	1	----	----	1
	Leptasterius sp.	----	----	----	----	1	----	----	1
Acaridae (marine mites)	*Copidognathus* sp.	12	6	54	34	12	20	26	164
	Halacaridae sp. 1	----	----	----	----	----	----	1	1
	Halacaridae sp. 2	----	----	1	----	----	----	----	1
	Halacaridae sp. 3	4	----	----	----	----	----	----	4
Pisces (fish)	*Aspidophoroides bortoni* embryo	----	----	----	----	----	----	68	68
	Pholis laeta	----	----	1	1	1	----	----	3
	Xiphister mucosus	----	----	----	----	1	----	----	1
Totals:									
Invertebrate individuals		1,927	54,035	478	7,655	2,390	2,101	1,811	70,397
Species		21	21	31	21	29	18	24	58
Average diversity[4]		2.19	0.36	3.99	1.36	3.26	2.95	3.19	----
Average diversity minus *Mytilus edulis*		3.01	2.00	3.92	3.29	3.19	2.85	3.07	----

[1] Species averaged for basket and multiplate samplers.
[2] Basket sampler only.
[3] Includes species for two multiplate and one basket sampler for one season.
[4] Average diversity, $d = -\sum_{1}^{s}(n_i/N)\log_2(n_i/N)$, where s=number of taxa, n_i=number of individuals per taxon, and N=total number of organisms.

TABLE 3.—*Average seasonal abundance of major epifauna groups collected at Jackson Point*

Major epifauna groups	Summer		Fall		Winter	Spring		Total
	1971	1972	1971	1972	1971–72	1971	1972	
Foraminifera	----	----	1	----	346	357	61	765
Turbellaria	----	----	1	----	----	----	----	1
Nematoda	4	49	17	76	152	650	32	980
Polychaeta	20	9	4	56	5	----	11	105
Ostracoda	68	26	35	52	88	70	21	360
Copepoda	100	95	150	818	1,625	690	1,219	4,697
Cumacea	----	----	----	2	----	----	----	2
Cirripedia	316	112	33	----	----	250	252	963
Isopoda	----	4	3	20	5	----	1	33
Amphipoda	3	1,293	3	70	46	----	9	1,424
Natantia	----	----	----	----	2	----	----	2
Brachyura	----	----	1	----	----	1	----	2
Anomura	----	8	3	8	1	----	----	20
Pelecypoda	1,084	51,534	106	6,158	53	10	77	59,022
Gastropoda	64	73	10	70	44	3	8	272
Insecta	252	826	55	290	7	50	25	1,505
Echinodermata	----	----	----	----	2	----	----	2
Acaridae	16	6	55	34	12	20	27	170
Pisces	----	----	1	1	2	----	68	72
Total	1,927	54,035	478	7,655	2,390	2,101	1,811	70,396

edulis (blue mussel) were the most abundant organisms in nearly all the samples collected during summer and fall. Most of these samples were collected shortly after sets of *M. edulis* had occurred. An average of 51,510 *M. edulis*, averaging 0.7 mm (0.3 in) in size, was collected during summer 1972.

The second most abundant group was the Copepoda; these species were most numerous during winter and spring. The dominant copepod shifted seasonally from "unknown sp. B" to *Harpacticus* sp. and *Halectinosoma* sp. B. There is some evidence that *Harpacticus* sp. migrates from the subintertidal zone in winter to the beach intertidal zone in summer (H. M. Feder, oral commun., 1974). Immature Insecta, the third most common group of organisms and represented primarily by

the midge *Clunio* sp., were more abundant during the summer and fall. The relative seasonal abundance of these three groups is summarized in figure 4.

During summer the dominant species in order of abundance (total numbers averaged for the 2 years) were the blue mussel (*Mytilus edulis*), fairy shrimp (unidentified amphipods), midges (*Clunio* sp.), and acorn barnacles (*Balanus balanoides*). During the fall the dominant species (total numbers averaged for the 2 years) were *Mytilus edulis*, copepods (*Halectinosoma* sp. A and *Harpacticus* sp.), *Clunio* sp., and unidentified nematodes. In winter the dominant species (total numbers for 1 year) were Copepoda (unknown sp. B and *Harpacticus* sp.), Foraminifera (*Elphidium frigidum*), unidentified nematodes, and seed shrimp (*Leptocythere* sp.). In spring dominant species were the Copepoda (*Harpacticus* sp. and "unknown sp. B"), unidentified nematodes, *Balanus balanoides*, and *Elphidium frigidum;* spring total numbers were averaged for the 2 years.

The average total numbers of epifauna organisms taken from the two sampler types ranged from 478 in the fall of 1971 to a high of 54,035 in the summer of 1972. Fifty-eight different species were collected, including three fish species. During spring 1971 only 18 different species were collected, as compared to a maximum of 31 species collected in fall 1971. Fall and winter collections averaged 26 and 29 species, respectively, whereas spring and summer collections had 21 species.

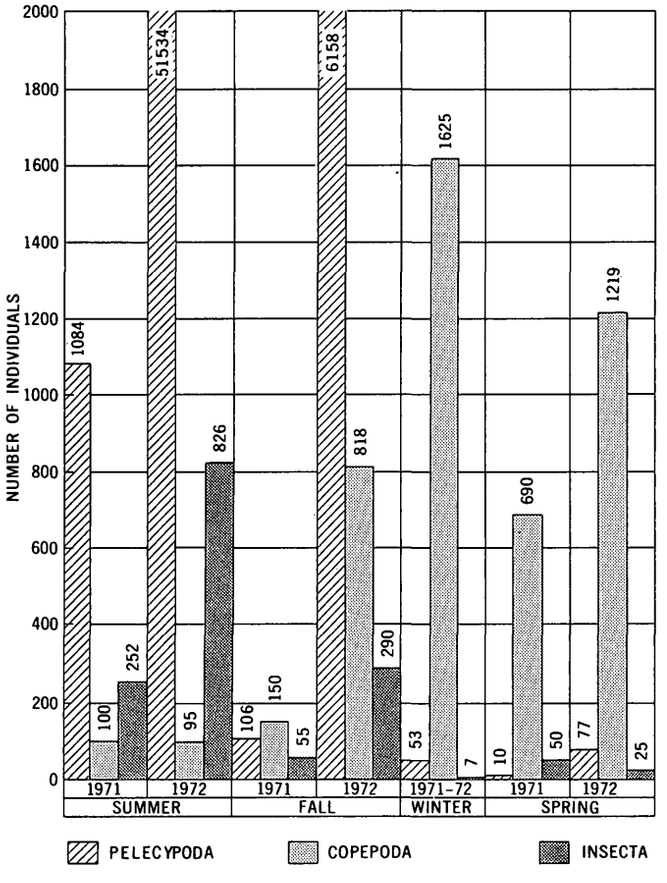

FIGURE 4.—Seasonal distribution of the three most abundant epifaunal groups from totals for the 14 samples collected.

Species diversities were calculated using information theory as described by Wilhm (1970). Diversity values for the combined samples from the two artificial substrates ranged from a low of 0.36 for summer 1972 to a high of 3.99 for fall 1971 (table 2). Except for spring 1972, diversity values were lower in 1972 than in 1971.

It should be noted that the lowest diversity values were due to the overwhelming dominance of the single species *Mytilus edulis*. If *M. edulis* were excluded from the calculations, the diversity values would increase to 1.99 during summer 1972 and 3.92 for fall 1971. These values are similar to those reported by Boesch (1972) for Puget Sound benthos and by Feder, Mueller, Dick, and Hawkins (1973) for Port Valdez benthos collected in the vicinity of this study during fall 1971.

The epifauna collections from the two types of samplers differed in the species composition and in individual abundance. These differences should be expected because of the construction of the two sampler types. Neither type collected all the species present on the natural substrate nor did both sampler types collect the same species. The basket sampler collected, on the average, three more species per sampler than did the multiplate sampler. The multiplate sampler, however, collected 1.6 times as many total specimens as the basket sampler (table 4).

Average diversity values (December 1970 to September 1972) for each individual sampler were 1.91 for the multiplate samplers and 2.51 for the basket samplers (table 4). Fullner (1971) compared collections from a multiplate sampler to those from a basket sampler without a net liner and concluded that the performance of the two samplers compared favorably. Mason, Weber, Lewis, and Julian (1973) found that some species preferred one sampler type to another. In this study, by using a net liner in the basket, both the number of species collected and the species diversity values were increased. It seems that the added inconvenience of increased size and weight of the basket sampler and the difficulty of retrieving the organisms are more than balanced by its ability to collect more of the available species. It is interesting to note that the isopod (*Limnoria* (*Phycolimnoria*) *algarum*) was collected only on the multiplate sampler. This species has not previously been recorded north of Oregon.

TABLE 4.—*Comparison of epifauna seasonal abundance determined from multiplate and basket samplers retrieved December 1970 to September 1972*

	Summer				Fall				Winter		Spring			
	1971		1972		1971		1972		1971–72		1971		1972	
	Multi-plate	Basket	Multi-plate	Basket	Multi-plate	Basket	Multi-plate	Basket	Multi-plate	Basket	Multi-plate [1]	Basket	Multi-plate	Basket
Number of specimens	1,836	2,023	70,444	37,620	442	546	6,722	9,021	1,334	3,457	----	2,101	424	3,205
Number of species	13	16	16	17	17	21	19	17	16	28	----	18	18	20
Average diversity [2]	1.78	2.31	0.16	0.67	2.85	3.69	1.28	1.54	2.59	3.23	----	2.95	2.78	3.19

[1] Multiplates not used.
[2] See footnote 4, table 2.
NOTE.—Average determined from individual values for each sample type are as follows:

Number of specimens for all multiplate samplers	13,534
Number of specimens for all basket samplers	8,282
Number of species for all multiplate samplers	16
Number of species for all basket samplers	19
Diversity for all multiplate samplers	1.91
Diversity for all basket samplers	2.51

SUMMARY

The seasonal diversity of the epifauna collected in the subintertidal zone of Jackson Point indicate that the water near Jackson Point in Port Valdez probably is clean and unpolluted. Basket samplers with net liners seem to collect epifauna organisms more representative of the community than do multiplate samplers; however, neither the basket nor multiplate samplers collect all available epifaunal species.

REFERENCES CITED

Boesch, P. F., 1972, Species diversity of marine macrobenthos in the Virginia area: Chesapeake Sci., v. 13, no. 3, p. 206–211.

Cory, R. L., 1967, Epifauna of the Patuxent River estuary, Maryland, for 1963 and 1964: Chesapeake Sci., v. 8, no. 2, p. 71–89.

Coulter, H. W., and Migliaccio, R. R., 1966, Effects of the earthquake of March 27, 1964, at Valdez, Alaska: U.S. Geol. Survey Prof. Paper 542–C, 36 p.

Feder, H. M., Mueller, G. J., Dick, M. H., and Hawkins, D. B., 1973, Preliminary benthos survey, *in* Hood, D. W., Shiels, W. E., and Kelley, E. J., eds., Environmental studies of Port Valdez: Fairbanks, Univ. of Alaska, Inst. Marine Sci. Occasional Pub. 3, p. 305–391.

Fullner, R. W., 1971, A comparison of macroinvertebrates collected by basket and modified multiplate samplers: Water Pollution Control Federation Jour., v. 43, no. 3, pt. 1, p. 494–499.

Haven, S. B., 1971, The Great Alaska Earthquake of 1964—Effects of land-level changes on intertidal invertebrates with discussion of post-earthquake ecological succession: Natl. Acad. Sci. Pub., p. 82–128.

Hood, D. W., Shiels, W. E., and Kelley, E. J., eds., 1973, Introduction, *in* Environmental studies of Port Valdez: Fairbanks, Univ of Alaska, Inst. Marine Sci. Occasional Pub. 3, p. 1–12.

Mason, W. T., Weber, C. I., Lewis, P. A., and Julian, E. C., 1973, Factors affecting the performance of basket and multiplate macroinvertebrate samplers: Freshwater Biology, v. 3, p. 409–436.

Mueller, G. J., 1973, Preliminary survey of intertidal fauna and flora of Glacier Bay National Monument—a final report: Fairbanks, Univ. of Alaska, Inst. Marine Sci., 24 p.

Muench, R. D., and Nebert, D. L., 1973, Physical oceanography, chap. 2, *in* Hood, D. W., Shiels, W. E., and Kelley, E. J., eds., Environmental studies of Port Valdez: Fairbanks, Univ. of Alaska, Inst. Marine Sci. Occasional Pub. 3, p. 103–150.

Nauman, J. W., and Kernodle, D. R., 1974, Aquatic organisms from selected sites along the proposed trans-Alaska pipeline corridor September 1970 to September 1972: U.S. Geol. Survey open-file rept., 23 p.

Nybakken, J. W., 1971, Preearthquake intertidal zonation of Three Saints Bay, Kodiak Island, Appendix *in* The great Alaska earthquake of 1964—Biology: Natl. Acad. Sci. Pub., p. 255–264.

Pearce, J. B., 1972, Invertebrate resources—available forms and potentials, *in* H. R. Frey, ed., Resources of the World's Ocean: New York Inst. of Ocean Resources, Inc., p. 75–90.

Searby, H. W., 1968, Climate along a pipeline from the Arctic to Gulf of Alaska: U.S. Weather Bur. Tech. Memo. 2, 16 p.

Slack, K. V., Averett, R. C., Greeson, P. E., and Lipscomb, R. G., 1973, Methods for collection and analysis of aquatic biological and microbiological samples: U.S. Geol. Survey Techniques Water-Resources Inv., book 5, chap. A4, 165 p.

U.S. Department of Commerce, 1971, Tide tables—high and low water predictions 1972, West Coast of North and South America including the Hawaiian Islands: Natl. Oceanic and Atmospheric Adm., Natl. Ocean Survey, 226 p.

Wilhm, J. L., 1970, Range of diversity index in benthic macroinvertebrate populations: Water Pollution Control Federation Jour., v. 42, no. 5, pt. 2, p. R221–R224.

Jour. Research U.S. Geol. Survey
Vol. 4, No. 3, May–June 1976, p. 305–315

ENHYDRA AND *ENHYDRIODON* FROM THE PACIFIC COAST OF NORTH AMERICA

By CHARLES A. REPENNING, Menlo Park, Calif.

Abstract.—Two lineages of the "crab-eating" otter *Enhydriodon*, from the Old World Miocene and Pliocene, are suggested by the fossil record. One appears to lead to the late Pliocene *Enhydriodon sivalensis* from Villafranchian-equivalent beds in India and can be characterized by the presence of a parastyle on P^4 and by the location of the protocone of this tooth, which is located as far lingually as is the hypocone. In the other lineage no parastyle is developed on P^4, the anteroposterior length of the carnassial blade is progressively reduced while the transverse width is increased, and the protocone of P^4 remains in its primitive position anterolateral to the hypocone. The second lineage, insofar as it is known, seems to lead toward the living sea otter *Enhydra*, particularly so because of the evolutionary direction shown by two species of *Enhydriodon* from the late Miocene and late Pliocene of California.

In 1967 I published a list of mammalian genera of Blancan (late Pliocene) age that I believed represented the first Western Hemisphere record of their lineage (Repenning, 1967, table 5). This list included both *Enhydra* and *Enhydriodon*. The *Enhydra* record was of a femur from the Elk River Formation of Oregon (Leffler, 1964), then tentatively considered to be of Blancan age. Since that time a large left scaphoid of *Mammuthus* has been found in a marine invertebrate bed at a locality near Eureka, Calif., called Moonstone Beach, along with seven bones of *Enhydra* (all in the collection of the Geology Department at California State University, Humboldt, under locality 205). The presence of *Mammuthus* suggests that the Moonstone Beach fossil bed is of Irvingtonian or younger (early Pleistocene or younger) age. The associated invertebrate fossils suggest that the Moonstone Beach locality is about the same age as, or somewhat older than, that part of the Elk River Formation in which the *Enhydra* femur was found (Allison and others, 1962). A Blancan age for *Enhydra* no longer seems defensible.

The *Enhydriodon* record was based on an isolated right P^4 (USNM 184083) from the *Pecten* zone of the San Joaquin Formation, North Dome, Kettleman Hills, Calif. The *Pecten* zone and underlying strata have produced a varied Blancan fauna (Durham and others, 1954, p. 69). Since 1967 some published note has been made of this record (van Zyll de Jong, 1972, p. 72; Hendey, 1974, p. 74), but description was postponed in the hope that additional material of similar age might be found; unfortunately, none was found.

However, there are two specimens assignable to *Enhydriodon* in the University of California Museum of Paleontology. One of these, UCMP 32970, is a fragment of a mandibular ramus bearing an incomplete M_1, and was collected from the middle of the Etchegoin Formation. The second specimen, UCMP 32972, is a cast of an isolated left P^4 of much more generalized form than that from the overlying Blancan fauna of the *Pecten* zone. This specimen is also from the Etchegoin Formation, but its locality is about 150 ft stratigraphically higher than that of the other specimen. Both specimens are of Hemphillian age, and a Blancan age for the earliest record of *Enhydriodon* in North America is also no longer defensible.

In this discussion and description, these three North American records of *Enhydriodon* are documented, and their relation to the living North Pacific sea otter is discussed.

The following abbreviations are used: AMNH, American Museum of Natural History; BM, British Museum (Natural History); GSI, Geological Survey of India; UCMP, University of California Museum of Paleontology; USGS, U.S. Geological Survey, and USNM, (U.S.) National Museum of Natural History.

Because of the international correlations involved in this report the Miocene, Pliocene, and Pleistocene Epochs are used in the sense of their Lyellian typification with subsequent clarifications by the International Geological Congress and following the correlations of Berggren and Van Couvering (1974). In this sense the Miocene-Pliocene boundary is about 5 m.y. old and the Pliocene-Pleistocene boundary is about 1.7 m.y. old. Where pertinent, the equivalent age in the sense of the Pacific coast provincial megainvertebrate chronology (Weaver and others, 1944; Addicott, 1972) is also

given. In this provincial sense the Miocene-Pliocene boundary is about 9.5 m.y. old and the Pliocene-Pleistocene boundary is approximately equal in age to this boundary in the Lyellian typification.

THE "CRAB-EATING" OTTERS

In 1919 Pohle (p. 201) divided the living otters into the "Fishotters" and the "Crabotters," presuming that these represented distinct phylogenetic groups since the early Miocene. The "Crabotters" include the living "clawless" or "small clawed" otters and *Enhydra*, the North Pacific sea otter. The fossil record is not yet adequate to document Pohle's presumption, and van Zyll de Jong (1972, p. 74) has suggested that the condition of the "crab-eating" otters was derived more than once from the more primitive "fish-eating" otters. Earlier Radinsky (1968, p. 500) suggested that the different arrangement of gyri in the forelimb cortical projection area of the brain of *Enhydra* indicates that its increased forelimb tactile sensitivity evolved independently of the other living "crab-eating" otters, *Amblonyx*, *Aonyx*, and *Paraonyx*. The "crab-eating" otters are noted for their manual dexterity, greater reliance on invertebrate food, and moderate preference for quiet water habitat. The "fish-eating" otters have greater sensitivity in their facial area and prefer vertebrate food and streams with faster currents.

Radinsky also examined a natural endocranial cast of *Aonyx aonychoides* (Zdansky) (AMNH 50575) from the Pontian (late Miocene) of the Paote District of China and noted strong similarities to living *Amblonyx* and *Aonyx*, rather than (by inference) to the living *Enhydra*. He concluded from this fossil that the "evolution of increased forepaw tactile sensitivity began at least five to ten million years ago" (Radinsky, 1968, p. 501). The dentition of *Aonyx aonychoides* also shows similarities to the living "small clawed" otters and no particular similarity to *Enhydra*. It is more similar to *Enhydra* than is the living *Aonyx capensis* only in the less prominent parastyle of P^4 and in an elevated medial lip on this tooth, which conceivably could have evolved into the P^4 "protocone" of *Enhydra* (fig. 1).

Aside from the low bulbous, or mastoid, tooth cusps, the most characteristic features in the dentition of *Enhydra* are found in the upper and lower carnassial teeth. The labial side of P^4 is longitudinally very short and no parastyle is present whereas the transverse dimension, from labial to lingual sides, is elongate and a prominent "protocone" is present. The talonid of M_1 is as short or shorter than the trigonid and has a hypoconid but no hypoconid crest, and the posterior margin

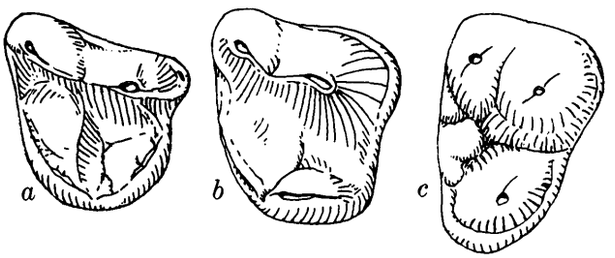

FIGURE 1.—Sketches of right upper carnassial tooth of *Aonyx capensis* (*a*), *Aonyx aonychoides* (*b*), and *Enhydra lutris* (*c*). Sketch *b* from cast of AMNH 50575. Anterior to right. Approximately × 2.

of the talonid is squared off with a prominent hypolophid that, however, is separated from the hypoconid by a valley. In the trigonid of M_1 the metaconid is the largest and highest cusp and extends posteriorly half the talonid length as measured behind the protoconid on the labial side of the tooth.

Genus *ENHYDRIODON* Falconer

Included species:

Enhydriodon sivalensis Falconer, 1868.
The type species. Late Pliocene or early Pleistocene, upper Siwalik Series, probably Tatrot Formation of Lewis (1937), Siwalik Hills, India.

Enhydriodon falconeri Pilgrim, 1931.
Early Pliocene, Dhok Pathan Formation of Lewis (1937), Siwalik Hills, India.

Enhydriodon africanus Stromer, 1931.
Early Pliocene, Kleinzee and Langebaanweg localities, South Africa.

Enhydriodon campanii (Meneghini, 1863).
Late Miocene, Monte Bamboli locality, Tuscany, Italy.

Enhydriodon lluecai Villalta and Crusafont, 1945.
Includes *Sivaonyx lehmani* Crusafont and Golpe, 1962. Late Miocene, several localities near Teruel, Spain.

Questionably included species:

Enhydriodon? latipes Pilgrim, 1931.
Lutrine foot bones included in the genus largely because of their great size. Late Miocene, Pikermi, Greece.

Enhydriodon? reevei (Newton, 1890).
Early Pleistocene, lower Norwich Crag, England.

Forms not assigned to species:

Enhydriodon cf. *E. lluecai*.
Late Miocene, middle and upper Etchegoin Formation, Kettleman Hills, Calif.

Enhydriodon n. sp.
Late Pliocene, middle San Joaquin Formation, Kettleman Hills, Calif.

Discussion of pertinent described specimens.—In 1931 Stromer described, as *Enhydriodon africanus*, an isolated M_1 bearing a strong resemblance to those of the type species *E. sivalensis*, especially that in a palate illustrated by Lydekker (1884, pl. 27, fig. 5); he also described a lower mandibular ramus with an M_1 bear-

ing a strong resemblance to the M_1 referred to *E. falconeri* by Pilgrim (1932, pl. 2, fig. 15; length 21.6 mm, p. 60). The M_1 of *E. africanus* was 22 mm long according to Stromer. This species is from the early Pliocene of South Africa. It represents the first described association of upper and lower teeth known for the genus, although Weithofer (1889, p. 59–60) mentioned lower jaws of *E. campanii* from Italy that he was unable to describe.

In 1863 Meneghini described *Lutra campanii* from the late Miocene fauna of Monte Bamboli, Tuscany, Italy. He illustrated, including both left and right upper tooth rows, the P^4 and M^1 a total of five times on his plate 1. None of the five matches any of the others. Weithofer (1889) referred this species to *Enhydriodon* although Lydekker (1884) had earlier recognized the relation but not the generic name. Lydekker's figure of one P^4 of *L. campanii* gives a better idea of the topography of the cusps than do Meneghini's illustrations, although the overall outline of the tooth seems incorrect. Matthew (1929) gave an outline drawing of the upper tooth row that appears to be proportioned properly. All authors since Weithofer have placed the species in *Enhydriodon.*

Enhydriodon campanii, in comparison with *E. sivalensis* and *E. falconeri*, has a number of features that most authors have taken as primitive, consistent with its greater antiquity (see fig. 2*a*). Most informative of these are the outline of P^4, which is more triangular than quadrate (best shown in Matthew's illustration); the total lack of a parastyle (all published illustrations); the more crestlike nature of the hypocone; and the position of the protocone anterolateral to the hypocone (both Matthew's and Lydekker's illustrations). In *E. sivalensis* the protocone is directly anterior to the hypocone. Tooth size and dental formula are essentially as in *E. sivalensis.*

Enhydriodon lluecai.—In 1945 Villalta and Crusafont described a mandible with right P_4, M_1, and M_2 from late Miocene deposits in the province of Teruel, Spain, as *Enhydriodon lluecai.* The locality is Los Algezares. The specimen had been imbedded in gypsum and was so corroded that little was left of the symphysis and the left ramus except the left M_2. Working partly with its impression in the rock, these authors determined that the jaw was short and lacked the first premolar as in *E. africanus.* The ramus is, however, less massive and the masseteric fossa extends more anteriorly and terminates beneath M_2, in contrast to *E. africanus* and the single mandibular fragment referred to *E. sivalensis* (Lydekker, 1884, p. 351, and pl. 45, fig. 3) in which species the anterior termination of the massteric fossa is behind M_2.

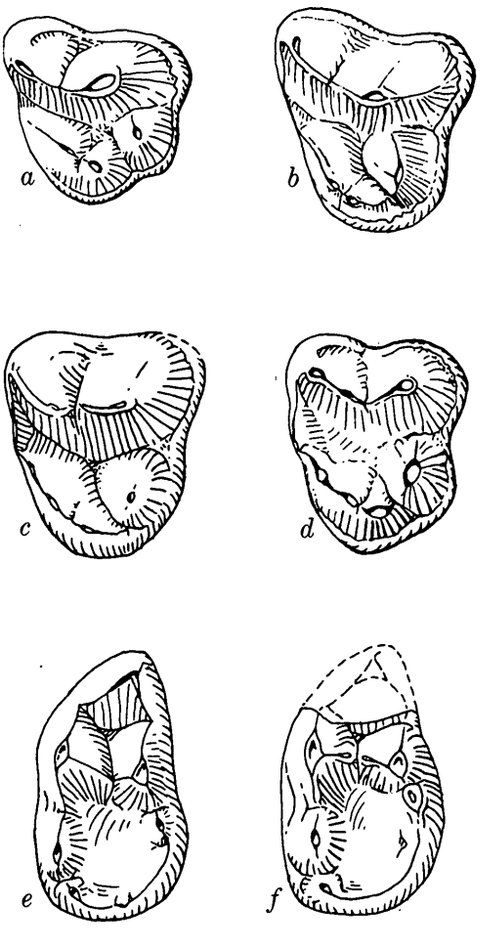

FIGURE 2.—Sketches of right upper and left lower carnassial teeth of species of *Enhydriodon.* Approximately × 2.

a. Enhydriodon campanii (Meneghini), right upper carnassial drawn from Matthew (1929) and Lydekker (1884). Late Miocene, Italy. Anterior to right.

b. Enhydriodon lluecai Villalta and Crusafont, left upper carnassial redrawn and reversed from Crusafont and Golpe (1962). Late Miocene, Spain. Anterior to right.

c. Enhydriodon cf. *E. lluecai*, left upper carnassial reversed, UCMP 32972. Late Miocene, California. Anterior to right.

d. Enhydriodon n. sp., right upper carnassial, USNM 184083. Late Pliocene, California. Anterior to right.

e. Enhydriodon lluecai Villalta and Crusafont, right lower carnassial redrawn and reversed from Villalta and Crusafont (1945). Late Miocene, Spain. Anterior up.

f. Enhydriodon cf. *E. lluecai*, left lower carnassial, UCMP 32970. Late Miocene, California. Anterior up.

The P_4 of *E. africanus* bears a relatively low and massive cusp with a prominent posterolateral secondary cusp. That of *E. lluecai* is considerably higher, is more slender, and has a very weak secondary cusp directly posterior to the principal cusp.

The M_1 of *E. lluecai* is very similar to that of *E. africanus* and to that referred to *E. falconeri* by Pilgrim except the metaconid appears to be uniquely

large, partly because a small secondary cuspid is present on its posterior side (see fig. 2*e*). This secondary cuspid is lacking on the M_1 metaconids of *E. africanus* and *E. falconeri*, which instead have a small secondary cuspid on the posterior side of the protoconid. The hypoconid of the M_1 in *E. lluecai* is contracted to a cusp, distinct but not crestlike as in the other two species. The M_1 of *E. lluecai* is similar to that of the type of *Sivaonyx bathygnathus* in anteroposterior length but does not otherwise resemble the slender tooth of the latter, and as pointed out by Villalta and Crusafont, *S. bathygnathus* has a P_1.

Crusafont and Golpe (1962, p. 11) listed two other records of *E. lluecai*, based on lower M_1, from "Los Mansuetos" and Concud, both in the Teruel basin and both of late Miocene age, although the Concud locality appears to be the oldest (Berggren and Van Couvering, 1974, fig. 11).

From a fourth locality in the upper Miocene beds of the Teruel basin, that of Rambla de Valdecebro II, Crusafont and Golpe (1962) described an upper P^4 (fig. 2*b*) that they name *Sivaonyx lehmani*. With hesitancy, they chose to put the specimen into *Sivaonyx*, rather than considering it to be the P^4 of *Enhydriodon lluecai* from the same deposits. Their decision was based on Pilgrim's discussion of the differences between *Enhydriodon sivalensis* and what he had lumped together to call *Sivaonyx bathygnathus*. Unfortunately, Crusafont and Golpe neglected comparison with *Enhydriodon campanii* from beds of approximately the same age in Italy.

The type species of *Enhydriodon* is *E. sivalensis*, one of the youngest and most specialized species of the genus; it bears slight resemblance to *S. lehmani*. The lectotype of *E. sivalensis* (selected by Matthew, 1929, p. 471) is a skull, BM 37153, from an unknown locality in the upper Siwalik Series. Except for one mandibular fragment bearing only an incomplete M_1, no lower dentition has been referred to *E. sivalensis*. It seems probable, however, that GSI D161, right lower M_1 referred to *E. falconeri* by Pilgrim (1932, p. 86), is actually referable to *E. sivalensis;* it is too large for *E. falconeri*.

The type species of *Sivaonyx* is *S. bathygnathus*. The holotype of *S. bathygnathus* is GSI D33, a left mandibular ramus from the middle Siwalik Series. It bears the alveolus of P_1 and an elongate M_1 that is damaged in the protoconid-hypoconid region. Lydekker (1884), author of the species, referred it to *Lutra*. Pohle (1919) referred it to *Potamotherium*. Matthew (1929) considered it inadequate for any interpretation. The specimen is characterized by having a P_1 and a noticeably narrow, elongate M_1.

To *S. bathygnathus* Pilgrim (1932) referred GSI D156, a mandibular fragment bearing a stout M_1, which appears identical to but smaller than GSI D161 and could more reasonably be referred to *E. falconeri;* GSI D244, the anterior portion of a mandibular ramus with P_1 and a unique P_4; three other mandibular fragments not illustrated; and, finally, GSI D157, an isolated left P^4. All specimens but one were collected from the Dhok Pathan stage of the middle Siwalik in the neighborhood of Hasnot. Pilgrim (p. 89) said that "In the circumstances it is highly probable that I am right in attributing it [the P^4] to this species." Until 1962 (Crusafont and Golpe), it was the only P^4 attributed the genus. Pilgrim illustrated it in two publications (1931 and 1932), and the illustrations clearly show the tooth to have a prominent parastyle and a prominent hypocone with an evident but very low hypoconal crest. In addition, from Pilgrim's illustrations it is evident that the only P^4 referred to *Sivaonyx* does have sharp cusps and crests, as Pilgrim described them, but these are small and very low features on the tooth.

In contrast, the P^4 from Teruel described by Crusafont and Golpe (1962) has large and stout cusps, lacks a parastyle, and does not have a prominent hypocone but rather only a twinned pair of very small cusps in this position on the hypoconal crest. Despite the fact that their tooth can be compared to *Sivaonyx* from Pilgrim's verbal description of the referred P^4, it bears no resemblance to his illustration of this questionably referred tooth. The P^4 from Teruel most resembles the P^4 of *Enhydriodon campanii*, particularly as represented in Falconer's (1868) and Matthew's (1929) illustrations. Because of this resemblance, and because of its stratigraphic association in deposits of late Miocene age in the region of Teruel with three lower carnassials assigned to *Enhydriodon lluecai*, *Sivaonyx lehmani* Crusafont and Glope is here included in *Enhydriodon lluecai* Villalta and Crusafont.

In summary, therefore, *Enhydriodon lluecai* may be characterized a small primitive species with P^4 most resembling that of *Enhydriodon campanii* in having no parastyle, a high and sharp paracone-metacone blade relative to *E. sivalensis*, protocone located anteromedial to the hypocone, and hypocone representing little more than the highest part of the prominent hypoconal crest. The M_1 is characterized by a prominent metaconid that is somewhat higher than the protoconid and has a posteriorly located secondary cuspid, protoconid without such secondary cuspid, hypoconid shortened to a prominent cusp rather than forming a hypoconid crest, and short talonid—especially if measured behind the metaconid. The M_1 ranges in length from 17.5 mm (type specimen) to 16.0 mm (specimen

from "Los Mansuetos;" Crusafont and Golpe, 1962, p. 12).

The P^4 has an anterioposterior length of 13.0 mm and a transverse width of 12.8 mm (Crusafont and Golpe, 1962, p. 11). Pilgrim (1932, p. 81, 83, and 93) made note that in the genus *Enhydriodon* the development of a parastyle on P^4 and the increase in transverse diameter, relative to the buccal longitudinal diameter, were progressive features of *E. sivalensis* not found in the older and more primitive *E. campanii*. In *E. lluecai* the longitudinal diameter of P^4 is somewhat greater than the transverse, as in *E. campanii*.

Enhydriodon* cf. *E. lluecai

Figures 2*c*, *f*; 3*a*, *g–i*

Material.—UCMP 32970, fragment of a left mandibular ramus with the alveolus for M_2 and bearing the M_1 which lacks the paraconid. UCMP 32972, cast of an isolated left P^4.

Localities.—UCMP 32970 is from locality UCMP V3634, near section line between secs. 8 and 17, T. 22 S., R. 18 E., La Cima quadrangle, east flank of North Dome, Kettleman Hills, King County, Calif. This is

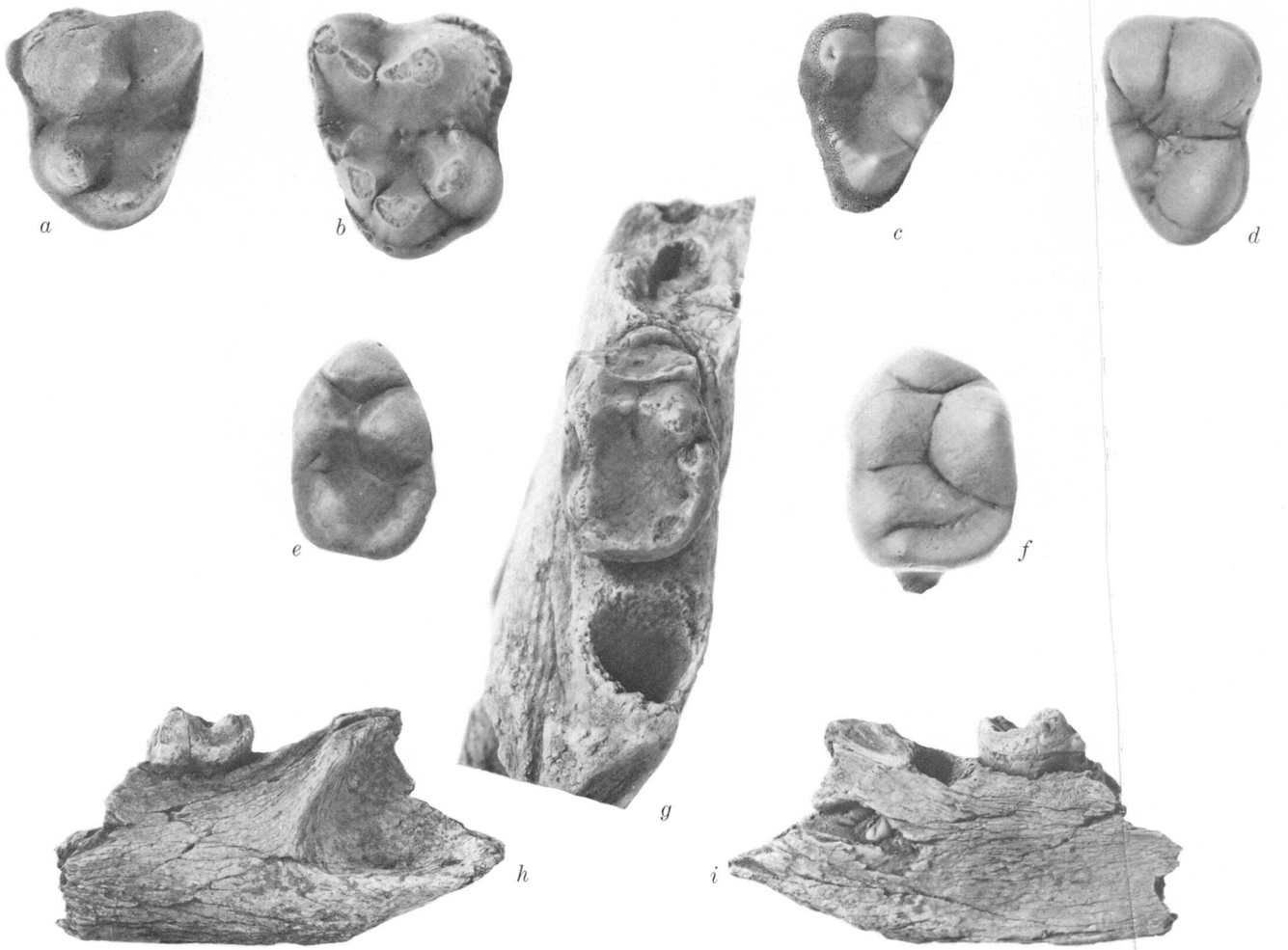

FIGURE 3.—Teeth of *Enhydriodon* and *Enhydra*.

a. *Enhydriodon* cf. *E. lluccai*, left upper carnassial, UCMP 32972. Late Miocene, California. Occlusal view, anterior to left, × 2.

b. *Enhydriodon* n. sp., right upper carnassial, USNM 184083. Late Pliocene, California. Occlusal view, anterior to right. × 2.

c. *Enhydra lutris* (Linnaeus), right upper deciduous carnassial. Modern. Occlusal view, anterior to right. × 2.

d. *Enhydra lutris* (Linnaeus), right upper permanent carnassial. Modern. Occlusal view, anterior to right. × 2.

e. *Enhydriodon*? *reevei* (Newton), right lower carnassial (reversed), Castle Museum (Norwich, England) 548. Early Pleistocene. Occlusal view, anterior up. × 2.

f. *Enhydra lutris* (Linnaeus), left lower carnassial. Modern. Occlusal view, anterior up. × 2.

g–i. *Enhydriodon* cf. *E. lluecai*, left lower carnassial, UCMP 32970. Late Miocene, California.

g. Occlusal view, anterior up. × 2.

h. Lateral view, anterior to left. × 1.

i. Medial view, anterior to right. × 1.

about 1.4 mi S. 30° E. of USGS vertebrate locality M1032—the Blancan record of the genus.

UCMP 32972 is from locality UCMP V3520, S½-NE¼ sec. 7, T. 22 S., R. 18 E., La Cima quadrangle, east flank of North Dome, Kettleman Hills, Calif. This is about 0.7 mi S. 11° E. of the Blancan record of the genus.

Collector.—Both specimens were collected by A. C. Hall, about 1936. Mr. Hall appears to have kept the P^4 and to have deposited only its cast in UCMP.

Horizon.—UCMP locality V3634 is in the upper part of strata between the *Pseudocardium* and *Macoma* zones of Woodring, Stewart, and Richards (1940), middle Etchegoin Formation. Probably latest Miocene or roughly mid-Pliocene in the sense of the Pacific coast provincial megainvertebrate chronology; that is in the upper part of the range of *Ostrea atwoodi* Gabb (Woodring and others, 1940; and Addicott and Galehouse, 1973). A few teeth of the horse *Pliohippus* have been found in this part of the Etchegoin Formation, and a Hemphillian North American Mammal Age is indicated. This locality is more than 1,100 ft downsection below the Blancan record of the genus.

UCMP locality V3520 is in the lower part of the strata between the *Littorina* zone of the Etchegoin Formation and the base of the San Joaquin Formation or from the *Littorina* zone itself (Woodring and others, 1940). This locality could be latest Miocene or early Pliocene. It is an estimated 950 feet downsection from the *Pecten* zone of the San Joaquin Formation.

Approximately 2.5 mi southeast of USGS locality M1032 (Blancan) and 1.5 mi east-southeast of UCMP locality V3634 (Hemphillian) J. D. Obradovich discovered a tuff bed in the lower part of the San Joaquin Formation, about 300 ft below the *Pecten* zone and more than 800 ft above the level of UCMP locality V3634. Obradovich dated this bed at 4.3 m.y.; he considered this to be a maximum age (oral commun., 1969). On the basis of this date and the great stratigraphic separation of the dated tuff from the underlying Etchegoin strata from which the UCMP specimens were collected, it seems most probable that the earliest record of *Enhydriodon* in the Western Hemisphere is of late Miocene age, if the Miocene-Pliocene boundary is placed at 5 m.y. (Berggren and Van Couvering, 1974).

Discussion.—The fragment of the mandibular ramnus shows a deep masseteric fossa that extends forward to a position beneath M_2, the metaconid of M_1 is slightly higher than the protoconid and has a distinct secondary cuspid on its posterior side that is part of a medial lip (entoconid crest) of the talonid basin. The entoconid area is low, the posterior margin of the talonid is squared off and marked by a hypolophid crest that is highest laterally but is separated from the hypoconid by a shallow valley and is continuous with the entoconid crest medially, and the hypoconid is a distinct cusp but is not developed into a crest. This specimen differs from the one illustrated specimen of *E. lluecai* (Villalta and Crusafont, 1945) in that the entoconid crest is more prominent anteriorly and the posterior margin of the talonid is more squared off, particularly in the region of the hypoconid. As does *E. lluecai*, this specimen differs from comparable parts of *E. africanus*, *E. sivalensis* (GSI D161 of Pilgrim, 1932, and the Ipswich Museum specimen of Lydekker, 1884, p. 351), and *E. falconeri* (GSI D156 of Pilgrim, 1932) in having a secondary cuspid behind the metaconid, in having none behind the protoconid, in a less trenchant hypoconid, and in the anterior extension of the masseteric fossa. There is a rather sharp bend in the ventral margin of the jaw slightly behind the anterior limit of the masseteric fossa, and the ventral margin is noticeably flattened posterior to this bend, reminiscent of the jaw of *Enhydra* and not evident on the jaws of *Enhydriodon africanus* or *E. sivalensis*.

The isolated P^4 from the Etchegoin Formation (UCMP 32972, figs. 2*c*, 3*a*) is nearly identical to that of *Enhydriodon lluecai* (nee *Sivaonyx lehmani*) (fig. 2*b*) except that its transverse diameter is greater (table 1).

***Enhydriodon* n. sp.**

Figures 2*d*, 3*b*

Material.—USNM 184083, isolated right P^4.

Locality.—USGS vertebrate locality M1032, NW¼ SE½ sec. 6, T. 22 S., R. 18 E., La Cima quadrangle, east flank of North Dome, Kettleman Hills, King

TABLE 1.—*Dimensions of teeth of* Enhydriodon *species and* Enhydra lutris

	P^4			Depth of ramus below M_1 (mm)
	Length (mm)	Width (mm)	(*L*/*W*)	
Enhydriodon campanii (Matthew, 1929, fig. 10)	17.1	16.1	1.06	---
E. falconeri (Matthew, 1929, fig. 11)	14.4	14.0	1.03	[1] 18.7
E. lluecai (Crusafont and Golpe, 1962)	13.0	12.8	1.01	[2] 24.0
E. cf. *E. lluecai* (UCMP 32972, 32970)	13.6	15.0	0.91	24.3
E. sivalensis (Lydekker, 1884, pl. 27)	16.2	18.4	0.88	[3] 31.7
E. n. sp. (USNM 184083)	14.5	16.7	0.87	---
Enhydra lutris	11.6	16.0	0.73	18.6

[1] GSI D156.
[2] Villalta and Crusafont (1945).
[3] Lydekker (1884, p. 351).

County, Calif. This is USGS locality 12335 (Washington, D.C., Tertiary invertebrate register; Woodring and others, 1940, their map locality 82).

Collector.—J. H. Beach, in 1963.

Horizon.—The *Pecten* zone of Woodring, Stewart, and Richards (1940), middle San Joaquin Formation. Late Pliocene and in a unit containing Blancan age land mammals. Late Pliocene in the sense of the Pacific coast provincial megainvertebrate chronology. This is a nearshore marine deposit.

Discussion.—This isolated P^4, of about the same age as *E. sivalensis*, differs from *E. lluecai* in more bulbous cusps, reduction of the metacone blade, prominent isolation of the hypocone from the hypoconal crest, development of two small cusps on the hypoconal crest, and greater enlargement of the transverse diameter. Its measurements are given in table 1.

The record of the several species of *Enhydriodon* is based on very few specimens scattered widely over the world. At present it can be summarized as follows:

Late Miocene.—Species from Spain, Italy, and North America. P^4 with no parastyle, length greater than width in the two European species and slightly less in the North American species, protocone anterolateral to hypocone, hypocone weak on hypoconal crest. M_1 with metaconid having a small secondary cusp on its posterior surface and larger than protoconid but undescribed in Italian species, talonid somewhat squared off in North American species.

Early Pliocene.—Species from South Africa and India, but P^4 known only from India. P^4 with parastyle, length greater than width, protocone positioned anterior to hypocone, hypocone prominent and crest weak, all cusps stouter. M_1 with small secondary cusp on posterior surface of protoconid and none on the metaconid, hypoconid trenchant, talonid rounded at back.

Late Pliocene.—Species from India and North America. P^4 with parastyle in India and without in North America, width greater than length, protocone anterolateral to hypocone in North America and anterior to hypocone in India, hypocone weak in North America and strong in India, cusps stout. M_1 like that of the early Pliocene forms in India, but not known in North America. A third lingual cusp, between the protocone and hypocone of P^4, has developed out of the cingulum in the species from India.

From this very sketchy record there appears to be a common generic tendency for increase in the width (or decrease in the length) of P^4 and increase in inflation of the tooth cusps. Beyond this, there seem to be marked differences in the trends of species evolution, as best illustrated by the late Pliocene forms from India and North America. The North American lineage retains the cusp pattern of the earlier forms, whereas the Indian and African (to judge by the similarity of M_1) modify this pattern. It should be noted, however, that this difference in pattern evolution is based entirely on the assumption that all species have evolved from an *E. campanii* condition, and that the lower dentition of *E. campanii* has not be described.

In the above summary, the wording is such that the M_1 of *E. lluecai* from the late Miocene of Spain appears to represent the most primitive condition known. It does not, however, because the emphasized metaconid, nontrenchant hypoconid, and posterior squareness of the talonid (in *E.* cf. *E. lluecai*) are more removed from the presumed condition of the "fish-eating" otters than are these structures on the M_1 of *E. africanus*, and, as here assigned *E. falconeri* and *E. sivalensis*. Regardless of whether the known record of *Enhydriodon* represents two branches from an *E. campanii*-like form or two lineages of separate origin from the "fish-eating" otters, the M_1 of *E. lluecai* was already more specialized in the late Miocene than the M_1 here assigned to *E. sivalensis* of the late Pliocene.

The next species under consideration, *Enhydriodon? reevei*, is based on a single M_1 of *Enhydra*-like specialization.

Enhydriodon? reevei (Newton)

Figure 3*e*

In 1890 Newton described, as *Lutra reevei*, an isolated lutrine right M_1 with mastoid cusps from the lower beds of the Norwich Crag in East Anglia, England. Its age is early Pleistocene. In all observable respects it appears intermediate between the M_1 of *Enhydriodon lluecai* and that of *Enhydra lutris*. The metaconid is somewhat stouter, and possibly higher, than the protoconid, and a low and rounded crest borders the medial side and posteromedial corner of the talonid.

Pohle (1919, p. 196) considered the tooth intermediate between that of *Enhydra* and the M_1 in a partial mandible from the late Miocene of Eppelsheim, Germany, which was named by Lydekker (1890) *Lutra hessica*, called by Pohle (1919) *Aonyx hessica*, and later called *Sivaonyx hessica* by Pilgrim (1931). To the extent that *Sivaonyx* is known, the last assignment may be the best. The M_1 of *Lutra hessica* has a notably high and slender protoconid and hypoconid, higher than in the living *Aonyx capensis*, and a remarkably short talonid, in contrast to the relatively elongate talonid of the M_1 of *Aonyx capensis*. However, the shortened talonid is not a result of a relative enlargement of the metaconid as in *Lutra reevei*, *Enhydrio-*

don lluecai, and *Enhydra lutris* as both protoconid and metaconid extend an equal distance to the rear, rather than only the enlarged metaconid as in the M_1 of the "Spanish-American" lineage of *Enhydriodon* (see Pohle, fig. 18). The similarity of *Lutra reevei* to *Enhydriodon lluecai* is thus greater than to "*Lutra*" *hessica* in the lowness of the anterior cusps and enlargement of the metaconid relative to the protoconid. The relation of the Eppelsheim tooth is not further considered here.

Because of its intermediate condition, Pohle considered *Lutra reevei* ancestral to *Enhydra lutris* and placed it in the genus *Latax* (=*Enhydra*) as *Latax reevei*. Several, but not all, subsequent authors have followed this assignment. However, Mitchell (1966) pointed out that *Enhydra* remains of the same age, early Pleistocene, are known from the Pacific coast of North America; that the dispersal to the Pacific from the North Atlantic, through the Arctic Ocean, seems difficult to assume in view of the sea otters' inability to survive under conditions of permanent winter sea ice (see Schneider and Faro, 1975); and that the lack of any other record in the North Atlantic does not suggest any large population that might have dispersed to the Pacific.

In addition, the recognition of *Enhydriodon* in the Miocene and Pliocene of Pacific North America provides a possible origin for *Enhydra* and one geographically more suitable than *Lutra reevei*. Thus it now seems quite unlikely that any direct relation exists between the North Pacific sea otter and *Lutra reevei*. *Enhydriodon* is the only available genus in which it could be placed, and it is not unreasonable to suppose that *Lutra reevei* evolved directly from one of the older European species of *Enhydriodon* by a continuation of the generic trend to increase cusp inflation. This cusp inflation has progressed so far that it has obscured the relatively minor differences by which the M_1 of the "Indian" and "Spanish" lineages are differentiated. The somewhat more massive metaconid, in comparison to the protoconid, of *Enhydriodon*? *reevei* suggests the "Spanish" lineage, and its rather squared off talonid does so also, although the squared talonid is not developed in the European species, *E. lluecai*.

Thus, as here conceived, *Enhydra lutris* and *Enhydriodon*? *reevei* evolved out of earlier species of the genus *Enhydriodon*, probably from the same subgeneric lineage, at the same time on the eastern shores of the North Pacific and of the North Atlantic, respectively, through a normal continuation of the generic trend toward inflated cusps.

Genus *ENHYDRA* Fleming

In historic times the North Pacific sea otter, *Enhydra lutris*, has had a geographic range from nearly lat 25° N. along the Baja California coast of Mexico northward along the Pacific coast of North America to Alaska and westward along the Aleutian Arc to Kamchatka and southward to northern Japan to almost lat 40° N. (Kenyon, 1969, fig. 67). In the southernmost Sea of Okhotsk it ranged somewhat northward to southern Sakhalin, and in the Bering Sea it ranged somewhat northward to the Pribilof Islands but it does not hibernate and starves to death in areas of permanent winter sea ice (Schneider and Faro, 1975). Its southern limits are tied closely to the 20° to 22°C surface-water isotherms for late summer, which approximate the southern limits of upwelling, which appear to be related to the southern limits of extensive giant kelp forests. It appears to be a product of the North Pacific and to have never escaped from there.

The earliest record of the genus *Enhydra* is uncertain. Early Pleistocene records are known from Cape Blanco, Oreg. (Leffler, 1964) and Moonstone Beach near Eureka, Calif. (Repenning, unpub. data, 1973), and an isolated deciduous P_4 is known from the Timms Point Silt Member of the San Pedro Formation, San Pedro, Calif. (Mitchell, 1966). The age of the silt has been uncertain. It is generally considered to be of early Pleistocene age, but a 3.0 m.y. date on glauconite from the underlying Lomita Marl Member (Obradovich, 1965) suggests a late Pliocene age because of close depositional relation and foraminiferal content of the two members.

In contrast to the glauconite date, Bandy (1972, p. 10) reported that

> The major left-coiling interval for *Globorotalia* (*Turborotalia*) *pachyderma* (Ehrenberg) is that corresponding with the Bruhnes and very uppermost part of the Matuyama above the Jaramillo event. In the Los Angeles Basin, this planktonic event marks the level near the base of the Lomita Marl–Timms Point Silt complex.

Thus Bandy's correlations suggest a maximum age of early Pleistocene and of about 1 m.y.

In an effort to confirm one or the other of these differing age assignments, L. N. Marincovich, who is very familiar with localities of the Timms Point Silt Member, collected fresh samples from about 10 ft above the locality of the deciduous sea otter tooth; the original locality is currently covered by talus. R. Z. Poore examined both planktonic foraminifers and calcareous nannoplankton from the samples and reported (written commun., 1975)

> Although *Globorotalia truncatulinoides* is very rare, its occurrence, as well as the presence of phylogenetically advanced

forms of *Neogloboquadrina pachyderma* (predominantly left coiling), in this sample indicates placement within zones N22/N23 of Blow . . . . I suggest that you can confidently assign a maximum age of 2.0 plus or minus m.y. B.P. to this sample.

It thus appears that the Timms Point *Enhydra* tooth is very likely early Pleistocene in age, more or less contemporaneous with other records from northern California and Oregon and distinctly younger than *Enhydriodon* n. sp. from the late Pliocene San Joaquin Formation.

One extinct species, *Enhydra macrodonta* Kilmer (1972), is known from the late Pleistocene and is distinguished from the living species by the greater size of its posterior cheek teeth, longer tooth row, and more generalized coronoid process of the mandible. This species has a masseteric fossa similar to that of *Enhydriodon lluecai* which terminates below the posterior part of M_1; the living species tends to have an anterior border of this fossa that runs ventrally from the anterior margin of the ascending ramus to the inferior margin of the ramus where it hooks forward in varying degrees. The masseteric fossa in the living species is highly variable, however, even bilaterally so in most individuals as the sea otter is a "left-" or "right-handed" chewer and the masseter develops preferentially.

The P^4 of *Enhydra lutris* (fig. 1*c*) is composed of closely appressed paracone and metacone, a prominent "protocone," and a plump but low hypoconal crest that may or may not form as one or two small cusps. All cusps are mastoid, and the tooth is surrounded by an inflated cingulum, more conspicuous on the lingual side. The transverse width greatly exceeds the longitudinal length (table 1).

The M_1 (fig. 3*f*) is easily characterized by its enlarged metaconid, which is not only higher than the protoconid but also extends backward as much as half the length of the talonid as measured behind the protoconid. This great backward extension was presumably accomplished by incorporation of the posterior secondary cuspid of the metaconid during the progressive inflation of the cusps. The entoconid crest on the lingual margin of the talonid is almost entirely removed by the backward extension of the metaconid, but it is present on the posterolingual corner of the tooth where it curves continuously into the hypolophid which extends straight across the posterior margin of the talonid to the rather angular posterolabial corner. The hypoconid is separated from the hypolophid by a shallow sulcus and is inflated, expanding medially to fill the talonid basin. The pattern is identical to that of the M_1 of *Enhydriodon* cf. *E. lleucai* from the middle of the Etchegoin Formation (compare in fig. 3); the *Enhydra* tooth is simply an inflated version of the late Miocene tooth.

The homologies between the P^4 of *Enhydriodon* cf. *E. lluecai* from the Etchegoin Formation and the P^4 of *Enhydra lutris* are not so easily seen. It has already been noted that the late Pliocene species from the San Joaquin Formation differs from the late Miocene species from the Etchegoin in that the hypocone is more prominently separated from the hypoconal crest, all cusps are stouter, and the transverse diameter of the tooth is much greater. But in the P^4 of *Enhydra lutris* it appears that the hypocone has been lost entirely and the "protocone" is the most lingual cusp of the tooth, suggesting that the hypocone of the P^4 of *Enhydriodon* n. sp. from the San Joaquin Formation should be suppressed rather than accentuated.

Examination of the roots of the tooth from the San Joaquin Formation provides another suggestion; the very stout lingual root is directly below the cusp here called the hypocone, although, because the root is large, the cusp called the protocone is also supported by the anterolateral part of the root. The root position thus suggests that the "protocone" of *Enhydra lutris* is the cusp called the hypocone on the P^4 of *Enhydriodon* sp. from the San Joaquin Formation. The same suggestion is provided by the deciduous P^4 of *Enhydra lutris* (fig. 3*c*) which shows one or a pair of small cusps anterolateral to the most medial cusp, the cusp called the "protocone." It therefore seems evident that the "protocone" of P^4 of *Enhydra lutris* is the same cusp as that called the hypocone on the P^4 of the late Pliocene *Enhydriodon* n. sp., that the *Enhydriodon* hypocone has continued the trend of accentuation noted between the late Miocene and late Pliocene forms, and also that the *Enhydriodon* protocone has become completely suppressed in adult *Enhydra lutris*.

CONCLUSIONS

Falconer (1868) introduced the generic name *Enhydriodon*, explaining as he did so that the name was derived from the Greek word for otter, as was the generic name *Enhydra*, and that his choice of the name implied no particular relation to the North Pacific sea otter. Despite this, he noted similarities with *Enhydra*. Since that time over a dozen authorities have considered the possible relation and about half have rejected it flatly. These rejections have usually been based on a comparison of *Enhydriodon sivalensis* with *Enhydra*, and it has been concluded that the trends in evolution shown by *E. sivalensis* were away, not toward, *Enhydra*. In addition, since 1919, Pohle has offered an alternate source for *Enhydra* in *Latax reevei*, and the question of the ancestry of *Latax reevei* has

been brushed aside into the uncertainties of "*Aonyx*" *hessica* and the evolution of the aonychoid otters. None of these workers had the advantage of knowing of *Enhydriodon* from North America, representing a lineage differing in its trends from those of the lineage leading to *Enhydriodon sivalensis*.

To judge from the different cortical patterns in the brain of recent and fossil "crab-eating" otters, *Enhydra* and presumably *Enhydriodon* because of its ancestral position represent a lineage that evolved independently from the small-clawed or aonychoid otters for at least as long as their known fossil record. Possibly the "crab-eating" otters represent two separate derivations from the "fish-eating" otters. The *Enhydriodon-Enhydra* group characteristically included and includes the largest of the otters and is marked by a strong tendency to lose all shearing ability in the teeth and to improve progressively upon their crushing ability; shortening and transversely broadening of the carnassial teeth and inflation of the tooth cusps are trends common to all members of the group. The group is marked in its earliest records by a distinct protocone on the upper carnassial and, progressively, a melininelike hypocone developed out of the lutrine hypoconal crest, at which point two branches are discernible. One, known from Asia and Africa, developed a quadrate upper carnassial in which the hypocone achieved an importance equal to that of the protocone and a prominent parastyle was present. This branch appears to have culminated in *Enhydriodon sivalensis* of the late Pliocene or early Pleistocene in northern India.

The other branch of the *Enhydriodon-Enhydra* group is known from the late Miocene of Italy, Spain, and California and retained a primitive triangular outline in the upper carnassial, did not develop a parastyle, did progressively accentuate the hypocone (apparently at the expense of the protocone) and progressed in tooth-cusp inflation to the point of acquiring mastoid cusps. This branch appears to have culminated in *Enhydriodon? reevei* of the early Pleistocene of England and in *Enhydra lutris* now living in the North Pacific Ocean.

REFERENCES CITED

Addicott, W. O., 1972, Provincial middle and late Tertiary molluscan stages, Temblor Range, California, *in* Symposium on Miocene biostratigraphy of California: Soc. Econ. Paleontologists and Mineralogists, Pacific Sec., Bakersfield, Calif., Proc. p. 1–26, pls. 1–4.

Addicott, W. O., and Galehouse, J. S., 1973, Pliocene marine fossils in the Paso Robles Formation, California: U.S. Geol. Survey Jour. Research, v. 1, no. 5, p. 509–514.

Allison, E. C., Durham, J. W., and Zullo, V. A., 1962, Coldwater late Cenozoic faunas of northern California and Oregon: Geol. Soc. America Spec. Paper 68, p. 2.

Bandy, O. L., 1972, Late Paleogene-Neogene planktonic biostratigraphy and some geologic implications, California, *in* Symposium on Miocene biostratigraphy of California: Soc. Econ. Paleontologists and Mineralogists, Pacific Sec., Bakersfield, Calif., Proc., p. 37–51.

Berggren, W. A., and Van Couvering, J. A., 1974, The late Neogene biostratigraphy, geochronology and paleoclimatology of the last 15 million years in marine and continental sequences: Palaeogeography, Palaeoclimatology, Palaeoecology, v. 16, no. 1/2, p. 1–216.

Crusafont-Pairo, Miguel, and Golpe, J. M., 1962, Nuevos hallazgos de Lutridos aonicoides (*Sivaonyx*, *Enhydriodon*) en el Pikermiense español (Cuenca de Teruel): Inst. Geol. y Minero de España Notas y Comuns., no. 67, p. 5–15.

Durham, J. W., Jahns, R. H., and Savage, D. E., 1954, Marine-nonmarine relationships in the Cenozoic section of California, pt. 7, *in* Chap. III *of* Jahns, R. H., ed., Geology of southern California: California Div. Mines Bull. 170, p. 59–71.

Falconer, Hugh, 1868, Fauna antiqua sivalensis. XVII. On *Enhydriodon* (*Amyxodon*), a fossil genus allied to *Lutra* from the Tertiary strata of the Sewalik hills: Falconer Paleont. Mem. I, p. 331–338.

Hendey, Q. B., 1974, The late Cenozoic carnivora of the southwestern Province: South African Mus. Annals, v. 63, p. 1–369.

Kenyon, K. W., 1969, The sea otter in the eastern Pacific Ocean: U.S. Bur. Sport Fisheries and Wildlife, North American Fauna No. 68, 352 p.

Kilmer, F. H., 1972, A new species of sea otter from the late Pleistocene of northwestern California: Southern California Acad. Sci. Bull., v. 71, no. 3, p. 150–157.

Leffler, S. R., 1964, Fossil mammals from the Elk River Formation, Cape Blanco, Oregon: Jour. Mammalogy, v. 45, no. 1, p. 53–61.

Lewis, G. E., 1937, A new Siwalik correlation: Am. Jour. Sci., v. 33, p. 191–204.

Lydekker, Richard, 1884, Siwalik and Narbada Carnivora, *in* Indian Tertiary and post-Tertiary Vertebrata, v. II, pt. VI: Geol. Survey India, Palaeontologia Indica, Ser. X, Mem., p. 178–355.

——— 1890, On a new species of otter from the lower Pliocene of Eppelsheim: Zool. Soc. London Proc. for 1890, pt. 1, p. 3–5.

Matthew, W. D., 1929, Critical observations upon Siwalik mammals: Am. Mus. Nat. History Bull., v. 56, art. 7, p. 437–560.

Meneghini, G. G. A., 1863, Descrizione dei resti di due fiere trovati nelli Ligniti Mioceniche de Monte Bamboli: Soc. Italiana Sci. Nat. e Museo Civico Storia Nat. Milano Atti, v. 4, p. 17–58.

Mitchell, E. D., 1966, Northeastern Pleistocene sea otters: Fisheries Research Board Canada Jour., v. 23, no. 12, p. 1897–1911.

Newton, E. T., 1890, On some mammals from the Red and Norwich Crags: Geol. Soc. London Quart. Jour., v. 46, p. 444–453.

Obradovich, J. W., 1965, Isotopic ages related to Pleistocene events: Internat. Union Quaternary Research, Cong., 7th, Boulder, Abs., p. 364.

Pilgrim, G. E., 1931, Catalogue of the Pontian Carnivora of Europe in the British Museum: British Mus. (Nat. History) Cat., p. 1–174.

——— 1932, The fossil Carnivora of India: Geol. Survey India, Palaeontologia Indica, New Ser., Mem., v. 18, p. 1–232.

Pohle, Hermann, 1919, Die Unterfamilie der Lutrinae: Berlin, Archiv Naturgeschichte, v. 85, ser. A, no. 9, p. 1–247.

Radinsky, L. B., 1968, Evolution of somatic sensory specialization in otter brains: Jour. Comp. Neurology, v. 134, no. 4, p. 495–506.

Repenning, C. A., 1967, Palearctic-Nearctic mammalian dispersal in the late Cenozoic, *in* Hopkins, D. M., ed., The Bering Land Bridge: Stanford, Calif., Stanford Univ. Press., p. 288–311.

Schneider, K. B., and Faro, J. B., 1975, Effects of sea ice on sea otters: Jour. Mammalogy, v. 56, no. 1, p. 91–101.

Strömer, Ernst, 1931, Reste Süsswasser und Land bewohnenden Wirbeltiere aus den Diamantenfeldern klein-Namaqualandes (Südwestafrika): Bayerische Akad. Wiss. Stitzungber., Math.-Naturw. Kl., p. 17–47.

van Zyll de Jong, C. G., 1972, A systematic review of the nearctic and neotropical river otters (genus *Lutra*, Mustelidae, Carnivora): Royal Ontario Mus. Life Sci. Contr., no. 80, p. 1–104.

Villalta Comella, J. F., and Crusafont Pairó, Miguel, 1945, *Enhydriodon lluecai nova sp.* el primer Lutrido del Pontiense español: Real Soc. Española Historia Nat. Bol., Sec. Geol., v. 43, no. 7–8, p. 383–396.

Weaver, C. E., and others, 1944, Correlation of the marine Cenozoic formations of western North America: Geol. Soc. America Bull., v. 55, no. 5, p. 569–598.

Weithofer, K. A., 1889, Ueber die Tertiären, Landsäugethiere Italiens: Austria, Geol. Reichanstalt, Jahrbuch, v. 39, no. no. 1, p. 55–82.

Woodring, W. P., Stewart, Ralph, and Richards, R. W., 1940, Geology of the Kettleman Hills Oil Field, California: U.S. Geol. Survey Prof. Paper 195, p. 1–170.

Jour. Research U.S. Geol. Survey
Vol. 4, No. 3, May–June 1976, p. 317–338

MISSISSIPPIAN HISTORY OF THE NORTHERN ROCKY MOUNTAINS REGION

By WILLIAM J. SANDO, Washington, D.C.

Abstract.—The Mississippian history of the northern Cordilleran region of the United States consists of two principal depositional cycles separated by a cycle of epeirogenic uplift and erosion. Each depositional cycle is divisible into phases that represent significant changes in depositional patterns. During Cycle I (early Kinderhookian–early Meramecian), predominantly carbonate and evaporite deposition took place on a broad cratonic shelf bordered on the east by land and on the west by a deep trough that received terrigenous sediments from an adjacent western landmass. Kinderhookian transgression was followed by regression during the Osagean and early Meramecian. Regional uplift during latest early Meramecian time (Cycle II) drained the shelf area and caused the sea to be confined to the western trough. During Cycle III (middle Meramecian–Chesterian), the sea again transgressed onto the craton, which was differentiated into the Big Snowy–Williston, Wyoming, and Uinta basins, where terrigenous and carbonate sediments were deposited. The Big Snowy–Williston basin was uplifted during latest Chesterian time and lost its identity, but the Wyoming basin continued to expand into the Pennsylvanian, when it engulfed most of the Cordilleran platform and breached the Transcontinental arch. Application of generalized carbonate, terrigenous, and evaporite depositional models results in specific models that explain the Mississippian depositional patterns.

Extensive exposures of Mississippian rocks in the mountain ranges of Idaho, Montana, and Wyoming, together with data from boreholes in the intervening topographic basins, provide an excellent opportunity to reconstruct the history of an ancient depositional platform and adjacent geosyncline. The Mississippian rocks of the northern Rocky Mountains have had a long history of study by many generations of American geologists since the earliest investigations of the Western States. In the past 25 years, the application of biostratigraphic techniques has resulted in considerable refinement of the outcrop stratigraphy, and intensive exploration for petroleum has contributed subsurface data that fill many voids in the network of stratigraphic control. This paper summarizes the tectonic and depositional history of the northern Cordilleran Mississippian on the basis of the latest physical and paleontologic data, much of which has not been published previously. Geologic studies currently in progress by W. E. Hall, R. A. Paull, and Betty Skipp in central Idaho may alter some of the conclusions concerning that area, where the rock sequence is structurally complex and paleontologic data are sparse.

Acknowledgments.—The present compilation is based upon the work of many geologists. Specific citations of published work in the text do not include all papers that have contributed to the concepts expressed herein. Many U.S. Geological Survey colleagues have contributed unpublished data and ideas; among the more noteworthy of these contributors are J. T. Dutro, Jr., M. Gordon, Jr., W. E. Hall, J. W. Huddle, J. D. Love, C. A. Sandberg, R. P. Sheldon, Betty Skipp, and the late Helen Duncan. B. L. Mamet of the University of Montreal was most helpful in providing foraminiferal determinations on many new samples. R. A. Paull and his students at the University of Wisconsin (Milwaukee) provided new data on the stratigraphy of south-central Idaho. I am also indebted to J. T. Dutro, Jr., J. W. Pierce, C. A. Sandberg, Betty Skipp, and J. L. Wilson for technical review of the manuscript.

PALEOTECTONIC ELEMENTS

During Mississippian time, most of the northern Rocky Mountains region of the United States was a part of the stable heartland of the North American continent known as the *North American craton.* The craton included the *Canadian Shield*, a vast northern stable land area composed of Precambrian basement rocks (fig. 1), and a linear positive area, the *Transcontinental arch*, which extended southwestward from the Canadian Shield. Physical and paleontologic evidence suggests that the Transcontinental arch was emergent throughout the Mississippian, but the ancient shorelines are not preserved and their precise locations are conjectural. Although the arch seems to have divided the southern part of the North American craton into two discrete areas of marine deposition

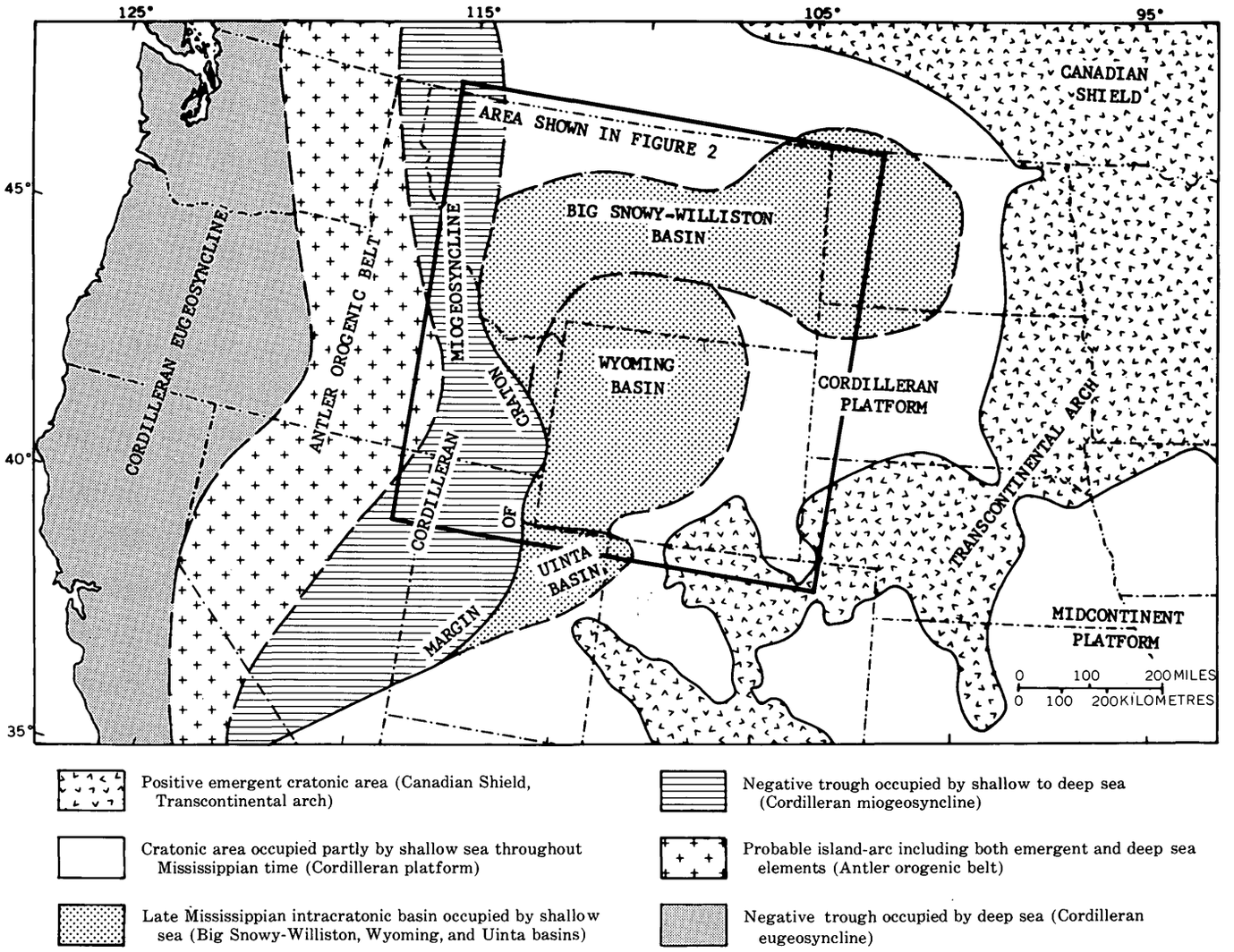

FIGURE 1.—Major structural features of the western United States during the Mississippian. Limits of Transcontinental arch are mainly the boundaries between Mississippian carbonate rocks and pre-Mississippian rocks modified from Mallory (1972) and Sloss and others (1960). Limits of Antler orogenic belt are generalized from Roberts (1972). Limits of Big Snowy–Williston basin are modified from Mallory (1972).

during the Mississippian, there may have been limited connections of the sea across the arch during some parts of the period. Moreover, the cratonic seas were connected around the southern terminus of the Transcontinental arch in New Mexico and Arizona.

West of the Transcontinental arch was the *Cordilleran platform*, a broad cratonic area of relatively thin marine sedimentation that extended from southern Canada southward into Mexico. During the Early Mississippian, the Cordilleran platform was a depositional shelf that received predominantly carbonate and evaporite sediments. In the Late Mississippian, the platform was differentiated into three intracratonic basins: the *Big Snowy–Williston basin*, which extended across Montana into parts of southern Canada and the Dakotas; the *Wyoming basin*, which covered most of Wyoming and extended into parts of Idaho, Utah, and Montana; and the *Uinta basin* in eastern Utah and northwestern Colorado. These basins received shallow-water terrigenous and carbonate sediments.

The Cordilleran platform was bordered on the west by a linear belt of thick sedimentation, which can be divided into an eastern *Cordilleran miogeosyncline*, a central *Antler orogenic belt*, and a western *Cordilleran eugeosyncline*. The Cordilleran miogeosyncline included both shelf and deeper water trough sedimentation of carbonates and terrigenous detritus during the Mississippian. The Antler orogenic belt, probably the site of an island chain, was undergoing sporadic tectonism throughout Mississippian time. The Cordiller-

an eugeosyncline was an area of predominantly deeper water sediments and volcanic materials.

This paper summarizes the Mississippian history of Montana, Wyoming, eastern Idaho, and adjacent parts of the Dakotas, Nebraska, Colorado, and Utah, an area that extends from the Transcontinental arch across the Cordilleran platform and Cordilleran migeosyncline into the Antler orogenic belt (fig. 1). Most of the major paleotectonic elements can be discerned on a thickness map for the Mississippian rocks in this area (fig. 2). The Cordilleran platform includes the area generally bounded by the 1,500-ft isopach line except for the Big Snowy–Williston basin, where the sedimentary rocks are more than 2,500 ft thick, and the Uinta basin, where they are more than 2,000 ft thick. The Wyoming basin, however, does not manifest itself in the total Mississippian thickness pattern because it was not an area of appreciable subsidence during deposition and it did not become evident as a discrete depositional unit until Late Mississippian time. The Cordilleran migeosyncline includes thicknesses that exceed 7,000 ft. The limited area of the Antler orogenic belt included in the study contains no record of Mississippian sedimentation and was probably emergent throughout the period.

Palinspastic reconstruction of depositional patterns has not been attempted. Distortion of geographic relations of lithofacies because of post-Mississippian folding and faulting is probably not significant on the Cordilleran platform. Moderate folding and thrust-faulting in the Cordilleran miogeosyncline undoubtedly reduced the width of sedimentary belts in this area, but no major translocations of original sedimentary facies have been noted.

STRATIGRAPHY

Many papers have been published on the local and regional stratigraphy of the Mississippian System in the Rocky Mountains area. A discussion of all previous work that laid the foundation for concepts presented herein is beyond the scope of this paper. Studies of regional lithostratigraphy by Andrichuk (1955a, b; 1958), Craig (1972), Craig and others (1972), Gries and Mickelson (1964), Huh (1967), Leatherock (1950), Love and others (1953), Mallory (1967, 1972), Maughan (1963), Maughan and Roberts (1967), Nordquist (1953), Paull and others (1972), R. P. Sheldon and M. D. Carter (unpub. data, 1976), and Sloss and Laird (1945) have been particularly helpful in providing basic data for the present compilation. Studies by Dutro and Sando (1963a, b), Easton (1962), Mamet and Skipp (1970, 1971), Mamet and others (1971), Mudge and others (1962), Sandberg (1963, 1967), Sandberg and Klapper (1967), Sandberg and Mapel (1967), Sandberg and others (1967), Sando (1960a, b; 1967a, b; 1972), Sando and Dutro (1960), Sando and others (1959, 1969, 1975), Shaw (1955), Shaw and Bell (1955), and Skipp and Mamet (1970) form the foundation for the biostratigraphic framework. Petrologic studies by Cotter (1965), Jenks (1972), Moore (1973), Smith (1972), Stone (1972), and Wilson (1969) contributed valuable information on aspects of Cordilleran Mississippian sedimentation that have received little attention in the literature.

Correlation of the Mississippian formations of the northern Rocky Mountains region (fig. 3) is based mainly on biostratigraphic studies utilizing the microfaunal and megafaunal zonations summarized by Sando and others (1969). The overall regional pattern of Mississippian sedimentation indicated by the correlation chart is that of two depositional cycles interrupted by uplift and erosion in all but the westernmost part of the area. The earliest Mississippian cycle (Cycle I) is a period of deposition that began in the early Kinderhookian and extended into early Meramecian time in the Cordilleran miogeosyncline and the Cordilleran platform. This was followed by a period of epeirogenic uplift and erosion (Cycle II) that began in latest early Meramecian time. Cycle II was relatively brief in the Cordilleran miogeosyncline but extended to the end of the Chesterian in some parts of the Cordilleran platform. A second marine transgression (Cycle III) began at the beginning of middle Meramecian time in the Cordilleran miogeosyncline; it extended into the Pennsylvanian in parts of the miogeosyncline and the platform, but was terminated by pre-Pennsylvanian erosion in other parts of the same area.

According to Sandberg and Mapel (1967, fig. 2), the base of the Mississippian coincides with the base of the *Siphonodella sulcata* conodont zone, which is near the base of megafaunal zone pre-A and microfaunal zone pre-7 of Sando and others (1969). Sandberg and Mapel (1967, fig. 2) have shown that sporadic sedimentation from latest Devonian time across the systemic boundary slightly into the Mississippian was followed by a widespread period of erosion in the northern Rocky Mountains region prior to the beginning of the main episode of Mississippian deposition, although sedimentation was continuous in a part of west-central Wyoming and possibly in South Dakota. For practical purposes of analyzing the depositional history of this area, the base of the Mississippian (base of Cycle I) is placed at the base of the depositional episode that followed regional uplift and erosion during earliest Mississippian time.

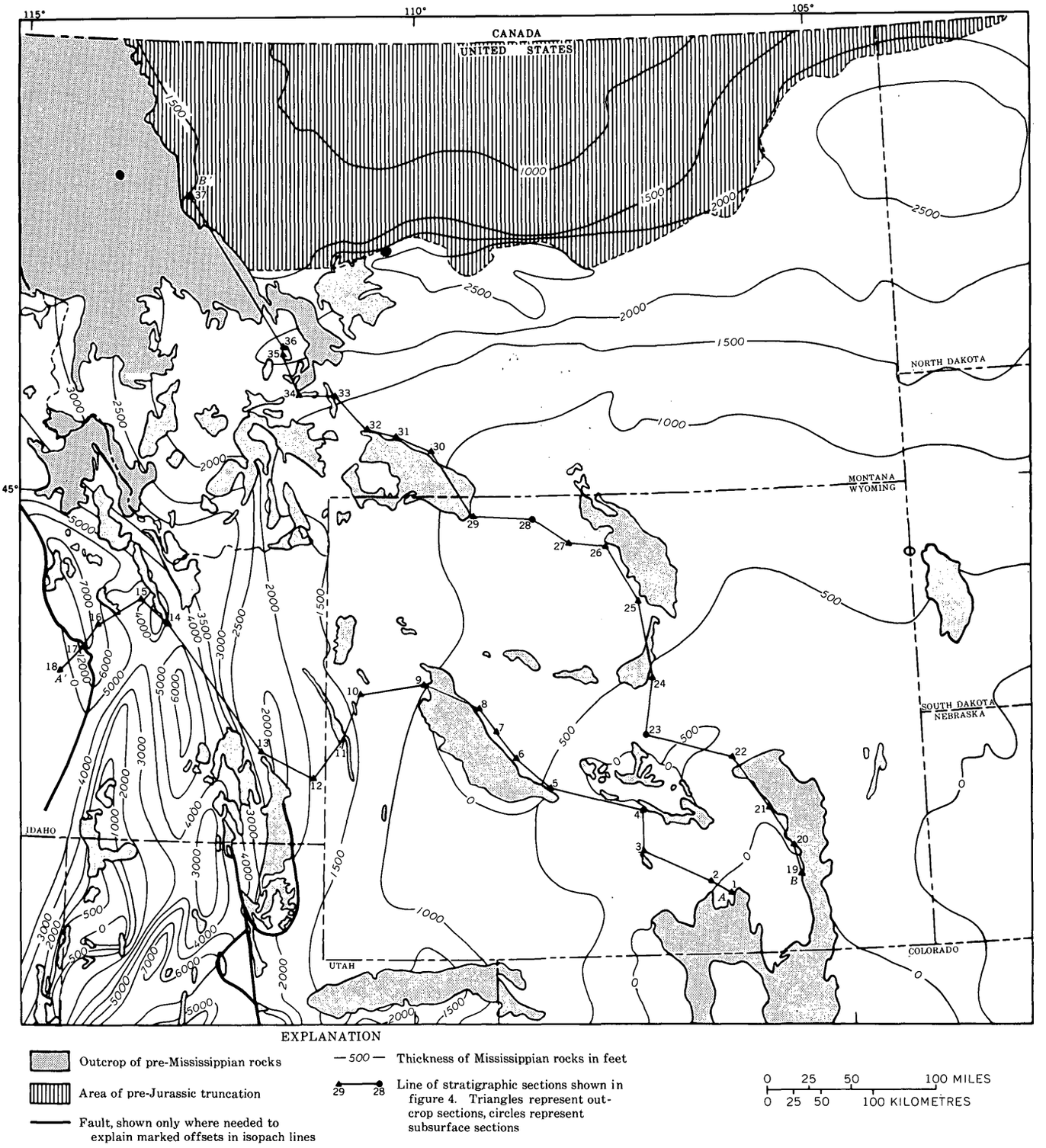

FIGURE 2.—Map showing total thickness of Mississippian rocks in northern Rocky Mountains region of the United States, trend of cross sections, and location of key stratigraphic sections (numbered) shown in figure 4. Modified from Craig and others (1972). Isopach lines in feet (metres=0.3048×feet).

Cycle I is represented by predominantly carbonate rocks included in the Madison Limestone or Group over most of the miogeosyncline and platform (fig. 3). The Madison Group is represented only by the Lodgepole Limestone in parts of southeast Idaho and northeast Utah; the Lodgepole is succeeded by the Brazer

Dolomite in the Crawford Mountains. Elsewhere, Madison correlatives include the Guernsey Formation of southeast Wyoming and the Pahasapa Limestone of the Black Hills. In the eastern part of south-central Idaho, argillites called Milligen Formation by Sandberg and others (1967) are the same age as the lower part of the Madison; these argillites are younger than and not continuous with the type Milligen (Sartenaer and Sandberg, 1974, p. 757) and should be given a new name.[1] Farther west, in the Pioneer Mountains of central Idaho, Madison time is represented by part of the "Milligen," the Drummond Mine, and the Scorpion Mountain Formations, and part of the Muldoon Canyon Formation of Paull and others (1972).

The more variable stratigraphic classification of the rocks of Cycle III reflects more complex paleogeographic conditions during the Late Mississippian. Terrigenous and carbonate rocks of this cycle are included in the Big Snowy Formation or Group of Montana, North Dakota, and part of Idaho, and in the Amsden Formation of Wyoming. In parts of northeastern Utah and southeastern and south-central Idaho, the lower sandy part of the cycle is included in three very similar time-equivalent units: the Little Flat, Middle Canyon, and Deep Creek Formations. Superjacent carbonate rocks of this area are referred to the Monroe Canyon Limestone, Scott Peak Formation, South Creek Formation, Surrett Canyon Formation, and Great Blue Limestone. Manning Canyon Shale tops the sequence in the Deep Creek Mountains of southeast Idaho. In the White Knob Mountains of south-central Idaho, the White Knob Limestone spans most of Cycle III. In the Pioneer Mountains, this later cycle is included in the upper part of the Muldoon Canyon Formation and the Brockie Lake Conglomerate of Paull and others (1972). Deposition was continuous into the Pennsylvanian over most of the area.

Two cross sections (fig. 2, 4) depict generalized stratigraphic and structural relations of the Mississippian strata. In cross-section *A–A′* (fig. 4*A*, *B*), a wedge of Cycle-I carbonate and evaporite rocks thickens uniformly westward from the Transcontinental arch to the margin of the Cordilleran platform, where the rocks were abruptly thinned by Cycle-II erosion in the Cordilleran miogeosyncline. The carbonate-evaporite facies passes into a thick argillite sequence in the miogeosyncline. This argillite sequence is bordered on the west by a thick sequence of carbonate rocks and coarse terrigenous rocks adjacent to the Antler orogenic belt.

In the same cross section, a thinner wedge of Cycle-III terrigenous rocks thickens uniformly westward across the Cordilleran platform and then thickens rapidly from the platform margin to the axis of the miogeosyncline. The upper part of Cycle III is represented by a wedge of carbonate rocks that thickens rapidly from the platform margin (fig. 4*A*, sec. 10) to the axis of the miogeosyncline. As in the previous cycle, the carbonate rocks of Cycle III intertongue with terrigenous rocks along the margin of the Antler orogenic belt (fig. 4*A*, secs. 16–17).

Cross section *B–B′* (fig. 4*C*) shows stratigraphic relations of the Mississippian strata from the Transcontinental arch to the north flank of the Big Snowy–Williston basin. Here also, the wedge of Cycle-I carbonate and evaporite rocks thickens gradually and fairly uniformly across the Cordilleran platform and then moderately in the Big Snowy–Williston basin. The Cycle-I lithic facies change only slightly in the Big Snowy–Williston basin, and no exclusively terrigenous facies is developed. Cycle-III terrigenous rocks show approximately the same thickness pattern as the rocks of Cycle I.

PALEOTECTONIC HISTORY

Each of the two depositional cycles (Cycles I and III) includes a complex of marine transgressions and regressions within the areas of deposition, and tectonic movements in adjacent landmasses that affect the character of the sedimentary deposits. Such changes are continuous and commonly difficult to delineate. Figure 5 presents a summary of paleotectonic events correlated by means of the Cordilleran Mississippian zonation systems and calibrated against a revised absolute time scale. Each of the depositional cycles is divided into phases that represent periods of significant changes in depositional patterns recognizable in some parts of the area.

Biostratigraphic and lithostratigraphic correlation of Mississippian sections measured at many localities in the northern Cordilleran region permits the construction of a series of paleogeographic maps (fig. 6) that depict patterns discernible at an identifiable moment or interval within each phase; they are not necessarily characteristic of the entire span of the phase. More detailed work will probably result in recognition of more phases or of subphases.

Cycle I, phase 1—early Kinderhookian (fig. 6)

Sandberg and Klapper (1967, p. B61–67) have summarized the paleotectonic history of the Late Devonian and Early Mississippian in the northern Cordilleran region. Prior to the deposition of the earliest sedi-

[1] The age, classification, and correlation of these beds are controversial. Sandberg (1975) has recently proposed a new formation name to include the argillite and siltstone beds placed by me in the overlying Middle Canyon Formation, which I regard as Meramecian in age and separated from the argillite by a regional disconformity.

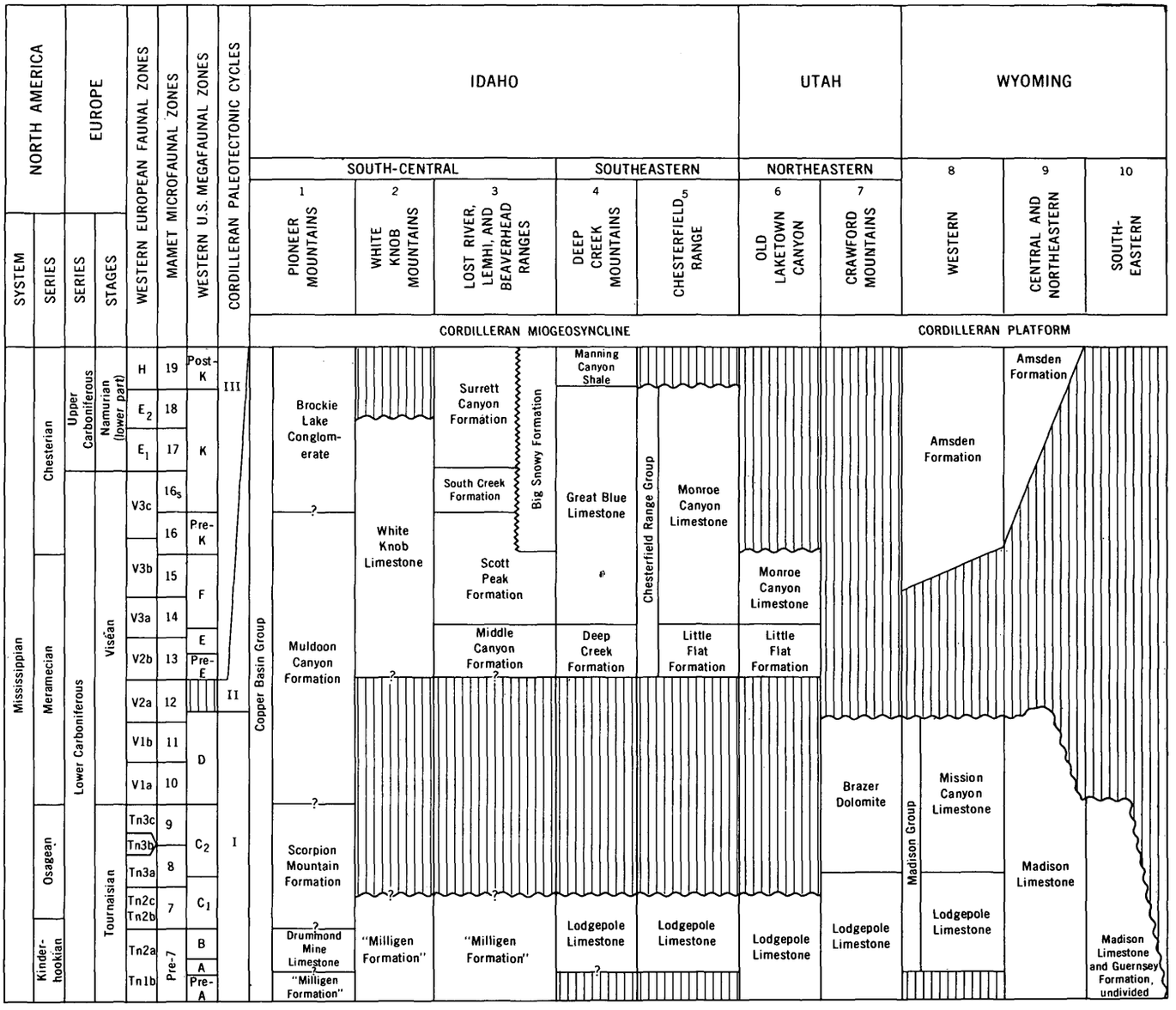

FIGURE 3.—Nomenclature and temporal relations of Mississippian rock units in the northern Rocky Mountains region of the United States. Vertical lines denote hiatus. Sources of data for stratigraphic columns: 1, modified from Paull and others (1972); 2, modified from Skipp and Mamet (1970); 3, Sando and others (1975); 4, Sando (1967b); 5, Sando and others (1969); 6, Sando and others (1969); 7, Sando (1967b); 8, Sando (1967b), Sando and others, (1969, 1975); 9, Sando (1967a), Sando and others (1969, 1975); 10, modified from Maughan (1963); 11, Sando and others (1969, 1975); 12, Mudge and others (1962); 13, Sandberg and Mapel (1967), Sando (1960b), Sando and others (1975); 14, Sandberg and Mapel (1967), Sando (unpub. data, 1975); 15, Sandberg and Mapel (1967), Sando (unpub. data, 1975).

ments of Cycle I, a mild orogenic episode, probably related to the Antler orogeny of Nevada and Idaho, created a land area of low relief on the Cordilleran platform and miogeosyncline. At the onset of Cycle I, a deep trough formed adjacent to the Antler orogenic belt and began receiving fine terrigenous sediments shed by a low-lying western landmass. As the Mississippian sea advanced rapidly onto the Cordilleran platform over a terrane composed of Cambrian, Ordovician, and Devonian rocks, terrigenous and carbonate sediments were deposited in several shallow marine basins separated by low-lying land. The rising Transcontinental arch was a land area bordered on the west by an apron of quartz sand derived from the arch.

Cycle I, phase 2—late Kinderhookian (fig. 6)

In phase 2, continued rapid transgression of the Cordilleran sea brought about the initiation of shelf car-

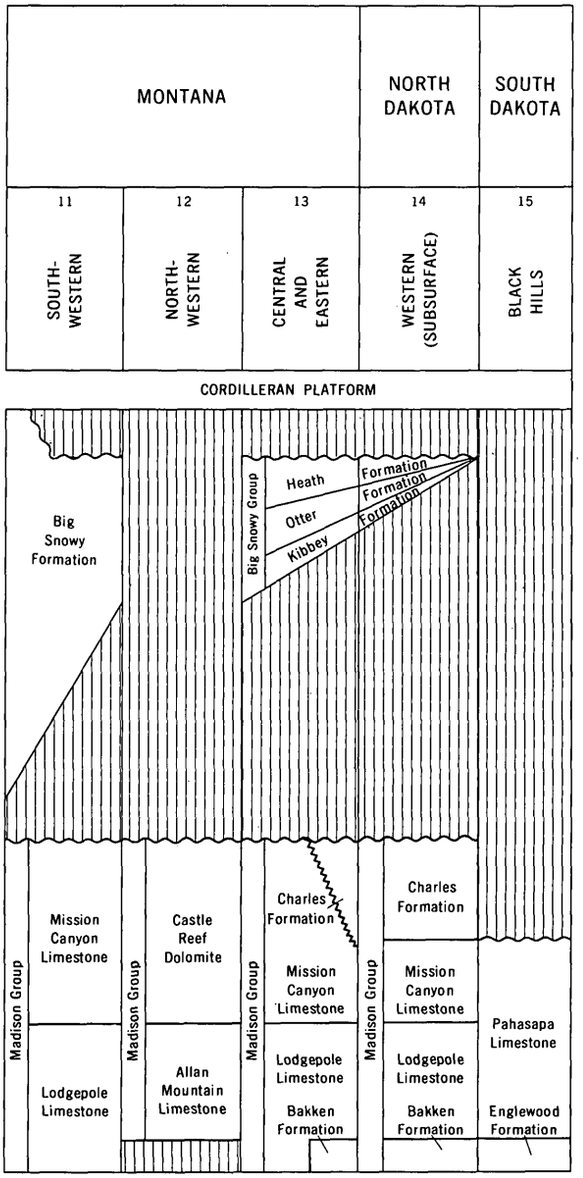

FIGURE 3.—Continued.

bonate deposition on the Cordilleran platform. The Transcontinental arch continued to rise and to contribute a marginal sand belt. The sand belt was bordered by a belt of dolomitized intertidal carbonate, which passed seaward into dolomitized and undolomitized subtidal carbonate to the edge of a prograding carbonate shelf. An island can be identified in south-central Wyoming. The sea floor adjacent to the shelf began to differentiate into slope and trough. While the deep trough of the miogeosyncline continued to receive fine terrigenous sediments from the Antler orogenic belt, the slope received argillaceous carbonate mud, the "deeper water limestones" of Wilson (1969).[2]

Cycle I, phase 3—latest Kinderhookian (fig. 6)

Phase 3 marked the height of the Cycle I transgression and was characterized by marked differentiation of the area into shelf, slope, and trough. The lithofacies belts are similar to those of the previous phase, but the shelf margin shifted landward, probably because of a rise in sea level. Waulsortian bioherms developed at several places on the slope (Wilson, 1969 and written commun., 1974; Smith, 1972; Stone, 1972). The Antler orogenic belt continued to supply fine terrigenous sediment to the deep trough in south-central Idaho.

Cycle I, phase 4—early Osagean (fig. 6)

Phase 4 marked a turning point in the depositional history. During this period, progradation of shelf carbonates caused the shelf margin to migrate seaward over the slope so that slope deposits cannot be distinguished. In Idaho, the deep trough was sharply demarcated from the shelf. Uplift in the Antler orogenic belt contributed a narrow marginal belt of coarse terrigenous sediments on the west flank of the trough. Quiescence in the Transcontinental arch reduced the supply of terrigenous detritus so that no marginal sand belt is evident on the Cordilleran platform. Instead, the arch was bordered by a belt of dolomitized intertidal to subtidal carbonate sediments. Most of the shelf was characterized by cyclical subtidal and intertidal carbonate sediments that record many minor transgressions and regressions of the sea. The sedimentary record on the Cordilleran platform suggests that phase 4 represents a change from net transgression to net regression.

Cycle I, phase 5—late Osagean (fig. 6)

Phase 5 is the first of several periods of restricted circulation during Osagean-early Meramecian regression on the Cordilleran platform. While a marginal dolomitized carbonate belt similar to that of the previous phase formed adjacent to the quiescent Transcontinental arch, an extensive area of evaporite deposition covered northern Wyoming, much of Montana, and extended eastward into the Dakotas. Evidence of widespread highly saline conditions is found in beds of anhydrite as well as in solution breccias that represent leached evaporite beds (Roberts, 1966; Sando, 1967a). A reflux system associated with evaporite deposition (Adams and Rhodes, 1960) was initiated during this

[2] Wilson's bathymetric interpretation has been challenged by Sloss (in Wilson, 1969, p. 18). A. B. Shaw (oral commun., 1974) believes that Wilson's "deeper water limestones" were deposited at the shelf edge in very shallow water, where fines were transported from slightly deeper but more turbulent environments on the shelf proper. Although the absence of benthonic algae in these beds suggests accumulation below the photic zone, this feature might be explained by increased turbidity in the area of deposition. Resolution of this controversy awaits more detailed study of the problem.

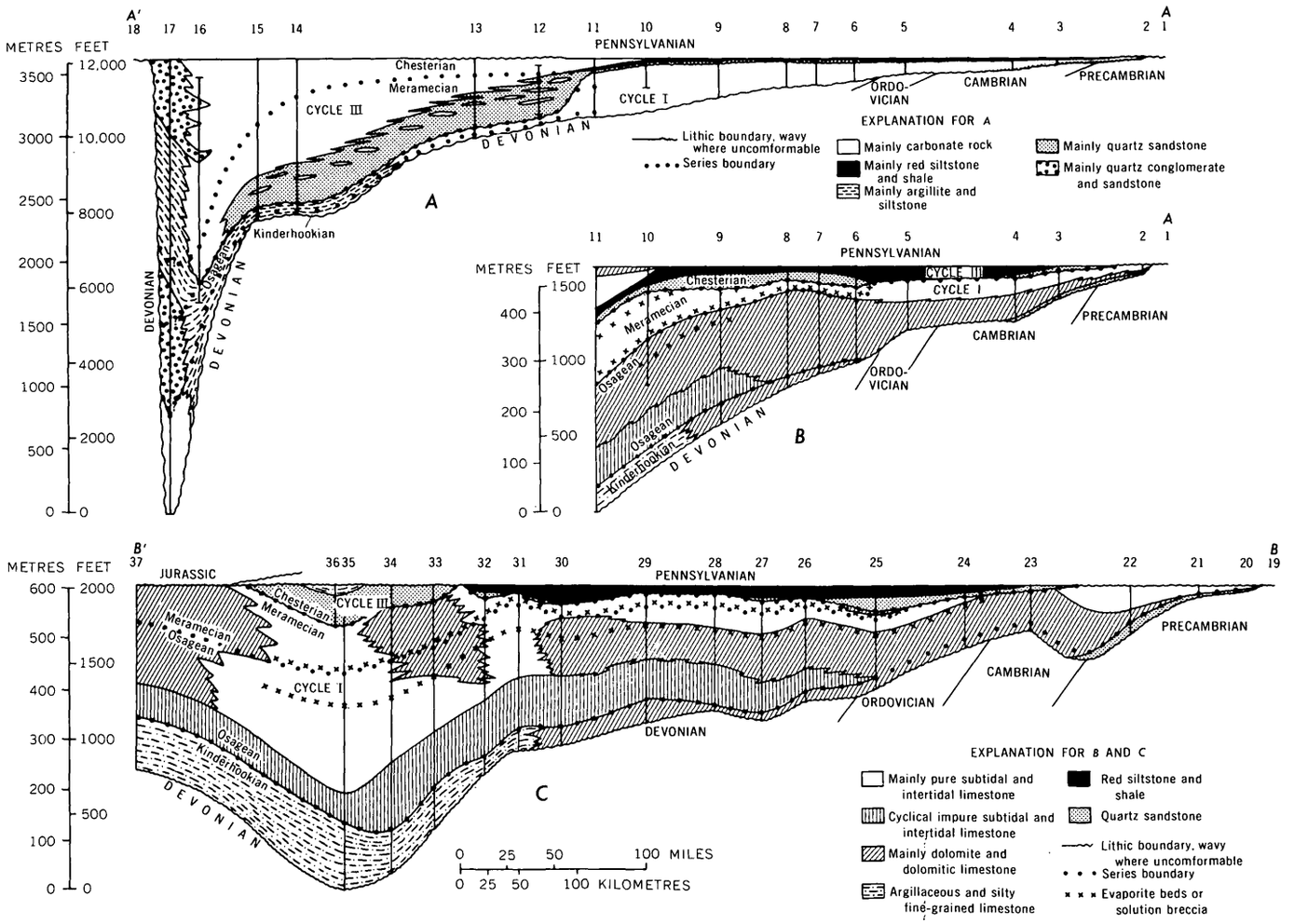

FIGURE 4.—Cross sections at different vertical scales showing stratigraphic and structural relations of Mississippian rocks in northern Rocky Mountain region of the United States. *A*, Section *A–A'* from southeast Wyoming to south-central Idaho. *B*, Eastern part of section *A–A'* from southeastern to western Wyoming. *C*, Section *B–B'* from southeast Wyoming to northwest Montana. Locations of stratigraphic sections shown in figure 2 and table 1.

phase and caused dolomitization of underlying carbonate rocks. Evidence of the shelf margin has been removed by subsequent erosion, but remnants of a seaward belt of subtidal limestone are preserved in western Montana. The Antler orogenic belt was bordered by a belt of coarse terrigenous sediments which intertongue with argillite that represents the deep trough in Idaho, but the true width of the trough at this time is unknown, owing to subsequent erosion.

Cycle I, phase 6—latest Osagean (fig. 6)

Phase 6 was characterized by a freshening of the shelf sea that occupied the Cordilleran platform. Subtidal carbonate sediments, subsequently dolomitized by reflux action in some places, were deposited at this time. This change in facies from the previous phase suggests a rise in sea level. Exact location of the shelf margin is unknown owing to subsequent erosion in Idaho, as in the previous phase. Deposition of coarse and fine clastic sediments in the deep trough adjacent to the Antler orogenic belt continued.

Cycle I, phase 7—early Meramecian (fig. 6)

Lithofacies patterns of phase 7 indicate a return to the restricted circulation pattern of phase 5, although subsequent erosion removed much of the record of deposition. The presence of an intertidal dolomite facies peripheral to a large area of evaporite deposition, including a halite facies in Montana and North Dakota, marks the culmination of the regression that began in the early Osagean. Again, the record of the shelf margin has been lost. Fine terrigenous sediment bordered the Antler orogenic belt in Idaho.

Cycle II,—latest early Meramecian (fig. 6)

Epeirogenic uplift drained the Cordilleran platform and most of the Cordilleran miogeosyncline during

Cycle II. Only a remnant of the sea remained in a narrow deep trough adjacent to the Antler orogenic belt in Idaho, where deposition of fine terrigenous sediment continued. Most of the rest of the previous area of deposition became a carbonate terrane except for part of the miogeosyncline east of the trough, where the land was composed of terrigenous rocks. The more extensive removal of the previous sedimentary record in the miogeosyncline suggests that the positive movements were more active in that area. Deposition of Cycle III also began earlier in the miogeosyncline and migrated eastward across the platform, parts of which were being eroded throughout Meramecian and Chesterian time. A karst topography developed on much of the platform (Roberts, 1966; Sando, 1974).

Cycle III, phase 1—early middle Meramecian (fig. 6)

At the onset of Cycle III, the Cordilleran platform was characterized by continued karst development and the formation of a river system that carried terrigenous sediment from the rising Transcontinental arch across the platform to the platform margin. The Uinta basin was formed as a reentrant into the platform margin and received quartz sand from the adjacent parts of the Transcontinental arch. The miogeosyncline was differentiated into a marine shelf where quartz sand and sandy carbonate were deposited, a slope where argillaceous and silty carbonate was deposited, and a trough where argillaceous and carbonaceous mud and silt were deposited. Open marine carbonate banks began to form on the shelf toward the end of this phase. The western landmass was quiescent.

Cycle III, phase 2—latest Meramecian (fig. 6)

During phase 2, subsidence of parts of the platform margin permitted encroachment of the Cordilleran sea into Wyoming and southwestern Montana. The remainder of the platform remained emergent and a second river system, which derived terrigenous detritus from the Canadian Shield, began to empty into the miogeosyncline. Differentiation into trough, slope, and shelf again characterized the miogeosyncline. Buildup of shelf carbonate banks restricted areas of terrigenous deposition to estuarine reentrants into the platform margin. A lagoonal area characterized by red beds began to form between the carbonate and quartz sand deposits at the platform margin in western Wyoming and southeastern Idaho.

Cycle III, phase 3—earliest Chesterian (fig. 6)

In phase 3, the embryonic Wyoming and Big Snowy–Williston basins were clearly evident as depositional entities, separated by a large peninsular area, the incipient Southern Montana arch. Another peninsular prong, the Bannock uplift, began to take shape in southwestern Wyoming and northeastern Utah. Tributaries of the northern river system began to encroach southward along the Transcontinental arch on the drainage area of the southern river system (Sando and others, 1975). The lagoonal red-bed and nearshore sand facies of the Wyoming basin migrated eastward. The Big Snowy–Williston basin was characterized by a landward area of quartz sand and a seaward area of argillaceous mud and carbonate. In the miogeosyncline, the area of pure shelf carbonate deposition was restricted by influx of fine terrigenous sediment from the southwest. Fine terrigenous sediment also continued to be deposited in a sharply defined deep trough adjacent to a quiescent western landmass in the Antler orogenic belt.

Cycle III, phase 4—middle Chesterian (fig. 6)

Phase 4 was marked by continued eastward migration and enlargement of the Big Snowy–Williston basin and Wyoming basin, separated by the Southern Montana arch. The Bannock uplift became an island that acted as a buttress restricting the mouth of the Wyoming basin. The sea also reentered the Uinta basin to the south. The miogeosyncline was characterized by expansion of the area of shelf carbonate deposition, which included a lobe that projected into the mouth of the Wyoming basin. Uplift in the Antler orogenic belt contributed coarse terrigenous sediment to the western trough.

Cycle III, phase 5—late Chesterian (fig. 6)

In phase 5, the Big Snowy–Williston basin attained its maximum areal extent and was characterized by an axial region of fine terrigenous sediment bordered landward by a terrigenous-carbonate belt and a nearshore sand belt. Continued expansion of the Wyoming basin reduced the Southern Montana arch to a narrow peninsula. The lagoonal red-bed facies occupied most of the Wyoming basin and was bordered by a narrow nearshore sand belt. The Bannock uplift continued to grow and to exert its influence on the restricted mouth of the Wyoming basin. Shelf carbonate deposition attained its maximum areal extent in the miogeosyncline. The western trough continued to receive coarse terrigenous sediment derived from a rising western landmass.

Cycle III, phase 6—latest Chesterian (fig. 6)

Phase 6 was a time of major earth movement in Montana, where the sea was drained by the emergence of the Big Snowy uplift. Evidence for complete with-

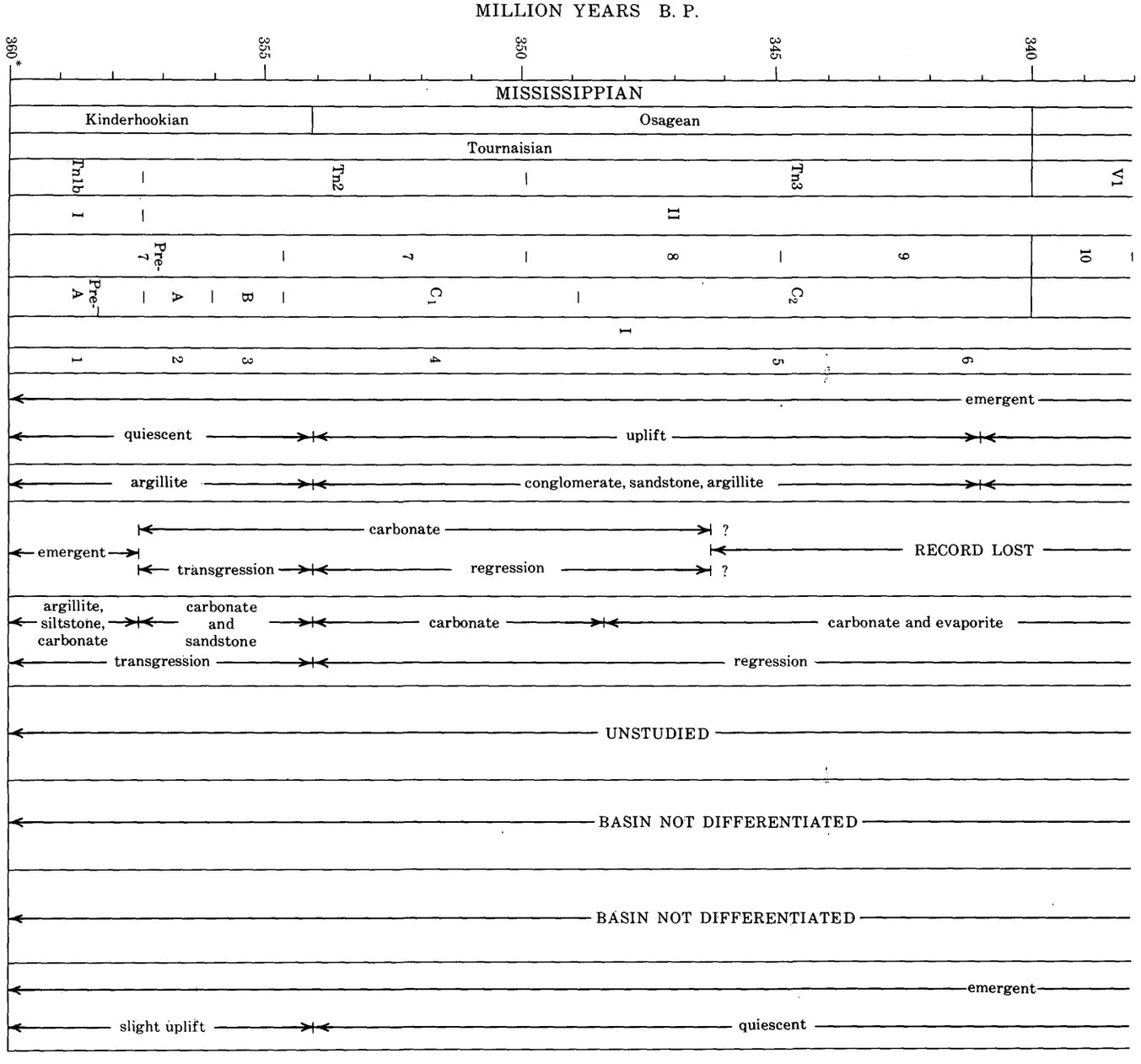

FIGURE 5.—Synthesis of Mississippian history of the northern Cordilleran region of the United

drawal of the sea from this area is largely lithostratigraphic and needs confirmation by more detailed paleontologic data; some remnants of the sea may have remained in the area shown on the map as land, but the Big Snowy–Williston basin ceased to exist as a depositional entity. The Wyoming basin continued to expand, and a restricted carbonate-terrigenous facies began to form at the mouth of the basin. The Bannock uplift attained its maximum areal extent. In the miogeosyncline, the area of shelf carbonate deposition was markedly reduced by the influx of fine terrigenous sediment from the southwest and northwest. The Antler orogenic belt continued to rise and contribute coarse terrigenous sediment to the western trough.

Early Pennsylvanian—early Morrowan (fig. 6)

The onset of Pennsylvanian time was marked by a great expansion of the Wyoming sea. It spread northward to cover most of Montana, reached eastward into the Dakotas and Nebraska, and breached the Transcontinental arch across the southeast corner of Wyoming and northeastern Colorado to mingle with the waters of the Midcontinent sea. In Montana, a small island area was all that remained of the Big Snowy uplift. Sources of terrigenous debris were now available northeast, east, and southeast of the Wyoming basin. The mouth of the basin was less restricted than before but was still partly blocked by the Bannock uplift, which

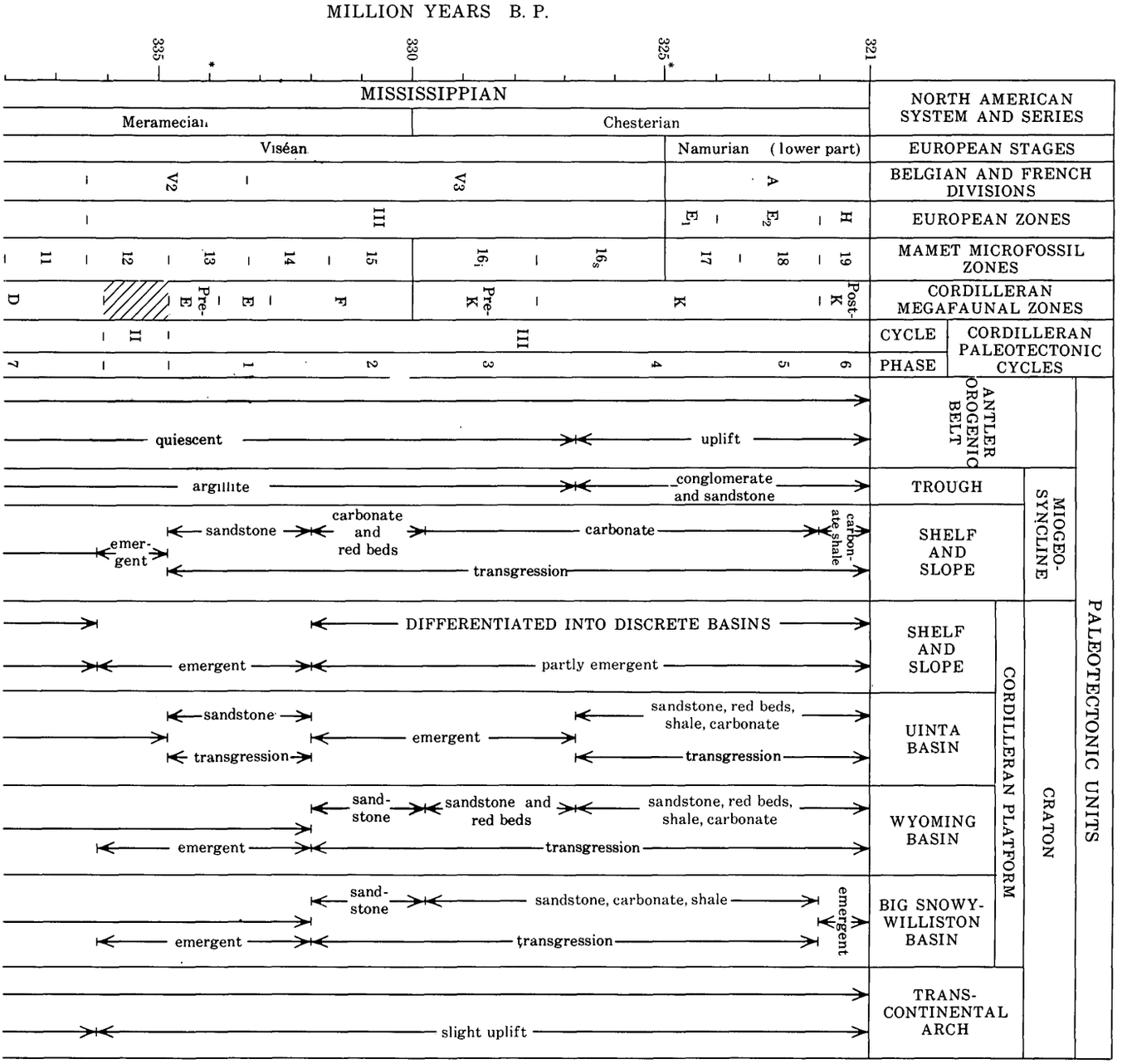

States. Absolute time scale revised from Francis and Woodland (1964) and Lambert (1971).

was diminishing in areal extent. At the southeast end of the basin, a highland area composed mostly of Precambrian crystalline rocks at the north end of the Front Range uplift began to influence sedimentation in that area. The restricted carbonate-terrigenous facies of latest Chesterian time was greatly expanded and occupied a central area of the basin. At the mouth of the Wyoming basin in south-central Idaho and westernmost Wyoming was a flood of quartz sand, probably derived from the Antler orogenic belt, which may have acted as a restrictive factor on deposition within the basin. This sand graded southward into carbonate and sand deposits in the miogeosyncline west of the Bannock uplift in southeastern Idaho. Fine terrigenous sediments and mixed carbonate and terrigenous sediments were deposited in the miogeosyncline of northern Utah.

RELATION BETWEEN MAJOR PALEOTECTONIC ELEMENTS AND PALEO-OCEANOGRAPHIC ELEMENTS

This analysis of the complex paleogeographic history of the northern Rocky Mountains Mississippian indicates that the morphology of the sea floor was not closely related to major paleotectonic elements in the area studied. The terms craton and miogeosyncline refer to tectonic elements characterized by different degrees of structural stability, as measured by the thickness of sediments accumulated during a given

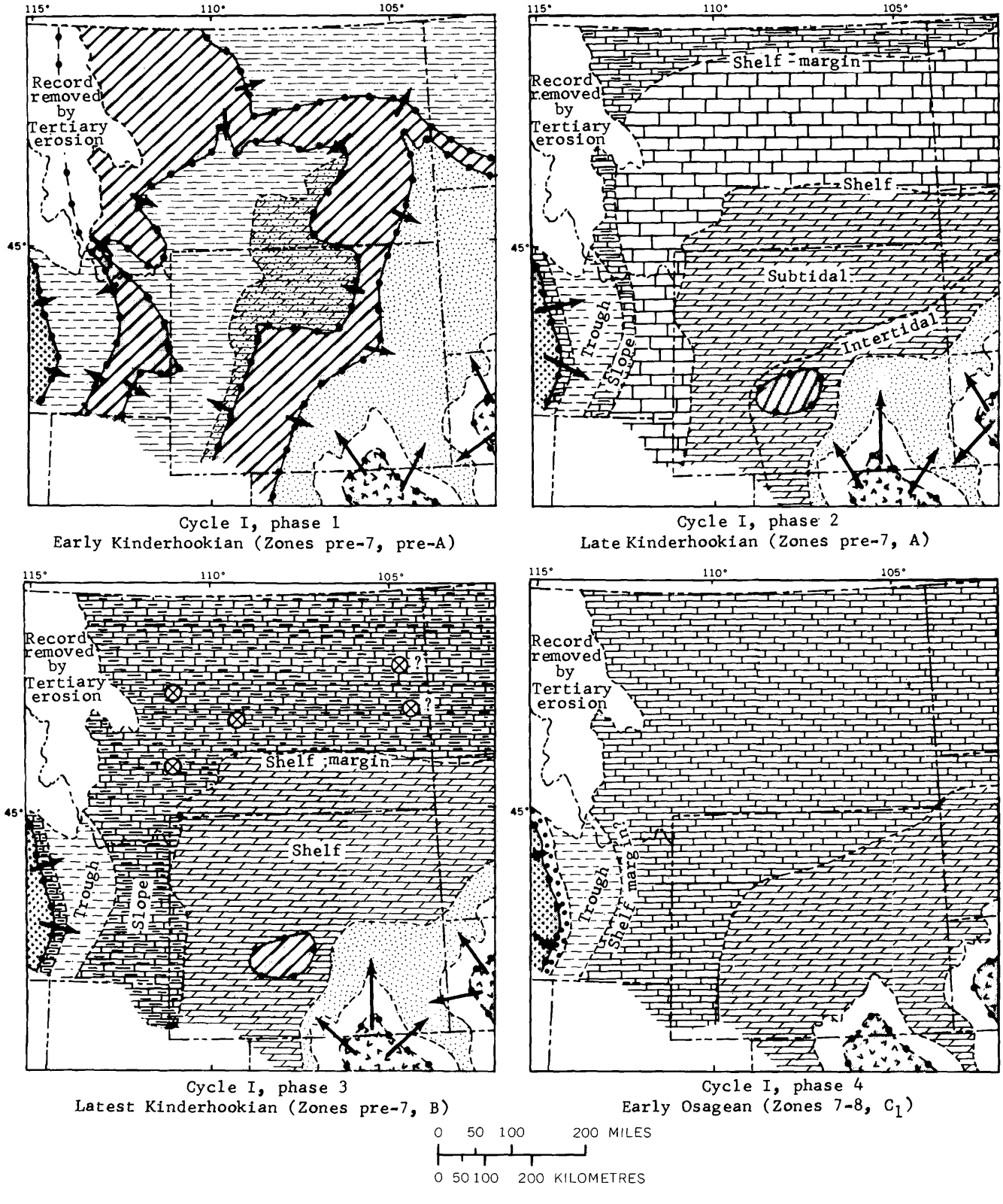

FIGURE 6.—Paleogeographic maps for Cycles I, II, III, and for Early Pennsylvanian.

EXPLANATION


Area of no control

Land areas


Upland composed of Precambrian crystalline rocks


Upland composed of lower Paleozoic terrigenous rocks


Lowland composed of lower Paleozoic carbonate and terrigenous rocks


Karst lowland composed of Madison Group (Mississippian) carbonate rocks


Lowland composed of "Milligen Formation" (Mississippian) terrigenous rocks


Lowland composed of Big Snowy Group (Mississippian) terrigenous and carbonate rocks

Marine depositional areas


Quartz sand and silt deposited in nearshore to offshore banks and bars on shelf


Quartz gravel and sand deposited nearshore on shelf adjacent to rising landmass


Quartz sand and sandy carbonate sediments deposited in open marine environments at shelf margin and in trough


Argillaceous and carbonaceous mud and quartz silt deposited in shallow basins


Argillaceous and carbonaceous mud and quartz silt deposited in trough


Argillaceous and silty carbonate mud deposited on slope between shelf and trough


Red argillaceous mud, silt, and sand and locally carbonaceous mud deposited in lagoons and nearshore swamps on shelf


Argillaceous mud and carbonate sediments deposited in shallow basin


Dolomitic carbonate, quartz silt, and sand deposited nearshore on shelf


Dolomitized intertidal to subtidal shelf carbonate sediments


Dolomitic carbonate, calcareous carbonate, argillaceous mud, and minor quartz sand deposited in restricted marine offshore banks in shallow basin on shelf


Cyclic intertidal and subtidal shelf carbonate sediments


Subtidal carbonate sediments deposited on open marine banks on shelf


Evaporitic sediments deposited in lagoons on shelf. H indicates halite facies

Postulated shoreline, dashed where uncertain


Postulated major paths of terrigenous sediment transport from land sources to sites of deposition


Waulsortian bioherm, question marks denote uncertain location

FIGURE 6.—Continued.

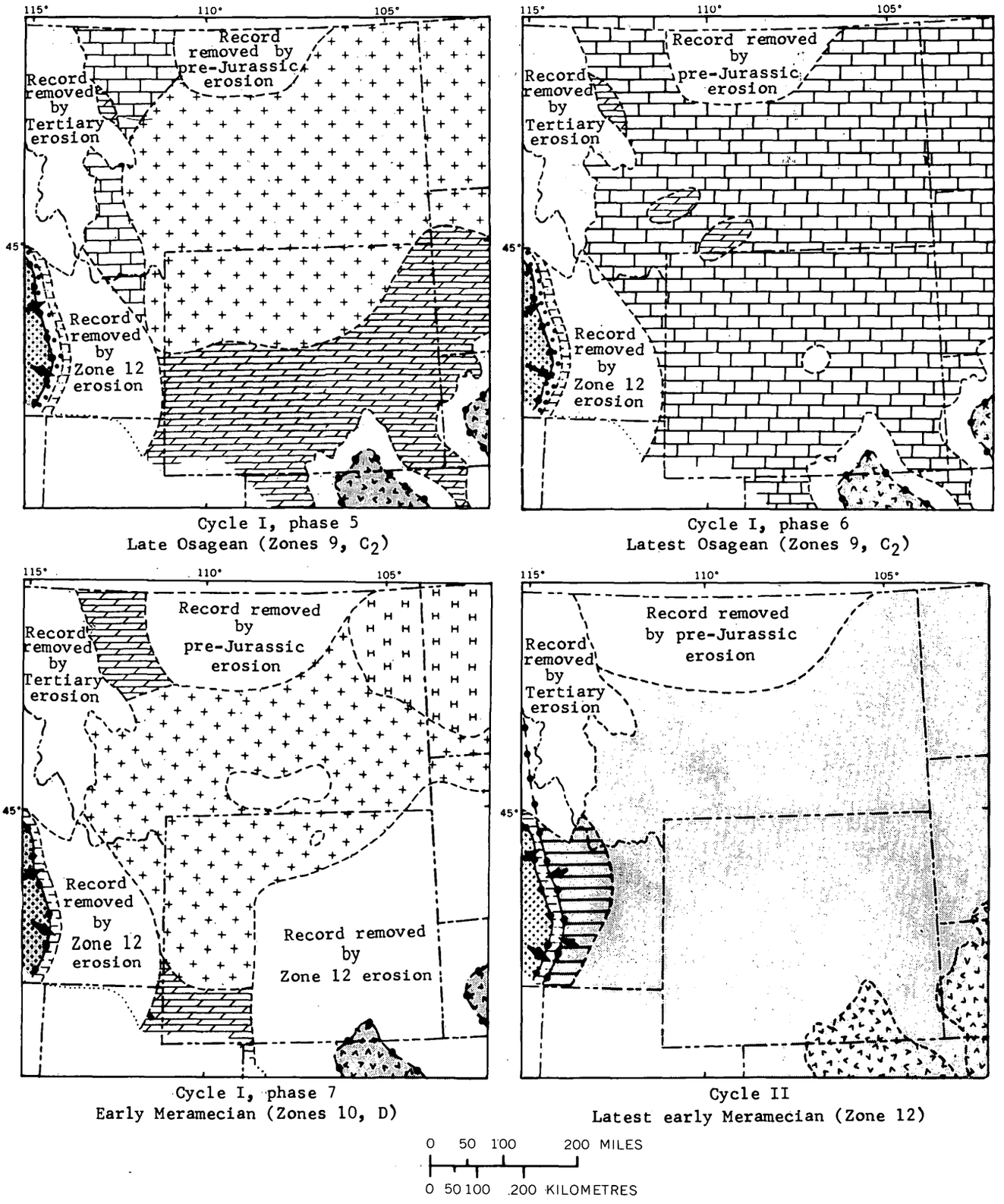

FIGURE 6.—Continued.

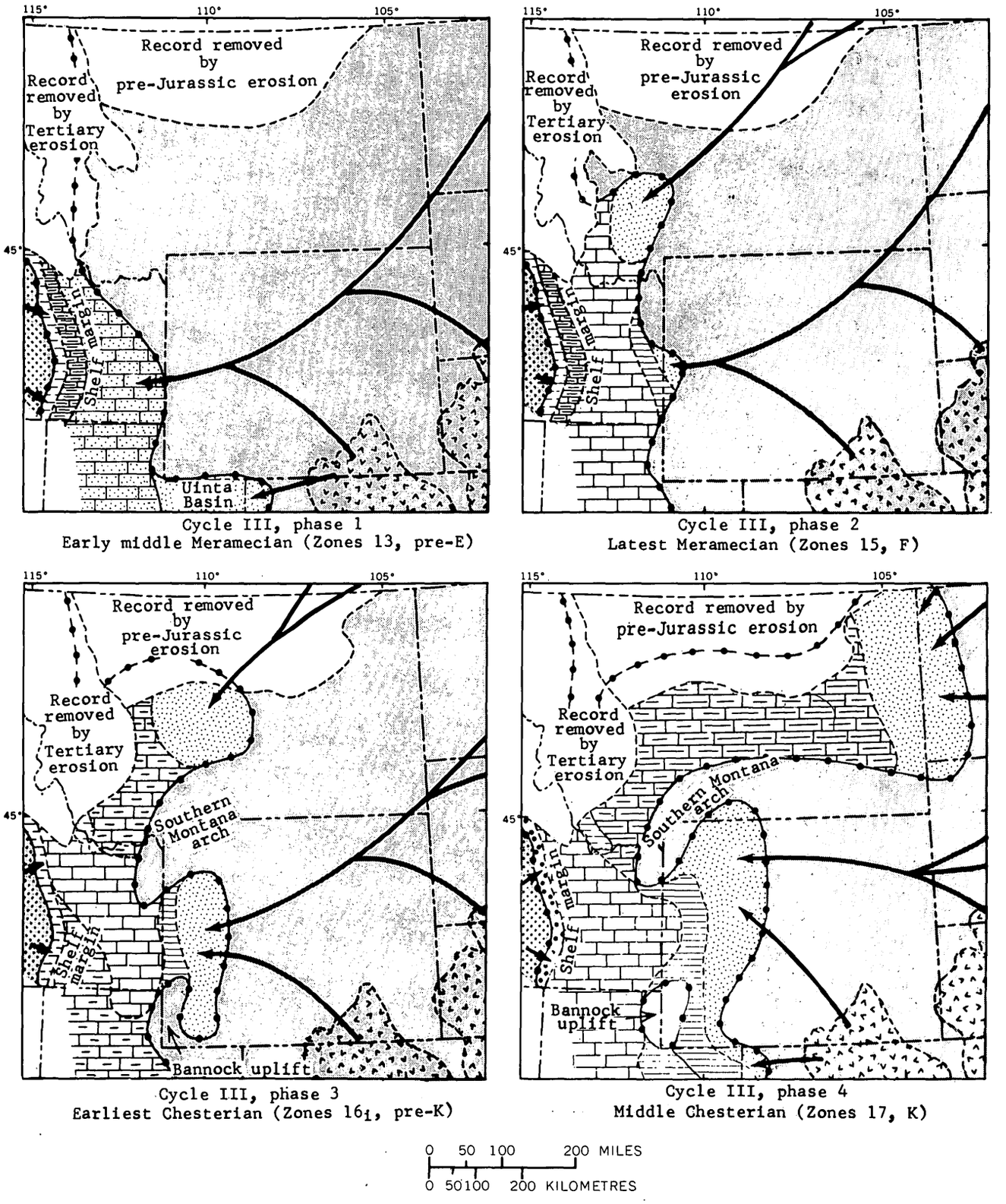

FIGURE 6.—Continued.

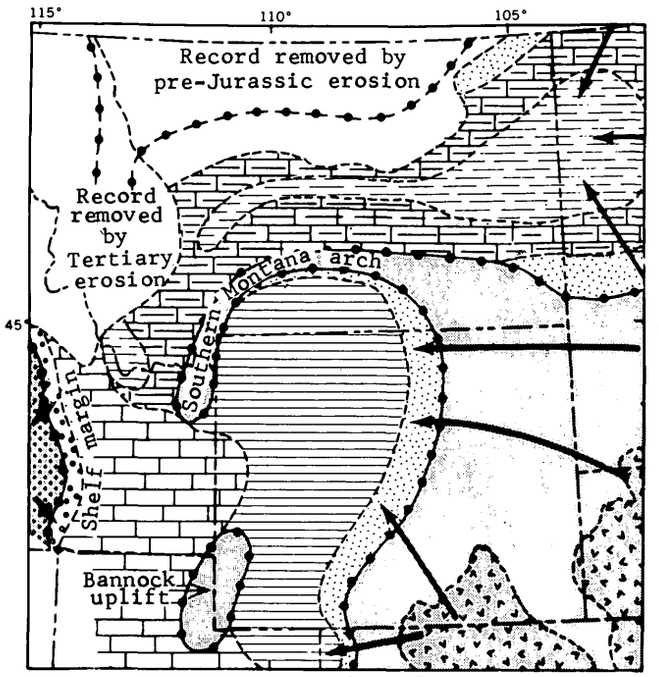

Cycle III, phase 5
Late Chesterian (Zones 18, K)

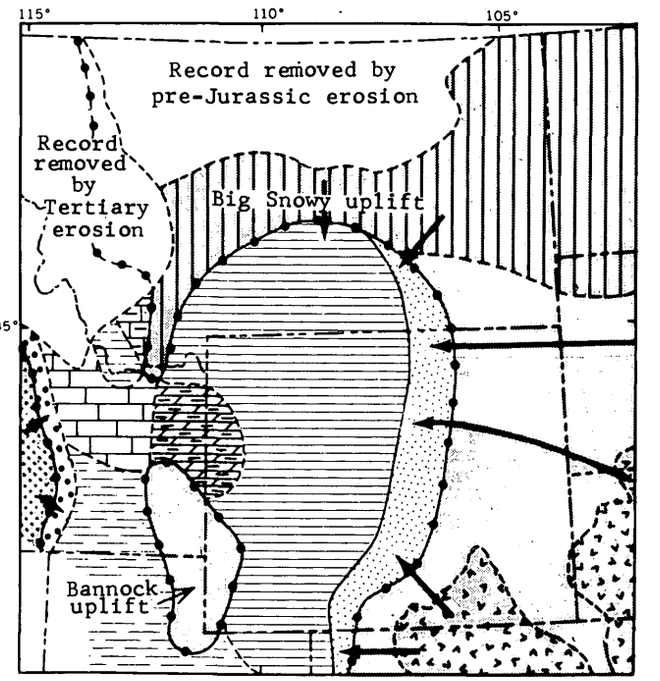

Cycle III, phase 6
Latest Chesterian (Zones 19, post-K)

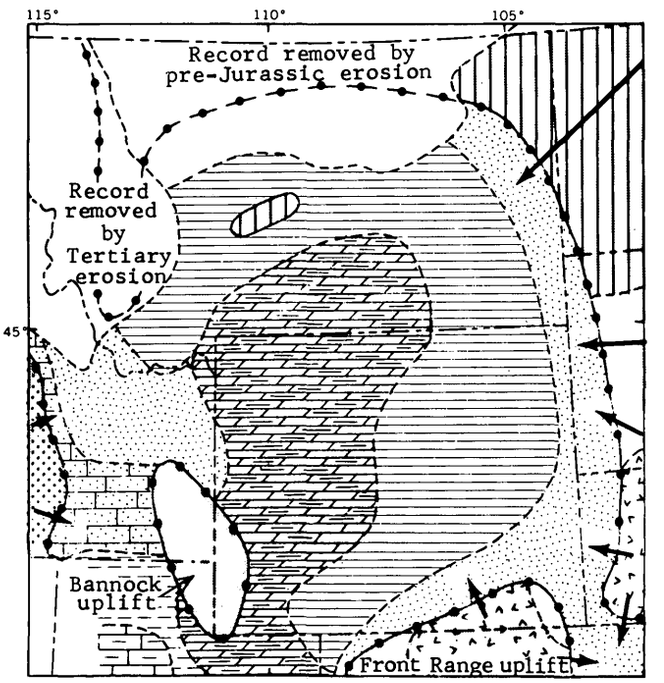

Early Pennsylvanian
Early Morrowan (Zone 20)

0 50 100 200 MILES
0 50 100 200 KILOMETRES

FIGURE 6.—Continued.

time interval. The craton margin, as commonly defined in the Cordilleran area, separates an area of thin sedimentation from an area of significantly thicker sedimentation. One might assume that there is a correlation between the craton margin and the margin of the Cordilleran depositional shelf, the paleooceanographic feature that dominated most of the area of Mississippian sedimentation. Figure 7 shows the position of the shelf margin with respect to the craton margin at various times during the Mississippian. The shelf receded during the transgressive part of Cycle I (phases 2 and 3) and then moved seaward during Cycle I regression (phase 4), reaching an extreme western position during Cycle II. The position of the shelf margin fluctuated slightly during Cycle III but maintained a position west of the craton margin. At no time during the Mississippian did the shelf margin coincide exactly with the craton margin. Although craton and miogeosyncline were important regional paleotectonic elements, they did not control sea-floor topography.

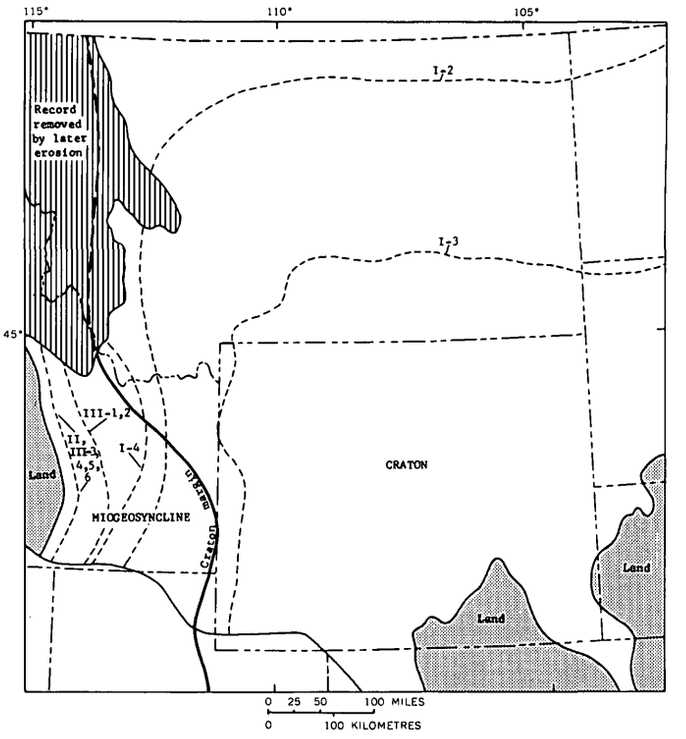

FIGURE 7.—Variation in location of shelf margin (dashed lines) with respect to craton margin in the northern Rocky Mountains during the Mississippian. Roman numerals refer to cycles and arabic numerals to phases discussed in text. Note generally western migration of shelf margin.

DEPOSITIONAL MODELS

Synthesis of the geographic distribution of contemporaneous lithofacies (fig. 6) and environmental comparisons of the Mississippian rocks and biota with modern and ancient counterparts permit tentative construction of depositional models for the Mississippian of the northern Rockies. Three generalized sedimentation models (fig. 8) form the basis for interpretation of the Mississippian sediments.

Ginsburg (1971) pointed out that modern carbonate shelves are characterized by net landward movement of sediment from a seaward production area (fig. 8*A*). Seaward progradation of a carbonate sediment wedge reduces the size of the source area until subsidence exceeds production and a new cycle begins. Although particle size distribution may be extremely variable and dependent on many factors, there is commonly a general shoreward progression of coarser to finer material.

In a typical model of constructive-deltaic or clastic-wedge terrigenous shelf sedimentation (fig. 8*B*), particulate matter is transported seaward from a production area on land. Ideally, size of the clastic particles decreases seaward, although the pattern may be complicated or even reversed by current distribution.

A third model that seems applicable to the Cordilleran Mississippian is that proposed by Adams and Rhodes (1960) for evaporite deposition on a broad shelf, generalized from the Permian of the southwestern United States (fig. 8*C*). In this model, an evaporite

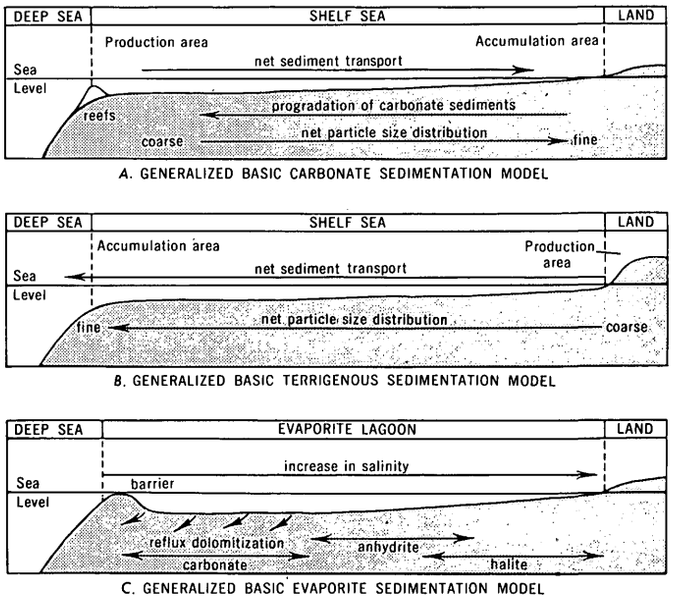

FIGURE 8.—Generalized basic models for carbonate, terrigenous, and evaporite sedimentation on shallow marine shelves. Carbonate model derived from Ginsburg (1971. Evaporite model after Adams and Rhodes (1960).

lagoon is formed when water circulation on the shelf is restricted by sediment buildup at the shelf margin, causing a salinity increase within the lagoon. Shoreward increase in salinity results in a shoreward progression of less soluble to more soluble sedimentary deposits. Dolomitization of carbonate rocks underlying the lagoon is caused by interaction with hypersaline brines that seep through the lagoon floor.

Application of the three generalized models to the Mississippian of the northern Rockies leads to the interpretations shown in figures 9 and 10. These diagrams depict profiles across the Cordilleran platform and geosyncline drawn to an approximate bathymetric scale based on lithic character, sedimentary structures, and biota of the strata at several times during the two main depositional cycles of the Mississippian. The vertical scale is greatly exaggerated in order to show differences in bathymetry on the shelf area.

The carbonate model was operative during the transgressive and regressive phases of Cycle I. The deeper

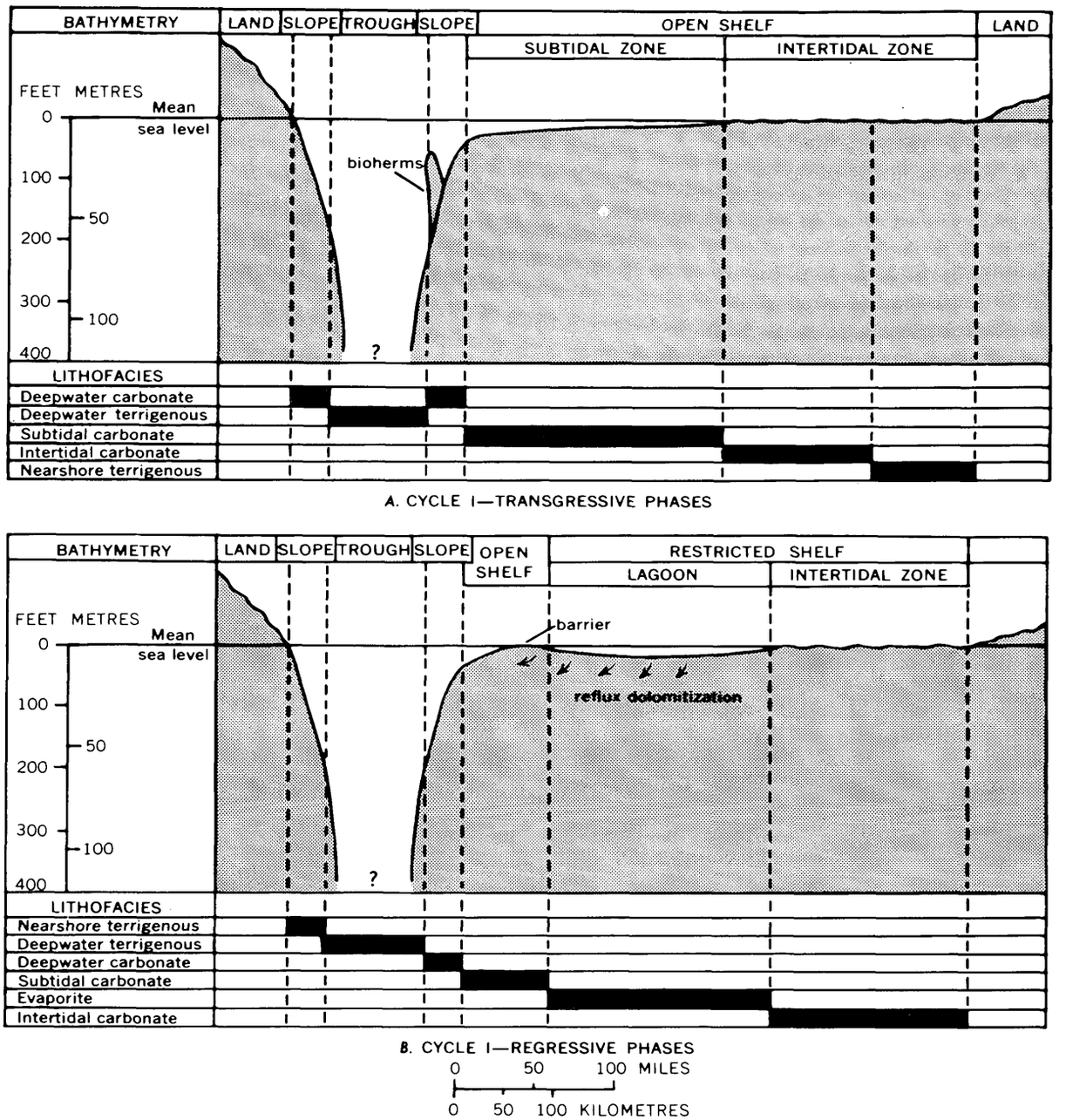

FIGURE 9.—Depositional models for transgressive and regressive phases of Cycle I (early Kinderhookian–early Meramecian). Profiles constructed to approximate vertical and horizontal scales; vertical scale exaggerated.

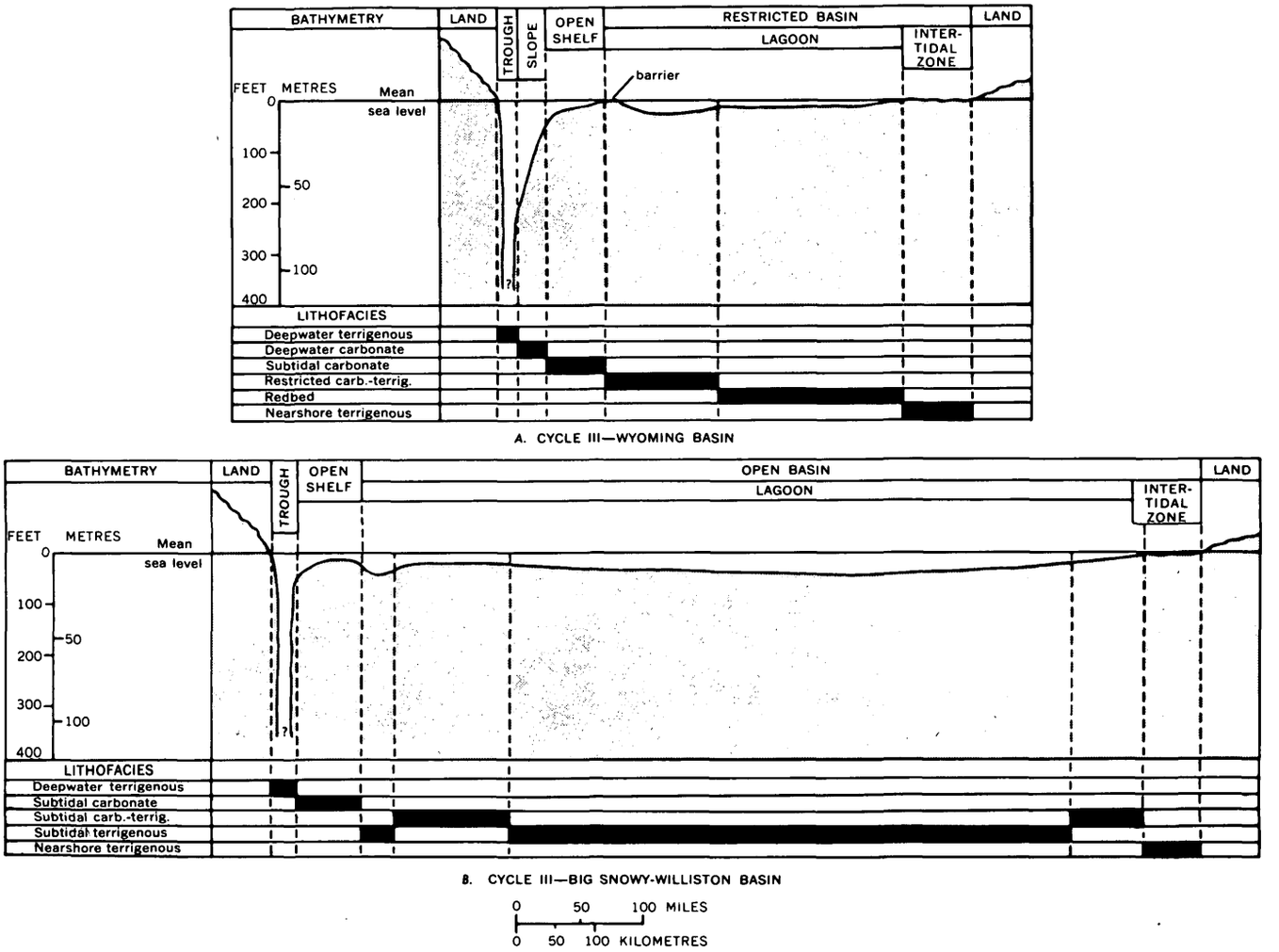

FIGURE 10.—Depositional models for Cycle III (early middle Meramecian–latest Chesterian). Profiles constructed to approximate vertical and horizontal scales; vertical scale exaggerated.

areas of the sea floor were differentiated into slope and trough, and an open shelf characterized by free circulation included subtidal and intertidal zones (fig. 9*A*). Sediment buildup near the shelf edge produced a restricted shelf divided into lagoon and intertidal zone behind a narrow open shelf area at the shelf margin during regressive phases of Cycle I (fig. 9*B*). Deposition of evaporite deposits and reflux dolomitization of underlying carbonate rocks followed the pattern of the evaporite model (fig. 8*C*).

Terrigenous sedimentation became an important ingredient of the depositional pattern on the Cordilleran platform and miogeosyncline during Cycle III (fig. 10). At the onset of Cycle III, the terrigenous model dominated the entire area of deposition, but as the terrigenous belts transgressed eastward, carbonate banks formed on an open shelf in the miogeosyncline adjacent to the mouths of the growing Wyoming and Big Snowy–Williston basins. Carbonate buildup at the seaward edge of the shelf restricted the terrigenous sediments to a lagoonal area in the Wyoming basin (fig. 10*A*). The Big Snowy–Williston basin was also essentially a lagoon but was characterized by freer circulation (fig. 10*B*).

TABLE 1.—*Geographic locations and sources of information for stratigraphic sections shown in figures 2 and 4*

Section No.	Locality name	Geographic location	Source of information
1 --	Arlington --	Approximately T. 18 N., R. 79 W., Carbon County, Wyo.	Maughan (1963, fig. 66.2).
2 --	Elk Mountain.	Approximately T. 19 N., R. 82 W., Carbon County, Wyo.	Do.
3 --	Buck Spring.	Sec. 33, T. 23 N., R. 88 W., Carbon County, Wyo.	Sando (1967a. fig. 3); Sando and others (1975).

TABLE 1.—*Geographic locations and sources of information for stratigraphic sections shown in figures 2 and 4*—Cont.

Section No.	Locality name	Geographic location	Source of information
4 --	Cottonwood Creek.	Secs. 27 and 34, T. 27 N., R. 88 W., Carbon County, Wyo.	Reynolds, M. W. (written commun., 1968).
5 --	Sweetwater Canyon.	Secs. 27 and 34, T. 29 N., R. 97 W.. Fremont County, Wyo.	Sando (1967a, fig. 3); Sando and others (1975).
6 --	Sinks Canyon.	Sec. 18, T. 32 N.. R. 100 W., Fremont County, Wyo.	Do.
7 --	Washakie Reservoir.	Sec. 18, T. 1 S., R. 2 W., Fremont County, Wyo.	Do.
8 --	Bull Lake Creek.	Secs. 2 and 3, T. 2 N., R. 4 W., Fremont County, Wyo.	Sando (1967a, fig. 3); Sando and others (1975).
9 --	Big Sheep Mountain.	Sec. 6. T. 38 N., R. 108 W., and sec. 31, T. 39 N., R. 108 W., Sublette County, Wyo.	Blackwelder, E (unpub. field notes); Richmond (1945).
10 --	Hoback Canyon.	Sec. 3, T. 38 N., R. 115 W., Teton County, Wyo.	Sando, 1967a (fig. 7); Sando and others (1975).
11 --	Haystack Peak.	Sec. 19, T. 34 N., R. 117 W., Lincoln County, Wyo.	Sando and Dutro (1960, pl. 1); Sando and others (1975).
12 --	Wells Canyon.	Secs. 10 and 11, T. 10 S., R. 45 E., Caribou County, Idaho.	Gulbrandsen and others (1956, p. 5).
13 --	Little Flat Canyon.	Secs. 17 and 20, T. 7 S., R. 40 E., Bannock County, Idaho.	Dutro and Sando (1963a, fig. 3).
14 --	East Canyon.	Lat 45° 52′ N., long 112° 57′ W., Butte County, Idaho.	Huh (1967, pl. 1).
15 --	Hawley Mountain.	Secs. 24 and 25, T. 9 N., R. 26 E., Butte County, Idaho.	Mamet and others (1971, fig. 2).
16 --	Cabin Creek.	Secs. 13, 14, 15, and 22, T. 6 N., R. 22 E., Custer County, Idaho.	Skipp and Mamet (1970, fig. 2).
17 --	Pioneer Mountains.	T. 4 N., R. 21 and 22 E., Blaine and Custer Counties, Idaho.	Paull and others (1972).
18 --	Wood River Region.	T. 2 N., R. 19 E., Blaine County, Idaho.	Hall, W. E. (unpub. notes, 1973).
19 --	Laramie Range.	Approximately T. 20 N., R. 72 W., Albany County, Wyo.	Maughan (1963, fig. 66.2).
20 --	Wheatland Reservoir.	Sec. 17, T. 23 N., R. 73 W., Albany County, Wyo.	Maughan (1963, fig. 66.1).
21 --	Marshall --	Approximately T. 26 N., and T. 27 N., R. 75 W., Albany County, Wyo.	Do.
22 --	Casper Mountain.	Sec. 9. T. 32 N., R. 79 W., Natrona County, Wyo.	Mytton (1954, pl. 1); Maughan (1963, fig. 66.2).
23 --	National Co-op Refining Co. Wallace Creek 2 well.	Sec. 16, T. 34 N., R. 87 W., Natrona County, Wyo.	American Stratigraphic Co.
24 --	Middle Buffalo Creek.	Secs. 20 and 21, T. 40 N., R. 86 W., Natrona County, Wyo.	Sando (unpub. data, 1975).
25 --	Tensleep Canyon.	Sec. 27, T. 48 N., R. 87 W., Washakie County, Wyo.	Do.
26 --	Shell Canyon.	Secs. 9 and 17, T. 53 N., R. 90 W., Big Horn County, Wyo.	Do.
27 --	Sheep Mountain.	Sec. 35, T. 54 N., R. 94 W., and Sec. 2, T. 53 N., R. 94 W., Big Horn County, Wyo.	Do.
28 --	Ohio Oil Co., Easton unit 6 well.	Sec. 28, T. 56 N., R. 97 W., Big Horn County, Wyo.	American Stratigraphic Co.
29 --	Clarks Fork Canyon.	Secs. 5, 6, and 7, T. 56 N., R. 103 W., Park County, Wyo.	Sando (1972, pl. 1).
30 --	Ben Bow Mine Road.	Secs. 20 and 29, T. 5 S., R. 16 E., Stillwater County, Mont.	Sando (1972, pl. 1).
31 --	Baker Mountain.	Secs. 34 and 35, T. 3 S., R. 12 E., Sweetgrass and Park Counties, Mont.	Do.
32 --	Livingston -	Secs. 1 and 2, T. 3 S., R. 9 E., and sec. 35, T. 2 S., R. 9 E., Park County, Mont.	Do.
33 --	Sacajawea Peak.	Sec. 27, T. 2 N., R. 6 E., Gallatin County, Mont.	Sando and Dutro (unpub. data 1975).
34 --	Logan -----	Sec. 25, T. 2 N., R. 2 E., Gallatin County, Mont.	Sando and Dutro (1960, pl. 1).
35 --	Limestone Hills.	Secs. 29 and 33, T. 6 N., R. 1 E., Broadwater County, Mont.	Klepper and others (1957, p. 17).

TABLE 1.—*Geographic locations and sources of information for stratigraphic sections shown in figures 2 and 4*—Cont.

Section No.	Locality name	Geographic location	Source of information
36 --	Indian Creek.	Sec. 32, T. 7 N., R. 1 E., Broadwater County, Mont.	Dutro and Sando (1963b).
37 --	Gibson Reservoir.	Sec. 36, T. 22 N., R. 10 W., Teton County, Mont.	Mudge and others (1962, p. 2005).

REFERENCES CITED

Adams, J. E., and Rhodes, M. L., 1960, Dolomitization by seepage refluxion: Am. Assoc. Petroleum Geologists Bull., v. 44, no. 12, p. 1912–1920, 4 figs.

Andrichuk, J. M., 1955a, Carboniferous stratigraphy in mountains of northwestern Montana and southwestern Alberta, *in* Billings Geol. Soc. 6th Ann. Field Conf., Sept. 1955, Guidebook; p. 85–95, 4 figs.

——— 1955b, Mississippian Madison group stratigraphy and sedimentation in Wyoming and southern Montana: Am. Assoc. Petroleum Geologists Bull., v. 39, no. 11, p. 2170–2210, 12 figs.

——— 1958, Mississippian Madison group stratigraphy and sedimentation in Wyoming and southern Montana, *in* Weeks, L. G., ed., Habitat of oil—a symposium: Tulsa, Oklahoma, Am. Assoc. Petroleum Geologists, p. 225–265.

Cotter, E., 1965, Waulsortian-type carbonate banks in the Mississippian Lodgepole Formation of central Montana: Jour. Geology, v. 73, no. 6, p. 881–888, 4 figs.

Craig, L. C., 1972, Mississippian System, *in* Mallory, W. W., ed., Geologic atlas of the Rocky Mountain region: Denver, Rocky Mountain Assoc. Geologists. p. 100–110.

Craig, L. C., and others, 1972, Map showing total thickness of Mississippian rocks in the conterminous United States: U.S. Geol. Survey open-file rept., 4 p., maps.

Dutro, J. T., Jr., and Sando, W. J., 1963a, New Mississippian formations and faunal zones in Chesterfield Range, Portneuf quadrangle, southeast Idaho: Am. Assoc. Petroleum Geologists Bull., v. 47, no. 11, p. 1963–1986, 6 figs.

——— 1963b, Age of certain post-Madison rocks in southwestern Montana and western Wyoming, *in* Geological Survey research 1963: U.S. Geol. Survey Prof. Paper 475–B, p. B93–B94, 2 figs.

Easton, W. H., 1962, Carboniferous formations and faunas of central Montana: U.S. Geol. Survey Prof. Paper 348, 126 p., 14 pls. 1 fig.

Francis, E. H., and Woodland, A. W., 1964, The Carboniferous period, *in* The Phanerozoic time scale—a symposium: Geol. Soc. London Quart. Jour., v. 120 supp., p. 221–232, 1 fig.

Ginsburg, R. N., 1971, Landward movement of carbonate mud —new model for regressive cycles in carbonates [abs.]: Am. Assoc. Petroleum Geologists Bull., v. 55, no. 2, p. 340.

Gries, J. P., and Mickelson, J. C., 1964, Mississippian carbonate rocks of western South Dakota and adjoining areas, *in* Williston Basin Symposium, 3d Internat. Regina, Saskatchewan, 1964, Proc.: Billings, Mont., Billings Geol. Soc., p. 109–118, 7 figs.

Gulbrandsen, R. A., McLaughlin, K. P., Honkala, F. S., and Clabaugh, S. E., 1956, Geology of the Johnson Creek quadrangle, Caribou County, Idaho: U.S. Geol. Survey Bull. 1042–A, 21 p., 2 pls., 1 fig.

Huh, O. K., 1967, The Mississippian System across the Wasatch line, east-central Idaho, extreme southwestern Montana, *in* Montana Geol. Soc., 18th Ann. Field Conf., 1967, Guidebook: p. 31–62, 1 pl., 13 figs.

Jenks, S., 1972, Environment of deposition and diagenesis of the Lodgepole Formation (Mississippian), central Montana, *in* Montana Geol. Soc., 21st Ann. Field Conf., Sept. 1972, Guidebook: p. 19–27, 5 figs.

Klepper, M. R., Weeks, R. A., and Ruppel, E. T., 1957, Geology of the southern Elkhorn Mountains, Jefferson and Broadwater Counties, Montana: U.S. Geol. Survey Prof. Paper 292, 82 p., 8 pls., 16 figs.

Lambert, R. St. J., 1971, The pre-Pleistocene Phanerozoic time-scale—a review, *in* Harland, W. B., and Francis, E. H., eds., The Phanerozoic time-scale, a supplement, part 1; Supplementary papers and items: Geol. Soc. London Spec. Pub. 5, p. 9–31, 3 figs.

Leatherock, C., 1950, Subsurface stratigraphy of Paleozoic rocks in southeastern Montana and adjacent parts of Wyoming and South Dakota: U.S. Geol. Survey Oil and Gas Inv. Chart OC–40.

Love, J. D., Henbest, L. G., and Denson, N. M., 1953, Stratigraphy and paleontology of Paleozoic rocks, Hartville area, eastern Wyoming: U.S. Geol. Survey Oil and Gas Inv. Chart OC–44.

Mallory, W. W., 1967, Pennsylvanian and associated rocks in Wyoming: U.S. Geol. Survey Prof. Paper 554–G, 31 p., 3 pls., 16 figs.

——— 1972, Regional synthesis of the Pennsylvanian System, *in* Mallory, W. W., ed., Geologic atlas of the Rocky Mountain region: Denver, Rocky Mountain Assoc. Geologists, p. 111–127.

Mamet, B. L., and Skipp, B. A., 1970, Preliminary foraminiferal correlations of early Carboniferous strata in the North American Cordillera, *in* Colloque sur la stratigraphie du Carbonifère: Liège Univ. Congr. et Colloques, v. 55, p. 327–348, 3 figs.

——— 1971, Lower Carboniferous calcareous Foraminifera—preliminary zonation and stratigraphic implications for the Mississippian of North America: Internat. Cong. Carboniferous Stratigraphy and Geology, 6th, Sheffield, 1967, Compte Rendu, v. 3, p. 1129–1146, 10 figs.

Mamet, B. L., Skipp, B., Sando, W. J., and Mapel, W. J., 1971, Biostratigraphy of Upper Mississippian and associated Carboniferous rocks in south-central Idaho: Am. Assoc. Petroleum Geologists Bull., v. 55, no. 1, p. 20–33, 3 figs.

Maughan, E. K., 1963, Mississippi rocks in the Laramie Range, Wyoming, and adjacent areas, *in* Geological Survey research 1963: U.S. Geol. Survey Prof. Paper 475–C, p. C23–C27.

Maughan, E. K., and Roberts, A. E., 1967, Big Snowy and Amsden Groups and the Mississippian-Pennsylvanian boundary in Montana: U.S. Geol. Survey Prof. Paper 554–B, p. B1–B27, 4 pls., 7 figs.

Moore, G. T., 1973, Lodgepole Limestone facies in southwestern Montana: Am. Assoc. Petroleum Geologists Bull., v. 57, no. 9, p. 1703–1713, 8 figs.

Mudge, M. R., Sando, W. J., and Dutro, J. T., Jr., 1962, Mississippian rocks of Sun River Canyon area, Sawtooth Range, Montana: Am. Assoc. Petroleum Geologists Bull., v. 46, no. 11, p. 2003–2018, 6 figs.

Mytton, J. W., 1954, The petrology and residues of the Madison Formation of the northern part of the Laramine Range, *in* Wyoming Geol. Assoc., 9th Ann. Field Conf., 1954, Guidebook: p. 37–43, 1 pl., 3 figs.

Nordquist, J. W., 1953, Mississippian stratigraphy of northern Montana, *in* Billings Geol. Soc., 4th Ann. Field Conf., Sept. 1953, Guidebook: p. 68–82, 8 figs.

Paull, R. A., Wolbrink, M. A., Volkmann, R. G., and Grover, R. L., 1972, Stratigraphy of Copper Basin Group, Pioneer Mountains, south-central Idaho: Am. Assoc. Petroleum Geologists Bull., v. 56, no. 8, p. 1370–1401, 21 figs.

Richmond, G. M., 1945, Geology of northwest end of the Wind River Mountains, Sublette County, Wyoming: U.S. Geol. Survey Oil and Gas Inv. Prelim. Map 31.

Roberts, A. E., 1966, Stratigraphy of Madison Group near Livingston, Montana, and discussion of karst and solution-breccia features: U.S. Geol. Survey Prof. Paper 526–B., p. B1–B23, 10 figs.

Roberts, R. J., 1972, Evolution of the Cordilleran fold belt: Geol. Soc. America Bull., v. 83, no. 7, p. 1989–2004, 4 figs.

Sandberg, C. A., 1963, Dark shale unit of Devonian and Mississippian age in northern Wyoming and southern Montana, *in* Geological Survey research 1963: U.S. Geol. Survey Prof. Paper 475–C, p. C17–C20, 2 figs.

——— 1967, Measured sections of Devonian rocks in northern Wyoming: Wyoming Geol. Survey Bull. 52, 93 p., 3 figs.

——— 1975, McGowan Creek Formation, new name for Lower Mississippian flysch sequence in east-central Idaho: U.S. Geol. Survey Bull. 1405–E, 11 p. 1 fig.

Sandberg, C. A., and Klapper, Gilbert, 1967, Stratigraphy, age, and paleotectonic significance of the Cottonwood Canyon Member of the Madison Limestone in Wyoming and Montana: U.S. Geol. Survey Bull. 1251–B, p. B1–B70, 5 figs.

Sandberg, C. A., and Mapel, W. J., 1967, Devonian of the northern Rocky Mountains and Plains, *in* Oswald, D. H., ed,. Internat. Symposium on the Devonian System, Calgary, Alberta, Sept. 1967: Calgary, Alberta, Soc. Petroleum Geologists, v. 1, p. 843–877, 10 figs. [1968].

Sandberg, C. A., Mapel, W. J., and Huddle, J. W., 1967, Age and regional significance of basal part of Milligen Formation, Lost River Range, Idaho, *in* Geological Survey research 1967: U.S. Geol. Survey Prof. Paper 575–C, p. C127–C131, 2 figs.

Sando, W. J., 1960a, Distribution of corals in the Madison Group and correlative strata in Montana, western Wyoming and northeastern Utah, *in* Geological Survey research, 1960: U.S. Geol. Survey Prof. Paper 400–B, p. B225–B227, figs. 100.1–100.3.

——— 1960b, Corals from well cores of Madison Group, Williston Basin. U.S. Geol. Survey Bull. 1071–F: p. 157–190, pls. 13–20, figs. 16, 17 [1961].

——— 1967a, Madison Limestone (Mississippian), Wind River, Washakie, and Owl Creek Mountains, Wyoming: Am. Assoc. Petroleum Geologists Bull., v. 51, no. 4, p. 529–557, 8 figs.

——— 1967b, Mississippian depositional provinces in the northern Cordilleran regions, *in* Geological Survey research 1967: U.S. Geol. Survey Prof. Paper 575–D, p. D29–D38, 3 figs.

——— 1972, Madison Group (Mississippian) and Amsden Formation (Mississippian and Pennsylvanian) in the Beartooth Mountains, northern Wyoming and southern Montana, *in* Montana Geol. Soc., 21st Ann. Field Conf., Sept. 1972, Guidebook: p. 57–63, 9 figs., 1 pl.

——— 1974, Ancient solution phenomena in the Madison Limestone (Mississippian) of north-central Wyoming: U.S. Geol. Survey Jour. Research, v. 2, no. 2, p. 133–141.

Sando, W. J., and Dutro, J. T., Jr., 1960, Stratigraphy and coral zonation of the Madison Group and Brazer Dolomite in northeastern Utah, western Wyoming, and southwestern Montana, *in* Wyoming Geol. Assoc., 15th Ann. Field Conf., 1960, Guidebook: p. 117–126, 1 pl., 3 figs.

Sando, W. J., Dutro, J. T., Jr., and Gere, W. C,, 1959, Brazer dolomite (Mississippian), Randolph quadrangle, northeast Utah: Am. Assoc. Petroleum Geologists Bull., v. 43, no. 12, p. 2741–2769, 5 figs.

Sando, W. J., Mamet, B. L., and Dutro, J. T., Jr., 1969, Carboniferous meagafaunal and microfaunal zonation in the northern Cordillera of the United States: U.S. Geol. Survey Paper 613–E, 29 p., 7 figs.

Sando, W. J., Gordon, M., Jr., and Dutro, J. T., Jr., 1975, Stratigraphy and geologic history of the Amsden Formation (Mississippian and Pennsylvanian) of Wyoming: U.S. Geol. Survey Prof. Paper 848–A, 82 p.

Sartenaer, Paul, and Sandberg, C. A., 1974, New North American species of upper Famennian rhynchonellid genus *Megalopterorhynchus* from Lost River Range, Idaho: Jour. Paleontology, v. 48, no. 4, p. 756–765, 1 pl., 3 figs.

Shaw, A. B., 1955, The Amsden Formation in southwestern and south-central Wyoming, *in* Wyoming Geol. Assoc., 10th Ann. Field Conf., 1955, Guidebook: p. 60–63, 1 fig.

Shaw, A. B., and Bell, W. G., 1955, Age of Amsden Formation, Cherry Creek, Wind River Mountains, Wyoming: Am. Assoc. Petroleum Geologists Bull., v. 39, no. 3, p. 333–337, 2 figs.

Skipp, Betty, and Mamet, B. L., 1970, Stratigraphic micropaleontology of the type locality of the White Knob Limestone (Mississippian), Custer County, Idaho, *in* Geological Survey research 1970: U.S. Geol. Survey Prof. Paper 700–B, p. B118–B123.

Sloss, L. L., Dapples, E. C., and Krumbein, W. C., 1960, Lithofacies maps, an atlas of the United States and southern Canada: New York, John Wiley and Sons, 108 p., maps.

Sloss, L. L., and Laird, W. M., 1945, Mississippian and Devonian stratigraphy of northwestern Montana: U.S. Geol. Survey Oil and Gas Inv. Prelim. Chart 15.

Smith, D. L., 1972, Depositional cycles of the Lodgepole Formation (Mississippian) in central Montana, *in* Montana Geol. Soc., 21st Ann. Field Conf., Sept. 1972, Guidebook: p. 29–35, 7 figs.

Stone, R. A., 1972, Waulsortian-type bioherms (reefs) of Mississippian age, central Bridger Range, Montana, *in* Montana Geol. Soc., 21st Ann. Field Conf., Sept. 1972, Guidebook: p. 37–55, 23 figs.

Wilson, J. L., 1969, Microfacies and sedimentary structures in "deeper water" lime mudstones, *in* Friedman, G. M., ed., Depositional environments in carbonate rocks: Soc. Econ. Paleontologists and Mineralogists Spec. Pub. 14, p. 4–19.

Jour. Research U.S. Geol. Survey
Vol. 4, No. 3, May–June 1976, p. 339–351

MARINE DIATOM AND SILICOFLAGELLATE BIOSTRATIGRAPHY OF THE TYPE DELMONTIAN STAGE AND THE TYPE *BOLIVINA OBLIQUA* ZONE, CALIFORNIA

By JOHN A. BARRON, Menlo Park, Calif.

Abstract.—Investigation of the marine diatom and silicoflagellate biostratigraphy of the type Delmontian Stage and and type *Bolivina obliqua* Zone in California shows that the type Delmontian Stage is equivalent to part of the supposedly older Mohnian Stage and is early late Miocene. The type *Bolivina obliqua* Zone, which conformably overlies the type Mohnian Stage, appears to be early Pliocene.

Miocene stratigraphy in California traditionally centered on the benthonic foraminiferal stages and zones of Kleinpell (1938). The upper Miocene was separated into the Mohnian (lower) and the Delmontian (upper) Stages. As the type locality for his Mohnian Stage, Kleinpell (1938, p. 127) chose Hoots' (1931, p. 103) section of units 1 through 16 of the Modelo Formation along the Topanga Canyon Road immediately north of Mohn Spring, near Los Angeles, Calif. The stratotype for the Delmontian Stage was chosen by Kleinpell (1938, p. 131) over 300 mi (480 km) to the north near Monterey, Calif. (fig. 1). The type area of the Delmontian Stage included the outcrops of Galliher's (1931) members 2 and 1 of the type Monterey Formation between Canyon Segundo and Canyon del Rey in Monterey County, Calif. (fig. 2). Kleinpell (1938, p. 134–135) recognized distinct lower Delmontian foraminiferal faunas throughout the State and included them in his *Bolivina obliqua* Zone. Although foraminiferal faunas are present in the type Delmontian, Hoots' units 17 and 18, which conformably overlie the type Mohnian Stage in southern California, were chosen arbitrarily as the stratotype for this lower Delmontian zone (fig. 3). Kleinpell did not define a biostratigraphic zone for his foraminifer-poor upper Delmontian Stage, nor was unit 19 zoned.

In recent years the validity of the Delmontian as a stage has been questioned by Pierce (1972) and others. Pierce correlated the benthonic foraminifers and fish of the type Delmontian with the lower and middle parts of the underlying Mohnian Stage (fig. 4). Pierce's belief that the Mohnian and Delmontian Stages are largely coeval was supported by Ruth (1972), who noted both the absence of post-Mohnian diatoms and the presence of characteristic Mohnian diatoms in the type Delmontian. Pierce (1972) favored expanding the Mohnian up to the base of the Repettian Stage. On the basis of a foraminiferal checklist in Ingle (1967), Pierce included Hoots' units 17 and 18 (the type *Bolivina obliqua* Zone) and part of unit 19 in his Mohnian stratotype (fig. 5).

Wornardt (1972) and others disagreed with Pierce. They believed that the foraminiferal faunas of the type *Bolivina obliqua* Zone and the type Delmontian

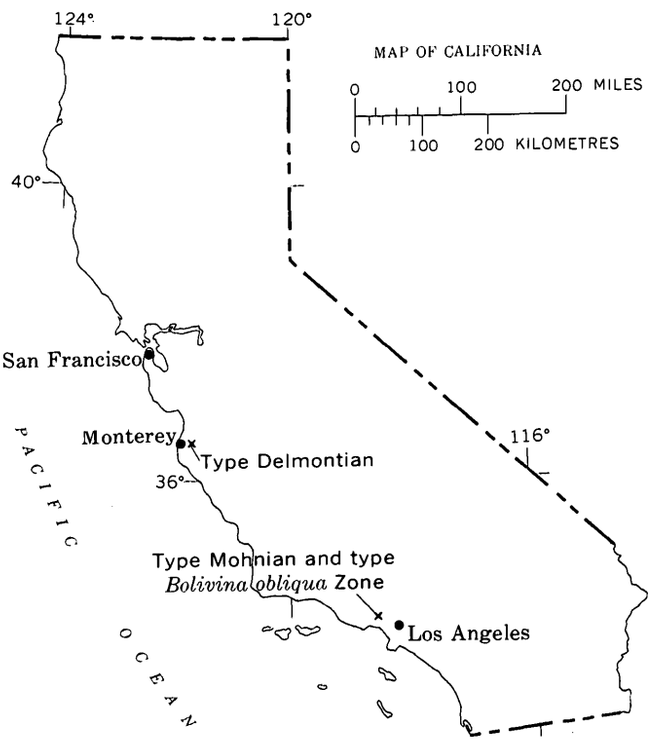

FIGURE 1.—Type localities of Kleinpell's (1938) Delmontian Stage, Mohnian Stage, and *Bolivina obliqua* Zone.

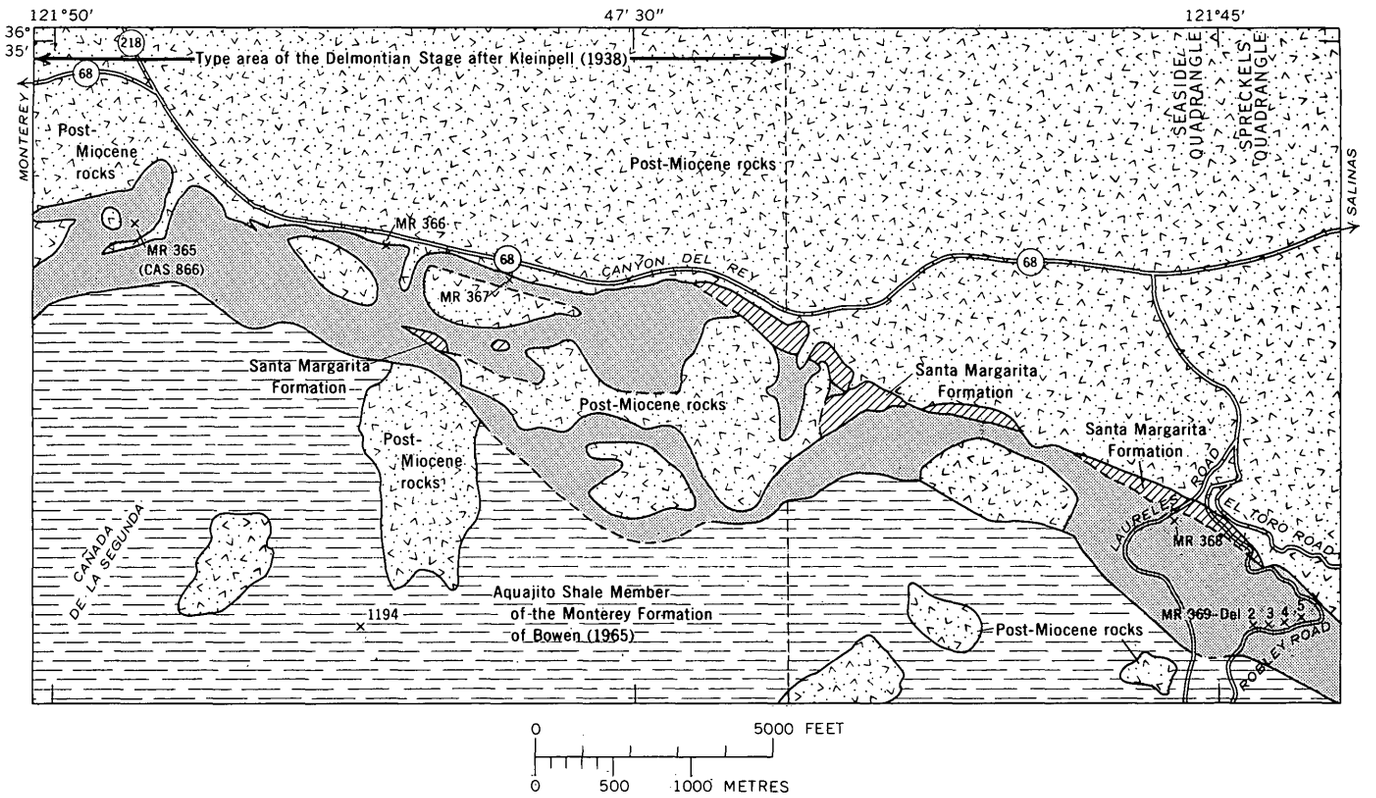

FIGURE 2.—Generalized geologic map showing type locality of Kleinpell's (1938) Delmontian Stage near Monterey, Calif., and correlative strata immediately to the east. Shaded area, outcrop area of Bowen's (1965) Canyon del Rey Diatomite Member (Member 1 of Galliher, 1931) of the Monterey Formation. Geology from Bowen (1965) and Clark, Dibblee, Greene, and Bowen (1974).

Stage are correlative and that Kleinpell's Delmontian Stage is, therefore, valid. Wornardt (1972) stated that the fauna of the type Delmontian is representative of a current-sheltered facies, whereas that of the type *Bolivina obliqua* Zone represents a more offshore facies. Differences in the two faunas were explained ecologically, but Wornardt pointed out that ten foraminiferal taxa are common to the two assemblages.

The diatoms of the type Delmontian area have been described and illustrated for more than 100 yr (Wornardt, 1967). Wornardt (1963, 1967) identified 116 diatom species and varieties from the type Delmontian and from correlative strata along Los Laureles Grade, east of Monterey. Wornardt (1967) followed Kleinpell in assigning the upper member of the type Monterey Formation (including the type Delmontian Stage) to the upper Miocene but failed to provide detailed correlations of the diatom flora with other stratigraphic sections.

Lohman (1931) identified 53 diatom species from Hoots' units 17 and 18 of the Modelo Formation (the type *Bolivina obliqua* Zone of Kleinpell, 1938) near Topanga Canyon in Los Angeles, Calif. He provided a floral checklist and stated that the flora was unlike the Monterey flora from the type locality. Presumably, he was referring to the Monterey flora described by Hanna (1928) from the type Delmontian Stage, which is included in the type area of the Monterey Formation.

Recent studies of deep sea cores have considerably improved Neogene diatom and silicoflagellate biostratigraphy in the North Pacific area. Reports by Schrader (1973, 1974) and Koizumi (1973) on diatoms and Bukry (1973) and Ling (1972, 1973) on silicoflagellates provide the biostratigraphic framework for a reexamination of the diatom and silicoflagellate biostratigraphy of the type Delmontian Stage and the type *Bolivina obliqua* Zone.

Acknowledgments.—I thank J. David Bukry and Harvey Sachs for their help. Peter Rodda of the California Academy of Sciences supplied sample CAS 866. Kenji Sakamoto of the U.S. Geological Survey processed the photographs.

MATERIALS AND METHODS

I collected samples for study from Bowen's (1965) Canyon del Rey Diatomite Member (Member 1 of

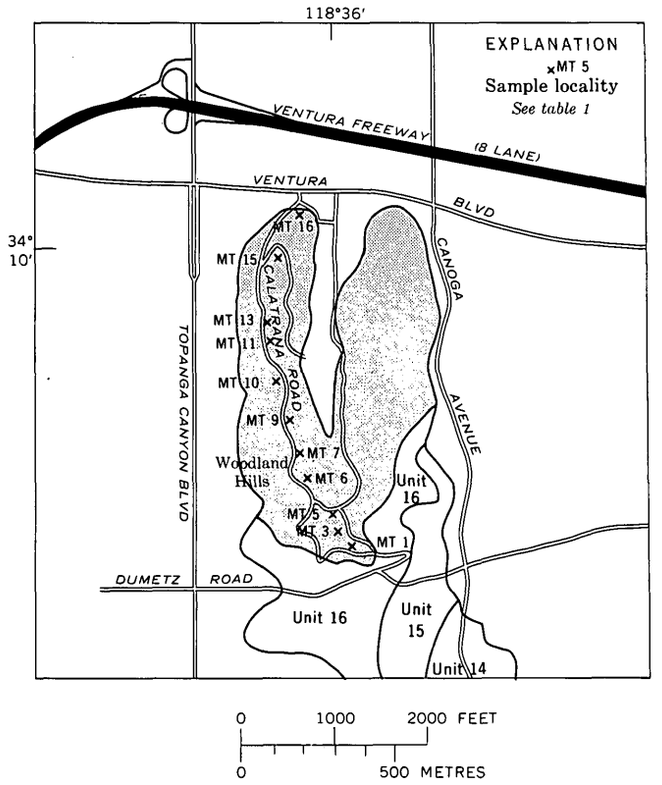

FIGURE 3.—Generalized geologic map showing type locality *Bolivina obliqua* Zone of Kleinpell (1938) near Los Angeles, Calif., and location of samples studied. Shaded area, outcrop area of units 17 and 18 (Hoots, 1931) of the Modelo Formation (the type *Bolivina obliqua* Zone). Canoga Park 7.5-minute quadrangle.

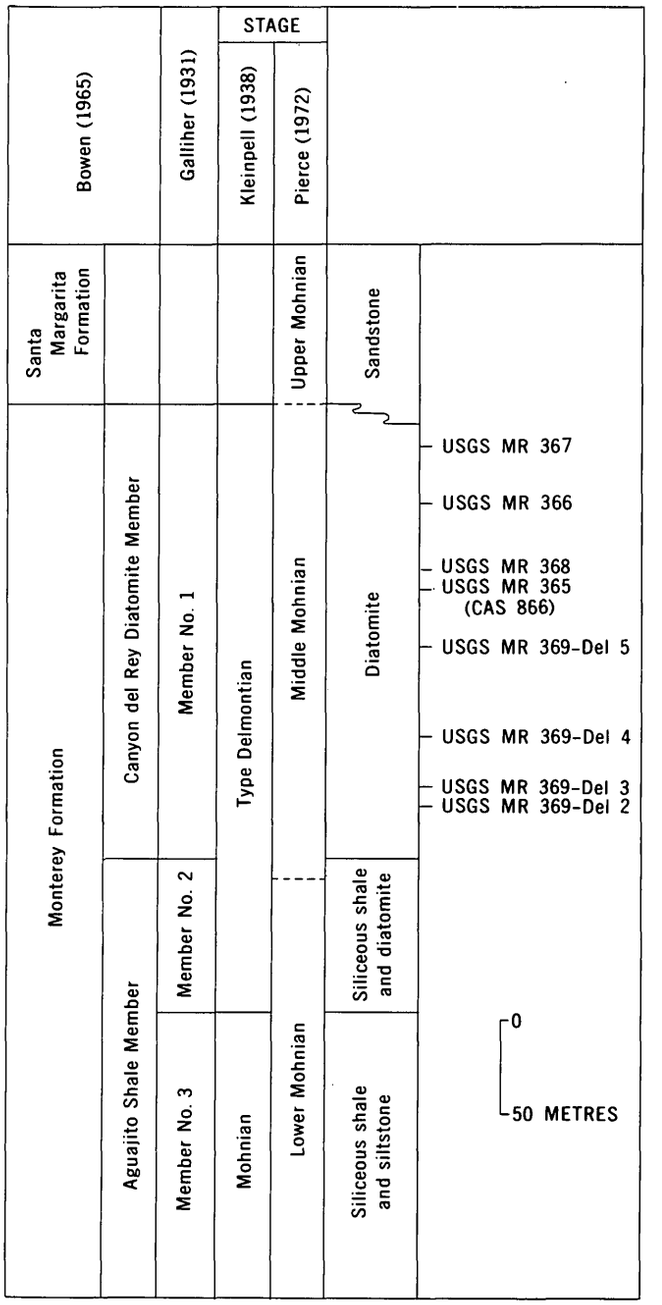

FIGURE 4.—Local stratigraphic column after Kleinpell (1938) of the type Delmontian Stage. Samples studied from the nearby Los Laureles Grade area are shown in inferred stratigraphic position.

Galliher, 1931) of the Monterey Formation in the type area of the Delmontian Stage and from the Los Laureles Grade area a few miles to the east (figs. 2, 4). In addition, a sample from California Academy of Sciences locality 866 in the type area of the Delmontian was obtained for study. Descriptive studies of the diatoms and silicoflagellates from locality 866 have been made by Hanna (1928) and Wornardt (1963, 1967). Galliher's unit 2, a transitional unit between underlying siliceous Monterey shales and the overlying diatomite, was not collected for this study.

Samples were also collected from Hoots' units 17 and 18 (the type *Bolivina obliqua* Zone of Kleinpell, 1938) near Topanga Canyon in the Los Angeles area (figs. 3, 6). These samples correspond closely to those of Hoots (1931) that were studied by Lohman (1931) (fig. 6).

Approximately 5 g of sample was broken into centimetre-size pieces and placed in a 400-ml beaker. The sample was disintegrated in 30 percent hydrogen peroxide and then flooded with distilled water. The liquid was decanted after 2 h of settling, and 50 ml of 37 percent hydrochloric acid and 20 ml of 61 percent nitric acid were added to the residue. The sample was then boiled until the nitrous oxide fumes disappeared and the sample became light in color. The acid was removed by successive 2-h decantations with distilled water. Strewn slides were prepared on 22- by 40-mm cover glasses and mounted in Hyrax on glass slides. At least two slides were examined in their entirety at

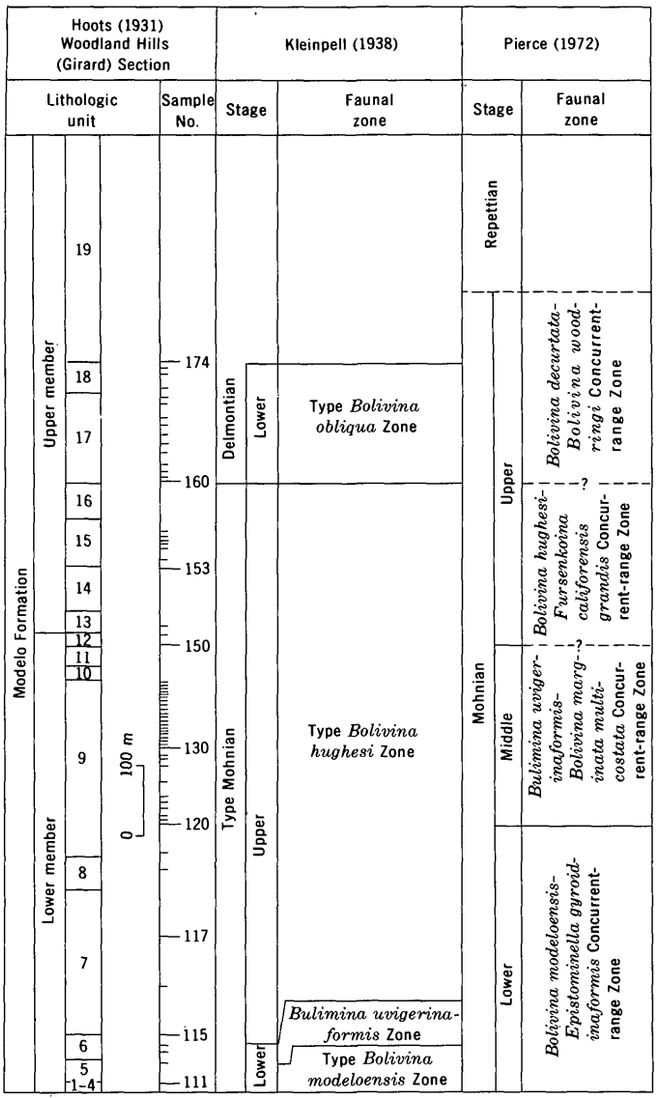

FIGURE 5.—Woodland Hills (Girard) stratigraphic section of Hoots (1931) with the interpretations of Kleinpell (1938) and Pierce (1972).

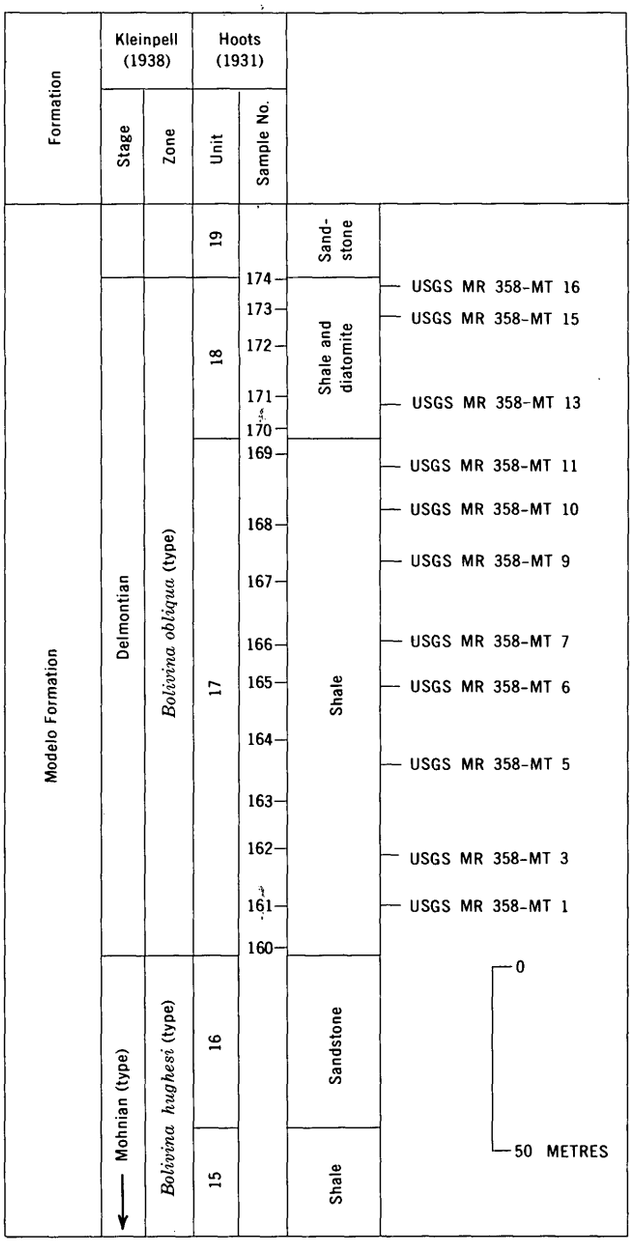

FIGURE 6.—Local stratigraphic column after Hoots (1931) of the type *Bolivina obliqua* Zone of Kleinpell (1938). Samples studied are shown in inferred stratigraphic position.

× 312. In addition, at least ten traverses at × 1,250 were made per slide. Identifications were made at × 1,250. Informal approximations of the abundance of the selected taxa relative to the whole assemblage were made. A Leitz Ortholux II light microscope with interference contrast optics was used in this investigation.

SAMPLE LOCALITIES

Type Delmontian Stage

All samples are from Bowen's (1965) Canyon del Rey Diatomite Member of the Monterey Formation ("Member 1" of Galliher, 1931). Samples USGS MR 365, 366, 367, and 368 are from the Seaside 7.5-minute quadrangle, Calif. Samples USGS MR 369–Del 2 to Del 5 are from the Spreckels 7.5-minute quadrangle, Calif. (fig. 2). Sample USGS MR 365 is from California Academy of Sciences locality 866 and was collected by G. D. Hanna in November 1923. All other samples were collected by the author in October 1974. All samples are USGS MR.

368 (Del 1): In roadcut on the east side of Laureles Road, 1.2 mi (1.9 km) south of the intersection with California Highway 68.
369–Del 2: In roadcut on the west side of Robley Road (the old Los Laureles Grade Road) 2.27 mi (3.65 km) (via Laureles Road) south of the intersection of Laureles Road and California Highway 68.
369–Del 3: In roadcut on the west side of Robley Road, 61 m north of sample Del 2.
369–Del 4: In roadcut on the west side of Robley Road, 115 m north of sample Del 3.
369–Del 5: In roadcut on the west side of Robley Road, 114 m north of sample Del 4.
366 (Del 6): In roadcut on the south side of California Highway 68, 3.17 mi (5.10 km) west of the intersection with Laureles Road.
367 (Del 7): In roadcut on the south side of California Highway 68, 2.7 mi (4.36 km) west of the intersection with Laureles Road.
365 (CAS 866): "Diatomaceous shale. Four miles (6.4 km) east of Del Monte on road to Salinas, Calif., at plant for preparation of diatomaceous earth. Soft, pure samples from near top of deposit."

Type *Bolivina obliqua* Zone

All samples are USGS MR 358–MT and are from Hoots' (1931, p. 103) units 17 and 18 of the Modelo Formation, Canoga Park 7.5-minute quadrangle, California (fig. 3). They were collected by J. A. Barron, 1972; refer to Hoots (1931, pl. 27).

1: West side of Medina Road, approximately equal to Hoots' sample 161.
3: West side of Medina Road, 40 m north of sample MT 1.
5: Top of the small hill on the west side of the intersection of Medina Road and Calatrana Road.
6: East side of Calatrana Road, approximately equal to Hoots' sample 165.
7: East side of Calatrana Road, 150 m north of sample MT 6.
9: West side of Calatrana Road, 200 m north of sample MT 7.
10: West side of Calatrana Road, 50 m north of sample MT 9.
11: East side of Calatrana Road, 100 m north of sample MT 10.
13: East side of Calatrana Road, approximately equal to Hoots' sample 171.
15: West side of road east of Calatrana Road, approximately equal to Hoots' sample 173.
16: East side of Calatrana Road, approximately equal to Hoots' sample 174.

BIOSTRATIGRAPHY

Table 1 is a checklist of the stratigraphically significant diatoms and silicoflagellates observed in samples from the type areas of the Delmontian Stage and the *Bolivina obliqua* Zone. Many of these taxa are illustrated in figures 7 and 8. Those that are not illustrated here are referenced to published figures in the floral reference list. Additional taxa may be found in the checklists of Hanna (1928) and Wornardt (1963) for the type Delmontian and in the checklist of Loḧman (1931) for the type *Bolivina obliqua* Zone.

In figure 9, the ranges of selected marine diatoms in the Neogene of California are referenced against the North Pacific Diatom Zones of Schrader (1973). Correspondingly, figure 10 is a range chart of selected silicoflagellates in the Neogene of California referenced against the silicoflagellate zones of Bukry (1973).

Diatom and silicoflagellate biostratigraphy of the type Delmontian

The presence of *Actinoptychus gruendleri* Schmidt, *Auliscus albidus* Brun, *Coscinodiscus lineatus* var. *leptopus* Grunow, *Craspedodiscus rhombiscus* Grunow, *Denticula lauta* Bailey, *Mediaria splendida* Sheshukova-Poretzkaya, and *Stephanopyxis spinossima* Grunow (table 1) indicate that the type Delmontian is correlative with the *Actinoptychus gruendleri* Assemblage Zone and the *Denticula dimorpha* Concurrent-range Subzone of Barron (1975a). This correlation is further supported by the restricted occurrence of *Cosmiodiscus elegans* Greville and *Pterotheca subulata* Grunow in the occurrence charts of Barron (1975b). Barron (1975a) correlated the *Actinoptychus gruendleri* Assemblage Zone and the *Denticula dimorpha* Concurrent-range Subzone with Schrader's (1973) North Pacific diatom zone XV (fig. 11).

The presence of the indicator species *Denticula lauta*, *Mediaria splendida* Sheshukova-Poretzkaya, *Lithodesmium minusculum* Grunow, *Rhizosolenia barboi* Brun, and *Rhizosolenia praebarboi* Schrader and the absence of *Coscinodiscus yabei* Kanaya (fig. 9) support a correlation of the type Delmontian with Schrader's (1973) North Pacific diatom zones XVI and XV (table 1, fig. 11). The occurrence of *Coscinodiscus endoi* Kanaya, *Nitzschia rolandii* Schrader, *Rhizosolenia miocenica* Schrader, and *Coscinodiscus plicatus* Grunow in the occurrence chart of Schrader (1973) for Deep Sea Drilling Project Site 173 off northern California also supports this correlation. Furthermore, Schrader (1974) indicated the restricted occurrence of *Coscinodiscus moholensis* Schrader to a sample correlated with North Pacific diatom zone XVI from the Experimental Mohole Drilling, Guadalupe Site, about 250 mi (400 km) south of California.

The silicoflagellates of the type Delmontian are correlative with the *Distephanus longispinus* Zone of Bukry (1973) (fig. 11). This is indicated by the presence of *Distephanus longispinus* (Schulz) Bukry and Foster and the absence of both *Dictyocha pseudofibula* (Schulz) Tsumura and *Corbisema triacantha* (Ehrenberg) Hanna (table 1, fig. 10). Furthermore, Ling

TABLE 1.—*Checklist of selected diatoms and silicoflagellates and one radiolarian from the type Delmontian Stage and the type* Bolivina obliqua *Zone of Kleinpell (1938)*

[*, reworked; R, rare; F, few; C, common; A, abundant; W, observed by Wornardt (1963, CAS 866 and 1277) but not here; H, observed by Hanna (1928, CAS 866) but not here. Preservation: P, poor; M, moderate; G, good. All samples are USGS]

	Type Delmontian								Type *Bolivina obliqua* Zone MR 358–MT										
	MR 369–Del				MR				Unit 17								Unit 18		
	2	3	4	5	365	368	366	367	1	3	5	6	7	9	10	11	13	15	16
Diatoms																			
Actinocyclus ingens Rattray	R	R	F	F	F	F	F	--	--	R	R	--	R	R	R	F	R	R	R
Actinoptychus gruendleri Schmidt	--	--	--	R	R	--	--	--	--	--	--	--	--	--	--	--	--	--	--
Auliscus albidus Brun	--	--	W	--	--	--	--	--	--	--	--	--	--	--	--	--	--	--	--
Brunia mirablis (Brun) Tempere	R	--	--	--	--	--	R	--	--	--	--	R	--	--	--	R	R	--	--
Cladogramma californicum Ehrenberg	--	R	R	--	--	--	--	--	--	R	R	--	--	--	--	--	R	--	--
dubium Lohman	R	--	R	--	R	--	--	--	--	R	--	--	--	--	--	--	R	--	--
Coscinodiscus endoi Kanaya	R	R	R	F	F	R	R	--	--	--	--	--	--	--	--	--	--	--	--
kurzii Grunow	--	--	--	--	--	--	--	--	--	R	--	--	--	--	R	--	R	R	R
lineatus var. *leptopus* Grunow	--	--	--	--	W	--	R	--	--	--	--	--	--	--	R	--	R	R	--
sp. aff. *C. miocenicus* Schrader	R	R	R	F	--	--	--	--	--	--	--	--	--	--	--	--	--	--	--
sp. aff. *C. moholensis* Schrader	--	--	R	R	R	--	--	--	--	--	--	--	--	--	--	--	--	--	--
plicatus Grunow s. str.	R	R	--	--	--	--	--	--	--	--	--	--	--	--	--	--	--	--	--
plicatus Grunow s. ampl.	--	--	--	--	R	--	--	--	--	--	--	--	--	--	--	--	--	--	--
sp. aff. *C. plicatus* Grunow	R	R	R	--	--	--	--	--	--	--	--	--	--	--	--	--	--	--	--
Cosmiodiscus elegans Greville	F	R	R	--	--	--	R	--	--	--	--	--	--	--	--	--	--	--	--
Craspedodiscus rhombicus Grunow	R	--	R	--	--	--	R	--	--	--	--	--	--	--	--	--	--	--	--
Denticula hustedtii Simonsen & Kanaya	A	A	F	F	F	F	A	--	--	R	R	--	--	R	R	R	R	R	R
lauta Bailey	R	R	R	R	R	R	F	--	--	*	--	--	--	*	*	*	*	--	*
Hemiaulus polymorphus Grunow	F	R	--	--	--	--	--	--	--	R	--	--	--	R	--	R	--	--	R
Hemidiscus simplicissimus Hanna & Grant	--	--	--	--	--	--	R	--	--	R	--	R	--	R	--	R	R	C	F
Lithodesmium minusculum Grunow	--	--	--	--	R	--	R	--	--	--	--	--	--	--	--	--	--	--	--
Mediaria splendida Sheshukova-Poretzkaya	R	R	--	--	--	--	--	--	--	--	--	--	--	--	--	--	--	--	--
Nitzschia kanayensis Schrader	R	--	--	--	--	--	--	--	--	--	--	--	--	--	--	--	--	--	--
reinholdii Kanaya ex Schrader	--	--	--	--	--	--	--	--	--	R	R	R	--	--	R	--	R	F	C
rolandii Schrader	R	--	--	--	--	--	--	--	--	--	--	--	--	--	--	--	--	--	--
Pterotheca subulata Grunow	R	--	R	--	R	--	R	--	--	--	--	--	--	--	--	--	--	--	--
Rhaphoneis surirella (Ehrenberg) Grunow	R	--	R	R	R	--	R	--	--	--	--	R	--	R	--	--	R	R	R
Rhizosolenia barboi Brun	--	--	R	R	R	F	R	--	--	--	--	--	R	--	R	--	R	R	--
miocenica Schrader	R	--	R	R	R	F	R	--	--	--	--	--	--	--	--	--	--	--	--
praebarboi Schrader	R	R	R	R	R	--	R	--	--	--	--	--	--	--	--	--	--	--	--
Rouxia californica Peragallo	R	R	R	--	--	--	--	--	--	R	R	--	--	R	--	--	--	R	R
peragalli Brun & Heribaud	F	--	--	--	--	--	--	--	--	--	--	--	--	--	--	--	--	--	--
Stephanopyxis spinossima Grunow	R	--	F	--	R	--	--	--	--	--	--	--	--	--	--	--	--	--	--
Thalassiosira antiqua (Grunow) Cleve-Euler	--	--	--	--	--	--	--	--	--	F	F	R	--	R	--	--	C	F	R
convexa? Muchina	--	--	--	--	--	--	--	--	--	--	R	--	--	--	--	--	--	--	--
oestrupii (Ostenfeld) Proshkina-Lavrenko	--	--	--	--	--	--	--	--	--	--	--	--	--	--	--	--	A	F	F
sp. 1	F	R	--	--	--	--	--	--	--	--	--	--	--	--	--	--	--	--	--
sp. 2	R	--	--	--	--	--	--	--	--	--	--	--	--	--	--	--	--	--	--
Silicoflagellates																			
Cannopilus sphaericus Gemeinhardt	--	--	--	--	H	--	--	--	--	--	--	--	--	--	--	--	--	--	--
Dictyocha pentagona (Schulz) Bukry	--	--	--	--	--	--	--	--	--	--	--	--	--	--	--	--	R	R	R
Distephanus boliviensis frugalis Bukry	--	--	--	--	--	--	--	--	--	--	--	--	--	F	R	--	A	C	A
longispinus (Schulz) Bukry & Foster	R	R	--	--	R	--	--	--	--	--	--	--	--	--	--	--	--	--	--
polyactis (Ehrenberg) Deflandre s. ampl.	--	--	--	--	--	--	--	--	--	--	--	--	--	--	--	--	R	--	R
speculum pseudocrux Schulz	--	--	--	--	--	--	--	--	--	--	--	--	--	--	--	--	--	--	R
Mesocena hexagona Haeckel	--	R	R	R	C	--	--	--	--	--	--	--	--	--	--	--	--	--	--
Radiolarian																			
Lamprocyrtis heteroporos (Hays)	--	--	--	--	--	--	--	--	--	--	--	--	--	R	--	--	R	--	R
Preservation	G	M	M	M	M	M	M	P	P	M	M	P	P	M	P	P	G	G	G

(1972) noted the only occurrence of *Mesocena hexagona* Haeckel from the Experimental Mohole, Guadalupe Site in sample EM 8–13 (125–126 cm). This corresponds to the *Distephanus longispinus* Zone (Bukry and Foster, 1973).

The *Actinoptychus gruendleri* Assemblage Zone and the *Denticula dimorpha* Concurrent-range Subzone were defined in the stratigraphic interval between (and inclusive of) Warren's (1972) samples NEW 42 and NEW 61 at Upper Newport Bay, Newport Beach, Calif. (Barron, 1975a). In subsequent studies, I have observed *Corbisema triacantha* in sample NEW 42 and *Dictyocha pseudofibula* in sample NEW 61. These silicoflagellates were not observed in the samples between NEW 42 and NEW 61. *Mesocena hexagona* was observed in one sample within this interval. Thus, the diatoms and the silicoflagellates both indicate that the type Delmontian is correlative with the stratigraphic

interval between Warren's (1972) samples NEW 42 and NEW 61 at Upper Newport Bay.

This stratigraphic interval was assigned to the *Bulimina uvigerinaformis* Zone (lower Mohnian Stage) by Warren (1972) (fig. 11), which supports Pierce's (1972) correlation of the benthonic foraminifers of the type Delmontian with the lower and middle parts of the Mohnian.

Schrader's (1973) North Pacific diatom zones XVI and XV are correlative with the *Distephanus longispinus* Zone of Bukry (1973) at Deep Sea Drilling Project Site 173 off northern California. Ingle (1973) placed the stratigraphic interval represented by the co-occurrence of these zones in the lower upper Miocene.

Diatom and silicoflagellate biostratigraphy of the type *Bolivina obliqua* Zone

Wornardt (1974) correlated the type *Bolivina obliqua* Zone with Schrader's (1973) North Pacific Diatom Zones XI (in part) and X. The presence of *Nitzschia reinholdii* Kanaya ex Schrader, *Actinocyclus ingens* Rattray, *Hemiaulus polymorphus* Grunow, and *Thalassiosira oestrupii* (Ostenfeld) Proshkina-Lavrenko (table 1, fig. 9) indicates that the type *Bolivina obliqua* Zone is correlative with North Pacific diatom zone X (fig. 11).

The presence of *Nitzschia reinholdii*, *Thalassiosira oestrupii*, *Actinocyclus ingens*, *Hemiaulus polymorphus*, *Rouxia californica* Peragallo, *Brunia mirabilis* (Brun) Tempère, and *Cladogramma californicum* Ehrenberg (table 1) indicates that the type *Bolivina obliqua* Zone is also correlative with the *Nitzschia reinholdii* Concurrent-range Zone of Barron (1975a); Barron correlated his zone with Schrader's (1973) North Pacific diatom zone X (fig. 11).

On the basis of the presence of *Distephanus bolivi-ensis frugalis* Bukry and *D. polyactis* (Ehrenberg) Deflandre s. ampl. and the absence of *Dictyocha pseudofibula* (table 1, fig. 10), the type *Bolivina obliqua* Zone is tentatively correlated with the *Distephanus speculum* Zone of Bukry (1973) (fig. 11). At Deep Sea Drilling Project Site 173 of northern California, the *Distephanus speculum* Zone is correlative in part with Schrader's North Pacific diatom zone X (Bukry, 1973; Schrader, 1973).

Schrader (1973, 1974) placed North Pacific diatom zone X in the lower Pliocene and estimated the age of its basal datum at 4.38 m.y. B.P. Wornardt (1974), however, correlated the diatoms of the type *Bolivina obliqua* Zone with the type Messinian (upper Miocene). Bukry (1973) placed the lower part of his *Distephanus speculum* Zone in the Pliocene (fig. 10). This supports Schrader's (1973) Pliocene age for North Pacific diatom zone X (fig. 11).

DISCUSSION

Diatoms and silicoflagellates indicate that the type Delmontian is substantially older than the type *Bolivina obliqua* Zone of Kleinpell. Inasmuch as the type *Bolivina obliqua* Zone conformably overlies the stratotype of the Mohnian Stage, the type Delmontian must be older than the youngest Mohnian. Recognition of type Delmontian diatoms in strata at Upper Newport Bay containing lower Mohnian benthonic foraminifers supports Pierce's (1972) correlation of the type Delmontian benthonic foraminifers and fish with the lower and middle parts of the Mohnian Stage.

As presently defined, the Delmontian is coeval with part of the Mohnian Stage and should be abandoned. Some workers have retained the term "Delmontian" to denote the interval between the highest demonstrable Mohnian strata and the lowest demonstrable Repettian strata and use quotation marks around the term to denote its ambiguity.

Pierce (1972) favored raising the top of the Mohnian stratotype to include all of Hoots' units 17 and 18 (the type *Bolivina obliqua* Zone of Kleinpell, 1938) up to the base of the Repettian Stage which Pierce estimated to be in the lower part of unit 19 (fig. 5). At present, Pierce's sugestion seems appropriate.

Age of the type *Bolivina obliqua* Zone

The diatoms and silicoflagellates indicate that the type *Bolivina obliqua* Zone is probably early Pliocene. This age is supported by the radiolarian evidence. Casey (1972) identified the radiolarian *Lamprocyrtis* (=*Lamprocyclas*) *heteroporos* (Hays) in Hoots' (1931) sample 172. This sample is stratigraphically between samples USGS MR 358–MT 13 and USGS MR 358–MT 15 of figure 6. Harvey Sachs (written commun., 1974) observed this radiolarian in sample USGS MR 358–MT 13. Casey and Jenkins (1974) stated that *L. heteroporos* first occurs in typical form in the upper part of the Gilbert reversed polarity epoch. Kennett and Watkins (1974) placed the Gilbert in the early Pliocene and estimated its absolute age from 5.10 to 3.32 m.y. B.P. This is consistent with an early Pliocene age for the type *Bolivina obliqua* Zone.

Reworking was not apparent in the samples studied from the type Delmontian. All of the diatoms from the type Delmontian observed by me are present in strata elsewhere in California correlative with Schrad-

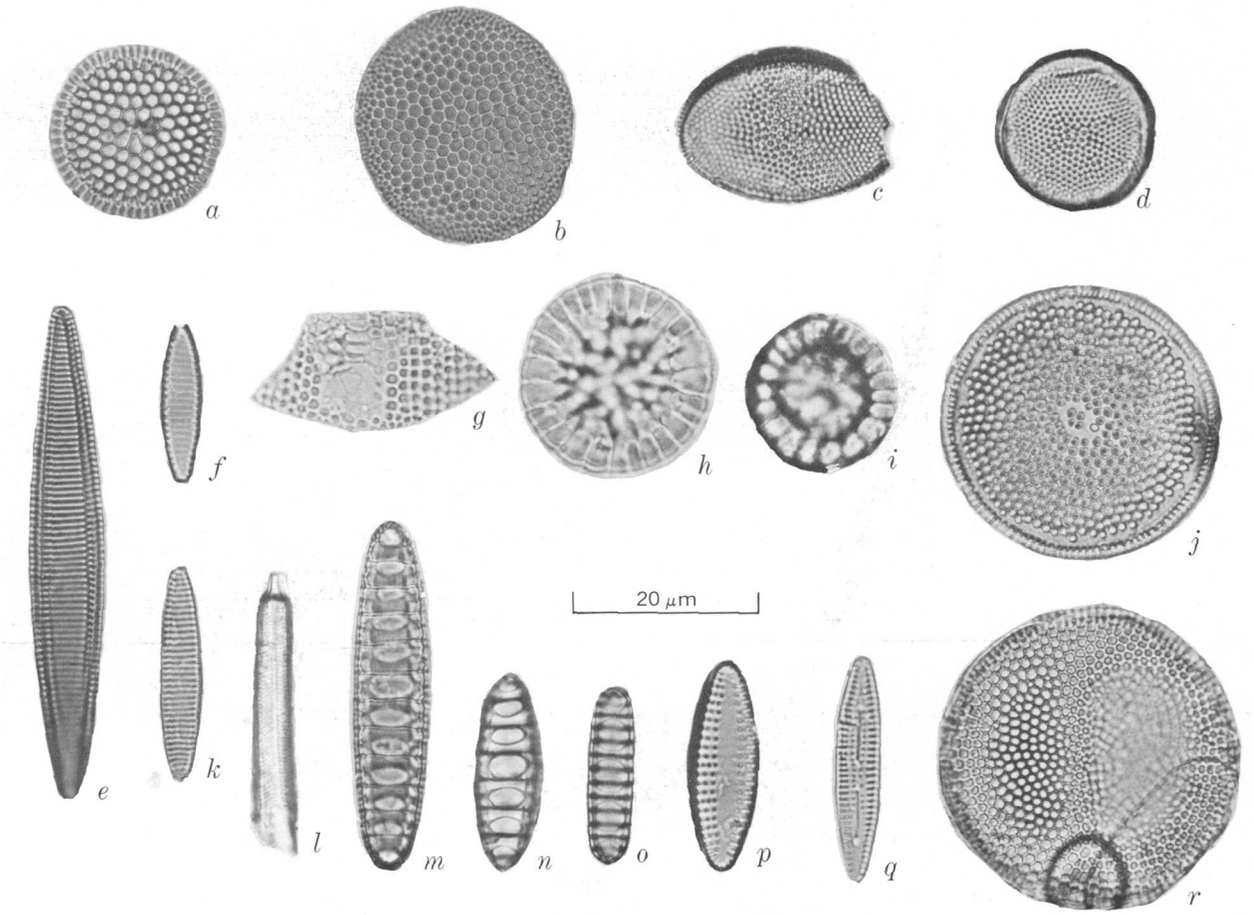
a
b
c
d
e
f
g
h
i
j
k
l
m
n
o
p
q
r
20 μm

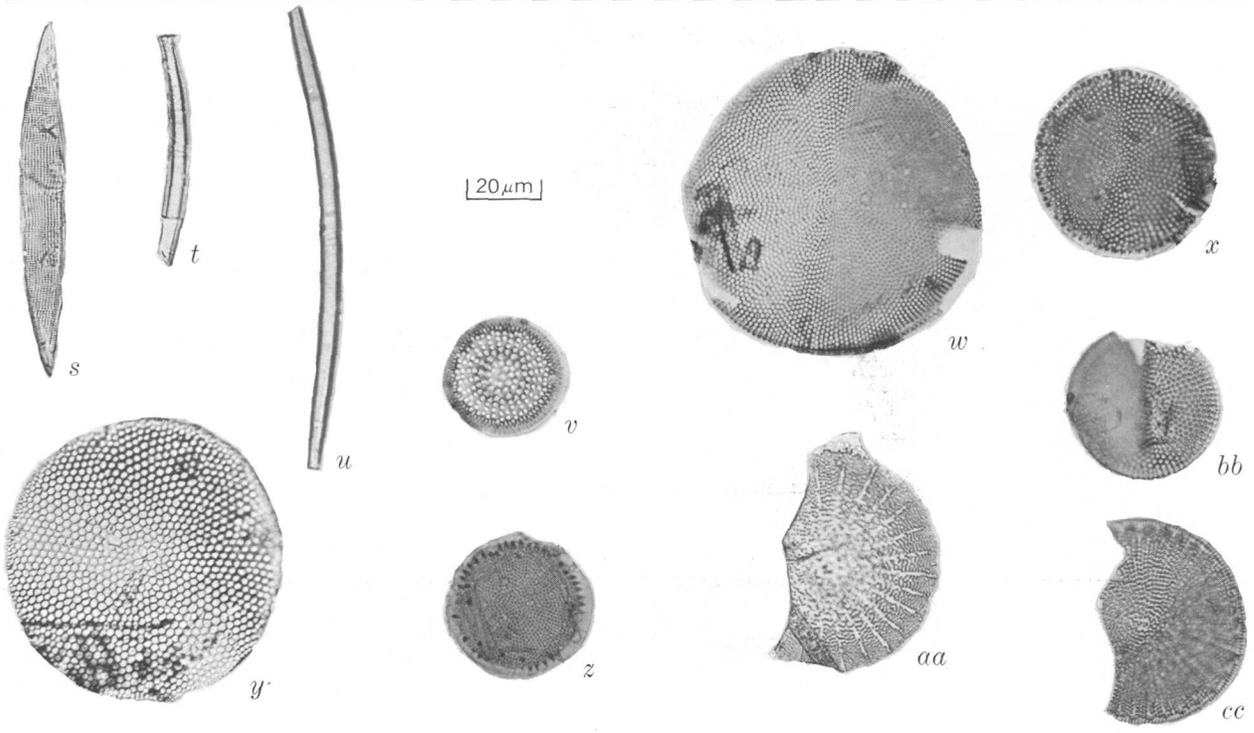
s
t
u
20 μm
v
w
x
y
z
aa
bb
cc

FIGURE 7.—Marine diotoms of the type Delmontian Stage and type *Bolivina oblique* Zone.

a. Thalassiosira antiqua (Grunow) Cleve-Euler. Type *Bolivina obliqua* Zone, Modelo Formation, USGS MR 358–MT 13. USNM 219029.

b. Thalassiosira oestrupii (Ostenfeld) Proshkina-Lavrenko. Type *Bolivina obliqua* Zone, Modelo Formation, USGS MR 358–MT 13. USNM 219030.

c. Hemidiscus simplicissimus Hanna & Grant. Type *Bolivina obliqua* Zone, Modelo Formation, USGS MR 358–MT 15. USNM 219033.

d. Thalassiosira sp. 1. Type Delmontian Stage, Monterey Formation, USGS MR 369–Del 2. USNM 219012.

e. Nitzschia reinholdii Kanaya ex Schrader. Type *Bolivina obliqua* Zone, Modelo Formation, USGS MR 358–MT 16. USNM 219034.

f. Nitzschia rolandii Schrader. Type Delmontian Stage, Monterey Formation, USGS MR 369–Del 2. USNM 219013.

g. Brunia mirabilis (Brun) Tempère. Type *Bolivina obliqua* Zone, Modelo Formation, USGS MR 358–MT 11. USNM 219027.

h. Cladogramma californicum Ehrenberg. Type *Bolivina obliqua* Zone, Modelo Formation, USGS MR 358–MT 15. USNM 219031.

i. Cladogramma dubium Lohman. Type *Bolivina obliqua* Zone. Modelo Formation, USGS MR 358–MT 15. USNM 219032.

j. Coscinodiscus endoi Kanaya. Type Delmontian Stage, Monterey Formation, USGS MR 365. USNM 219026.

k. Nitzschia kanayensis Schrader. Type Delmontian Stage, Monterey Formation, USGS MR 369–Del 2. USNM 219014.

l. Rhizosolenia miocenica Schrader. Type Delmontian Stage, Monterey Formation, USGS MR 369–Del 5. USNM 219018.

m, n. Denticula lauta Bailey, Type Delmontian Stage, Monterey Formation, USGS MR 365. USNM 219021 and 219024.

o. Denticula hustedtii Simonsen & Kanaya. Type Delmontian Stage, Monterey Formation, USGS MR 369–Del 2. USNM 210008.

p. Rhaphoneis surirella (Ehrenberg) Grunow. Type Delmontian Stage, Monterey Formation, USGS MR 365. USNM 219025.

q. Rouxia peragalli Brun & Héribaud. Type Delmontian Stage, Monterey Formation, USGS MR 369–Del 2. USNM 219015.

r. Coscinodiscus sp. aff. *C. miocenicus* Schrader. Type Delmontian Stage, Monterey Formation, USGS MR 369–Del 2. USNM 219016.

s. Mediaria splendida Sheshukova-Poretzkaya. Type Delmontian Stage, Monterey Formation, USGS MR 369–Del 3. USNM 219017.

t. Rhizosolenia barboi Brun. Type Delmontian Stage, Monterey Formation, USGS MR 366. USNM 219020.

u. Rhizosolenia praebarboi Schrader. Type Delmontian Stage, Monterey Formation, USGS MR 365. USNM 219022.

v. Actinocyclus ingens Rattray. Type *Bolivinia obliqua* Zone, Modelo Formation, USGS MR 358–MT 13. USNM 219028.

w. Coscinodiscus sp. aff. *C. plicatus* Grunow. Type Delmontian Stage, Monterey Formation, USGS MR 369–Del 2. USNM 219007.

x. Coscinodiscus plicatus Grunow s. str. Type Delmontian Stage, Monterey Formation, USGS MR 369–Del 2. USNM 219010.

y. Coscinodiscus kurzii Grunow. Type *Bolivina obliqua* Zone, Modelo Formation, USGS MR 358–MT 16. USNM 219035.

z. Thalassiosira sp. 2. Type Delmontian Stage, Monterey Formation, USGS MR 369–Del 2. USNM 219009.

aa. Cosmiodiscus elegans Greville. Type Delmontian Stage, Monterey Formation, USGS MR 369–Del 2. USNM 219011.

bb. Coscinodiscus plicatus Grunow s. ampl. Type Delmontian Stage, Monterey Formation, USGS MR 365. USNM 219023.

cc. Coscinodiscus sp. aff. *C. moholensis* Schrader .Type Delmontian Stage, Monterey Formation, USGS MR 369–Del 5. USNM 219019.

er's North Pacific diatom zones XVI and XV. Likewise, all of the silicoflagellates that others and I have observed may be found in strata correlative with Bukry's *Distephanus longispinus* Zone. Wornardt (1967), however, noted *Coscinodiscus lewisianus* Greville in California Academy of Sciences sample 866 from the type Delmontian. This diatom is probably reworked from older strata.

In the samples studied from the type *Bolivina obliqua* Zone, *Denticula lauta* Bailey and possibly *Denticula hustedtii* Simonsen & Kanaya are reworked from older strata. The youngest diatoms present, however, are those indicative of Schrader's North Pacific diatom zone X.

CONCLUSIONS

1. The type Delmontian Stage of Kleinpell (1938) near Monterey, Calif., is correlative with Schrader's (1973) North Pacific diatom zones XVI and XV and with Bukry's (1973) *Distephanus longispinus* (silicoflagellate) Zone. As such, the type Delmontian Stage is probably early late Miocene in age.
2. The type *Bolivina obliqua* Zone of Kleinpell (1938) near Los Angeles, Calif., is correlative with Schrader's (1973) North Pacific diatom zone X and probably with Bukry's (1973) *Distephanus speculum* (silicoflagellate) Zone. As such, the type *Bolivina obliqua* Zone is apparently early Pliocene in age. This supports the radiolarian data of Casey (1972).
3. The diatoms and silicoflagellates of the type Delmontian Stage are correlative with strata assigned to the *Bulimina uvigerinaformis* Zone of the

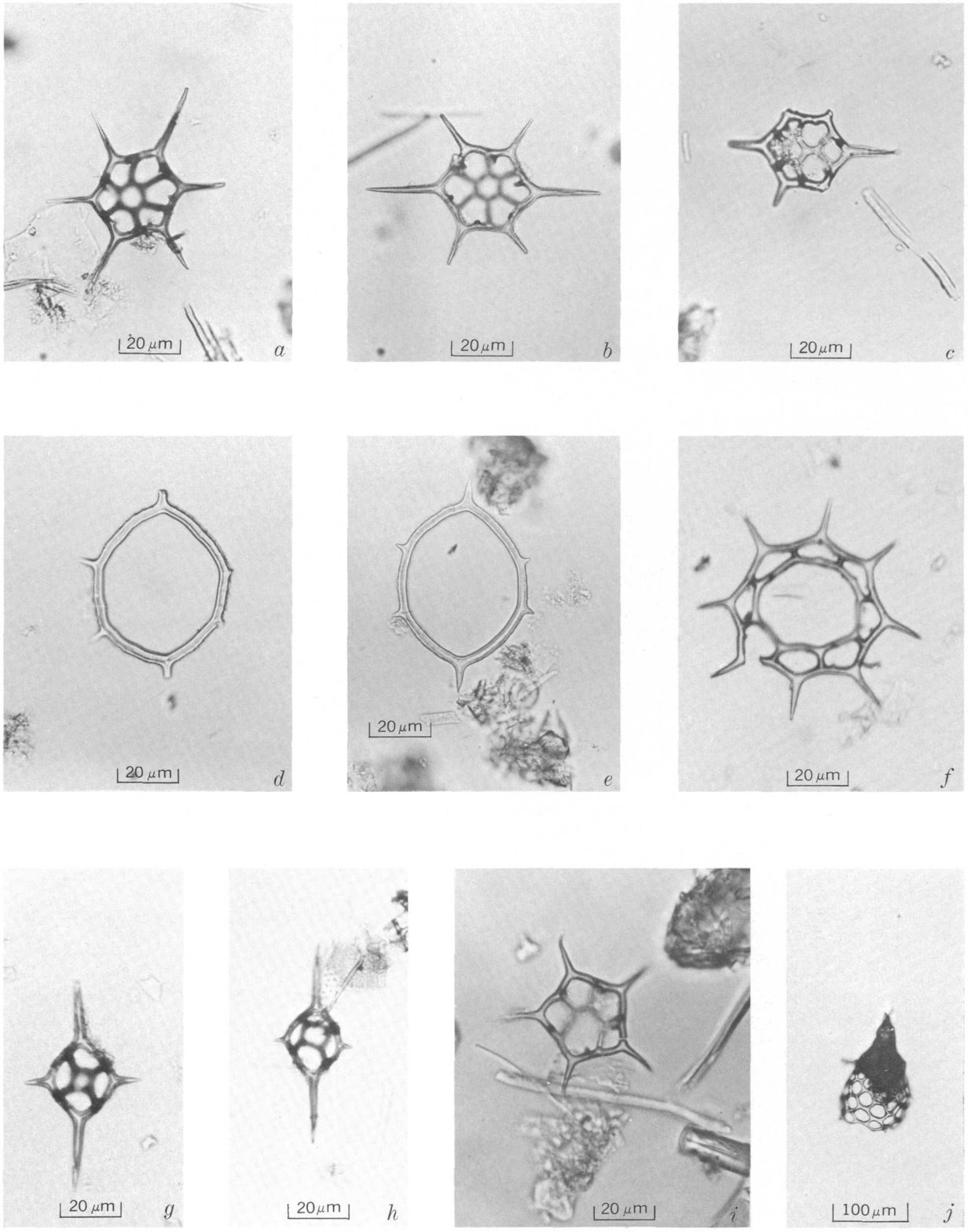

FIGURE 8.—Silicoflagellates (*a–i*) and one radiolarian (*j*) of the type Delmontian Stage and the type *Bolivina obliqua* Zone.

a, b. Distephanus boliviensis frugalis Bukry. Type *Bolivina obliqua* Zone, Modelo Formation, USGS MR 358–MT 16. USNM 219042 and 219043.

c. Distephanus speculum pseudocrux Schultz. Type *Bolivina obliqua* Zone, Modelo Formation, USGS MR 358–MT 16. USNM 219044.

d, e. Mesocena hexagona Haeckel. Type Delmontian Stage, Monterey Formation, USGS MR 365. USNM 219038. and 219039.

f. Distephanus polyactis (Ehrenberg) Deflandre s. ampl.

Type *Bolivina obliqua* Zone, Modelo Formation, USGS MR 358–MT 13. USNM 219040.

g, h. Distephanus longispinus (Schulz) Bukry & Foster. Type Delmontian Stage, Monterey Formation, USGS MR 369–Del 2 and Del 3. USNM 219037 and 219036.

i. Dictyocha pentagona (Schulz) Bukry & Foster. Type *Bolivina obliqua* Zone, Modelo Formation, USGS MR 358– MT 16. USNM 219041.

j. Lamprocyrtis heteroporos (Hays). Type *Bolivina* Zone, Modelo Formation, USGS MR 358–MT 13. USNM 219045.

---

lower Mohnian Stage at Upper Newport Bay, Newport Beach, Calif.

4. As strictly defined, the Delmontian Stage is no longer valid. There remains, however, an interval of strata between the uppermost Mohnian Stage and the lowermost Repettian Stage. At present, it seems preferable to follow Pierce (1972, fig. 3) and extend the Mohnian stratotype up to the base of the Repettian Stage which Pierce interpreted to be in Hoots' unit 19.

FLORAL REFERENCE LIST

Diatoms

Actinoptychus gruendleri Schmidt 1874. Wornardt, 1967, fig. 66.

Auliscus albidus Brun *in* Schmidt 1882. Wornardt, 1967, fig. 86.

Coscinodiscus lewisianus Greville 1866. Wornardt, 1967, fig. 26.

lineatus var. *leptopus* Grunow *in* Van Heurck 1881. Wornardt, 1967, fig. 24.

yabei Kanaya 1959. Schrader, 1973, pl. 6, figs. 1–6.

Craspedodiscus rhombicus Grunow *in* Schmidt 1881. Wornardt, 1967, figs. 44, 45.

Denticula seminae Simonsen & Kanaya 1961. Schrader, 1973, pl. 1, figs. 1–11, 36, 47.

Hemiaulus polymorphus Grunow 1884. Barron, 1975b, pl. 9, fig. 6.

Lithodesmium minusculum Grunow *in* Van Heurck 1883. Barron, 1975b, pl. 10, fig. 4.

Pterotheca subulata Grunow *in* Van Heurck 1883. Barron, 1975b, pl. 11, fig. 18.

Rouxia californica Peragallo *in* Tempère and Peragallo 1910. Schrader, 1973, pl. 3, figs. 18–20.

Stephanopyxis spinossima Grunow 1884. Barron, 1975b, pl. 12, fig. 18.

Silicoflagellates

Cannopilus sphaericus Gemeinhardt 1931. Ling, 1972, pl. 23, figs. 8–10. (Illustrated as the radiolarian, *Petalospyris* sp. by Hanna, 1928, pl. 10, fig. 2.)

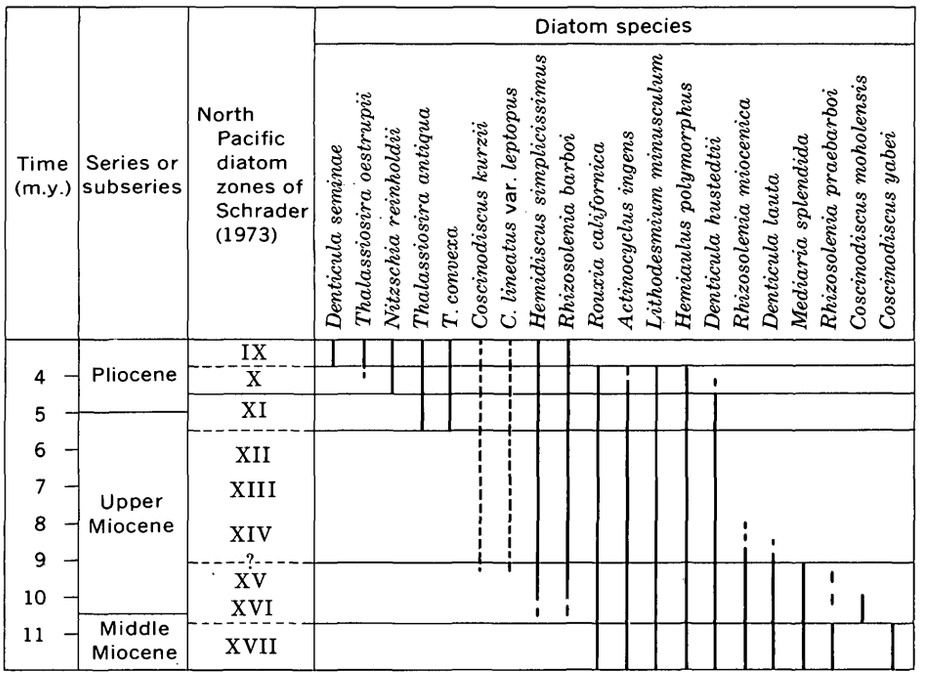

FIGURE 9.—Ranges of selected diatoms in the Neogene of California referenced against the North Pacific diatom zones of Schrader (1973). Compiled from Schrader (1973, 1974) and Barron (1975a). Modified in part after Ingle (1973). Vertical dashed line, inferred range after Barron (1975a).

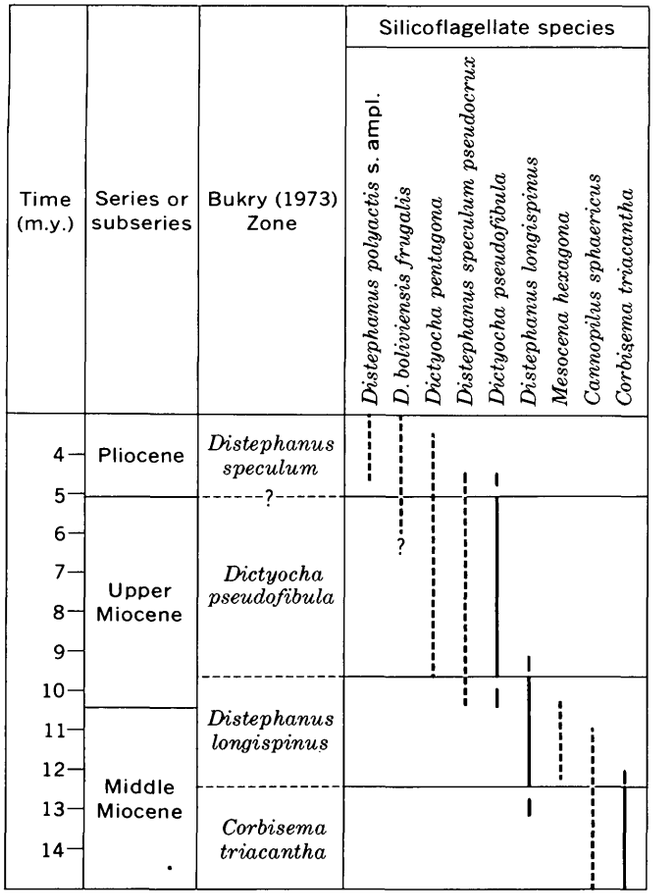

FIGURE 10.—Ranges of selected silicoflagellates in the Neogene of the eastern Pacific referenced against Bukry's (1973) silicoflagellate zones. Compiled from Bukry (1973), Bukry and Foster (1973), and Ling (1972). Modified in part after Ingle (1973). Vertical dashed line, inferred range from occurrence chart of Bukry (1973).

Corbisema triacantha (Ehrenberg) Hanna 1931. Bukry, 1973, pl. 1, fig. 2.

Dictyocha pseudofibula (Schulz) Tsumura 1963. Bukry, 1973, pl. 1, figs. 7–9.

REFERENCES CITED

Barron, J. A., 1975a, Marine diatom biostratigraphy of the upper Miocene–lower Pliocene strata of southern California: Jour. Paleontology, v. 49, no. 4, p. 619–632.

——— 1975b, Late Miocene–early Pliocene marine diatoms from southern California: Palaeontographica, v. 151, pt. B, p. 97–170.

Bowen, O. E., Jr., 1965, Stratigraphy, structure, and oil possilibities in Monterey and Salinas quadrangles, California: Am. Assoc. Petroleum Geologists, 40th Ann. Mtg., Pacific Sec., Bakersfield, Calif., p. 48–67.

Bukry, David, 1973, Coccolith and silicoflagellate stratigraphy, Deep Sea Drilling Project Leg 18, eastern North Pacific: Deep Sea Drilling Proj. Initial Repts., v. 18, p. 817–831.

Bukry, David, and Foster, J. H., 1973, Silicoflagellate and diatom stratigraphy, Leg 16, Deep Sea Drilling Project: Deep Sea Drilling Proj. Initial Repts., v. 16, p. 815–871.

Casey, R. E., 1972, Remarks made at S.E.P.M. Miocene symposium, March 10, 1972, *in* The Proceedings of the Pacific Coast Miocene Biostratigraphic Symposium: Soc. Econ. Paleontologists and Mineralogists, Pacific Sec., Bakersfield, Calif., 1972, p. 349.

Casey, R. E., and Jenkins, J. L., 1974, "Cosmopolitan" radiolarian datum planes using supposed tropical submergent radiolarians [abs.], *in* Symposium "Marine Plankton and Sediments": Planktonic Conference, 3d, Kiel, W. Germany, p. 16.

Clark, J. C., Dibblee, T. W., Jr., Greene, H. G., and Bowen, O. E., Jr., 1974, Preliminary geologic map of the Monterey and Seaside 7.5-minute quadrangles, Monterey County, Calif., with emphasis on active faults: U.S. Geol. Survey Misc. Field Studies Map MF–577, scale: 1:24,000.

Galliher, E. W., 1931, Stratigraphic position of the Monterey Formation: Micropaleontology Bull., v. 2, no. 4, p. 71–74.

Hanna, G. D., 1928, The Monterey Shale of California at its type locality with a summary of its fauna and flora: Am. Assoc. Petroleum Geologists Bull., v. 12, no. 10, p. 969–983.

Hoots, H. W., 1931, Geology of the eastern part of the Santa Monica Mountains, Los Angeles County, Calif.: U.S. Geol. Survey Prof. Paper 165–C, p. 83–134.

Ingle, J. C., Jr., 1967, Foraminiferal biofacies variation and the Miocene-Pliocene boundary in southern California: Bull. Am. Paleontology, v. 52, p. 217–394.

1973, Summary comments on Neogene biostratigraphy, physical stratigraphy and paleooceanography in the marginal northeastern Pacific Ocean: Deep Sea Drilling Proj. Initial Repts., v. 18, p. 949–960.

Kennett, J. P., and Watkins, N. D., 1974, Late Miocene–early Pliocene paleomagnetic stratigraphy, paleoclimatology, and biostratigraphy in New Zealand: Geol. Soc. America, v. 85, no. 9, p. 1385–1398.

Kleinpell, R. M., 1938, Miocene stratigraphy of California: Tulsa, Okla., Am. Assoc. Petroleum Geologists, 450 p.

Koizumi, Itaru, 1973, The Late Cenozoic diatoms of Sites 183–193, Leg 19, Deep Sea Drilling Project: Deep Sea Drilling Proj. Initial Repts., v. 19, p. 805–855.

Ling, H. Y., 1972, Upper Cretaceous and Cenozoic silicoflagellates and ebridians: Bull. Am. Paleontology, v. 62, p. 135–229.

——— 1973, Silicoflagellates and ebridians from Leg 19: Deep Sea Drilling Proj. Initial Repts., v. 19, p. 751–763.

Lohman, K. E., 1931, Floral checklist, *in* Hoots, H. W., Geology of the eastern part of the Santa Monica Mountains, Los Angeles County, California: U.S. Geol. Survey Prof. Paper 165–C, p. 114–115.

Pierce, R. L., 1972, Revaluation of the late Miocene biostratigraphy of California: summary of evidence, *in* The Proceedings of the Pacific Coast Miocene Biostratigraphic Symposium: Soc. Econ. Paleontologists and Mineralogists, Pacific Sec., Bakersfield, Calif., 1972, p. 334–340.

Ruth, J. W., 1972, Remarks made at S.E.P.M. Miocene symposium, March 10, 1972, *in* The Proceedings of the Pacific Coast Miocene Biostratigraphic Symposium: Soc. Econ. Paleontologists and Mineralogists, Pacific Sec. Bakersfield, Calif., 1972, p. 352–353.

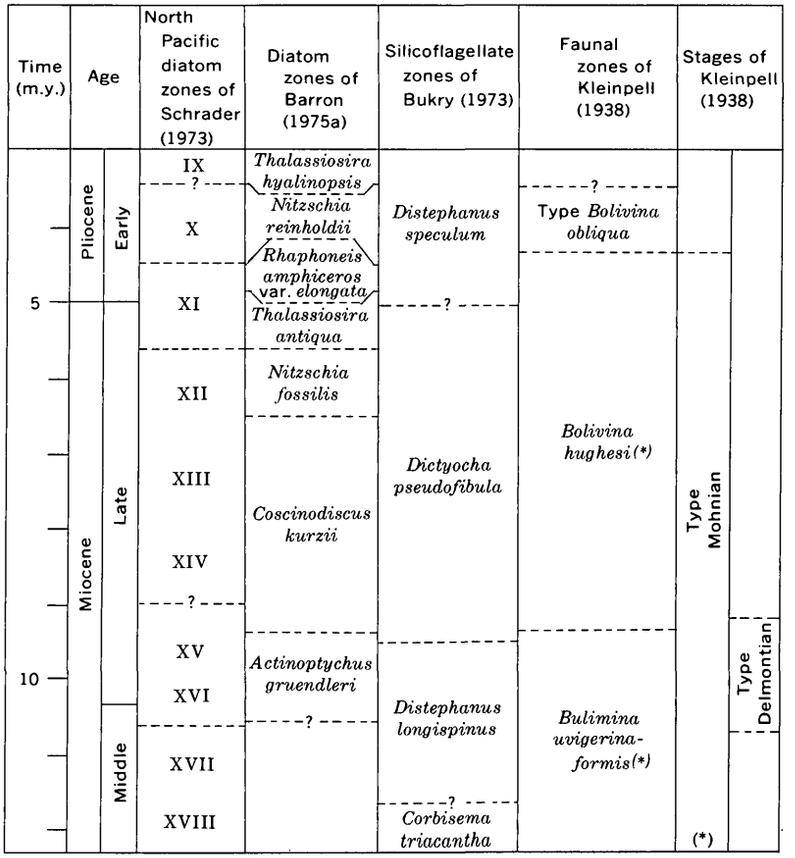

FIGURE 11.—Correlation of type Delmontian Stage and type *Bolivina obliqua* Zone of Kleinpell (1938) with the diatom bones of Schrader (1973) and Barron (1975a) and the silicoflagellate zones of Bukry (1973). Asterisk indicates estimation at Upper Newport Bay.

Schrader, H. J., 1973, Cenozoic diatoms from the northeast Pacific, Leg 18: Deep Sea Drilling Proj. Initial Repts., v. 18, p. 673–797.

——— 1974, Revised diatom stratigraphy of the Experimental Mohole Drilling, Guadalupe Site: California Acad. Sci. Proc., v. 39, p. 517–562.

Warren, A. D., 1972, Luisian and Mohnian biostratigraphy of the Monterey Shale at Newport Lagoon, Orange County, California, *in* The Proceedings of the Pacific Coast Biostratigraphic Symposium: Soc. Econ. Paleontologists and Mineralogists, Pacific Sec., Bakersfield, Calif., 1972, p. 27–36.

Wornardt, W. W., Jr., 1963, Stratigraphic distribution of diatom floras from the "Mio-Pliocene" of California: Berkeley, California Univ., Ph. D. thesis, 208 p.

——— 1967, Miocene and Pliocene marine diatoms from California: California Acad. Sci. Occasional Paper, 63, p. 1–108.

——— 1972, Late Miocene and early Pliocene correlations in the California province, *in* The Proceedings of the Pacific Coast Miocene Biostratigraphic Symposium: Soc. Econ. Paleontologists and Mineralogists, Pacific Sec., Bakersfield, Calif., 1972, p. 284–333.

——— 1974, Late Miocene Messinian correlations in various parts of the world based on diatoms [abs.]: Geol. Soc. America Abs. with Programs, v. 6, no. 7, p. 1010.

Jour. Research U.S. Geol. Survey
Vol. 4, No. 3, May–June 1976, p. 353–358

SEDIMENT-FILLED POTS IN UPLAND GRAVELS OF MARYLAND AND VIRGINIA

By LOUIS C. CONANT,[1] ROBERT F. BLACK,[2] and JOHN W. HOSTERMAN,
Washington, D.C., Storrs, Conn., Reston, Va.

Abstract.—Pot-shaped depressions filled with sandy clayey silt are found in "Upland" gravels (previously termed Brandywine) of probable Miocene age, in northeastern Maryland and in Virginia near Washington, D.C. The pots are about 7 ft (2 m) deep and commonly are about as wide. In plan, many are strongly elliptical. Sides are steep or even bulbous, and the filling in some pots shows faint stratification paralleling the sides. Strata in the enclosing gravel commonly bend downward and are thinner beside and below the pots. The gravel deposits are remnants of alluvial deposits of the ancestral Susquehanna and Potomac Rivers. All the pots are at the present gravel surface. We suggest that the pots originated when seasonal frost in an overlying layer of sandy clayey silt provided a confining upper layer. The freezing plane in the silt moved downward, reaching the gravel at some points before others. Water in the gravel moved toward the freezing plane by capillarity or by cryostatic head, forming ice lenses in the silt. Each winter, ice growth forced unfrozen clayey silt a short distance downward and outward into the gravel, increasing the irregularity of the silt-gravel contact and promoting more rapid movement. The pots probably reflect some centuries of growth, probably during the Illinoian Glaciation.

During the last few years, the senior author has observed peculiar pot-shaped or truncated spherical masses of sandy clayey silt (fig. 1*A*) at the top of nearly all high-level gravel deposits exposed in gravel pits in Cecil and Harford Counties, northeastern Maryland (fig. 2), and in Virginia near Washington, D.C. Hosterman made and interpreted X-rays of several clay samples, and Black has offered an explanation for the formation of the pots.

R. N. Oldale (written commun., 1971) has called attention to similar features in glacial outwash on Cape Cod, Mass., considered by Mather and others (1942, p. 1159–1160, pls. 1 and 2) to be "till clumps." Their published photographs, and others supplied by Oldale, show features much like our pots. Somewhat similar features have been described by Bertouille (1969, p. 21–22, 56–57) in France, by Karacsonyi and Scheuer (1970) in Hungary, and by Dionne (1970) in Canada. Black has seen similar features in high stream terraces in Austria and Hungary. Since this paper was presented orally (Conant and others, 1974), other features have been compared with our pots (Mickelson and Evenson, 1974). This note calls attention to these peculiar forms and solicits information on other localities and on their origin and significance.

Acknowledgments.—We are indebted to Charles S. Denny and James P. Minard, U.S. Geological Survey, for visiting many of the localities with the senior author, for taking part in many helpful discussions on the subject, and for suggesting improvements to the manuscript.

LOCATION AND PROVENANCE

Some of the pots, as they are here termed, are on undissected uplands; others are on the side slopes of scattered erosional remnants (fig. 3). Some are on the top of gravel deposits 50 ft (15 m) or more thick, and others are at places where the gravel is only a few feet thick. As the pots are only at or close to the present-day surface of much-dissected ancient gravel deposits, it appears that they were formed after the present topography had evolved and not at the time the gravel was deposited.

The gravel deposits known to contain the pots are clearly remnants of once broad gravel sheets formed by the ancestral alluviating Susquehanna and Potomac Rivers before uplift and deep dissection of the land. In Cecil and Harford Counties, where most of the pots have been seen (fig. 2), the base of the gravels is now about 400 ft (125 m) above the Susquehanna River, which there is at sea level. About 75 mi (120 km) to the southwest, just north of Tysons Corner in Fairfax County, Va., and about 6 mi (10 km) west of the District of Columbia, a large abandoned gravel pit shows one well-developed double pot and a single one. That gravel is about 500 ft (150 m) above sea level and 450 ft (135 m) above the Potomac River,

[1] U.S. Geological Survey (retired), 3070 Porter St. N.W., Washington, DC 20008.
[2] University of Connecticut.

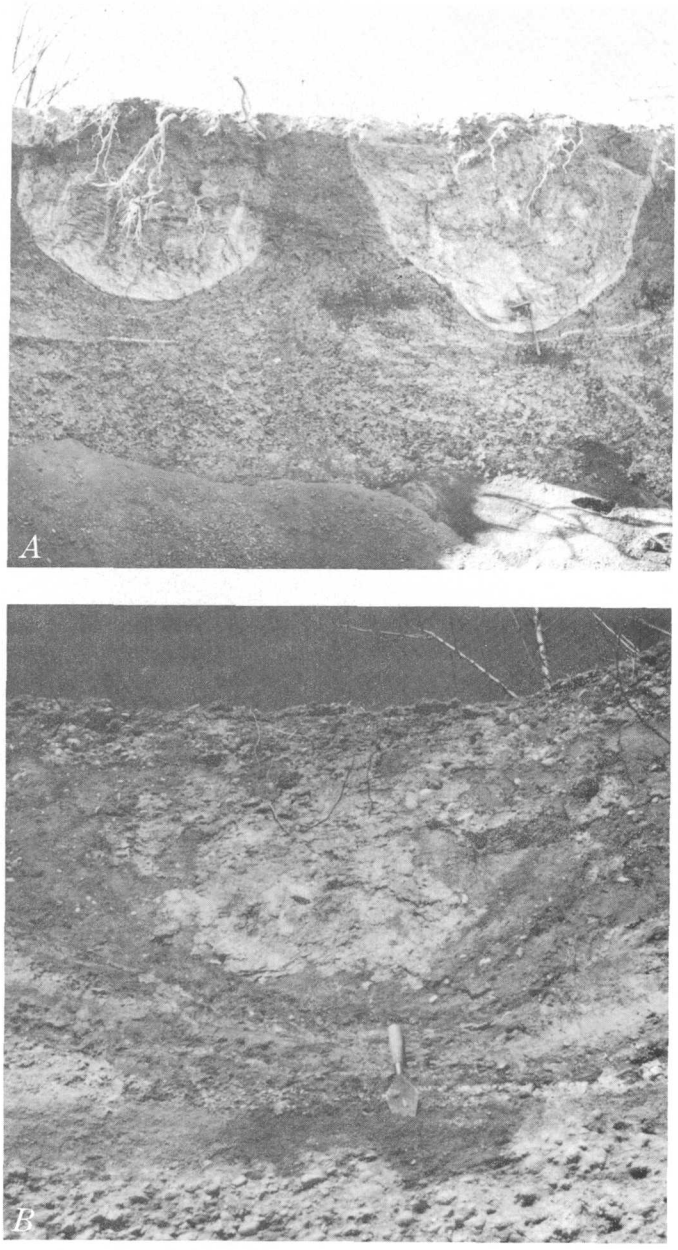

FIGURE 1.—Typical pots of clayey silt enclosed by downwarped gravel strata. Shovel handle at base of larger pot in *A* is 21 in. (53 cm) long. *B* is a closer view of another pot. Both photographs in Julian gravel pit, Cecil County, Md.

which is 3½ mi (5½ km) to the north. All these gravels have customarily been termed the Brandywine or Bryn Mawr but are here termed Tertiary "Upland" gravels of probable Miocene age (Owens and Denny, 1974). Presumably other adequate exposures in high-level gravel deposits would show similar pots along the Patapsco River near Baltimore and at other places outside the range of present observations.

DESCRIPTION OF POTS

Size and shape

Where best developed, the pots are typically 6 to 7 ft (2 m) wide and about as deep. They range in width, as exposed on the walls of gravel pits, from about 3 to 25 ft (1–8 m); some are shallower than 6 ft (2 m), but none is significantly deeper. In cross section (fig. 4), the outline of a typical pot is a truncated imperfect circle. In most of the pots, the walls are vertical or nearly so, and in some places, at least part of one or both walls of the host gravel overhangs the pot. Rounded V-shapes are also common. Typically the bases are rounded, but in a few pots they are nearly flat. Locally, two or more have merged (fig. 4*C*). A few pots have a nearly horizontal "pipestem" or wedge (fig. 4*A*) extending outward a few feet from the lower part; one is about 5 ft (1½ m) long. Some pots having reduced fillings are adjacent to pots having oxidized fillings. In a few places where poor horizontal sections could be seen, some of the pots are subcircular or strongly elliptical in plan and as much as 25 ft (8 m) long, but such exposures are rare.

The active Julian pit in Cecil County has afforded a succession of several dozen excellent exposures, and two large inactive pits near Earlton in Harford County expose several dozen pots. In some other pits the pots are isolated, no others being visible along several hundred feet (100 m) or more of wall, but at Earlton, 18 pots can be seen within a distance of about 125 yd (115 m) along the straight north wall of the south pit. In the Earlton pits, some features resemble, but are not, true pots; these features appear to be zones of reduced sediments enclosed by oxidized sediments in which stratification is continuous across the boundary between reduced and oxidized areas. The gravel strata are warped around the true pots.

Filling

The filling of the pots is chiefly a clayey silt containing a few percent to perhaps 40 percent of admixed sand and gravel (table 1). The silt is generally medium gray and mostly structureless, but in some pots it is faintly or distinctly stratified parallel with the margins (fig. 4*E*). In some pots, flat pebbles also tend to be alined parallel with the margins. The uppermost 1 ft (30 cm) of the filling is commonly somewhat more gravelly.

UPLAND GRAVELS

The gravel enclosing the pots is reddish brown, in marked contrast with the gray material filling the pots. Except for the upper 3 ft (1 m) or so, which is

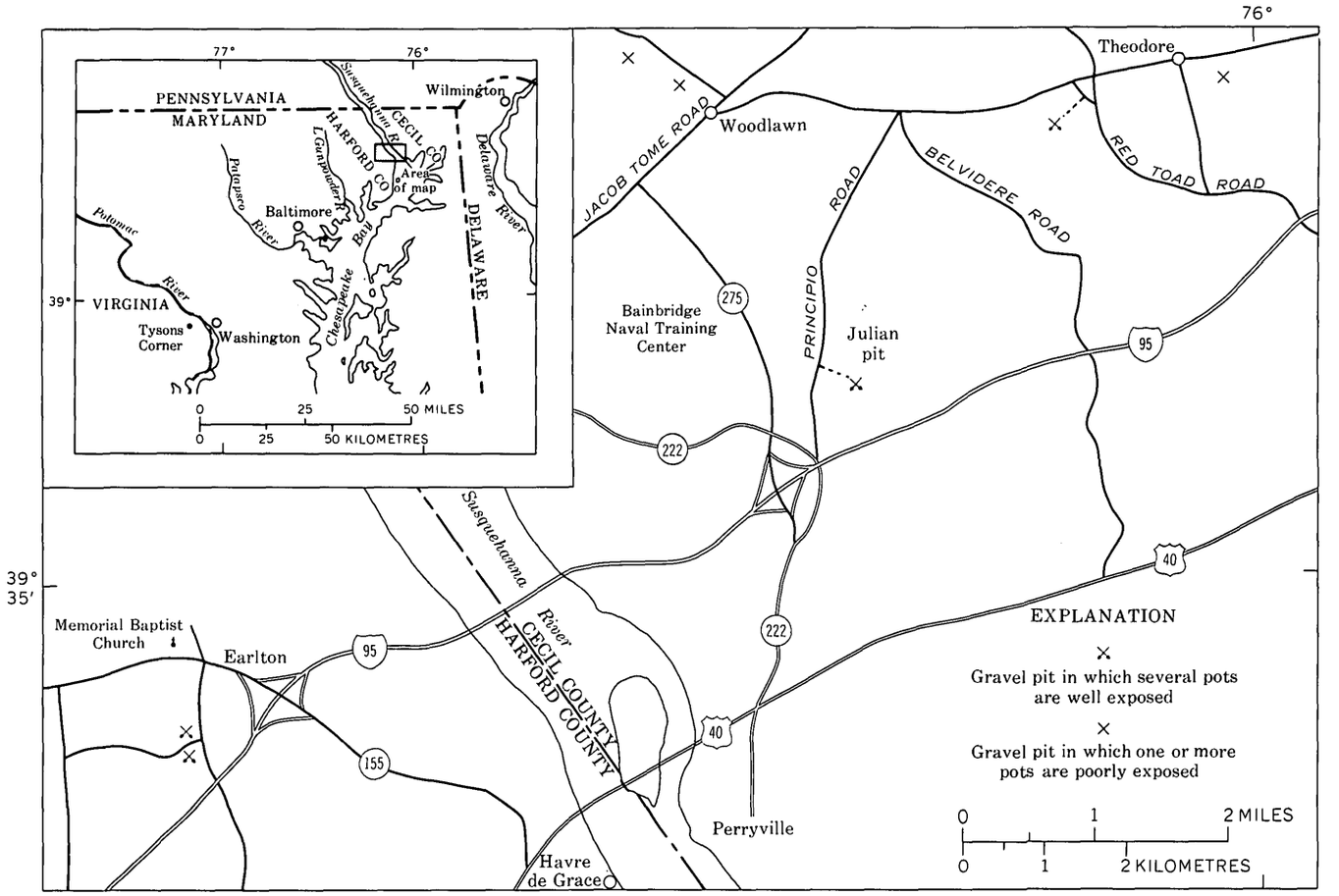

FIGURE 2.—Locations of gravel pits in Cecil and Harford Counties, Md., in which pots have been seen. Several pots are also poorly exposed at an abandoned pit at Bay View, 2½ mi (4 km) east of Theodore. Five well-exposed pots and several poorly exposed ones were seen in 1970 in the north and west walls of the excavation for the Memorial Baptist church at Earlton. Shaded area on inset map shows area of the larger map.

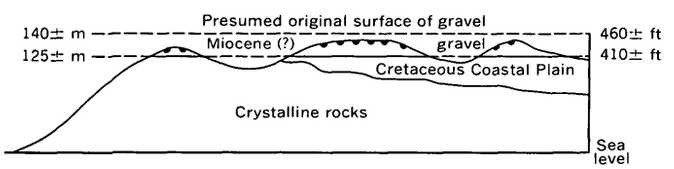

FIGURE 3.—Schematic drawing showing topographic and stratigraphic relationships of the pots, which are at the top of the gravel.

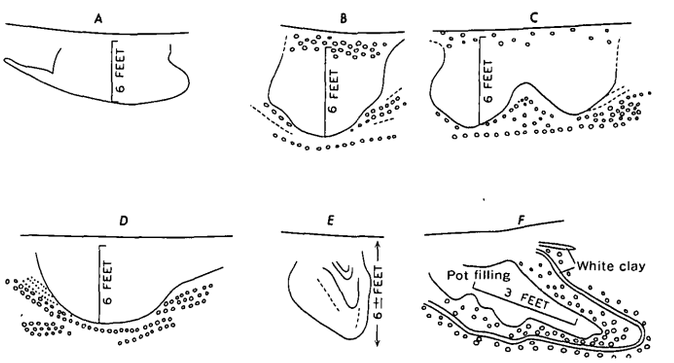

FIGURE 4.—Drawings from photographs, showing various shapes of pots. Stratification in fine-grained sediments shown by solid and dashed lines; in gravel, by circles. *A*, South pit at Earlton, Harford County, Md.; *B*, *C*, Tysons Corner, Fairfax County, Va.; *D*, *E*, *F*, Julian gravel pit, Cecil County, Md.

commonly unstratified, the gravel is distinctly stratified and has scattered thin beds or lenses of sand, silt, and silty clay. Adjacent to the pots, the strata commonly bend downward, some thinning and passing below the pots; the beds underlying many pots are slightly depressed (figs. 1 and 4 *B*). Locally, the enclosing gravel beds are warped upward on the flanks of the pots. Platy pebbles in the gravel near the pots, as well as those in the pots, are commonly alined parallel with the margins. One long narrow pot, about 1 ft (30 cm) wide and 6 ft (2 m) long, inclined at about 45°, was especially interesting because a layer of white clay 1 to 2 in. (3–5 cm) thick, was wrapped around it (fig. 4*F*).

TABLE 1.—*Wet-sieve analyses of the clayey-silt layer, the pot fillings, and the enclosing gravel, Julian gravel pit, Cecil County, Md.*

[Sieve analyses of pot filling and gravel by William Raspet; analysis of clayey-silt layer and all silt and clay separations by Hosterman. All analyses given in percentage. Tr., trace]

Size	Clayey-silt layer	Lower 40 in. (1.0 m) of pot filling	Upper 28 in. (0.7 m) of pot filling	Enclosing 28–68 in. (0.7–1.7 m) below surface
½ in. (12.7)[a]	Tr.	3.8	8.8	37.0
4 (4.76)[a]	Tr.	14.3	23.5	15.9
10 (2.00)[a]	---	8.3	12.5	7.0
40 (0.420)[a]	.12	10.9	16.7	13.2
200 (0.074)[a]	---	9.8	13.6	11.6
Silt	52	30.8	14.2	2.0
Clay	36	20.9	6.3	10.1
Total	100	98.8	95.6	96.8

[a] U.S. standard sieve. Metric equivalent in millimetres given in parentheses.

TABLE 2.—*X-ray analyses of the clay fraction of the clayey-silt pot filling, and the enclosing gravel, in percentage, Julian gravel pit, Cecil County, Md.*

Mineral	Clayey-silt layer	Lower 40 in. (1.0 m) of pot filling	Enclosing gravel, upper 28 in. (0.7 m)	Enclosing gravel, 28–68 in. (0.7–1.7 m) below surface
Kaolinite	55	45	65	65
Chlorite	--	25	--	--
Illite	10	20	10	5
Mixed-layer clay	15	10	5	Trace
Montmorillonite	20	--	Trace	5
Gibbsite	--	--	20	25
Quartz	Trace	Trace	--	--

SILT CAP

Recent operations at the large Julian pit (fig. 2) have revealed a surface layer of gray clayey silt as much as 3 ft (1 m) thick, exposed in two right-angle directions for distances of about 100 to 125 ft (30–38 m). Wet-sieve analyses of this material and of the main (lower) part of the filling of a nearby pot (table 1) indicate that both materials have nearly identical ratios of silt to clay. The upper part of the pot filling also has a similar ratio of silt to clay but differs markedly from that ratio in the gravel. Although the pot filling, especially the upper part, has sand and gravel similar to that of the host gravel (table 1), sand and gravel are insignificant in the overlying silt layer. Thus, the main filling of the pots seems to have been derived from the silt layer and to have been somewhat contaminated by the host gravel. Contamination is much higher in the upper part of the pot filling. This may have resulted from collapse of the enclosing gravel after the intrusion of the silt.

If the sand and gravel in the pots is derived from the host gravel, as seems likely, a small part of the silt and as much as half the clay in the pots may also have come from the host (table 1). Results of X-ray studies of the clay fractions of the various materials involved neither confirm nor deny this (table 2). Kaolinite is the dominant clay mineral in all units, but the gravel has the highest content of kaolinite. The presence of gibbsite is compatible with the presumed strongly oxidizing conditions of the enclosing gravel. The presence of chlorite in the pots reflects the nonoxidizing conditions resulting from long moist periods in the fine clastic fillings which did not dry out as rapidly as gravel. The lack of chlorite in the enclosing gravels is due to oxidation during downward movement of water in the gravels. This oxidation process altered the chlorite to kaolinite, which is more abundant in the enclosing gravels.

ORIGIN

Except for those pots on Cape Cod, the other previously described similar features known to us, in Europe and Canada, are apparently on flood-plain or low terraces of clay, silt, sand, or gravel. They have been variously attributed to frost action or the melting of underlying ice blocks, and all are apparently in deposits where the water table was at or near the surface.

In contrast, all our pots are in high-level deposits (fig. 3) in which the water table today is at considerable depth. Because the pots are clearly a phenomenon related to the present-day topography, the water table was probably low at the time of pot formation. However, slight induration of the upper several feet by iron oxide, resulting from weathering processes, may have caused that part to be more moist than the underlying unconsolidated gravel.

The process by which our pots were produced and the time of their formation are not obvious. Stream channeling and refilling can hardly be involved, nor can solution. Kettle formation from glacial ice blocks is not possible. The fabric of the pots and of the immediately adjacent host gravel implies a physical intrusion of the clayey silt, forcing aside the host gravel. No evidence has been seen suggesting that the pots are the result of loading of the silt layer by superposition of glacial ice or by other strata.

The suggestion is strong that some force within the filling has displaced the enclosing gravel beds, both laterally and downward. The bulk of the clayey silt seems unlikely to have been derived from the gravel. Thus, two major problems have to be considered in an explanation of the formation of the pots: (1) the source of the silt and clay that are the dominant constituents of the filling, and (2) the process by which

the gravel beds were displaced to permit emplacement of the filling.

Layers of clayey silt and silty clay are scattered irregularly in, and are part of, the upland gravel deposits. One of these layers is apparently fortuitously preserved at the top of part of the Julian pit. As no other likely source for the pot fillings is known, we assume that such a layer was once present at the surface wherever the pots have formed. Such a layer would have supplied an adequate source of material to have formed the pots but was apparently contaminated in later stages by material from the host gravel.

Charles Denny has suggested (oral commun., 1971) that the clayey silt may be a remnant of a loess that was deposited over the area during a Pleistocene glacial stage. Such loess deposition is common today in forests adjacent to glacial streams in Alaska, as it was in the midcontinental United States during several glacial substages. The presence of ancient sand dunes on the central Delmarva Peninsula, some 100 mi (160 km) to the south, suggests an episode of aeolian activity in that area during late Pleistocene time (Denny, 1974). We cannot determine the origin of the silty relict layer by using the limited data available. We believe, however, that the silty pot filling probably came originally from silty beds within the gravel deposit. The absence of a silty cap above the pots at most places suggests that the silt has been removed by erosion since the pots were formed.

We suggest that the pots originated as the result of a seasonal frost process at a time when seasonal freezing penetrated about 3 ft (1 m) on the average into the ground (much more than the few inches of penetration now observed). The 3-ft (1-m) depth is recorded in some places by an abrupt zone of demarcation separating horizontally stratified gravel from the overlying unstratified disturbed gravel. The contact of the lithologically and texturally similar gravels is too regular to have been produced by such processes as tree throw, root penetration, and burrowing animals. Depressions and mounds produced by fallen trees, however, could have produced irregularities in the contact of a silt layer on the gravel.

The downward injection of the clayey silt into the gravel required that part of the silt over the gravel be rigid and impermeable. Seasonal frost could have provided such a confining horizon (fig. 5). Downward penetration of seasonal frost in the layer of clayey silt would reach gravel at some points before others. Water in the gravel would migrate to the freezing plane in the silt, in part by capillarity and in part by cryostatic head, and build ice lenses. The direct expulsion of clayey silt by the growing ice lenses, and the local cryostatic pressure under the confining seasonal frost zone would forcibly move unfrozen silt downward and outward into the porous gravel. If we assume that the gravel was loosely packed, the clayey silt would shoulder some aside, increasing the irregularity of the silt-gravel contact and promoting movement. The process might move the unfrozen silt a fraction of an inch or so (perhaps a few millimetres) each winter. The pots would grow by small annual increments over a period ranging from many decades to some centuries.

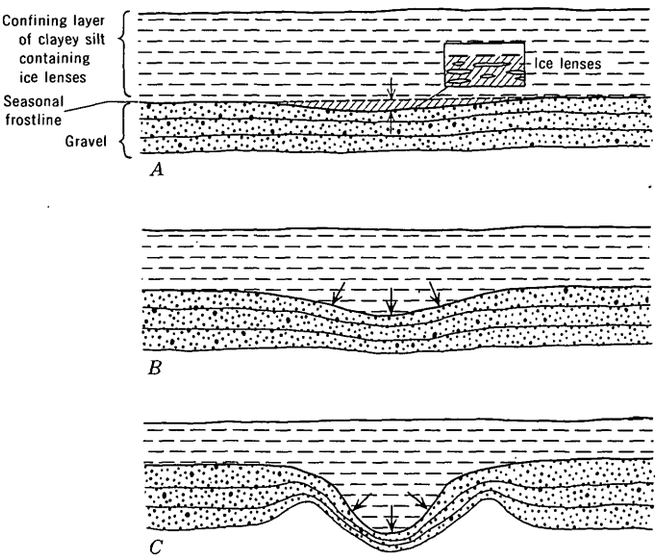

FIGURE 5.—A hypothetical method of generating pots by seasonal frost action.

A. Seasonal frost pentrates to part of the irregular contact of clayey silt over gravel. Detail: In original depressions in the contact of clayey silt on gravel, ice lenses grow as the freezing surface continues to move downward.

B. Growth of ice lenses generates cryostatic pressure below the frost zone. Expansion and movement of material is mostly downward and sideways because of the confining layer above. Loose packing of gravel allows clayey silt to push in and shoulder aside some gravel.

C. Seasonal frost over a period of many years enlarges the downwarped area into a pot.

Seasonal frost processes could explain the contamination of the silt layer of the gravel and also the tendency of the pots to become almost spherical with flat tops. The depths of the pots may be a function of the thickness, therefore the confining ability, of the overlying zone of seasonal frost. A possible weakness in the hypothesis is that the upland gravel should have been well drained because of its high topographic position. However, internal drainage in the gravel may have been impeded by the slight ferruginous induration resulting from weathering.

The origin here proposed requires loose packing in the gravel, especially in a horizontal direction. Even so, the sharp silt-gravel contact at the bases of some pots is puzzling. If the clayey silt shouldered the gravel aside, the silt must have had unusually high viscosity and adhesion. This could be possible if the silt-clay were selectively frozen to such depths that size separation was maintained as injection was achieved. The physical characteristics of silt are such that it is the most active and expandable of the size fractions under freeze-thaw conditions. However, no evidence was found that freezing took place to such depths. Wetting and drying of expandable clays as an emplacement agent was not considered effective because of the lack of such clays at present. It has not been proved, however, that such clays never were present. Gravity movement, as in loading, was not considered a viable mechanism for emplacing the pots because the material in the pots is less dense than the host material.

The sphericity of the pots may be partly attributable to nearly equal directional growth of a cryogenic bulb in fairly homogeneous material. Deviations from sphericity may have resulted from growth along weaker zones in the enclosing material. The flat tops on some pots and their shallower depths may be the result of subsequent truncation by colluviation.

An alternative hypothesis proposes that permafrost provided an impervious horizon that trapped appreciable soil moisture in the overlying active layer. The pots would grow each fall and early winter as the active layer was refrozen, mainly from the top downward. However, this requires an active layer of 8 ft (2½ m) or more—an unlikely situation. Furthermore, no evidence of a permafrost table or even of freezing at the base of the pots has been seen. In fact, the undisturbed primary fluvial fabric in the gravel below about 3 ft (1 m), and disturbance of that fabric above, suggests that freezing never reached a depth below 3 ft (1 m).

By analogy, the time of formation of the pots should be the glacial stage that brought the deepest frostline to the Maryland-northern Virginia area—presumably the Illinoian, which reached the farthest south. This would allow for the uplift and dissection of the landscape before middle Pleistocene time. However, formation of the pots could also have taken place in Wisconsinan time.

REFERENCES CITED

Bertouille, Horace, 1969, Quaternaire de l'Artois (France): Biul. Peryglacjalny, no. 19, p. 5–84.

Conant, L. C., Black, R. F., Hosterman, J. W., 1974, Pots in deposits of upland gravels in Maryland and Virginia [abs.]: Geol. Soc. America Abs. with Programs, v. 6, no. 1, p. 15.

Denny, C. S., 1974, Sand dunes on the lower Delmarva Peninsula, Maryland and Delaware [abs.]: Geol. Soc. America Abs. with Programs, v. 6, no. 1, p. 18–19.

Dionne, Jean-Claude, 1970, Structures sédimentaires dans du fluvio-glaciare, Lac-Saint Jean, Quebec: Rev. Géographie Montréal, v. 24, no. 3, p. 255–263.

Karacsonyi, S., and Scheuer, Gy., 1970, The building-geological evaluation of the Pleistocene soil-freezing phenomenons: Internat. Assoc. Eng. Geology, Internat. Cong., 1st, Paris, 1970, [Papers], v. 1, p. 37–48.

Mather, K. F., Goldthwait, R. P., and Thiesmeyer, L. R., 1942, Pleistocene geology of western Cape Cod, Massachusetts: Geol. Soc. America Bull., v. 53, no. 8, p. 1127–1174.

Mickelson, D. M., and Evenson, E. B., 1974, Large scale involutions (convolutions?-pots?) in red till in the Mahotowoe–Two Rivers–Two Creeks area of Wisconsin—Periglacial features or load structures, *in* Knox, J. C., and Mickelson, D. M., eds., Late Quaternary environments of Wisconsin: Wisconsin Geol. and Nat. History Survey, Misc. Pub., p. 182–186. (Prepared for Am. Quaternary Assoc., 3d Bienn. Mtg., Univ. Wisconsin, Madison, July 28–Aug. 2, 1974.)

Owens, J. P., and Denny, C. S., 1974, Provisional stratigraphic sequence in the Maryland-Delaware parts of the lower Delmarva Peninsula [abs.]: Geol. Soc. America Abs. with Programs, v. 6, no. 1, p. 61–62.

Jour. Research U.S. Geol. Survey
Vol. 4, No. 3, May–June 1976, p. 359–365

OCHER AS A PROSPECTING MEDIUM IN THE MONTEZUMA DISTRICT OF CENTRAL COLORADO

By GEORGE J. NEUERBURG, THEODORE BOTINELLY,
and JOHN R. WATTERSON, Denver, Colo.

Abstract.—Ocher occurs widely in the Montezuma district as small sinters and as bedded deposits of bog iron and ocher-cemented conglomerates. The iron of the ochers is derived from pyrite-rich veins and from pyritic hydrothermally altered rocks. Trace amounts of ore metals in the ocher and its admixed detritus are partly from the pyritic source rocks but also include contributions from other rocks and ores in the watershed, both during and after formation of the ocher deposit. Ocher is evidence for the presence and character of the generally ill exposed pyritic rocks, which are important in evaluating the porphyry-metal system of ore deposits. The trace-element composition of the ocher is at best a qualitative guide to the ore metals present in the provenance of the ocher deposit but not to their abundance or necessarily to their mode of occurrence.

Ochers are a conspicuous component of surficial deposits in the Montezuma mining district of central Colorado (fig. 1) and evidently occur widely in the Colorado mineral belt (Harrer and Tesch, 1959). Large bedded ocher deposits below pyritic sericitized rocks occur in the cirques of Geneva Creek, Snake River, and Handcart Gulch, along both sides of the Continental Divide. Trace amounts of ore metals in the ocher further relate them to mineralized rock. The water from which the ocher precipitates carries metals dissolved from all contacted materials in the ocher provenance, and some part of these metals is deposited with the ocher. Also, ocher is a reactive substance under surface conditions and may scavenge metals (Hawkes and Webb, 1962; Jenne, 1968) from any waters that contact it. Hydrous iron and manganese oxides have long been thought to scavenge and concentrate trace metals from water and thus would appear to be a useful medium in geochemical exploration. The abundance and variety of ocher deposits in the Montezuma district seem well suited to a test of this thesis.

GEOLOGY

The mineralized and altered rocks in the Montezuma district are a structurally complex example of the porphyry-metal class of ore deposit (Neuerburg and others, 1974) focused on the Oligocene Montezuma stock in Precambrian gneisses and granites. The explored mineral deposits of the district are silver-lead-zinc veins with some copper; these veins are characteristic of the outer propylitic zones of the porphyry-metal deposits. Stockworks of molybdenite veins centered on apophyses of the Montezuma stock are barely exposed in the Geneva Creek and Snake River cirques and occur in sericitized rocks having more than 1 percent pyrite and few added metals other than traces of copper and molybdenum. The ore elements that are expected to occur in the ocher, and for which a source

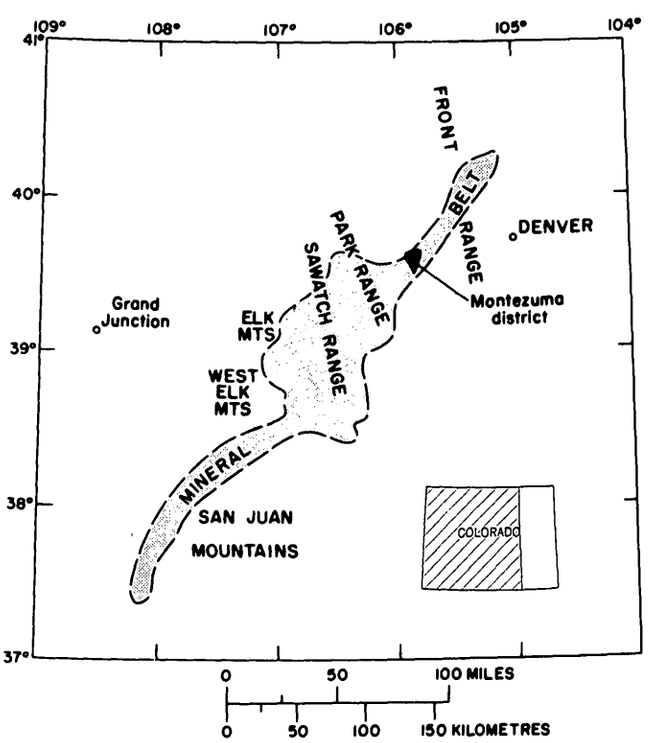

FIGURE 1.—Index map of central and western Colorado, showing Montezuma district in relation to the Colorado mineral belt.

can usually be identified, are Sb, As, Ba, Bi, Cd, Cu, Fe, Pb, Mn, Mo, Ag, W, and Zn.

Ocher occurs as sinters on hillsides and at mine entrances and as bedded deposits of bog iron and ocher-cemented gravels in valley bottoms. Ocher is a sparse-to-abundant cementing material in conglomerates and in talus and makes up essentially the whole mass of some sinters and bog irons. Textures of the ocher range from dense and compact to very fine grained and powdery. Porosity is generally high and has, in large measure, resulted from degradation of entrained plant fragments. Structure of the ocher component varies from massive in the conglomerates to unevenly and finely laminated in the pure bog irons and sinters. Rounded-to-subrounded pebbles and angular talus fragments are largely "floating" in ocher. Addition of ocher has inflated the volume of the gravels and has even "shattered" and pried outcrops apart, probably by the freezing and thawing of the water from which the ocher precipitated. Ocher precipitation is continuous to the present, but the site of precipitation has continually moved over the area of each deposit.

Bedded ocher deposits cover large areas over and downslope from pyritic sericitized rocks (fig. 2), mostly in the notably marshy areas below the intersection of the water table with the lower valley slopes. Ocher-cemented stream gravels and sands containing lenses of bog iron in the stream courses grade up the side slopes of the valley into a varied assemblage of ocher-cemented talus, slopewash, and glacial debris, all interfingering with large, irregular masses of sinter. Generally, the larger bedded deposits are near proportionally large volumes of leached, once-pyritic rocks.

Isolated epaulets of ocher sinter occur in the outer parts of the phyllic alteration zones and in the propylitic alteration zones in the western part of the district (fig. 2). Sinter epaulets are small and are on or close to one of the following equally small iron sources: pyrite-quartz veins, pyritic lead-zinc veins, small masses of pyritic altered rock, and unidentified sources under talus. Fragments of the pyritic source rock are common detrital components, although the outer edges of many epaulets contain very little detritus, which is mostly plant trash and windblown dust. The sinters and ocher-cemented slope gravels on the flanks of Tiptop Peak, northeast of Montezuma (fig. 2), are composed mostly of manganese oxides; they are structurally and texturally like the corresponding bedded and epaulet (iron) ochers.

The chemistry of ocher formation is a complex and controversial subject, though simple in broad outline. Oxidation of pyrite-bearing rocks above the water table generates sulfuric acid, which leaches ore metals from the pyritic source rock as well as from other adjacent rocks. Dissolved oxygen is all consumed in the process, and iron is transported in the ferrous state. Where this iron-bearing ground water emerges in seeps and springs, the ferrous iron is oxidized to ferric iron by atmospheric oxygen and bacterial action (Deul, 1947; Hanshaw, 1976; Wentz, 1974, p. 15–20) and precipitates typically (Krause and Lewandowski, 1963) as an amorphous hydrated iron oxide. Eventual crystallization to goethite or to hematite is hindered by phosphate and silicate anions and by organic compounds (Schwertmann, 1966). The modes of occurrence of ore elements in the ocher deposits are as (1) ions sorbed on the iron oxide (Jenne, 1968; Dyck, 1970; Hanshaw, 1976); (2) iron compounds of other metals (Hem, 1976); (3) co-precipitated independent compounds (Mikhailov, 1962); and (4) components of detrital materials, including human litter. Unlike the iron of gossans, the iron of ochers is transported from its source and, further, is exceptionally subject to addition and deletion of metals after deposition. Thus, the iron and chemically associated metals in ocher deposits represent many dispersed sources, chemical processes, and events.

SAMPLING AND ANALYSIS

Grab samples from the deposits shown in figure 3 were collected to test the metal contents of the observed variety of ocher deposits in the Montezuma district. Ocher-rich portions were preferentially sampled. Two artificially exposed parts in each of the extensive bedded ocher deposits of the Snake River and Geneva Creek cirques were selected to test the metal contributions from the two highest watersheds of each cirque; the number and type of ore deposits differ between these watersheds. Twenty-five samples were taken in each of these four areas to test the nature of any variation in metal content.

Duplicate spectrographic analyses (table 1) were made of most samples by using different fragments from the districtwide samples but splits from single fragments of each sample from the Geneva Creek and Snake River bedded deposits. Chemical analyses for copper of the north-area samples in Geneva Creek are given in table 1 for comparison with the spectrographic analyses. The differences between chemical and spectrographic analyses and between spectrographic analyses of different parts of the same sample are small.

Arsenic, antimony, and molybdenum were generally not detected spectrographically. Because these elements are derived from distinct sources (lead-zinc veins and molybdenum stockworks), chemical analyses were

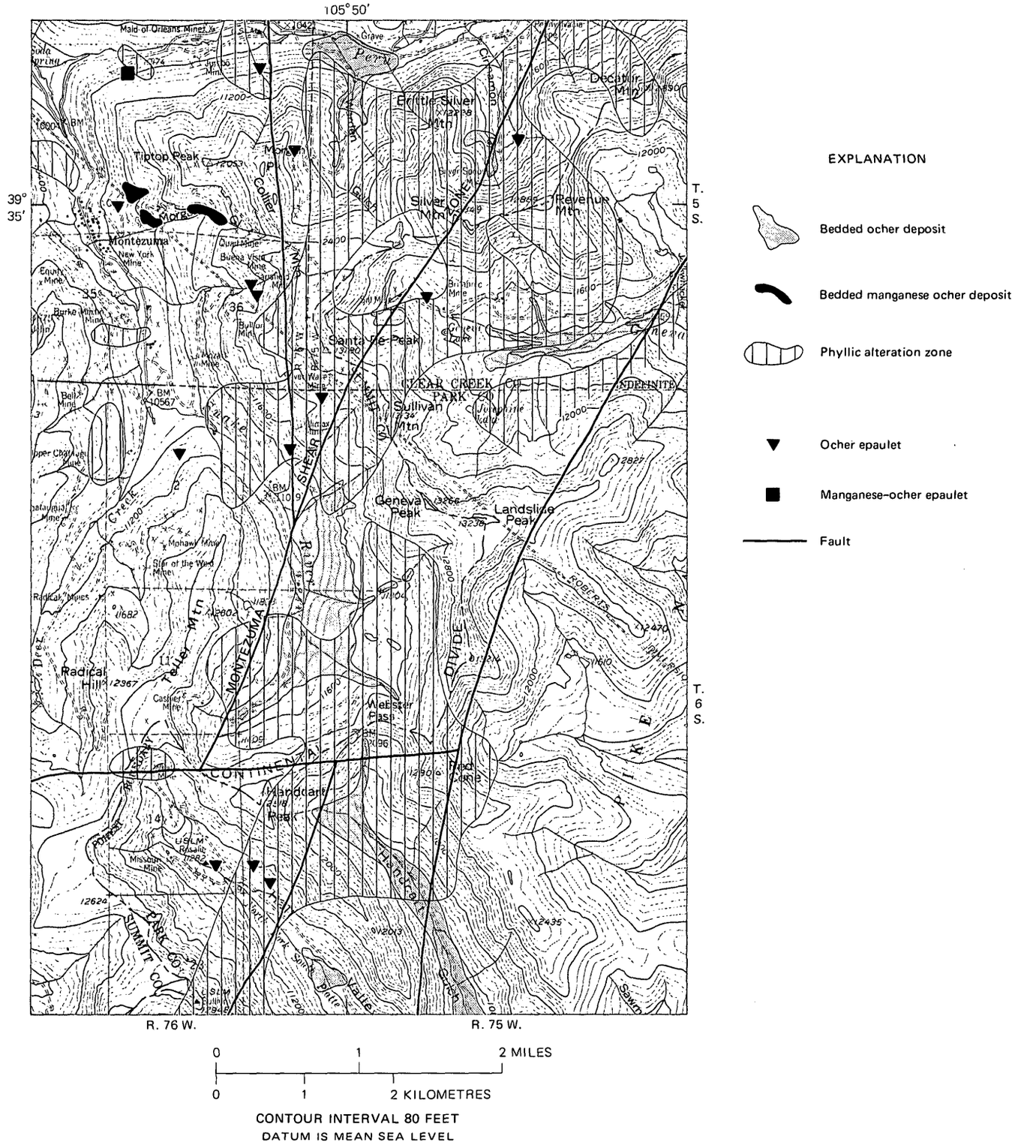

FIGURE 2.—Distribution of ocher deposits in relation to the phyllic alteration zones of the Montezuma porphyry-metal system. Base from U.S. Geological Survey Montezuma 15-minute topographic quadrangle, 1958.

made for these elements in the Geneva Creek and Snake River deposits (table 2). Waters percolating through and over the Geneva Creek bedded deposit were analyzed for molybdenum (table 2). Light-colored crusts

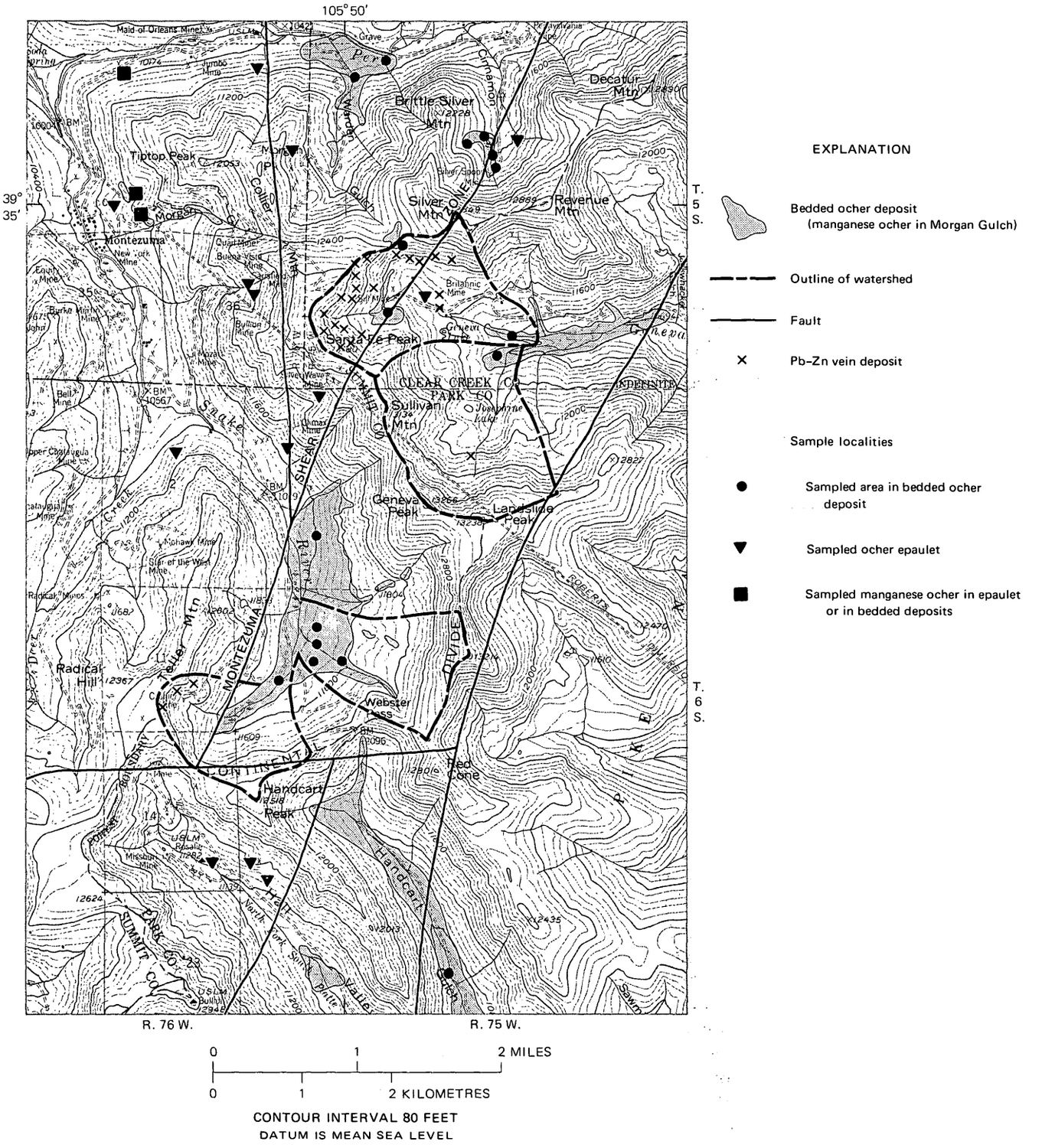

FIGURE 3.—Locations of sampled areas in ocher deposits and outlines of watersheds tested by detailed sampling of bedded ocher deposits in the Geneva Creek and Snake River cirques. Base from U.S. Geological Survey Montezuma 15-minute topographic quadrangle, 1958.

precipitated from waters draining the Geneva Creek deposit were spectrographically analyzed (table 1); these crusts are mostly amorphous, but some are jarosite, and one, not analyzed, is barite.

TABLE 1.—*Spectrographic analyses of ochers and related materials from the Montezuma district*

[Analyses reported in parts per million in the series 1, 0.7, 0.5, 0.3, 0.2, 0.15, 0.1 and so forth. N, below limit of measurement. Numbers in parentheses indicate lower limit in parts per million of measurement for each metal. Analysts are W. D. Crim, G. W. Day, R. T. Hopkins, E. L. Mosier, Harriet Neiman, and D. Siems]

Sample locality	Number of samples	Barium (20)			Manganese (10)			Silver (0.5)		
		Median	Range	Number with measurable Ba	Median	Range	Number with measurable Mn	Median	Range	Number with measurable Ag
Bedded ochers										
Warden Gulch	3	300	20–700	3	300	70–500	3	1	N–2	2
Montezuma:										
Shear zone[1]	9	700	20–1,000	9	200	70–700	9	10	N–100	8
Geneva Creek:										
North	25	N	N	0	N	N–10	4	N	N	0
South	25	N	N–200	1	10	N–30	14	N	N	0
Snake River:										
North	1	50	———	1	100	———	1	N	———	0
Middle	25	200	N–500	24	20	10–100	25	N	N	0
South	25	100	N–300	17	10	N–50	21	N	N	0
Handcart Gulch	1	300	———	1	50	———	1	1	———	1
Ocher epaulets										
Districtwide[2]	13	500	N–1,000	13	500	100–5,000	13	1	N–10	9
Manganese ochers										
Tiptop Peak[3]	3	700	500–1,500	3	(4)	(4)	--	2	N–20	2
Crusts on bedded ochers										
Geneva Creek[5]	7	N	N–200	1	N	N–150	2	0.5	N–150	4

Sample locality	Number of samples	Copper (5)			Lead (5)			Zinc (200)		
		Median	Range	Number with measurable Cu	Median	Range	Number with measurable Pb	Median	Range	Number with measurable Zn
Bedded ochers—Continued										
Warden Gulch	3	50	N–150	2	70	20–150	3	N	N	0
Montezuma:										
Shear zone[1]	9	200	50–500	9	1,000	20–3,000	9	N	N–500	1
Geneva Creek:										
North	25	150	20–300	25	N	N	0	N	N	0
		[6]195	[6]33–370	[6]25	N					
South	25	70	30–100	25	N	N–10	10	N	N	0
Snake River:										
North	1	100	———	1	30	————	1	500	————	1
Middle	25	30	10–300	25	15	N–100	22	N	N	0
South	25	30	N–30	24	15	N–50	23	N	N	0
Handcart Gulch	1	100	———	1	20	————	1	N	————	0
Ocher epaulets—Continued										
Districtwide[2]	13	70	N–500	12	200	30–7,000	13	300	N–10,000	7
Manganese ochers—Continued										
Tiptop Peak[3]	3	500	200–1,500	3	7,000	5,000–15,000	3	10,000	7,000–15,000	3
Crusts on bedded ochers—Continued										
Geneva Creek[5]	7	20	7–200	7	N	N	0	N	N	0

[1] One sample contained 200 ppm Bi; one sample 30 ppm Sn.
[2] One sample contained 70 ppm Cd; one sample 10 ppm Sn; one sample 5 ppm Bi; one sample 50 ppm Bi.
[3] One sample contained 100 ppm Cd, 5 ppm Mo, 500 ppm As; one sample 100 ppm Cd; one sample 150 ppm Sn.
[4] Major constituent.
[5] One sample contained 200 ppm As; one sample 300 ppm As.
[6] Data from chemical analysis of splits of Geneva Creek north samples.

METAL CONTENT

The metal content of Montezuma ochers is generally quite small; it is comparable with that of other ocher deposits in the Colorado mineral belt (Harrer and Tesch, 1959; Hanshaw and Spiker, 1972). Metals are not concentrated by ochers, the deposits being more a subdued expression of the metal content of their provenances. Ocher epaulets, like their vein sources, show a higher and more varied metal content than do bedded deposits derived mainly from stockwork deposits and their barren pyritic mantles. However, the difference is more directly attributable to the detrital component of the ocher deposits than to any chemical property of the ferric hydroxide; detritus-poor ochers in general have metal contents at the lower limit of the ranges listed in table 1. The bedded ocher deposits along the Montezuma shear zone (table 1) are not an exception, inasmuch as this structure hosts some of the more productive silver-lead-zinc veins of the district; the veins have contributed appreciable detritus to the ocher-cemented gravels. Ferric hydroxides experimentally (Chao and Anderson, 1974) and observationally (table

TABLE 2.—*Chemical analyses of bedded ocher samples and waters, Geneva Creek and Snake River cirques (fig. 3)*

[N, not detected; NA, no analyses]

Locality	Insoluble residue (percent)[1]		Arsenic (ppm)[2]			Antimony (ppm)[3]			Molybdenum in ocher (ppb)[4]			Molybdenum in water (ppb)[4]		
	Median	Range	Median	Range	Proportion above detection limit, 10 ppm	Median	Range	Proportion above detection limit, 1 ppm	Median	Range	Proportion above detection limit, 10 ppb	Median	Range	Proportion above detection limit, 0.1 ppb
Geneva Creek cirque:														
North	0.5	<0.5–2.5	80	20–200	25/25	3	1–6	25/25	100	N–1,100	24/25	0.27	N–1.0	6/7
South	1.0	<.5–15.5	10	N–40	20/25	2	1–3	25/25	N	N–20	2/25	.13	N–.20	9/10
Snake River cirque:														
Middle	29	4.0–58.5	10	N–20	23/25	2	1–3	25/25	20	N–60	13/25	NA	NA	NA
South	8	.5–43.5	20	N–80	23/25	2	1–3	25/25	20	N–80	21/25	NA	NA	NA

[1] Residue from 24-hour digestion in concentrated HCl, air dried.
[2] Colorimetric; J. G. Viets, analyst.
[3] Colorimetric; J. D. Huffman, analyst.
[4] Atomic absorption; J. R. Watterson, analyst.

1) contain lower amounts of metals than do manganese ochers, but the data are too few for further comment.

The samples from the Geneva Creek and Snake River cirques were taken from ocher deposits in drainages from metallized areas and from nearly barren areas. It was expected that the metal contents of these ochers would reflect this difference and would give some indications of the type of ore deposit in the drainage. The results are much more complex and much less definitive than expected.

The bedded ocher deposit of the southernmost sample area in the Snake River cirque (fig. 3) is thin-bedded bog iron and ocher-cemented fluviatile pebble conglomerate. The watershed is divided by the Montezuma shear zone. East of the shear zone are sericitized rocks containing sparsely disseminated chalcopyrite and molybdenite. West of the shear zone, mildly propylitized rocks host the Cashier mine and two prospects, all Ag-As-Ba-Cu-Pb-Zn veins. The middle sample area of the Snake River deposit comprises four localities in ocher-cemented talus and slope gravels. The rocks in the contributing watershed are a continuation from the southern-sample-area watershed of the sericitized rocks containing sparsely disseminated chalcopyrite and molybdenite. This area also contains a stockwork-vein deposit of molybdenite (Neuerburg and others, 1974).

The arsenic content (table 2) is slightly higher in the southern sample area of the Snake River ocher deposit, which is in keeping with the cited differences in watershed mineralization. No significant difference in copper content of the two ocher sample areas was found; the small traces of disseminated chalcopyrite are evidently sufficient to overwhelm any contribution of copper from the veins of the southern watershed. The molybdenite deposit in the middle watershed does not contribute significantly to the ocher, probably because it is mostly below the zone of leaching. Silver is reported from manganese and iron oxides on stream bottoms below the Cashier mine (Chao and Anderson, 1947) and upstream from the southern sample area but is not present in the ocher deposit. Presumably, silver was scavenged before it could reach the sample area.

The watershed draining into the southern sample area in the Geneva Creek cirque (fig. 3) contains a single small Ag-Cu-Pb-Zn vein in propylitized gneisses. The watershed for the northern sample area contains numerous Ag-Pb-Zn veins, some with bismuth and tungsten minerals, in propylitized gneisses; these veins are topographically above sericitized rocks containing disseminated molybdenite and quartz-molybdenite stockworks in pebble breccias. Both sample areas are of exceptionally pure ocher (table 2) and are saturated with flowing meteoric waters.

The greater content of arsenic, copper, and molybdenum in the northern sample area is in agreement with the more extensive mineralization in its watershed. The paucity of barium, lead, manganese, and silver in these pure ochers is noteworthy. These metals are present in the crusts that are precipitated at the surface of the bog from the water flowing through and over the bog. A similar contrast in molybdenum content is shown by these ochers and the saturating waters. The southern-area ocher samples have almost no molybdenum; yet the molybdenum content of the waters of the southern area is only slightly lower than that of the waters of the northern area, whose ocher samples are 10 times or more richer in molybdenum. These observations evoke a variety of explanations involving metal interchanges in either direction, or not at all, between ocher and waters but all underlining the uncertain significance of the metal contents of ocher as a practical indicator of mineralization.

CONCLUSIONS

The principal prospecting value of ocher deposits in the Montezuma district and other similar districts is as evidence of the presence of ill-exposed pyritic rocks and of their probable location and areal extent. The metal content of the ocher deposit is a qualitative and subdued inventory of the ore metals in the provenance. There is little evidence that these nearly pure iron ochers selectively scavenge and(or) concentrate metals to an extent useful for prospecting. The manganese ochers are accumulating metals but are inadequately represented for evaluation.

REFERENCES CITED

Chao, T. T., and Anderson, B. J., 1974, The scavenging of silver by manganese and iron oxides in stream sediments collected from two drainage areas of Colorado: Chem. Geology, v. 14, no. 3, p. 159–166.

Deul, Maurice, 1947, The origin of the bog iron deposits near Montezuma, Summit County, Colorado: Boulder, Colorado Univ. M.S. thesis, 37 p.

Dyck, Willy, 1971, The adsorption and coprecipitation of silver on hydrous oxides of iron and manganese: Canada Geol. Survey Paper 70–64, 23 p.

Hanshaw, B. B., 1976, Geochemical evolution of a geothite deposit: [Czechoslovakia] Ustřed. Ústav. Geol. Věstník. (In press.)

Hanshaw, B. B., and Spiker, E., 1972, Unusual wood preservation used to determine the geochemical kinetics of an iron spring deposit: Internat. Conf. on Radiocarbon Dating, 8th, Wellington [New Zealand], Proc., sec. F, v. 2, p. F41–F51.

Harrer, C. M., and Tesch, W. J., Jr., 1959, Reconnaissance of iron occurrences in Colorado: U.S. Bur. Mines Inf. Circ. 7918, 82 p.

Hawkes, H. E., and Webb, J. S., 1962, Geochemistry in mineral exploration: New York, Harper & Row, Publishers, 415 p.

Hem, J. D., 1976, Some mechanisms for coprecipitation of metal ions with ferric hydroxide, *in* Krenkel, P., ed., Progress in water technology, Volume 7: Oxford, England, Pergamon Press. (In press.)

Jenne, E. A., 1968, Controls on Mn, Fe, Co, Ni, Cu, and Zn concentrations in soils and water—The significant role of hydrous Mn and Fe oxides, [Chap.] 21 *in* Baker, R. A., ed., Trace inorganics in water: Washington, D.C., Am. Chem. Soc. (Advances in Chemistry Ser. 73), p. 337–387.

Krause, Alfons, and Lewandowski, Anzelm, 1963, Die Struktur eines Raseneisenerzes: Tschermaks Mineralog. u. Petrog. Mitt,, 3d ser., v. 8, no. 3, p. 439–443.

Mikhailov, A. S., 1962, On the formation of molybdenum-bearing hydrous iron oxides: Geochemistry, 1962, no. 10, p. 1050–1053.

Neuerburg, G. J., Botinelly, Theodore, and Watterson, J. R., 1974, Molybdenite in the Montezuma district of central Colorado: U.S. Geol. Survey Circ. 704, 21 p.

Schwertmann, U., 1966, Die Bildung von Goethit und Hämatit in Böden und Sedimenten: Internat. Clay Conf., Jerusalem, Israel, 1966, Proc., v. 1, p. 159–165.

Wentz, D. A., 1974, Effect of mine drainage on the quality of streams in Colorado, 1971–1972: Colorado Water Conserv. Board Colorado Water Resources Circ. 21, 117 p.

Jour. Research U.S. Geol. Survey
Vol. 4, No. 3, May–June 1976, p. 367–377

A RECONNAISSANCE STUDY OF THE URANIUM AND THORIUM CONTENTS OF PLUTONIC ROCKS OF THE SOUTHEASTERN SEWARD PENINSULA, ALASKA

By THOMAS P. MILLER and CARL M. BUNKER,
Anchorage, Alaska, Denver, Colo.

Abstract.—Large granitic Cretaceous plutons are exposed along and adjacent to an arcuate belt of igneous and high-grade metamorphic rocks in the southeastern Seward Peninsula of Alaska. Reconnaissance studies of these plutons have shown that the Darby pluton has well above average amounts of uranium and thorium (11.2 ppm and 58.7 ppm, respectively), the Kachauik pluton contains average to above average uranium and thorium (5.7 ppm and 22.5 ppm, respectively), and the Bendeleben pluton contains average amounts of uranium and thorium (3.4 ppm and 16.7 ppm, respectively). The three plutons show compositional and textural differences indicative of different source materials that may have controlled the distribution of uranium and thorium.

The high uranium and thorium contents of the Darby pluton, similar to those of the Conway Granite of New Hampshire which has been mentioned as a possible low-grade thorium resource, suggest that this pluton may be a favorable area for economic concentrations of uranium and thorium.

Reconnaissance sampling and mapping of three large granitic masses, the Bendeleben, Darby, and Kachauik plutons, in the southeastern part of the Seward Peninsula (fig. 1) have shown that the Darby pluton contains above average amounts of uranium and thorium and that the uranium and thorium contents of the three plutons are significantly different. Reconnaissance petrologic studies of the three plutons and analytical results reported herein provide a framework for future studies of radioactive materials in the region and call attention to areas of anomalous concentrations of uranium and thorium.

The southeastern Seward Peninsula is dominated physiographically by the rugged Bendeleben and Darby Mountains, which together form an arcuate trend convex to the southwest. The Darby and Bendeleben plutons underlie the respectively named mountain ranges, and the Kachauik pluton lies in the uplands adjacent to the Darby Mountains. These plutons were first noted by Mendenhall (1901) and Smith and Eakin (1911) during reconnaissance traverses along and across the Darby Mountains. No other studies of these plutons were done until West (1953) investigated the radioactivity of pan concentrates taken from streams draining the Darby and Kachauik plutons. More recently, the plutons were mapped at a scale of 1:250,000 by Miller, Grybeck, Elliott, and Hudson (1972), and much of this report is based on that work. A preliminary geochemical report by Miller and Grybeck (1973) mentioned the high uranium and thorium values obtained from three rock samples of the Darby pluton.

Approximately 70 modal analyses have been made of the plutonic rocks, and 28 chemical analyses were obtained along with the 31 gamma-ray spectrometric analyses reported here. It is emphasized that much of this study is based on reconnaissance mapping and the number of samples analyzed is too small to define in detail the total range of uranium and thorium contents in the plutons sampled. Smaller plutons in the general region such as the Windy Creek stock and the Dry Canyon Creek stock (fig. 1) have not yet been analyzed for uranium and thorium.

Acknowledgments.—We are indebted to Donald Grybeck, R. L. Elliott, and T. L. Hudson for assistance in the mapping and to M. H. Staatz for information on some of the radioactive minerals. C. A. Bush assisted with the analyses of the radioelement contents.

GEOLOGIC SETTING

The Darby, Bendeleben, and Kachauik plutons are among the largest bodies of granitic rock on the Seward Peninsula and form part of an arcuate belt of plutonic and high-grade metamorphic rocks extending for 270 km across the peninsula through the Darby, Bendeleben, and Kigluaik Mountains (fig. 1). The metamorphic rocks of this igneous-metamorphic complex consist chiefly of Precambrian pelitic schist and

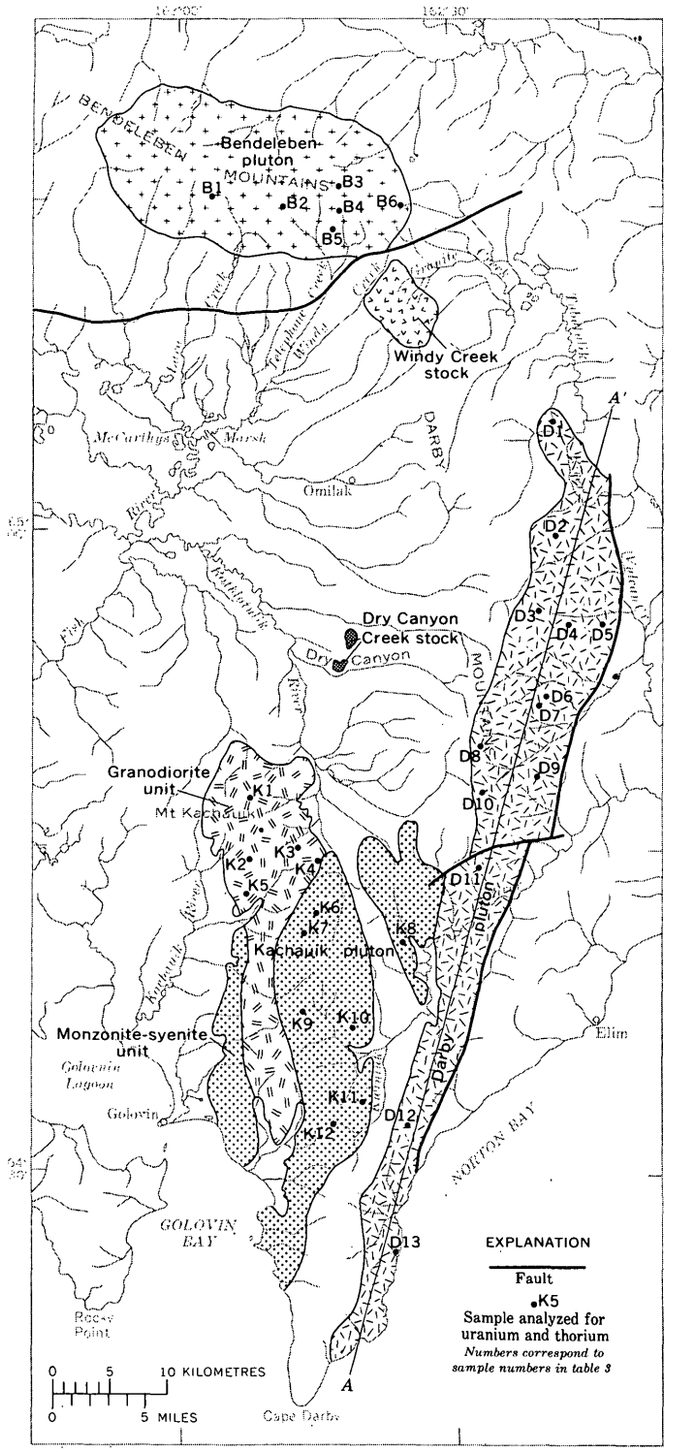

FIGURE 1.—Distribution of plutonic rocks in southeastern Seward Peninsula.

gneiss with intercalated marble, calc-silicate gneiss, and minor amounts of rock of the amphibolite facies. The plutonic rocks that intrude this assemblage in the southeastern Seward Peninsula are chiefly Cretaceous in age and range in composition from quartz monzonite and granodiorite to monzonite and syenite. Associated with some of the syenite and monzonite bodies are small intrusive complexes and dikes of alkaline subsilicic rocks that form part of a lithologically similar belt that extends from west-central Alaska through the southeastern Seward Peninsula and St. Lawrence Island into Siberia (Miller, 1972; Csejtey and Patton, 1974). Bounding the igneous-metamorphic complex in the southeastern Seward Peninsula are low-grade Precambrian rocks of the greenschist facies consisting chiefly of quartz-mica schist with lesser amounts of metavolcanic rocks, graphitic schist, and marble. Paleozoic (chiefly Devonian) carbonate rocks (Miller and others, 1972) are associated with these low-grade metamorphic rocks and appear to be in fault contact with them. The change in facies between low- and high-grade metamorphic rocks is so abrupt in most places that it appears to mark a fault contact. Cretaceous nonmarine sedimentary rocks crop out east of the Darby Mountains, and Late Cenozoic basalts, which cover large areas to the north and east, occur locally in the southeastern Seward Peninsula. Both the Bendeleben and Darby Mountains were subjected to valley glaciation of probable Illinoian and Wisconsin age (Hopkins, 1963) that produced numerous U-shaped valleys and arêtes.

The southeastern Seward Peninsula is structurally complex, and its dominant structural grain changes from east-west in the Bendeleben Mountains to north-south in the Darby Mountains. Parts of the area have been subjected to east-directed thrust faulting (Sainsbury, 1969b), and both mountain ranges appear to be at least partly bounded by range-front faults. A narrow but continuous north-south belt of ophiolite rocks of probable Permian age crops out east of the Darby and Bendeleben Mountains (Miller and others, 1972); these rocks locally contain glaucophane and may mark an old suture zone.

PETROLOGY

The Darby and Bendeleben plutons are composed of relatively homogeneous quartz monzonite that is similar in gross composition in both plutons but differs in grain size and texture. The Kachauik pluton is a much more heterogeneous composite pluton composed of rocks ranging from granodiorite to syenite. Plots of felsic modal components based on point counts of stained slabs (fig. 2) show the compositional character of the plutons. Because the sampling density of these large plutons is relatively low, the modes shown in figure 2 only approximately represent the range in

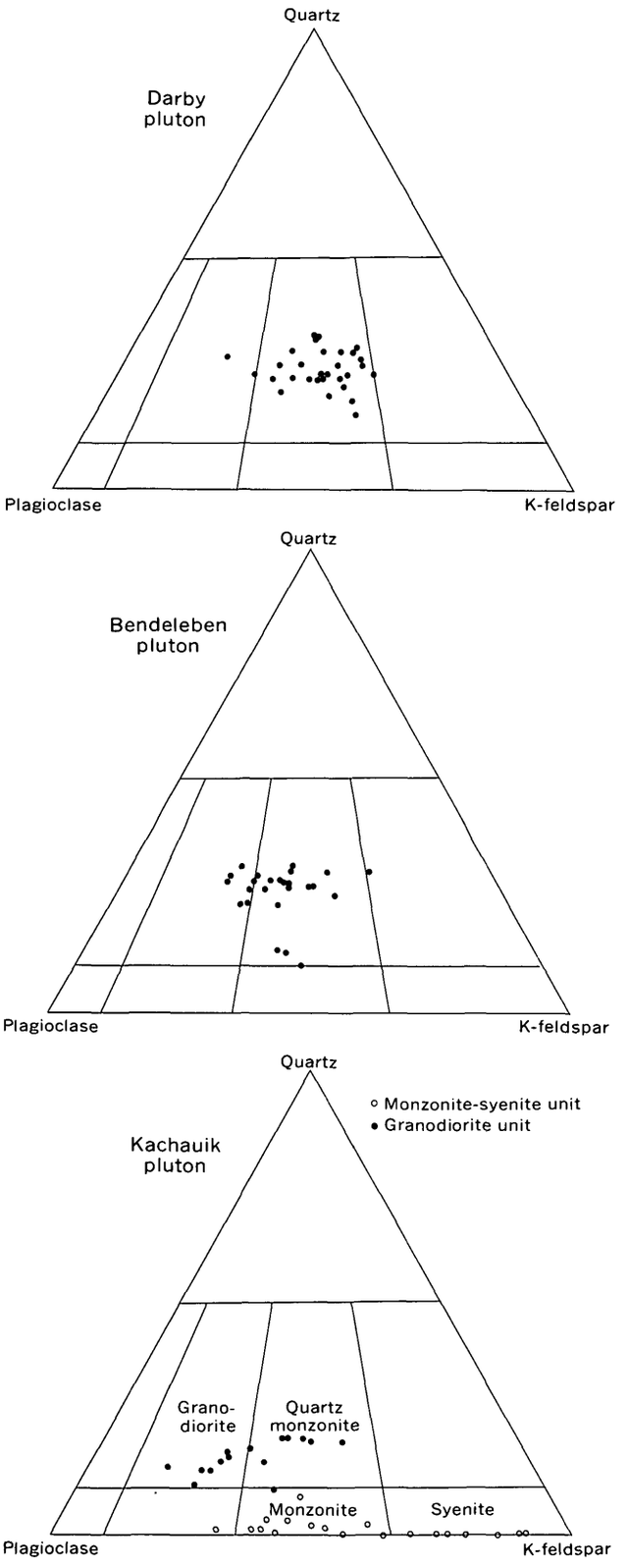

FIGURE 2.—Modal plots of plutonic rocks of southeastern Seward Peninsula.

composition. The same is true for the average chemical analyses given in table 1.

The Darby pluton, a long, thin body extending more than 80 km in a N. 18° E. direction and only 3 to 8 km in width, underlies an area of about 400 km² in the eastern Darby Mountains. Exposures are good in the glaciated northern part of the pluton, particularly in the higher cirque walls, and along the southern seacoast; elsewhere in the pluton, frost action has reduced many outcrops to rubble. Enough pinnacle outcrops remain, however, to give a fair outcrop pattern. The rocks are generally fresh although commonly somewhat friable in the pinnacle outcrops. The Darby pluton is composed of granitic rocks that have a characteristic coarse-grained porphyritic texture with large tabular pink potassium-feldspar phenocrysts (up to 50 mm long) in a gray to cream-colored, medium- to coarse-grained groundmass of feldspar and quartz mottled with 5 to 10 percent dark minerals. Foliation and lineation are almost totally lacking except locally along the west contact north of the headwaters of Dry Canyon Creek. Large (>30 cm long) mafic ellipsoidal inclusions are very abundant in the sea cliff exposures at the southern tip of the pluton just east of Cape Darby (fig. 1).

The Darby pluton is composed chiefly of quartz monzonite consisting primarily of perthitic potassium-feldspar and plagioclase (An_{20-34}) in approximately equal amounts with slightly less quartz. Varietal mafic minerals are biotite and hornblende; hornblende is less abundant than biotite and almost totally absent from the northern third of the pluton. Ubiquitous accessory minerals are abundant magnetite and allanite with lesser amounts of sphene, apatite, zircon, and a little fluorite and rutile. Alteration effects are weak, minor amounts of sericite replacing plagioclase, chlorite replacing biotite, and goethite and lepidocrocite replacing magnetite.

Although megascopically the pluton appears to show little change in composition over its entire 80-km length, the modes show a slight and gradual decrease in mafic-mineral and plagioclase content from south to north and a corresponding increase in quartz and potassium-feldspar, indicating lateral zoning. This lateral zoning is illustrated in figure 3 where mafic-mineral content is plotted along the axis of the pluton.

Aplite dikes, commonly tourmaline-bearing and generally less than 40 cm thick, are present throughout the pluton, and a swarm of lamprophyre dikes occurs near the south end of the pluton.

The most distinguishing characteristics of the Darby pluton are its uniform coarse-grained porphyritic tex-

TABLE 1.—*Chemical composition of the Darby, Bendeleben, and Kachauik plutons*

	Darby pluton (10 analyses)		Bendeleben pluton (6 analyses)		Kachauik pluton			
					Granodiorite (2 analyses)		Monzonite-syenite (7 analyses)	
	Avg	Range	Avg	Range	Avg	Range	Avg	Range
SiO_2	71.5	68.8 –74.1	70.2	68.2 –70.7	64.4	64.1 –64.8	57.0	54.4 –60.1
Al_2O_3	14.6	13.5 –15.7	15.6	15.2 –16.1	16.2	16.2	17.9	17.0 –18.9
Fe_2O_3	1.05	.66– 1.5	.31	.2 – .4	1.0	.9 – 1.0	1.5	.8 – 2.7
FeO	.97	.60– 1.7	1.9	1.6 – 2.3	2.8	2.8	3.8	3.0 – 4.6
MgO	.53	.28– .90	.64	.58– .83	2.3	2.1 – 2.4	2.0	1.1 – 2.8
CaO	1.5	1.1 – 2.2	2.1	1.8 – 2.6	3.7	3.1 – 4.2	5.0	3.8 – 6.6
Na_2O	3.55	3.1 – 3.9	3.3	3.0 – 4.1	3.2	3.0 – 3.3	3.2	2.3 – 4.1
K_2O	4.97	4.7 – 5.4	3.85	2.6 – 4.4	4.6	4.6	6.6	5.2 – 8.8
H_2O+	.50	.31– .75	.70	.41– .80	.47	.15– .80	.94	.66– 1.0
H_2O-	.15	.08– .23	.17	.10– .26	.17	.11– .24	.19	.08– .24
TiO_2	.24	.14– .37	.41	.35– .52	.54	.54	.75	.65– .98
P_2O_5	.10	.04– .18	.15	.12– .19	.17	.15– .18	.36	.23– .44
MnO	.05	.00– .10	.07	.07	.00	.00	.11	.00– .18
CO_2	.02	.01– .08	.01	.01– .02	.02	.02	.03	.01– .08
Fe_2O_3/FeO	1.08	----------	.16	----------	.36	----------	.39	----------

ture, consistent mineralogy, relatively homogeneous composition, and relative abundance of magnetite and allanite. The Darby granitic rocks are rich in SiO_2 and K_2O with a high Fe_2O_3/FeO ratio (table 1). This high Fe_2O_3/FeO ratio is reflected in the abundant magnetite in the Darby pluton, which in turn results in a high magnetic intensity for the pluton particularly as compared to the Bendeleben pluton (Alaska Division of Geological and Geophysical Surveys, 1973a, b).

The Bendeleben pluton forms the core of the eastern Bendeleben Mountains underlying an ellipsoidal-shaped area of about 300 km². Exposures of rock actually in place are generally confined to the higher cirque walls because most outcrops are reduced to frost-riven blocks. This pluton is composed chiefly of fine- to medium-grained, pinkish-gray quartz monzonite mottled with up to 11 percent mafic minerals. The rock is generally massive and equigranular although porphyritic and foliated varieties occur near the border of the pluton.

In contrast to the abrupt country-rock contacts of the Darby pluton, the Bendeleben consists of a central core of granitic rocks enclosed in a broad zone of alternating thin bands of granitic and high-grade metamorphic rocks with a gradual increase in metamorphic rocks away from the pluton. Aplite dikes cut both the pluton and country rocks, and pegmatites are also common in the country rock.

The Bendeleben pluton is a quartz monzonite that consists mainly of plagioclase (An_{25-37}) and slightly lesser amounts of perthitic potassium-feldspar and quartz. The varietal mafic minerals, biotite and hornblende, make up about 7 percent of the rock. Both biotite and hornblende are present, but biotite is generally much more abundant as indicated by a biotite-hornblende ratio of more than 9. Locally, in more mafic (perhaps contaminated) phases, hornblende is more abundant and clinopyroxene also occurs. Accessory minerals are sphene, zircon, and apatite. Allanite and opaque minerals are less common and much less abundant than in the Darby pluton; monazite is a rare constituent.

Distinguishing characteristics of the Bendeleben pluton are its relatively fine grained and equigranular

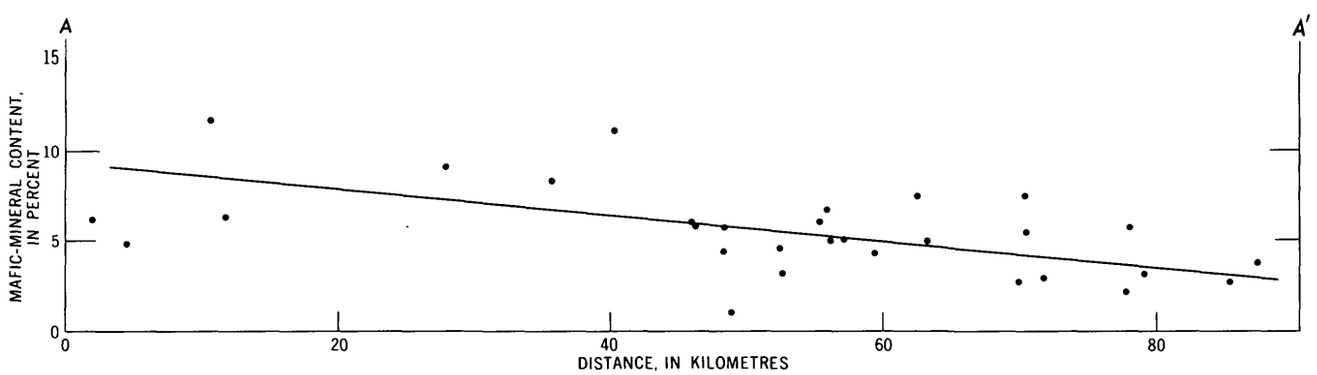

FIGURE 3.—Mafic-mineral content of the Darby pluton plotted in relation to distance along line *A–A'*, figure 1. The line on the graph represents a least-squares approximation of the data.

texture and its relative paucity of magnetite and allanite as compared to the Darby pluton. Chemically the Bendeleben is a silicic quartz monzonite with a low Fe_2O_3/FeO ratio.

The Kachauik pluton occupies the upland region west of the Darby Mountains and has an aggregate area of about 530 km² (fig. 1). It is a composite intrusion with granodiorite and quartz monzonite forming most of the west half of the pluton and a monzonite-syenite unit, subdivided by Miller and others (1972) into four subunits, forming the eastern part. An alkaline dike swarm consisting of pulaskite and pseudoleucite porphyry has intruded much of the north half of the pluton (Miller and others, 1971); the dike set has a consistent N. 40° E. strike. Exposures of rock actually in place are confined chiefly to scattered outcrops in the coarse-grained monzonite-syenite unit.

The granodiorite and quartz monzonite are porphyritic with large cream-colored plagioclase phenocrysts up to 25 cm long and abundant mafic-mineral phenocrysts in a grayish-cream-colored medium-grained groundmass of feldspar and quartz. Essential minerals are plagioclase (An_{33-45}), perthitic orthoclase, and less abundant quartz; varietal mafic minerals, which constitute as much as 27 percent of the rock, are biotite, hornblende, and clinopyroxene. The average modal composition is approximately that of a granodiorite. Adjacent to the alkaline rock dikes, the granodiorite has commonly been metasomatized with incipient development of aegirine and riebeckite. Accessory minerals are ubiquitous sphene, zircon, and apatite; allanite is less common, and magnetite is rare. Tourmaline is common in the form of thin veinlets cutting feldspar.

Distinguishing characteristics of the granodiorite are the large cream-colored plagioclase phenocrysts, relatively low quartz content, the occurrence of clinopyroxene with hornblende and biotite, the almost total lack of magnetite, the tourmaline veinlets, and the local alkali-metasomatized rocks.

The two chemical analyses reported in table 1 are of granodiorite in which little or no alkali metasomatism is apparent. They show the unaltered rock to be a granodiorite fairly rich in mafic minerals, relatively low in SiO_2, and high in K_2O. Metasomatized rocks show lower SiO_2 but higher alkalies.

The monzonite-syenite unit is composed of a variety of rocks including obvious contaminated and hybrid phases. Rocks of this unit are characteristically porphyritic with large pink to cream-colored potassium-feldspar phenocrysts (as much as 75 mm long) in a similarly colored medium-grained groundmass of feldspar; large hornblende and pyroxene phenocrysts are also abundant. Trachytoid and gneissic textures caused by alinement of potassium-feldspar phenocrysts and grains are common.

Essential minerals are perthitic potassium-feldspar and subordinate plagioclase (An_{30-45}); quartz content ranges from none to 5 percent. Varietal mafic minerals are dark-greenish-brown hornblende and green clinopyroxene; biotite is rare except in hybrid phases, and melanite garnet is locally present in contaminated border phases. Accessory minerals are ubiquitous sphene, apatite, and zircon, sporadically distributed magnetite, and allanite.

Distinguishing characteristics of the monzonite-syenite unit are the high potassium-feldspar and mafic-mineral content and the variation in composition and texture. The chemical analyses in table 1 show the general low-SiO_2, high-K_2O character of the rock as well as its generally more mafic character as indicated by relatively high FeO, Fe_2O_3, MgO, and CaO contents.

AGE OF PLUTONS

The plutons of the southeast Seward Peninsula intrude rocks of probable Precambrian age and are not stratigraphically bracketed. Although K-Ar ages have been obtained from the plutons in the area, only on the Darby pluton has sufficient dating been done to be relatively confident of the age. Two biotite samples from the northern part of this pluton yielded ages of 92.1 ± 2.8 and 94.0 ± 3 m.y. (table 2), and coexisting hornblende and biotite from a sample from the middle of the pluton yielded ages of 92.8 ± 2.6 and 88.3 ± 1.5 m.y., respectively. This second pair of ages, although not quite within the range of analytical error, together with the two biotite dates indicate a Late Cretaceous age of 88 to 94 m.y. for the pluton. A previously reported hornblende date of 81.4 ± 3 m.y. for the Darby pluton (Miller and others, 1972) appears to be wrong owing to an incorrect K_2O analysis.

A date of 79.8 ± 2.4 m.y. was obtained on biotite from the Bendeleben pluton, and a date of 97.5 ± 3 m.y. was obtained on hornblende from the monzonite-syenite unit of the Kachauik pluton (table 2). These dates should be regarded as only preliminary until supporting K-Ar age data are obtained; however, they are similar to those reported on plutons of similar composition elsewhere in western Alaska (Miller, 1970a; Csejtey and others, 1971). Also, that part of the Kachauik pluton adjacent to the Darby pluton is intruded by dikes similar in composition to the Darby, indicating that the Kachauik pluton is older.

The absolute age of the granodiorite unit of the Kachauik pluton is uncertain. Although an age of 86.1 ± 3 m.y. was reported on hornblende from this

TABLE 2.—K-Ar *age dates of the Darby, Bendeleben, and Kachauik plutons*

[Ages were calculated using the following constants: ^{40}K decay constants: $\lambda_\epsilon = 0.585 \times 10^{-10} yr^{-1}$, $\lambda_\beta = 4.72 \times 10^{-10} yr^{-1}$; abundance ratio: $^{40}K/K = 1.19 \times 10^{-4}$ atom percent. Potassium analyses were done by L. Schlocker by flame photometry using a lithium internal standard. Argon measurements using standard isotope-dilution techniques were made by J. Von Essen on samples 1, 2, and 6, by J. Von Essen and L. Alba on sample 3, and by J. Von Essen and S. J. Kover on samples 4 and 5]

Sample[1]	Field No.	Pluton	Mineral	K_2O (percent)		$^{40}Ar_{rad}$ (mol/g)	$\frac{^{40}Ar_{rad}}{^{40}Ar_{total}}$	Calculated age (m.y.)
1	68AMm280	Bendeleben	Biotite	8.14		9.799×10^{-10}	0.82	79.8±2.4
2	68AMm285	Darby	Biotite	8.93 8.96	8.94	1.247×10^{-9}	.73	92.1±2.8
3	71AMm415A	Darby	Biotite	8.96		1.275×10^{-9}	.78	94.0±3
4	70AMm158B	Darby	Hornblende	.893 .896		1.250×10^{-10}	.81	92.8±2.6
5	70AMm158B	Darby	Biotite	7.74 7.87		1.042×10^{-9}	.93	88.3±1.5
6	70AMm150	Kachauik	Hornblende	1.583 1.590	1.586	2.346×10^{-10}	.89	97.5±3

[1] Sample locations are as follows:
1. Lat 65°16′ N., long 162°55′ W.
2. Lat 65°01′ N., long 162°11′ W.
3. Lat 64°57′ N., long 162°20′ W.
4. Lat 64°45.2′ N., long 162°25.2′ W.
5. Lat 64°45.2′ N., long 162°25.2′ W.
6. Lat 64°34′ N., long 162°45′ W.

unit (Miller and others, 1972), biotite from a nepheline syenite dike intruding this unit has since yielded a 93.9±3 m.y. age. Additional dating is currently being conducted on this unit in an attempt to resolve this problem. K-Ar dates from other alkaline rocks in the western Alaska alkaline rock province, including the nearby Dry Canyon Creek stock (fig. 1), yielded ages of 105 to 107 m.y. (Miller, 1972).

The K-Ar ages on these three large plutons range from 80 m.y. to 98 m.y., suggesting emplacement in Cretaceous time. The Kachauik pluton is similar in composition to a suite of plutons in western Alaska that yielded K-Ar ages of 98 to 110 m.y. (Miller, 1972), and the single available date of 98 m.y. from the Kachauik pluton indicates that it belongs to this suite. A Late Cretaceous time of emplacement of around 92 m.y. for the Darby pluton appears to be fairly well documented by the four K-Ar ages obtained from the pluton. Csejtey and others (1971) referred to a 93-m.y. age for a mineralized granitic pluton on St. Lawrence Island, and the Kugruk pluton (Sainsbury, 1974) north of the Bendeleben Mountains likewise gave a 93-m.y. age (T. P. Miller, unpub. data, 1976). The relation of the Bendeleben pluton to other nearby plutonic rocks is uncertain since only a single date of 80 m.y. is available. A suite of calc-alkaline granitic rocks yielded ages of 78 to 82 m.y. in the Yukon-Koyukuk province to the east (Miller, 1970b), and a date of 75 m.y. was reported on the Brooks Mountain granitic stock in the western Seward Peninsula (Sainsbury, 1969a).

ANALYTICAL METHOD

Uranium, thorium, and potassium analyses of 31 samples from the Darby, Bendeleben, and Kachauik plutons are given in table 3. These analyses were done by gamma-ray spectrometry, and the basic operational procedures and calibration techniques are described by Bunker and Bush (1966, 1967).

Uranium concentrations are determined indirectly by measuring the radium daughters to obtain radium equivalent uranium (RaeU) values. Radium equivalent uranium is the amount of uranium, under the assumption of radioactive equilibrium, required to support the amount of daughter products that emit the radioactivity measured in a sample. Throughout the report where "U" and "uranium" are used "radium equivalent uranium" is implicit. Although thorium is also measured from daughter products, disequilibrium is improbable because of short half-lives; therefore, the concentrations are considered to be a direct measurement of parent thorium. Potassium is determined from its ^{40}K content, which is proportional to the total potassium. The coefficients of variation for the accuracy of the data included in this report (table 3) are about 3 percent for uranium and thorium and 1 percent for potassium when compared to standards analyzed by isotope dilution and flame photometer methods.

DISTRIBUTION OF URANIUM AND THORIUM

The Darby pluton has the highest uranium and thorium content of the three plutons with an average of 11.2 and 58.7 ppm, respectively, or about two to three times various reported averages (Rodgers and Adams, 1969) for granitic rocks. The uranium and thorium content appears to be high over the entire 80-km length of the pluton; samples D1 and D13 (fig. 1), for example, are about 75 km apart yet show 7.92 ppm uranium and 55.15 ppm thorium and 14.61 ppm uranium and 52.92 ppm thorium, respectively. The consistency of high values is also indicated by the range in these elements, which is 6.18 to 19.89 ppm for uranium and 40.84 to 83.75 ppm thorium. The number of sam-

TABLE 3.—*Radioactivity parameters for some southeastern Seward Peninsula plutons*

[Sample locations shown in figure 1. Analyses by C. M. Bunker and C. A. Bush]

Sample	Field No.	U (ppm)	Th (ppm)	K (percent)	Heat (μcal/g·yr)	Th/U	U/K×10⁻⁴	Th/K×10⁻⁴
BENDELEBEN PLUTON								
B1	70AMm59	4.07	15.63	3.34	7.00	3.84	1.22	4.68
B2	70AMm60	3.84	21.37	3.80	8.10	5.57	1.01	5.62
B3	70AEr66	4.38	17.69	3.35	7.64	4.04	1.31	5.28
B4	70AMm70A	9.49	50.84	3.51	18.04	5.36	2.70	14.48
B5	68AMm28	1.82	16.89	3.48	5.65	9.28	0.52	4.85
B6	70AMm67	2.68	11.69	2.21	4.89	4.36	1.21	5.29
Average		4.38	22.35	3.28	8.6	5.4	1.33	6.7
Average excluding sample B4		3.36	16.7	3.24	6.7	4.63	1.05	5.14
Range		1.82– 9.49	11.69–50.84	2.21– 3.80	4.89–18.04	3.84– 9.28	.52– 2.70	4.85–14.48
DARBY PLUTON								
D1	68AMm276	7.92	55.15	4.31	17.98	6.96	1.84	12.80
D2	71AMm409	10.29	51.92	3.86	18.94	5.05	2.67	13.45
D3	70AMm212	19.89	83.75	4.08	32.37	4.21	4.88	20.53
D4	71AMm421	17.73	68.80	3.73	27.71	3.88	4.75	18.45
D5	70AMm186A	10.36	64.65	3.72	21.50	6.24	2.78	17.38
D6	70AMm160B	13.50	50.76	4.19	21.24	3.76	3.22	12.11
D7	70AMm160A	8.81	48.77	4.54	17.41	5.54	1.94	10.74
D8	70AMm161	6.18	54.89	4.39	16.67	8.88	1.41	12.50
D9	70AMm159B	7.02	55.16	4.23	17.30	7.86	1.66	13.04
D10	70AMm146	11.71	66.58	4.11	22.97	5.69	2.85	16.20
D11	70AMm145	8.33	68.58	4.02	20.88	8.23	2.07	17.06
D12	70AMm210	9.32	40.84	3.99	16.05	4.38	2.34	10.24
D13	70AMm225	14.61	52.92	3.92	22.31	3.62	3.73	13.50
Average		11.2	58.7	4.08	21.0	5.2	2.78	14.46
Range		6.18–19.89	40.84–83.75	3.72– 4.54	16.05–32.37	3.62– 8.88	1.41– 4.88	10.24–20.53
KACHAUIK PLUTON **Granodiorite**								
K1	71AMm546	4.86	36.07	3.76	11.78	7.42	1.29	9.59
K2	71AMm549	12.46	34.25	3.71	16.95	2.75	3.36	9.23
K3	71AMm545	4.41	10.68	4.17	6.48	2.42	1.06	2.56
K4	70AMm130	6.10	13.59	2.82	7.93	2.23	2.16	4.82
K5	70AMm236	4.33	18.63	3.03	7.70	4.30	1.43	6.15
Average		6.4	23.4	4.15	10.17	3.82	1.86	6.47
Range		4.33–12.46	10.68–36.07	2.82– 4.17	6.48–16.95	2.23– 7.42	1.06– 3.36	2.56– 9.59
Monzonite-syenite								
K6	71AMm552	3.58	18.05	5.38	7.68	5.04	0.67	3.36
K7	70AMm135	5.46	29.24	4.37	11.01	5.36	1.25	6.69
K8	70AMm143	3.96	17.68	5.82	8.00	4.46	.68	3.04
K9	71AMm602	8.74	22.66	4.83	12.22	2.59	1.81	4.69
K10	70AMm141	5.14	20.58	5.54	9.36	4.00	.93	3.71
K11	70AMm151	1.97	11.26	7.35	5.67	5.72	.27	1.53
K12	70AMm229	8.62	39.15	5.71	15.66	4.54	1.51	6.86
Average		5.2	21.9	5.25	9.94	4.53	1.02	4.27
Range		1.97– 8.74	11.26–39.15	4.37– 7.35	5.67–15.66	2.59– 5.72	.27– 1.93	1.53– 6.86

ples is too small to pinpoint any local areas within the pluton with significantly higher uranium and thorium; however, samples D3, D4, and D5 just west of Vulcan Creek in the northern part of the pluton include some of the highest amounts of uranium and thorium reported. This is the same general area where West (1953) reported the occurrence of an unidentified "uranium-titanium niobate" mineral in pan concentrates. Heavy-mineral fractions (specific gravity >2.89) of a few of the pan concentrates contained as much as 5 to 10 percent of a mineral that consists chiefly of niobium, uranium, titanium, and calcium with traces of silicon, iron, and thorium (West, 1953). The combination of these elements suggests that the mineral is a multiple oxide mineral, such as euxenite or samarskite. Euxenite-bearing granitic rocks are rare but have been reported in the Idaho batholith (Mackin and Schmidt, 1956) where they are the source material for uranium- and thorium-bearing placer deposits.

With one exception analyzed samples from the Bendeleben pluton contain average uranium and thorium contents; five of the six samples show a range of 1.8 to 4.4 ppm uranium with an average of 3.4 ppm and a range of 11.7 to 21.4 ppm thorium with an average of 16.7 ppm. Sample B4 (fig. 1) contains much higher uranium and thorium, 9.5 ppm and 50.8 ppm, respectively, which is similar to amounts found in the Darby pluton; the potassium content, however, is similar to

the other Bendeleben samples and less than any value of potassium reported for the Darby pluton. The reason for the high uranium and thorium content in sample B4 is not known.

The granodiorite and monzonite-syenite units of the Kachauik pluton show a considerable but roughly similar range in uranium and thorium content. The Kachauik generally has more uranium and thorium than the Bendeleben pluton but less than the Darby pluton. The small number of analyzed samples makes generalizations difficult, but the two samples of relatively fresh granodiorite, K1 and K2, both have above average amounts of thorium (36 and 34 ppm) and K2 has above average uranium (12.5 ppm). The samples with lower quartz content and visible signs of potassium and sodium metasomatism contain smaller amounts of uranium and thorium.

Variation diagrams indicating the relation between uranium, thorium, and potassium (figs. 4 and 5) show that for the Bendeleben pluton and for the granodiorite of the Kachauik pluton, thorium generally increases as potassium increases. Such an increase is common for igneous rock series because thorium and uranium generally increase as differentiation proceeds, and the potassium content in silicic rocks such as these serves as a differentiation index. For the potassium-rich monzonite-syenite of the Kachauik pluton, however, the trend is anomalous in that thorium decreases as potassium increases. The range of potassium for the Darby pluton is so small that no trend relative to thorium is discernible.

Individual units show little or no relation between uranium and potassium, but excluding the monzonite-syenite of the Kachauik pluton, the plutons as a whole show a general increase of uranium with respect to potassium. The monzonite-syenite shows little variation of uranium with respect to potassium.

The Darby pluton has the highest U/K and Th/K ratios (table 3), which is to be expected since it is composed of the most silicic and presumably the most highly differentiated rock of the three plutons, and these ratios characteristically increase as rocks become more differentiated (Rodgers and Adams, 1969). A fairly good positive correlation exists between uranium and thorium in the Darby pluton (fig. 5); the U/Th ratio is the highest of the three plutons and relatively high for granitic rocks in general. A similar relation appears to exist for the monzonite-syenite of the Kachauik pluton, whereas no clear trend is apparent for the remainder of the Kachauik pluton or the Bendeleben pluton.

Radiogenic heat produced by the plutonic rocks from the southeast Seward Peninsula has been calculated

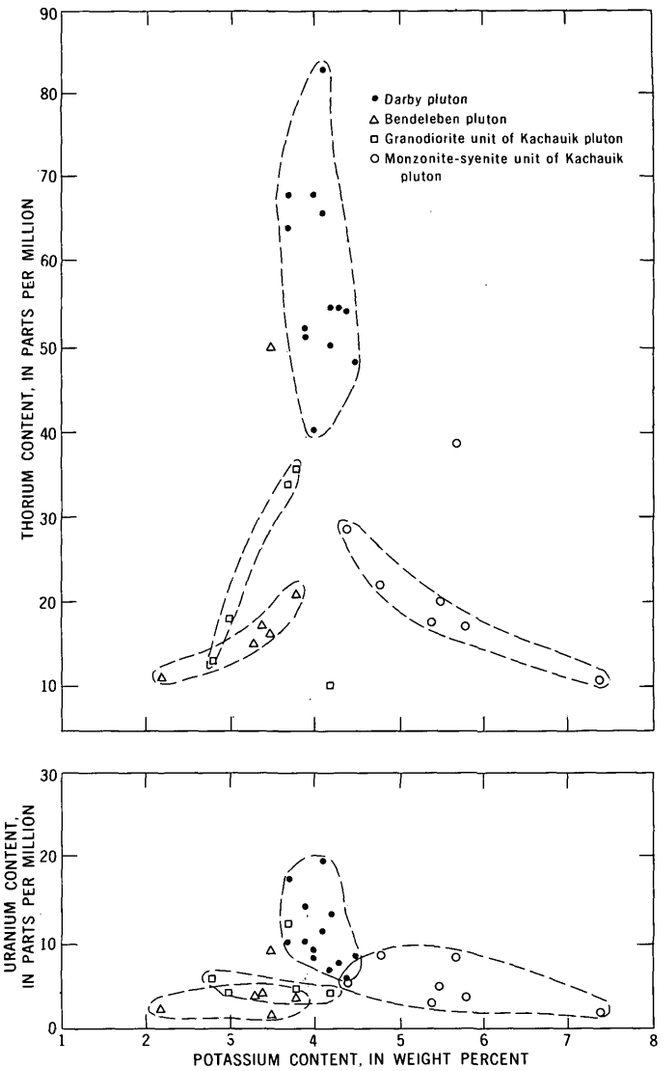

FIGURE 4.—Uranium and thorium content of the Darby, Bendeleben, and Kachauik plutons plotted in relation to potassium content.

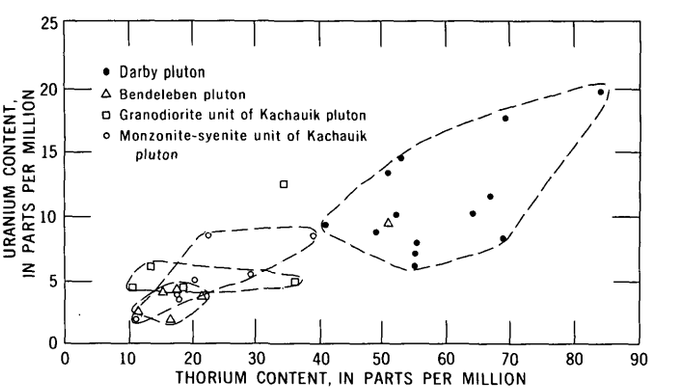

FIGURE 5.—Uranium content of the Darby, Bendeleben, and and Kachauik plutons plotted in relation to thorium content.

(table 3) from the uranium, thorium, and potassium contents (table 3) on the basis of Birch's (1954) estimates of heat generation (1 ppm Th=0.20 μcal/g·yr; 1 ppm U=0.73 μcal/g·yr; 1 percent K=0.27 μcal/g·yr). The Darby pluton, as is to be expected from its high uranium, thorium, and potassium content, has the greatest heat production. The heat yield from this pluton ranged from 16.0 to 32.4 μcal/g·yr and averages 21. This range is considerably above typical values reported for granitic rocks from the western United States by Tilling and Gottfried (1969). For example, the Boulder batholith has a reported average heat production of 6.8 μcal/g·yr, and the southern California batholith, 2.7 μcal/g·yr. The Kachauik pluton has a lower average heat production of about 10 μcal/g·yr, and the Bendeleben pluton has an average heat production of 8.67 μcal/g·yr (6.7 μcal/g·yr excluding sample B4), which is more typical of granitic rocks.

All three plutons contain accessory minerals such as allanite, sphene, and zircon that commonly are host minerals for uranium and thorium. West (1953) reported that the radioactivity of the concentrates taken from streams draining the Kachauik and Darby plutons was largely due to these accessory minerals. The Darby pluton has a much higher uranium and thorium content than the Bendeleben and Kachauik plutons, and allanite is certainly more abundant in the Darby pluton than in either of the other two plutons. A quantitative spectrographic analysis of allanite from sample D10 showed 12,000 ppm thorium.

Assuming normal thorium contents for the remaining accessory minerals as well as the major minerals present, a total of 0.4 to 0.5 percent allanite would have to be present in order to account for the 67 ppm thorium reported for sample D10. Point counts of the amount of allanite in the rock range from 0.15 to 0.21 percent. This estimate of the amount of allanite may be too low because accurate estimates of modal abundance of accessory minerals based on thin section study are difficult to obtain. This would be particularly true in regard to the coarse-grained Darby rocks. Other possibilities are that one of the major minerals in the rock contains much more thorium than it typically does, or an as yet unidentified uranium- and thorium-bearing mineral is present. X-ray studies of heavy mineral concentrates from this sample do not reveal any such minerals, however, nor has West (1953) reported any, other than the euxenitelike mineral, in the pan concentrates.

DISCUSSION

This study shows that the Darby pluton contains well above average amounts of uranium and thorium, the uranium and thorium content of the Kachauik pluton ranges from average to slightly above average, and the Bendeleben pluton contains only average amounts of uranium and thorium. The reason for the variation in uranium and thorium between plutons as close together as these is not readily apparent but may be a reflection of a difference in uranium and thorium content of the pregranitic source rocks of the three plutons.

It has been suggested, for example, that the decrease in the uranium content and radioactivity from east to west across the Sierra Nevada batholith, noted by Dodge (1972) and Wollenberg and Smith (1968) among others, reflects a regional distribution of uranium and thorium that predates the intrusion of the granitic rocks (Wollenberg and Smith, 1968). In the southeastern Seward Peninsula, however, the same sillimanite-bearing high-grade metamorphic rock unit occurs in the country rock surrounding all three plutons. The plutons, underlying an aggregate area of over 1,200 km^2, occur within a relatively small area of 7,000 km^2. They range in composition from highly silicic quartz monzonite to subsilicic nepheline syenite and in age from 105 m.y. to 80 m.y. This close juxtaposition of plutonic rocks that differ considerably in major- or minor-element composition but cover a time interval of only 25 m.y. and intrude the same country rock makes it unlikely that their composition results from lateral variation in the pregranitic source rocks. A more likely possibility is a vertical variation in the composition of the pregranitic source rocks coupled with the formation of magma at different levels. The high potassium content, low silica content, and generally more mafic character of the Kachauik pluton, for example, suggest that the source material for the Kachauik pluton, be it crustal material, deep-seated magma, or a combination of the two, was considerably different from that of the other two plutons. The close association in time and space of the large monzonite-syenite plutons (Kachauik-type rocks) in western Alaska with a regional belt of alkaline subsilicic rocks has lead to the suggestion (Miller, 1972) that the composition of the former is due at least partly to deep-seated alkaline magmas.

The Darby and Bendeleben plutons also show some indications that their respective magmas formed at different levels. The two plutons are relatively similar in gross composition, the Darby pluton being slightly higher in K_2O and Na_2O and the Bendeleben slightly higher in CaO and Al_2O_3. Perhaps the most significant chemical difference between the two plutons, however, is in their respective Fe_2O_3/FeO ratios. Although their

total Fe content is about the same, the Darby pluton has an average Fe_2O_3/FeO ratio of 1.08; the Bendeleben, 0.16. Converting the Fe_2O_3/FeO ratio to the molecular ratio $(2Fe_2O_3 \times 100)/(2Fe_2O_3 + FeO)$, termed the oxidation ratio by Chinner (1960), gives some insight into the behavior of oxygen during magmatic processes. The oxidation ratio appears to be dependent on the magnetite content, and the Darby pluton contains much more magnetite than the Bendeleben pluton; this dependence is similar to that pointed out by Dodge (1972) for the Sierra Nevada batholith. The average oxidation ratio for the Darby pluton is 50 as compared to 13 for the Bendeleben pluton, which indicates that the Darby pluton had a higher oxygen pressure and thus a higher degree of water saturation although neither magma was probably water saturated. This difference in water saturation of the magmas may be a reflection of the water content of the pregranitic source rocks. If more anhydrous rocks are to be expected at depth, for example, then the Bendeleben magma was formed at depths greater than that of the Darby magma.

Alkaline rocks are commonly host rocks for uranium and thorium deposits, and the western Alaska alkaline province with its associated large monzonite and syenite plutons were included within a uranium-thorium metal province that extends 300 km north and east of the southeastern Seward Peninsula (Clark and others, 1972). Uranothorianite and gummite were found associated with copper sulfides, molybdenite, gold, silver, bismuth, and thorite in placer deposits in the headwaters of the Peace River within this province (Gault and others, 1953). The streams in this area drain a mineralized alkaline stock (Miller and Elliott, 1969). Uranium and thorium analysis of selected plutonic rocks from plutons and alkaline complexes located within this uranium-thorium province are as great as 31 ppm uranium and 179 ppm thorium (Miller and Bunker, 1975).

The occurrence of above average amounts of uranium and thorium in the Darby pluton shows that anomalous amounts of uranium and thorium in this part of Alaska are not necessarily confined to alkaline and kindred intrusive rocks. The Darby pluton is slightly younger than the alkaline rocks and is much more silicic. This close spatial association of two different rock types both with above average uranium and thorium indicates that the area is indeed a uranium-thorium province and that this part of the crust is enriched in uranium and thorium.

Other occurrences of uranium and thorium have been reported in the Seward Peninsula. Small stocks of pyroxene-bearing granitic rocks in the Kigluaik and western Bendeleben Mountains have been described by Sainsbury (1974) as being unusually rich in thorium and containing abundant allanite. West and White (1952) reported the occurrence of zeunerite, a secondary hydrous copper-uranium arsenate mineral, in a small granitic stock at Brooks Mountain in the western Seward Peninsula. Most of the zeunerite is disseminated in hematite, which partly fills openings in an oxidized pegmatitic phase of the intrusion. The primary source of the uranium is not known. Moxham and West (1953) reported small amounts of radioactive material in Serpentine Hot Springs pluton of the northwest Seward Peninsula which result in above average radioactivity. Sainsbury and others (1970) stated that the southeast edge of the Serpentine Hot Springs pluton has the highest radioactivity. Killeen and Ordway (1955) discussed a lode deposit containing uranium in the nearby Ear Mountain pluton. The primary uranium mineral was not identified, but a secondary mineral described as intermediate between metazeunerite and metatorbernite was found. The lode deposit was not considered to have economic potential by Killeen and Ordway. Anomalous radioactivity has been reported in the Windy Creek stock (fig. 1) by Sainsbury (1974); the anomaly may be related to a mineralized zone on the west side of the stock or to alkaline subsilicic rocks known to occur in the pluton (Miller and others, 1971). Whether these scattered occurrences of uranium and thorium elsewhere in the Seward Peninsula mean that the uranium-thorium province extends beyond the area outlined in Clark and others (1972) is uncertain at present.

The Darby pluton has a uranium and thorium content similar to that of the Conway Granite of New Hampshire, which has been cited as a low-grade uranium-thorium resource (Adams and others, 1962). In addition to whatever potential the Darby pluton might have as a low-grade resource, however, its high uranium and thorium content plus the occurrence of the euxenitelike mineral in the pan concentrates of some streams draining the northeastern part of the pluton suggest the possibility of local concentrations of uranium and thorium that could have more immediate economic potential. The Darby pluton is therefore a favorable area for future exploration.

REFERENCES CITED

Adams, J. A. S., Kline, M. C., Richardson, K. A., and Rogers, J. J. W., 1962, The Conway Granite of New Hampshire as a major low-grade thorium resource: Natl. Acad. Sci. Proc., v. 48, p. 1898–1905.

Alaska Division of Geological and Geophysical Surveys, 1973a, Aeromagnetic map, northern part of Solomon quadrangle, Alaska: Alaska Div. Geol. and Geophys. Surveys open-file rept. 6, 1 sheet, scale 1:250,000.

——— 1973b, Aeromagnetic map, Bendeleben quadrangle, Alaska: Alaska Div. Geol. and Geophys. Surveys open-file rept. 3, scale 1:250,000.

Birch, Francis, 1954, Heat from radioactivity, *in* Faul, Henry, ed., Nuclear geology: New York, John Wiley and Sons, 414 p.

Bunker, C. M., and Bush, C. A., 1966, Uranium, thorium, and radium analyses by gamma-ray spectrometry (0.184–0.352 million electron volts), *in* Geological Survey research 1966: U.S. Geol. Survey Prof. Paper 550–B, p. B176–B181.

——— 1967, A comparison of potassium analyses by gamma-ray spectrometry and other techniques: U.S. Geol. Survey Prof. Paper 575–B, p. B164–B169.

Chinner, G .A., 1960, Pelitic gneisses with varying ferrous/ferric ratios from Glen Cova, Angus, Scotland: Jour. Petrology., v. 1, p. 178–217.

Clark, A. L., Berg, H. C., Cobb, E. H., Eberlein, G. D., MacKevett, E. M., Jr., and Miller, T. P., 1972, Metal provinces of Alaska: U.S. Geol. Survey open-file rept., 3 p.

Csejtey, Bela, Jr., and Patton, W. W., Jr., 1974, Petrology of the nepheline syenite of St. Lawrence Island, Alaska: U.S. Geol. Survey Jour. Research, v. 2, no. 1, p. 41–47.

Csejtey, Bela, Jr., Patton, W. W., Jr., and Miller, T. P., 1971, Cretaceous plutonic rocks of St Lawrence Island, Alaska: A preliminary report, *in* Geological Survey research 1971: U.S. Geol. Survey Prof. Paper 750–D, p. D68–D76.

Dodge, F. C. W., 1972, Trace-element contents of some plutonic rocks of the Sierra Nevada batholith: U.S. Geol. Survey Bull. 1314–F, 13 p.

Gault, H. R., Killeen, P. L., West, W. S., and others, 1953, Reconnaissance for radioactive deposits in the northeastern part of the Seward Peninsula, Alaska, 1945–47 and 1951: U.S. Geol. Survey Circ. 250, 31 p.

Hopkins, D. M., 1963, Geology of the Imuruk Lake area, Seward Peninsula, Alaska: U.S. Geol. Survey Bull. 1141–C, 101 p.

Killeen, P. L., and Ordway, R. J., 1955, Radioactivity investigations at Ear Mountain, Seward Peninsula, Alaska: U.S. Geol. Survey Bull. 1024–C, 36 p.

Mackin, J. H., and Schmidt, D. L., 1956, Uranium- and thorium-bearing minerals in placer deposits in Idaho, *in* Page, L. R., Stocking, H. E., and Smith, H. B., compilers, 1956. Contributions to the geology of uranium and thorium by the United States Geological Survey and Atomic Energy Commission for the United Nations International Conference on Peaceful Uses of Atomic Energy, Geneva, Switzerland, 1955: U.S. Geol. Survey Prof. Paper 300, p. 375–380.

Mendenhall, W. C., 1901, A reconnaissance in the Norton Bay Region, Alaska, in 1900, p. 181–222, *in* Brooks, A. H., Richardson, G. B., Collier, A. J., and Mendenhall, W. C., Reconnaissance in Cape Nome and Norton Bay regions, Alaska: U.S. Geol. Survey Spec. Pub., 222 p.

Miller, T. P., 1970a, Preliminary correlation of Mesozoic plutonic rocks in Bering Sea region [abs.]: Am. Assoc. Petroleum Geologists Bull., v. 54, no. 12, p. 2496.

——— 1970b, Petrology of the plutonic rocks of west-central Alaska: U.S. Geol. Survey open-file rept., 132 p.

——— 1972, Potassium-rich alkaline intrusive rocks of western Alaska: Geol. Soc. America Bull., v. 83, p. 2111–2128.

Miller, T. P., and Bunker, C. M., 1975, U, Th, and K analyses of selected plutonic rocks from west-central Alaska: U.S. Geol. Survey open-file rept., 5 p.

Miller, T. P., and Elliott, R. L., 1969, Metalliferous deposits near Granite Mountain, eastern Seward Peninsula, Alaska: U.S. Geol. Survey Circ. 614, 19 p.

Miller, T. P., Elliott, R. L., Grybeck, D. G., and Hudson, T. L., 1971, Results of geochemical sampling in the northern Darby Mountains, Seward Peninsula, Alaska: U.S. Geol. Survey open-file rept., 12 p.

Miller, T. P., and Grybeck, D. G., 1973, Geochemical survey of the eastern Solomon and southeastern Bendeleben quadrangles, Seward Peninsula, Alaska: U.S. Geol. Survey open-file rept., 115 p.

Miller, T. P., Grybeck, D. G., Elliott, R. L., and Hudson, T. L., 1972, Preliminary geologic map of the eastern Solomon and southeastern Bendeleben quadrangles, eastern Seward Peninsula, Alaska: U.S. Geol. Survey open-file rept.

Moxham, R. M., and West, W. S., 1953, Radioactivtiy investigations in the Serpentine-Kougarok area, Seward Peninsula, Alaska: U.S. Geol. Survey Circ. 265, 11 p.

Rodgers, J. J. W., and Adams, J. A. S., 1969, Handbook of geochemistry, Volume 11, Chapter 90 and 92, K. H. Wedepohl, ed.: Berlin, Springer-Verlag.

Sainsbury, C. L., 1969a, Geology and ore deposits of the Central York Mountains, western Seward Peninsula, Alaska: U.S. Geol. Survey Bull. 1287, 101 p.

——— 1969b, The A. J. Collier thrust belt of the Seward Peninsula: Geol. Soc. America Bull., v. 80, no. 12, p. 2595–2596.

——— 1974, Geologic map of the Bendeleben quadrangle, Seward Peninsula, Alaska: Anchorage, Alaska, The Mapmakers, 31 p.

Sainsbury, C. L., Hudson, T. L., Kachadoorian, Reuben, and Richards, Thomas, 1970, Geology, mineral deposits, and geochemical and radiometric anomalies, Serpentine Hot Springs area, Seward Peninsula, Alaska: U.S. Geol. Survey Bull. 1312–H, 19 p.

Smith, P. S., and Eakin, H. M., 1911, A geologic reconnaissance in southeastern Seward Peninsula and the Norton-Bay-Nulato region, Alaska: U.S. Geol. Survey Bull. 449, 146 p.

Tilling, R. L., and Gottfried, David, 1969, Distribution of thorium, uranium, and potassium in igneous rocks of the Boulder batholith region, Montana, and its bearing on radiogenic heat production and heat flow: U.S. Geol. Survey Prof. Paper 614–E, 29 p.

West, W. S., 1953, Reconnaissance for radioactive deposits in the Darby Mountains, Seward Peninsula, Alaska, 1948: U.S. Geol. Survey Circ. 300, 7 p.

West, W. S., and White, M. G., 1952, The occurrence of zeunerite at Brooks Mountain, Seward Peninsula, Alaska: U.S. Geol. Survey Circ. 214, 7 p.

Wollenberg, H. A., and Smith, A. R., 1968, Radiogeologic studies in the central part of the Sierra Nevada batholith, California: Jour. Geophys. Research, v. 73, no. 4, p. 1481–1495.

*U.S. GOVERNMENT PRINTING OFFICE: 1976-211-295-5/13

RECENT PUBLICATIONS OF THE U.S. GEOLOGICAL SURVEY

(The following books may be ordered from the Branch of Distribution, U.S. Geological Survey, 1200 South Eads Street, Arlington, VA 22202 (an authorized agent of the Superintendent of Documents, Government Printing Office). Payment is required. Remittances should be sent by check or money order payable to U.S. Geological Survey. Give series designation and number, such as Bulletin 1368–A, and the full title. Prices of Government publications are subject to change. Increases in costs make it necessary for the Superintendent of Documents to increase the selling prices of many publications offered. As it is not feasible for the Superintendent of Documents to correct the prices manually in all the previous announcements and publications stocked, the prices charged on your order may differ from the prices printed in the announcements and publications)

Professional Papers

726–E. Gravity and aeromagnetic study of part of the Yakima River basin, Wash., by S. L. Robbins, R. J. Burt, and D. O. Gregg, 1975, p. E1–E6; plate in pocket. $1.05.

729–D. Geology of sedimentary rocks in southern Yellowstone National Park, Wyo., by J. D. Love and W. R. Keefer. 1975. p. D1–D57. $2.55.

743–D. Dimorphism in two new genera of Devonian tabulate corals, by W. A. Oliver, Jr. 1975. p. D1–D11; 7 plates showing fossils. $1.15.

774–C. Mount Abbot quadrangle, central Sierra Nevada, Calif.—Analytic data, by J. P. Lockwood. 1975. p. C1–C18. 85¢.

823. A, Geologic and paleogeographic setting of Paleozoic corals in Alaska, by Michael Churkin, Jr. p. 1–11; B, Ordovician, Silurian, and Devonian corals of Alaska, by W. A. Oliver, Jr., C. W. Merriam, and Michael Churkin, Jr. p. 13–44; 25 plates, showing fossils: C. Carboniferous corals of Alaska, a preliminary report, by A. K. Armstrong. p. 45–57; D, Stratigraphic distribution of Permian corals in Alaska, by C. L. Rowett. p. 59–75; 3 plates showing fossils. $3.40.

860. Geochemical and geologic relations of gold and other elements at the Gold Acres open-pit mine, Lander County, Nev., by C. T. Wrucke and T. J. Armbrustmacher. 1975. 27 p.; 1 plate in pocket. $1.45.

865. Normapolles pollen from the Mississippi embayment, by R. H. Tschudy. 1975. 42 p.; 20 plates showing fossils. $2.20.

937. The 1973 Mississippi River basin flood: Compilation and analyses of meteorologic, streamflow, and sediment data, by E. H. Chin, John Skelton, and H. P. Guy. 1975. 137 p.; plates in pocket. $7.10.

941–A. Studies for seismic zonation of the San Francisco Bay region, edited by R. D. Borcherdt. 1975. p. A1–A102. $2.80.

Bulletins

1383–B. Upper Pleistocene pyroclastic-flow deposits and lahars south of Mount St. Helens volcano, Washington, by J. H. Hyde. 1975. p. B1–B20. 45¢.

1388. Influence of rainfall and ancient landslide deposits on recent landslides (1950–71) in urban areas of Contra Costa County, Calif., by T. H. Nilsen and B. L. Turner. 1975. 18 p.; plates in pocket. $1.90.

1401. Rapid analysis of silicate, carbonate, and phosphate rocks—revised edition, by Leonard Shapiro. 1975. 76 p. $1.10.

1405–B. A summary of Tertiary volcanic stratigraphy of the southwestern High Plateaus and adjacent Great Basin, Utah, by P. D. Rowley, J. J. Anderson, and P. L. Williams. 1975. p. B1–B20. 45¢.

1408. New and refined methods of trace analysis useful in geochemical exploration, by F. N. Ward, Editor. 1975. 105 p. $1.40.

1417. Annotated bibliography of studies on the density and other volumetric properties for major components in geothermal waters 1928–74, by R. W. Potter II, D. R. Shaw, and J. L. Haas, Jr. 1975. 78 p. $1.10.

Water-Supply Paper

2039–A. Chemical quality and temperature of water in Flaming Gorge Reservoir, Wyo. and Utah, and the effect of the reservoir on the Green River, by E. L. Bolke and K. M. Waddell. 1975. p. A1–A26; plate in pocket. $1.05.